HAL
open science

Characterization and optimization of high density plasma etching processes for advanced memories application

Maria Mercedes Rizquez Moreno

To cite this version:

Maria Mercedes Rizquez Moreno. Characterization and optimization of high density plasma etching processes for advanced memories application. Other. Université de Lyon, 2016. English. NNT : 2016LYSEM024 . tel-02918008

HAL Id: tel-02918008

https://theses.hal.science/tel-02918008

Submitted on 20 Aug 2020

HAL is a multi-disciplinary open access archive for the deposit and dissemination of scientific research documents, whether they are published or not. The documents may come from teaching and research institutions in France or abroad, or from public or private research centers.

L'archive ouverte pluridisciplinaire **HAL**, est destinée au dépôt et à la diffusion de documents scientifiques de niveau recherche, publiés ou non, émanant des établissements d'enseignement et de recherche français ou étrangers, des laboratoires publics ou privés.

N°d'ordre NNT : 2016LYSEM024

THESE de DOCTORAT DE L'UNIVERSITE DE LYON

opérée au sein de

L'Ecole des Mines de Saint-Etienne

Ecole Doctorale N° 488

Sciences, Ingénierie, Santé

Spécialité de doctorat : Microelectronics/ Microélectronique

Soutenue publiquement le 08/11/2016, par :

María Rízquez

Characterization and optimization of high density plasma etching processes for advanced memories application

---

« Caractérisation et optimisation des procédés de gravure plasma haute densité pour application sur des dispositifs de type mémoires électroniques avancées »

Devant le jury composé de:

REIS Marco/ Professeur/ Université Coimbra (Portugal)	Présidente
LANDESMAN, Jean-Pierre/ Professeur–Directeur/Université Rennes 1 (France)	Rapporteur
DUSSART, Rémi/ Professeur/ Université d'Orleans (France)	Rapporteur
REIS Marco/ Professeur/ Université Coimbra (Portugal)	Examinateur
PINATON Jacques/ Responsible process control group/ STMicroelectronics	Examinateur
PASQUET Julien/ Responsible plasma etching group/ STMicroelectronics	Examinateur
ROUSSY Agnès/ Maitre-Assistant-HdR/ EMSE CMP-SGC	Directrice de thèse

Spécialités doctorales	Responsables :	Spécialités doctorales	Responsables
SCIENCES ET GENIE DES MATERIAUX	K. Wolski Directeur de recherche	MATHEMATIQUES APPLIQUEES	O. Roustant, Maître-assistant
MECANIQUE ET INGENIERIE	S. Drapier, professeur	INFORMATIQUE	O. Boissier, Professeur
GENIE DES PROCEDES	F. Gruy, Maître de recherche	IMAGE, VISION, SIGNAL	JC. Pinoli, Professeur
SCIENCES DE LA TERRE	B. Guy, Directeur de recherche	GENIE INDUSTRIEL	X. Delorme, Maître assistant
SCIENCES ET GENIE DE L'ENVIRONNEMENT	D. Graillot, Directeur de recherche	MICROELECTRONIQUE	Ph. Lalevée, Professeur

EMSE : Enseignants-chercheurs et chercheurs autorisés à diriger des thèses de doctorat (titulaires d'un doctorat d'Etat ou d'une HDR)

ABSI	Nabil	CR	Génie industriel	CMP
AUGUSTO	Vincent	CR	Image, Vision, Signal	CIS
AVRIL	Stéphane	PR2	Mécanique et ingénierie	CIS
BADEL	Pierre	MA(MDC)	Mécanique et ingénierie	CIS
BALBO	Flavien	PR2	Informatique	FAYOL
BASSEREAU	Jean-François	PR	Sciences et génie des matériaux	SMS
BATTON-HUBERT	Mireille	PR2	Sciences et génie de l'environnement	FAYOL
BEIGBEDER	Michel	MA(MDC)	Informatique	FAYOL
BLAYAC	Sylvain	MA(MDC)	Microélectronique	CMP
BOISSIER	Olivier	PR1	Informatique	FAYOL
BONNEFOY	Olivier	MA(MDC)	Génie des Procédés	SPIN
BORBELY	Andras	MR(DR2)	Sciences et génie des matériaux	SMS
BOUCHER	Xavier	PR2	Génie Industriel	FAYOL
BRODHAG	Christian	DR	Sciences et génie de l'environnement	FAYOL
BRUCHON	Julien	MA(MDC)	Mécanique et ingénierie	SMS
BURLAT	Patrick	PR1	Génie Industriel	FAYOL
CHRISTIEN	Frédéric	PR	Science et génie des matériaux	SMS
DAUZERE-PERES	Stéphane	PR1	Génie Industriel	CMP
DEBAYLE	Johan	CR	Image Vision Signal	CIS
DELAFOSSE	David	PR0	Sciences et génie des matériaux	SMS
DELORME	Xavier	MA(MDC)	Génie industriel	FAYOL
DESRAYAUD	Christophe	PR1	Mécanique et ingénierie	SMS
DJENIZIAN	Thierry	PR	Science et génie des matériaux	CMP
DOUCE	Sandrine	PR2	Sciences de gestion	FAYOL
DRAPIER	Sylvain	PR1	Mécanique et ingénierie	SMS
FAVERGEON	Loïc	CR	Génie des Procédés	SPIN
FEILLET	Dominique	PR1	Génie Industriel	CMP
FOREST	Valérie	MA(MDC)	Génie des Procédés	CIS
FOURNIER	Jacques	Ingénieur chercheur CEA	Microélectronique	CMP
FRACZKIEWICZ	Anna	DR	Sciences et génie des matériaux	SMS
GARCIA	Daniel	MR(DR2)	Génie des Procédés	SPIN
GAVET	Yann	MA(MDC)	Image Vision Signal	CIS
GERINGER	Jean	MA(MDC)	Sciences et génie des matériaux	CIS
GOEURIOT	Dominique	DR	Sciences et génie des matériaux	SMS
GONDRAN	Natacha	MA(MDC)	Sciences et génie de l'environnement	FAYOL
GRAILLOT	Didier	DR	Sciences et génie de l'environnement	SPIN
GROSSEAU	Philippe	DR	Génie des Procédés	SPIN
GRUY	Frédéric	PR1	Génie des Procédés	SPIN
GUY	Bernard	DR	Sciences de la Terre	SPIN
HAN	Woo-Suck	MR	Mécanique et ingénierie	SMS
HERRI	Jean Michel	PR1	Génie des Procédés	SPIN
KERMOUCHE	Guillaume	PR2	Mécanique et Ingénierie	SMS
KLOCKER	Helmut	DR	Sciences et génie des matériaux	SMS
LAFOREST	Valérie	MR(DR2)	Sciences et génie de l'environnement	FAYOL
LERICHE	Rodolphe	CR	Mécanique et ingénierie	FAYOL
MALLIARAS	Georges	PR1	Microélectronique	CMP
MOLIMARD	Jérôme	PR2	Mécanique et ingénierie	CIS
MOUTTE	Jacques	CR	Génie des Procédés	SPIN
NIKOLOVSKI	Jean-Pierre	Ingénieur de recherche	Mécanique et ingénierie	CMP
NORTIER	Patrice	PR1		SPIN
OWENS	Rosin	MA(MDC)	Microélectronique	CMP
PERES	Véronique	MR	Génie des Procédés	SPIN
PICARD	Gauthier	MA(MDC)	Informatique	FAYOL
PIJOLAT	Christophe	PR0	Génie des Procédés	SPIN
PIJOLAT	Michèle	PR1	Génie des Procédés	SPIN
PINOLI	Jean Charles	PR0	Image Vision Signal	CIS
POURCHEZ	Jérémy	MR	Génie des Procédés	CIS
ROBISSON	Bruno	Ingénieur de recherche	Microélectronique	CMP
ROUSSY	Agnès	MA(MDC)	Génie industriel	CMP
ROUSTANT	Olivier	MA(MDC)	Mathématiques appliquées	FAYOL
STOLARZ	Jacques	CR	Sciences et génie des matériaux	SMS
TRIA	Assia	Ingénieur de recherche	Microélectronique	CMP
VALDIVIESO	François	PR2	Sciences et génie des matériaux	SMS
VIRICELLE	Jean Paul	DR	Génie des Procédés	SPIN
WOLSKI	Krzystof	DR	Sciences et génie des matériaux	SMS
XIE	Xiaolan	PR1	Génie industriel	CIS
YUGMA	Gallian	CR	Génie industriel	CMP

Mise à jour : 01/02/2016

A mis abuelos.
Por haberme llenado el corazón
de los más bellos recuerdos.

Acknowledgements

(Agradecimientos, Remerciments)

I would like to thank all these people who helped me and support during this time. I will express my gratitude in English, but I will also address to them in their native language if it is Spanish or French.

Many people contributed in different ways to my experience as a PhD student. First of all, I want to thank all the people from CMP.
Tout d'abord, un grand merci à ma directrice de thèse, Agnès Roussy, *pour toutes ces années. Merci pour ton soutien constant, en particulier dans les moments difficiles. Et merci aussi de m'avoir supportée au quotidien dans ton bureau … que du bonheur*!
Je tiens également à remercier Stéphane Dauzère-Pérès, *directeur du CMP à l'époque, de m'avoir donné l'opportunité de faire la thèse dans son laboratoire.*
I would like to particularly thank Jakey, for all his help and for all the interesting discussions where I have always learnt a lot (even if we did not always agree!).
And of course, thank you to all the SFL-people! …*Pour les pauses, pour les séminaires, pour partager la merveilleuse cantine*… It has been great doing the PhD with you and belonging to this group!

I would also like to extend my gratitude to all the people from STMicroelectronics who helped me during these years, especially those from the groups of plasma etching and process control, for their precious collaboration.
Un grand merci à Jacques Pinaton*, de m'avoir accueilli chez ST Rousset et d'avoir été toujours là… toujours avec la bonne humeur*! *Merci aussi* à Julien Pasquet, *responsable de l'équipe de gravure chez ST pour son aide et de m'avoir laissé tester mes idées dans un réacteur industrielle ! Merci également à Yoann Goasduff, toujours présent en quelque sorte, de m'avoir appris les enjeux de la gravure plasma. Je tiens à remercier également tous les thésards, stagiaires et alternants pour les repas du midi, les pauses cafés, les discussions… En particulier,* Richard *et* Romain ! *Je voudrais aussi remercier tout particulièrement* Marylaine. *Merci pour toutes les conversations (professionnels et personnels!), de m'avoir fait connaître tous ces plats fantastiques, pour ta confiance et soutien…*« *On n'est riche que de ses amis* »*…merci!*

A big thanks to my friends and my "family" here (*la famiglia!).*
Dario, Vincenzo, Babeth, Diego, Steffy, Les Knopp, Dino, Sebastian…thanks to all of you for driving these days as wonderful as they were! *Pour les voyages, pour les fêtes, por la "cultura"... Merci!*
Gracias especialmente a Laura *y* Carlos*, por ser una parte tan importante de estos años…¡y los que quedan por llegar!. Gracias también "a los de siempre", especialmente a Natalia, Ana y Dani, por estar siempre tan presentes pese a no estarlo.*

And finally, my most sincerely thanks goes to my family, my biggest support.
GRACIAS por todo el apoyo que me brindáis cada día. GRACIAS por haberme dado la oportunidad de vivir esta vida y por haberme acompañado todo el camino.
A mi padre por transmitirme y compartir conmigo su pasión por la ciencia, por confiar y creer siempre en mí, por ser mi cable a tierra. A mi madre por saber sacarme siempre una sonrisa, por la complicidad, por estar siempre ahí (a cualquier hora del día y de la noche). A mi hermano, por ese link que crece cada día, porque incluso en los silencios sabemos encontrarnos. A mis abuelos, culpables de las más duras despedidas cada regreso a Francia, por haberme llenado el corazón de los más bellos recuerdos. En especial a mi abuelo Juan, mi "big fish", que ha vivido esta tesis como si fuese la suya. Y a Alex, mi compañero de viaje, por su incondicionalidad. Esta aventura no hubiera sido lo mismo sin ti. No hay palabras suficientes para agradecerte lo que me aportas, lo que me complementas… « *Las palabras nunca alcanzan cuando lo que hay que decir desborda el alma* ».

To all you,

Thank you, Merci, Grazie, Danke, 谢谢, Gracias.

Contents

Work done in conjunction with others **7**

Acronyms **8**

Thesis Overview **9**

I. Introduction **11**

1. MICROELECTRONICS: AN OVERVIEW 12
2. CMOS TECHNOLOGY 14
   - 2.1. Basics 14
     - 2.1.1. The MOSFET Structure and Principle of Operation 16
     - 2.1.2. From MOS to CMOS 18
     - 2.1.3. Semiconductor Memories 19
   - 2.2. Fabrication Processes 22
     - 2.2.1. Front End of Line (FEOL) 24
     - 2.2.2. Back End of Line (BEOL) 25
   - 2.3. The Role of Plasma Etching in CMOS Technology 25
3. PLASMA ETCHING 27
   - 3.1. Introduction 27
   - 3.2. Basic Plasma Properties 28
   - 3.3. Physics and Chemistry of Plasma Etching 30
     - 3.3.1. The chemical etching 30
     - 3.3.2. The physical Etching 31
     - 3.3.3. Ion-Enhanced Etching 31
   - 3.4. Key Parameters in Plasma Etching 35
     - 3.4.1. Influence of Plasma Parameters 35
     - 3.4.2. Parameters for Evaluating Plasma Etching Performance 36
   - 3.5. State-of-the-art in Plasma Etching 38
4. OBJECTIVES 39

II. Experimental: Materials and Equipment 41

1. MATERIALS 42

1.1. Stack 42

1.2. Photolithography Mask 44

1.2.1. Areas of Study 45

2. PLASMA ETCH EQUIPMENT 47

2.1. The Etch Platform 47

2.1.1. Lam Versys 2300 Etch Chamber 48

2.1.2. Process Etch and Chamber Conditioning 49

3. DIAGNOSTIC TECHNIQUES 52

3.1. End Point Detection Technique (EPD) 53

3.1.1. What is an Endpoint? 53

3.1.2. Light Signal Reflectometry (LSR) 54

3.1.3. Optical Emission Spectroscopy (OES) 56

3.2. Scatterometry 60

3.2.1. Principle 61

3.2.2. Instrumentation 61

3.2.3. New Model for STI Measures 62

3.3. X-Ray Photoelectron Spectroscopy (XPS) 63

3.3.1. Principle 63

3.3.2. Instrumentation 65

3.3.3. Spectral Analysis 65

3.3.4. Angle-Resolved XPS (ARXPS) 67

3.3.5. Floating Sample Method 68

3.4. Scanning Electron Microscopy (SEM) 70

3.5. CD-Scanning Electron Microscopy (CDSEM) 71

3.6. Transmission Electron Microscopy (TEM) 71

4. SUMMARY 71

III. eSTM: Characterization and Process Optimization 73

1. INTRODUCTION 74

1.1. Embedded Select Trench Memory (eSTM) 74

1.1.1. The Starting Point: The 2T cell 75

1.1.2. Literature Review of the Polysilicon Vertical Trenches 75

1.1.3. The Polysilicon Trench of the eSTM: The Vertical Transistor 78

1.2. Plasma Etching Considerations 79

1.2.1. Pure Plasma Chemistries 80

1.2.2. Etch Directionality in RIE 82

1.2.3. Etch Selectivity in RIE 83

1.2.4. Literature Review on the Mechanistic Studies of Si and SiO2 Etching 83

2. EXPERIMENTAL APPROACH 90

2.1. Fabrication Process 90

2.1.1. The Necessary Steps for Reaching the eSTM Trench 90

2.1.2. The Selected Chemistry for the eSTM Trench 91

2.2. Specifications 93

2.2.1. Stack 93

2.2.2. Etching Specifications 93

2.2.3. Morphological Study of each Step 95

3. CHARACTERIZATION 96

3.1. Plasma Diagnostics 96

3.1.1. Background 97

3.1.2. Experimental 100

3.1.3. Results 102

3.1.4. Summary 107

3.2. Surface Characterization 107

3.2.1. Background 108

3.2.2. Experimental 112

3.2.3. Results 114

3.2.4. Discussion 129

4. OPTIMIZATION 132
4.1. Background 132
4.2. Experiments 135
4.2.1. Choice of the Factors 136
4.2.2. Design of Experiments 141
4.3. Results 143
4.3.1. DOE Analysis 143
4.3.2. Predictions and Validation 146
4.3.3. Further Details 147
4.4. Summary and Industrialization 149
5. CONCLUSION 150

IV. Plasma-Reactor Walls Interactions: The Fluorine Problem 153
1. LITERATURE REVIEW 154
1.1. Influence of Reactor Wall Conditions on Etch Processes 154
1.2. Contamination: The Fluorine Problem 156
2. PROCESS AND CLEANING CONSIDERATIONS 157
3. CHARACTERIZATION 158
3.1. State-of-the-art 158
3.2. Experimental 160
3.2.1. Substrates 162
3.3. Results 162
4. OPTIMIZATION 165
4.1. State-of-the-art 165
4.2. Strategy 167
4.2.1. Protocol 167
4.3. Results 168
5. CONCLUSIONS 171

V. STI: Plasma Etch Process Control for Critical Dimensions 173

1. INTRODUCTION 174

1.1. The STI Process 174

1.2. Process Variation 175

1.2.1. Measures of Variation 176

1.3. Process Control in Semiconductor Manufacturing 177

1.3.1. Statistical Process Control (SPC) 177

1.3.2. Advanced Process Control (APC) 178

2. EXPERIMENTAL 180

2.1. Stack 180

2.2. Etching Specifications 181

2.3. Industrial Context 182

3. CHARACTERIZATION 182

3.1. Process Variability 182

3.2. Impact of Previous Steps 183

3.3. The Influence of Etching 187

4. OPTIMIZATION 188

4.1. The EWMA R2R Strategy 189

4.2. The STI-Etch R2R Controller 190

4.2.1. R2R Operation 191

4.2.2. Model Validation 193

4.2.3. New Metrology 194

5. CONCLUSIONS 195

Conclusions and Future Work 197

Résumé (French) 201

Bibliography 231

List of Publications/ Communications 248

Work done in conjunction with others

The work presented in this thesis was carried out by the author, with the following exceptions:

Process

1. All the CMOS processes were done at STMicroelectronics Rousset. All the etching steps were performed by the author.
2. Al_2O_3 depositions were provided by ENCAPSULIX SAS.
3. Y_2O_3 substrates were provided by Pr. Rolly GABORIAUD, Departement Physique et Mecanique des Materiaux, CNRS-Universite de Poitiers.

Characterization

1. SEM, TEM and EDX images of full devices were taken at the ST Rousset characterization laboratory.
2. XPS analyses realized at CIMPACA were carried out by B. Bortolotti and A. James.
3. Electrical measures of the devices were made by the electrical characterization group at ST Rousset.
4. The scatterometry model was developed with Julian Martinez (metrology group).
5. The R2R was developed in collaboration with Dennis Pompier (automation team).

The evaluation of all the results was carried out by the author.

Acronyms

a-C:H Amorphous Hydrogenated Carbon
AHM Ashable Hard Mask
ARXPS Angle-Resolved X-ray Photoelectron Spectroscopy
BEOL Back End of Line
BL Bit Line
BT Breakthrough
CD Critical Dimensions
CD-SEM CD- Scanning Electron Microscopy
CG Control Gate
CMOS Complementary Metal-Oxide Semiconductor
CMP Chemical-Mechanical Polishing
CVD Chemical Vapor Deposition
DOE Design of Experiment
DTI Deep Trench Isolation
ECR Electron Cyclotron Resonance
EDX Energy Dispersive X-ray spectrometry
EEPROM Electrically Erasable Programmable Read Only Memory
eSTM Embedded Select Trench Memory
FEOL Front End of Line
FG Floating Gate
FN Fowler Nordhein
IC Integrated Circuit
ICP Inductively Coupled Plasma
ITRS International Technology Roadmap for Semiconductors
ME Main Etch
MOS Metal-Oxide Semiconductor
MOSFET Metal-Oxide-Semiconductor Field Effect Transistor
NVM Non-Volatile Memory
OE Over Etch
OES Optical Emission Spectroscopy
ONO Oxide-Nitride-Oxide
PECVD Plasma Enhanced Chemical Vapor Deposition
PW/NW P-Well/N-Well
PVD Physical Vapor Deposition
RAM Random Access Memory
RF Radio-Frequency
RIE Reactive Ion Etching
ROM Read Only Memory
R2R Run-to-Run
SEM Scanning Electron Microscopy
SHEI Substrate Hot Electron Injection
SL Source Line
STI Shallow Trench Isolation
TCP Transformer Coupled Plasma
TCR Top Corner Rounding
TOFSIMS Time of Fly Secondary ion mass spectroscopy
WL Worl Line
XPS X-ray Photoelectron Spectroscopy

Thesis Overview

The Critical Dimension (CD) is highly influenced by the Reactive Ion Etching (RIE) of silicon in the CMOS technology. The CD has to be well-controlled since it is one of the most important features related to process stability and product quality. However, the RIE process involves a lot of parameters which are highly confounded and entangled and thus it is very difficult to analyze the process. The main objectives of this thesis are to have an understanding of the fundamental mechanisms of the etching process and to propose innovative solutions to reduce the variations of CD by reaching the good control of the process desired.

This research was carried out in parallel between STMicroelectronics Rousset and the Center Microelectronic of Provence (CMP).

The structure of this thesis is organized in five chapters. The experimental results of this study are presented through chapters III to V (Figure 1). These chapters begin with an introduction to the relevant literature and the experimental details related to the process. Then, the results are expressed in two parts; the characterization and the optimization of the process. A summary of the result is presented at the end of each part and finally the conclusions are drawn.

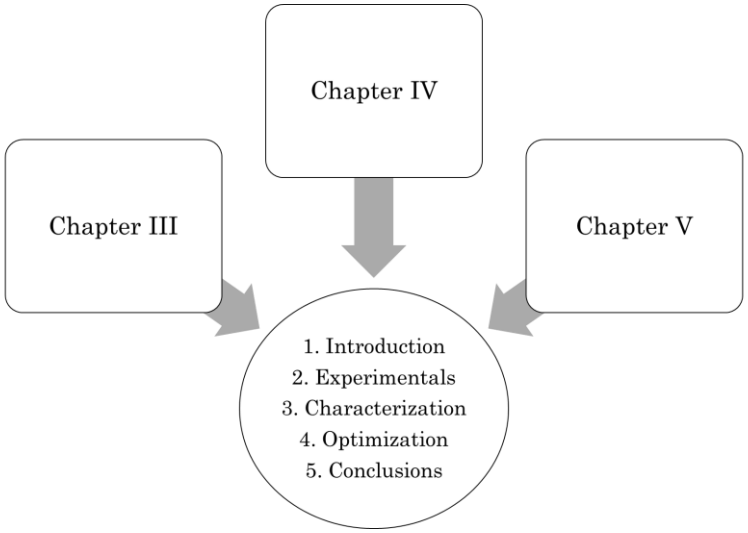

Figure 1. Structure of the three experimental chapters that compose the thesis.

The main propose of each chapter is:

In Chapter I, the main aspects and actual tendencies in CMOS technology and plasma etching is introduced.

Chapter II, describes the experimental systems regarding the plasma etching equipment and the characterization techniques.

Chapter III, is dedicated to a detailed understanding of the main mechanism involved in the etching of the mask and specially the silicon during the etch of the new vertical transistor of the eSTM structure. Characterizations of the plasma itself, and the surface of the wafer are discussed. After understanding the mechanism involved in this process, a model able to predict the optimum CD in terms of electrical results is proposed by means of DOE.

Chapter IV, presents to the characterization of the reactor walls during the eSTM process. Since this technology is still in development, the cleaning recipe has to be optimized in order to get the best results without contaminating the chamber from process to process due to fact of working in an industrial environment (ST Microelectronics).

Chapter V, contains the study of the source of variability during the STI trench etch process. The development of a R2R control for the CD of this trench to improve the uniformity 3sigma total of the CD is described.

Finally, the main conclusions are summarized, as well as the proposition of the possible applications of the results obtained and future directions of this work.

"Science knows no country, because knowledge belongs to humanity, and is the torch which illuminates the world" (L. Pasteur)

Chapter I

Introduction

This chapter presents the general motivation of this thesis, based on the past and present state-of-the-art related to the plasma etching in semiconductor manufacturing. An overview of the microelectronics with emphasis in the CMOS technology will be introduced followed by some of the most important plasma etching concepts. Finally, the objectives of the thesis are presented.

Picture of cold plasma discharge [I].

Great advances in semiconductor technology and circuit design techniques have been observed in recent years. Yet, chip manufacturing is a very challenging undertaking, primarily because of the complexity and sensitivity of its production process [1].

1. MICROELECTRONICS: AN OVERVIEW

As the name suggests, microelectronics is related to the study and manufacture of very small electronic designs and components. Over the last decades, the semiconductor industry has played a major role in social and economic development since the invention of the transistor. Every remarkable modern innovation has been made possible by the transistor, but they are most commonly known for their contribution to the world of computers.

The beginning of semiconductor research is well established by the mid-1930s, when the quantum theory of solids began to be interesting to industrial scientists seeking solid-state alternatives to vacuum-tube amplifiers and electromechanical relays [2]. In 1947, the most important invention of the past century, the transistor, emerges from the Bell laboratories by J. Bardeen, W. Brattain and W. B. Shockley. Eleven years later, in 1958, Jack Kilby created the first Integrated Circuit (IC) while working at Texas Instruments laboratories [3]. Up to 1970 the integrated circuit's innovation and business was almost completely a U.S. phenomenon. In 1971, appears the first commercially microprocessor by Intel which held 2300 transistors and announcing a new era in Integrated Electronics [4]. Figure I-1 shows the first Integrated Circuit from Texas Instrument (1958) and the first microprocessor from Intel (1971).

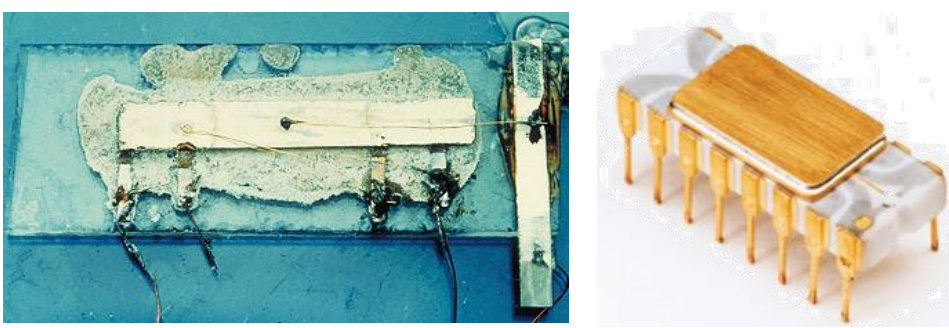

Figure I-1. First Integrated Circuit Texas Instruments, 1958 (source: Texas Instruments) and first microprocessor Intel, 1971 (source: Intel).

As the semiconductor technology improved, the technology of transistors grew making them faster, cheaper, smaller and more reliable. The object was to miniaturize electronics equipment to include increasingly complex electronics functions in limited space with minimum weight.

According to the empirical theory of Gordon Moore in 1965 [5], the number of transistors on an Integrated Circuit (IC) roughly doubles every year, whereas the cost per transistor is

reduced at the same time. Ten years later, in 1975, he reformulated this theory explaining that the number of transistors per integrated circuit doubles every 18 months.

This prediction has been surprisingly accurate. As a result, the scale gets smaller, and transistor count increases at a regular pace to provide improvements in IC functionality and performance while decreasing costs. The exponential growth that continues today is shown in Figure I-2.

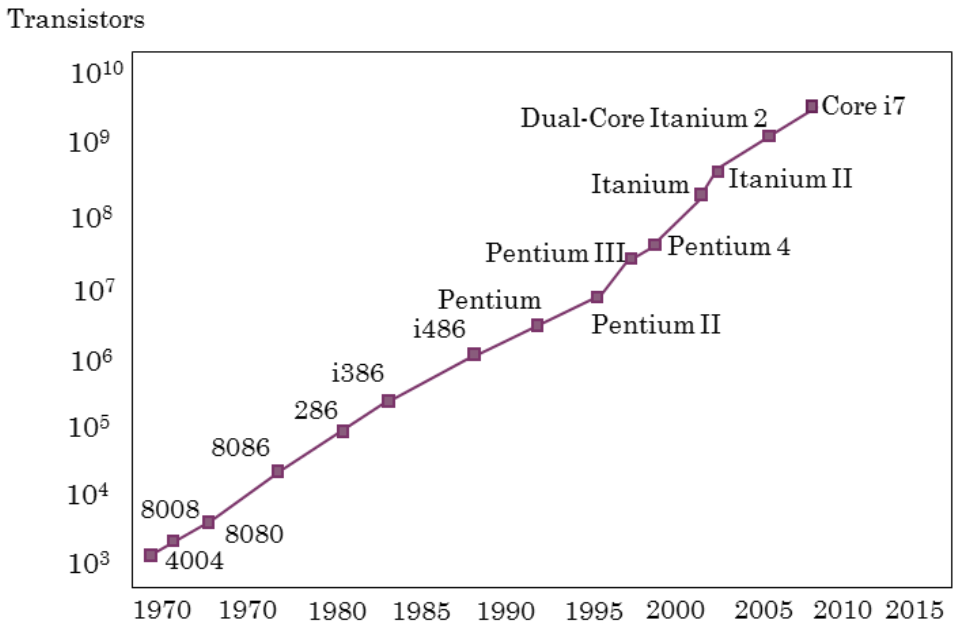

Figure I-2. Moore's Law for transistor counts since 1970 [Data from 6].

Since 1977, the Moore's law is showed as a technology roadmap in the International Technology Roadmap for Semiconductors (ITRS) where the evolution of the microelectronics is predicted in a short, medium and long term [7]. The ITRS synchronizes the technology development and the timely availability of manufacturing tools and methods. However, as the physical limits are approached, other factors such as design cost, manufacturing economics and device reliability, make progress through device scaling alone ever more challenging, and alternative ways forward must be sought [8].
Microelectronics therefore seeks to develop in new ways for keeping the miniaturization going, as it has been coming until now. This miniaturization has been possible thanks to the control of processes implied on the fabrication of Integrated Circuits based on CMOS technologies.

Introduction to the CMOS technology and its main aspects are presented in the next section.

2. CMOS TECHNOLOGY

CMOS (Complementary Metal-Oxide Semiconductor) is the semiconductor technology used in the transistors that are manufactured into most of today's computer microchips such as microprocessors, microcontrollers, static RAM and other digital logic circuits. CMOS derives its name from the basic physical structure of these devices; the MOS capacitor, composed of a semiconductor, oxide and a metal gate.

In the following sections, some key aspects of this technology will be discussed. In the first section a quick overview of CMOS basics is given, such as the principal element used in microelectronics, the integration of this element into the technology and the classification of semiconductor memories. The second will deal with the fabrication process and finally, the role of plasma etching in CMOS technology is shown.

2.1. Basics

The most basic element in the design of a large scale integrated circuit is the transistor. For the processes we will discuss, the type of transistor available is MOSFET [9,10], which becomes imperative when the problems of high power consumption become dominant. Even if the bipolar transistors are faster than MOSFET's, these devices have low power consumption and can be scaled down easily than other transistor types. MOSFET is a compromised of an MOS capacitor (gate and substrate terminals) and two pn junctions (source and drain terminals) as illustrated by Figure I-3. The MOS capacitor [10,11,12] consists of a Metal-Oxide-Semiconductor structure. It is actually a "sandwich" consisting of the underlying substrate material, which is a single crystal of semiconductor material (usually silicon heavily-doped); a thin insulating layer (usually thermal silicon dioxide); and an upper metal layer. Actually, the transistors that we will discuss do not use metal for their gate regions, but instead use heavily-doped polycrystalline silicon (Poly-Si).

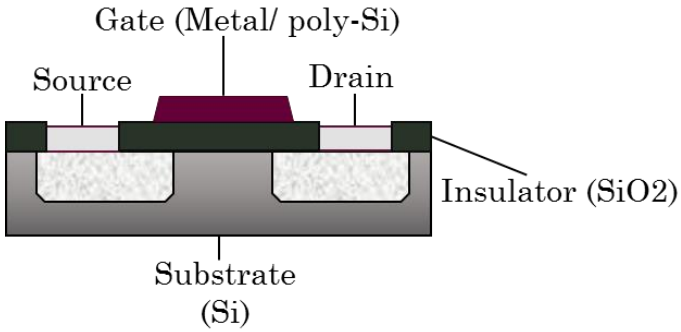

Figure I-3. Basic schematic view of a MOSFET structure.

As capacitor, the MOS is able to store charge; however, the MOSFET, as transistor, acts as a current switch and amplifies the current. The electrical charge, or current, can flow from the source to the drain depending on the charge applied to the gate region. Details of the MOSFET structure and physical operation are explained in 2.1.1.

Almost universally, the MOSFET structure utilizes doped silicon as the semiconductor on the substrate and its native oxide, silicon dioxide, as the insulator. The semiconductor material in the source and drain regions is “doped” with a different type of material than in the region under the gate, so an NPN or PNP structure exists between the source and drain regions [10,13,14,15].

The most commonly used semiconductor since the early 1960s is silicon (Si) [16,17] which is today the cornerstone of modern CMOS technology. The main reasons we use silicon [18] are that silicon devices exhibit better properties at room temperature, and high-quality silicon dioxide can be grown thermally. There is also an economic consideration, device-grade silicon cost much less than any other semiconductor material [19].

Semiconductors [20] are a group of materials having conductivities between those of conductors and insulators. Silicon atoms form covalent bonds and can crystallize into a regular lattice. Each of these elements has four valence electrons and needs four more to complete the valence energy shell. If a silicon atom, has four nearest neighbors, with each neighbor atom contributing one valence electron to be shared, then the atom of the center will have eight electrons in its outer shell. This structure is called an intrinsic semiconductor and can conduct a small amount of current. In intrinsic semiconductors, the conductivity is determined by both electrons and holes and depends on the carrier density. A two-dimensional representation of the covalent bonding in silicon is shown in Figure I-4.

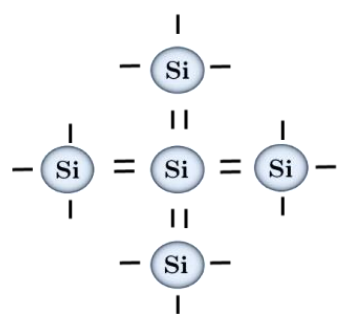

Figure I-4. 2D Schematic representation of the covalent bonding in silicon.

It is possible to shift the balance of electrons and holes in a silicon crystal lattice by "doping" it with other atoms. This doping process, described in [21,22], can greatly alter the electrical characteristics of the semiconductor. Semiconductors in its pure form are called intrinsic whereas that impure semiconductors are called extrinsic.

Depending on the type of impurity added we have two types of semiconductors: N-type and P-type. An extrinsic semiconductor will have either a preponderance of electrons (n-type) or a preponderance of holes (p-type). These effects are schematically shown in Figure I-5.

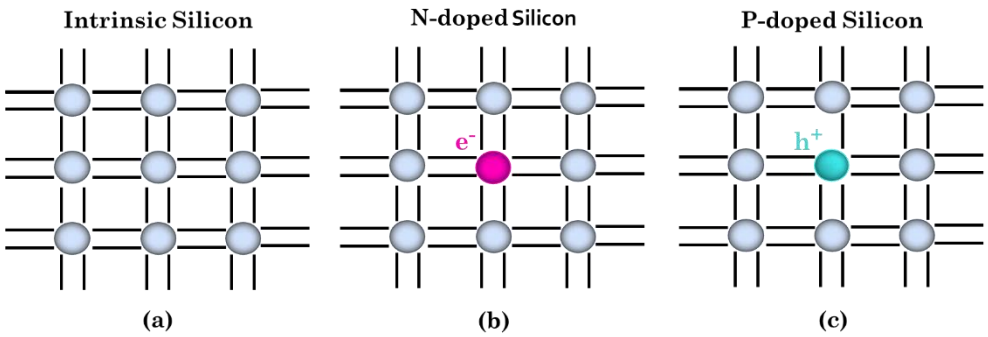

Figure I-5. Representation of the intrinsic silicon lattice (a), N-doped Si (b), P-doped Si (c).

Atoms with more valence electrons than silicon, mainly from group V [23], are used to produce "n-type" silicon material, which adds electrons to the conduction band and hence increases the number of electrons. Atoms with less valence electrons than silicon, mainly from group III [24], result in "p-type" silicon material. In p-type, the number of electrons trapped in bonds is higher, thus effectively increases the number of holes. Table I-1 summarizes the properties of semiconductor types.

Table I-1. Properties of P-type and N-type semiconductors.

	P-type (positive)	**N-type (negative)**
Dopant	Group III (e.g. Boron)	Group V (e.g. Phosphorous)
Valence Electrons	3	5
Polarity	Positive	Negative
Charge carriers	Missing Electrons (Holes)	Excess Electrons

The intrinsic silicon is not useful due to the low conductivity. The extrinsic semiconductors are the primary reason we can fabricate the various semiconductor devices [25] that we will consider in this thesis.

2.1.1. The MOSFET Structure and Principle of Operation

The Metal-Oxide-Semiconductor Field Effect Transistor (MOSFET) is by far the most common type of transistor. The basic MOSFET structure was proposed by Atalla [26], but the first MOSFET transistor was reported in 1960 by Kahng and Atalla [27].
As explained before, it is a compromise between a MOS capacitor and two pn junctions: the Source and the Drain (S/D). These regions, heavily-doped, are quite similar and are labelled depending on what they are connected to. The source is the terminal or node, which acts as the source of charge carriers. The charge carriers leave the source and travel to the drain.
In the case of an N channel MOSFET, the source is the more negative of the terminals; in the case of a P channel, it is the most positive of the terminals. The area under the gate oxide

is called the "channel", which is lightly doped. Table I-2 summarizes the properties of the transistor types [28].

Table I-2. Composition of NMOS and PMOS.

Transistor type	S/D	channel	Inversion layer created
NMOS	n-type	p-type	n-type
PMOS	p-type	n-type	p-type

The basic device parameters are the channel length L, which is the distance between the two metallurgical n+-p junctions; the channel width W; the insulator thickness d and the substrate doping N_A. In a silicon integrated circuit, a MOSFET is surrounded by a thick oxide (called the field oxide to distinguish it from the gate oxide) or a trench filled with insulator to electrically isolate it from adjacent devices [10]. The insulation trenches that isolate the different transistors between them are called STI (Shallow Trench Isolation). The basic structure of a MOSFET is illustrated in Figure I-6.

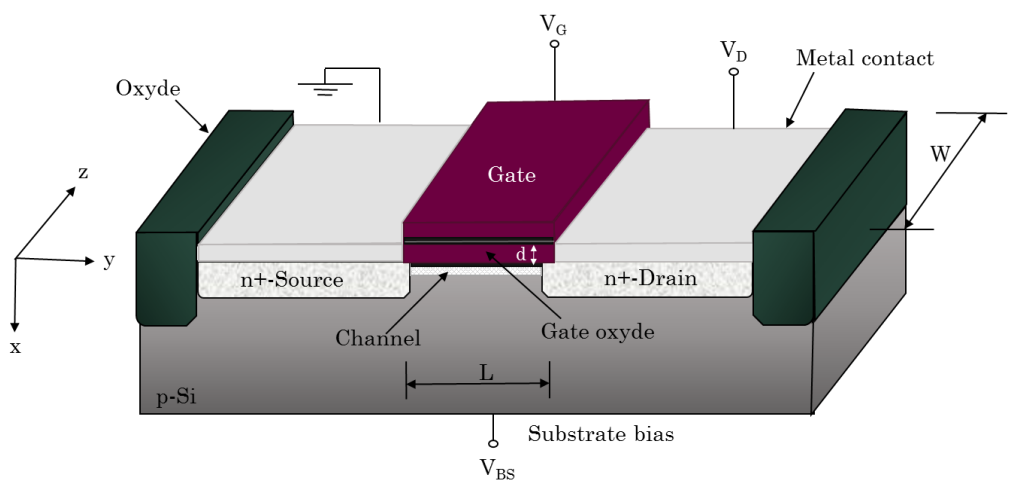

Figure I-6. Schematic diagram of a basic MOSFET [Adapted from 10].

MOSFET works [13,29] by electronically varying the width of a channel along which charge carriers flow (electrons or holes). The charge carriers enter into the channel trough the source and exit via the drain. The width of the channel is controlled by the voltage on the gate. The flow of the current between the source and the drain depends on the voltages that are applied to these terminals.

Corresponding to whether the transistor is in an ON state or an OFF state at zero gate–source voltage, two basic forms of MOSFET are available [30,31]: "Depletion-mode" and "Enhancement-mode". A channel marks the main difference between the two types (the so-called conducting "path"). It is located between the source and drain. With the depletion-mode MOSFET it is formed in the doping process during fabrication. In the enhancement-

mode device there is no channel between the source and drain. Both types of MOSFET devices have either an n-channel or a p-channel depending on their added impurities. However, MOSFET is a unipolar device, its operation depends on only one type of charge, either electrons or holes, but never both.

The operational principle of MOSFET depends on the MOS capacitor, since it is the main part of the device. We will consider subsequently the case of an n-MOS as an example. MOSFET having n-channel region between source and drain is a four terminal device, where the terminals are gate, drain, source and substrate or body. The drain and source are heavily doped n+ region and the substrate is p-type. The current flows of the negatively charged electrons, that is why it is known as n-channel MOSFET. When we apply positive voltage to the gate, the holes present beneath the oxide layer experience repulsive force and they are pushed downwards in to the bound negative charges which are associated with the acceptor atoms. The positive gate voltage also attracts electrons from n+ source and drain region in to the channel, thus the electron rich channel is formed. Now, if a voltage is applied between the source and drain, current flows freely between them. The gate voltage controls the electron concentration in the channel. N-channel is preferred over p-channel MOSFET as the mobility of electrons are higher than holes [32]. The diagrams of enhancement mode and depletion mode for an n-MOS are given in Figure I-7.

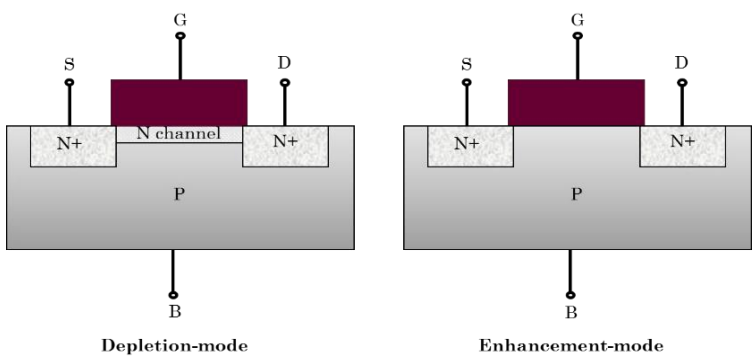

Figure I-7. Schematic of n-MOS in depletion-mode and enhanced-mode [Adapted from 32].

CMOS circuits require n-MOS and p-MOS transistors, the integration of these transistors on the same substrate for CMOS processes is explained in next section.

2.1.2. From MOS to CMOS

MOSFET is the most-important device for forefront high-density integrated circuits such as microprocessors and semiconductor memories. These circuits, fabricated with the CMOS technique, require an nMOS and pMOS transistor technology on the substrate to enable the logic functions. To this end, an n-type is usually provided in the p-type substrate or an n-type and p-type in a low-doped substrate.

The advantage of CMOS is that the output can be as high as the power supply voltage and as low as ground. In addition, there is no power dissipation in either logic state. Instead the power dissipation occurs only when a transition is made between logic states. CMOS circuits are the most suited for very/ultra-large-scale integration (VLSI/ULSI) [29,33].

Several applications are possible such as microprocessors, microcontrollers and other digital logic circuits [34-37]. Even if this technology is also used for several analogy circuits, one of the most widespread is the microprocessor, which takes several million transistors and at least 10 levels of metal for the interconnections. Figure I-8 shows the photograph of a microprocessor including in the same circuit the microcontroller (logic) dedicated to the processing of inputs and outputs and the memory where the information is stored.

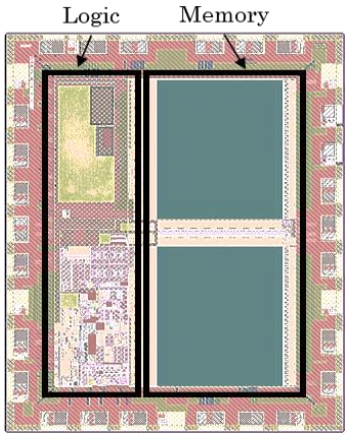

Figure I-8. Microprocessor including the memory and the logic.

The microprocessor allows managing a large amount of stored data in the RAM (Random Access Memory) memory cells, the so-called Volatile Memories. The memory part used to stock the information is the so-called Non Volatile Memory (NVM) [38-41]. As the names imply, a volatile memory loses the content when there is no voltage whereas a nonvolatile memory does not need voltage to maintain the data.

As the memory market enters the Gigabit and GHz range with consumers demanding ever higher performance and more diversified applications, new types of devices are being developed in order to keep up with the scaling requirements for cost reduction [42]. In this scenario, memories [43,44] play an important role. The most important semiconductor memories will be summarized in the next section.

2.1.3. Semiconductor Memories

Semiconductor memories can be classified by regarding different criteria, Figure I-9 shows a first classification of these memories.

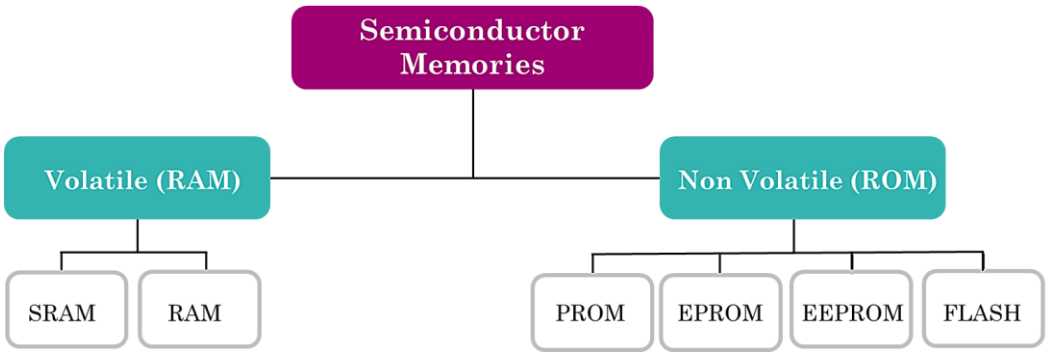

Figure I-9. Classification of semiconductor memories.

The Volatile Memories are fast and are used for temporary storage of data since they lose the information when the power is turned off. This means that they need to be permanently under tension to keep their information. The Non Volatile Memories (NVM) [39,49] retain the information even when the power is down. They have been conceived in order to store the information without any power consumption for a long time.

The first Non Volatile semiconductor memory is the ROM (Read Only Memory). This new device appears when the gate electrode of a conventional MOSFET is modified so that semipermanent charge storage inside the gate stack is possible. Since the first nonvolatile memory device proposed by Kahng and Sze in 1967 [50] various device structures have been made, and nonvolatile memory devices have been extensively used in commercial products. The two groups of nonvolatile memory devices are the floating-gate devices [51] and the charge-trapping devices [52].

The characterization and optimization which have been carried out during the development of this thesis is related to the Floating-gate's structure, but before getting into details about the memories studied here, we should first clarify what a Floating gate transistor is. A floating gate is basically a MOSFET with two supplementary levels of polysilicon. These two levels of polysilicon are separated by a tri-insulating layer of ONO (Oxide / Nitride / Oxide), whose role is to prevent the pass from the floating-gate to the control-gate.

For the understanding of this thesis, the difference between the EEPROM and the Flash memories, both of them floating-gate based, should be introduced. The basic structure of each memory is presented in Figure I-10 and the main different between these two NVM are explained as follows:

- **EEPROM (Electrically Erasable Programmable Read Only Memory).** An electrically erasable/programmable ROM, can be erased not only electrically, but also selectively by byte address. To erase selectively, a select transistor is needed for each cell, leading to a two-transistor cell (2T); the floating-gate and the select-transistor.

The select transistor increases the size of the memories and the complexity of array organization, but the memory array can be erased bit per bit.

- **Flash memory.** The name "flash" comes from its fast erasing mechanism. It looks like EEPROM memory but without the select transistor. As opposed to a full-feature EEPROM, can be erased electrically but only by a large block of cells simultaneously. It loses byte selectivity but maintains one-transistor cell (just the floating-gate). Today it is the most produced memory.

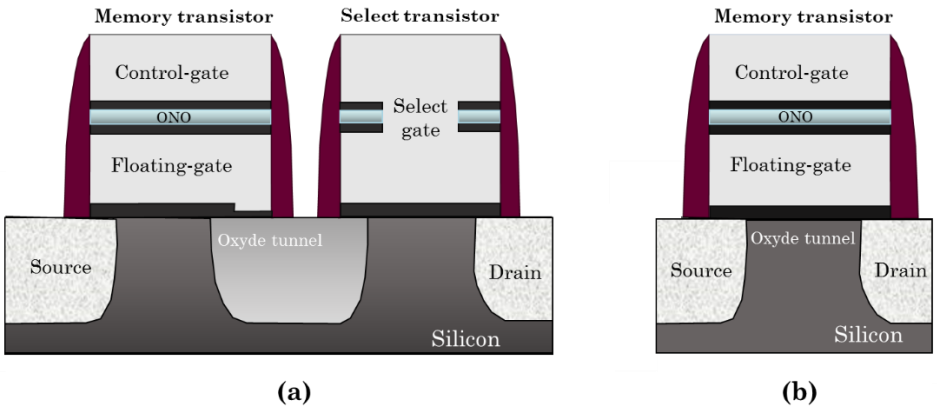

Figure I-10. Schematic of EEPROM (a) and Flash (b) memories.

Among other characteristics, the ideal memory should have low power consumption, fast read/write/erase and high density solution… But the "ideal" device does not exist yet. However, different types of memories have been invented in order to pursuit these specific properties [43,44]. Example of this attempt is the eSTM (Embedded Select Trench Memory) which is represented in Figure I-11. This memory has been presented by STMicroelectronics in 2012 [53,54].

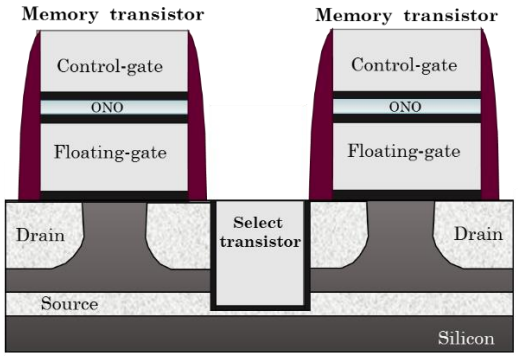

Figure I-11. Schematic of eSTM structure.

The eSTM aims to have the advantages of consumption and isolation from the EEPROM, due to its select transistor, together with the advantage of the Flash by reducing its size. Based on this, two select-transistors have been merged into a single vertical transistor of selection.

Thanks to this, it is possible to convert a large cell (2T) as the EEPROM, into a new cell, smaller in size and still with low consumption, at the expense of a slightly more complex manufacturing process but still compatible with a CMOS technology. The properties of EEPROM, Flash and eSTM memories are compared below in Table I-3.

Table I-3. EEPROM, Flash and eSTM properties.

	EEPROM	FLASH	eSTM
Low Consumption	x		x
Fully-Bit alterable	x		x
High Density		x	x
Fast Write/Erase		x	x

The main characteristics of this new structure are:

- A vertical transistor, used as the selection transistor.
- The Niso, serving to isolate transistors to the substrate, is also used in the eSTM as a source line to win a contact.
- Two floating gate transistors, with a length of 100 nm, presented on either side of the selection transistor separated by an N^+ implant.
- The trench where the select-transistor will be placed consist of 450nm of depth (corresponding to the Niso) and 150 nm of width.

In this thesis, two different trenches have been studied. Chapter III and Chapter IV are related to the characterization and optimization of the eSTM trench process; Chapter V will be focused on the STI trench. Details of those fabrication processes will be explained in their respective chapters, but first it is important to present the basic steps of the fabrication processes in CMOS technology that all these structures follow.

2.2. Fabrication Processes

Integrated-circuits are now fabricated industrially by using wafers. Wafers are thin circular slices, usually of monocrystalline silicon. On each wafer hundreds or thousands of individual chips are fabricated, as represented in Figure I-12. Technically, each of these individual chips is called die, and each die might represent an Integrated Circuit (IC) [55]. For economic reasons, the size of the wafer increases gradually on the semiconductor manufacturing industries, up to 300mm today. Due to the size of the devices on the IC, it is essential to work in a very-clean environment, the so-called *clean room*, keeping temperature and humidity under control in order to prevent the contamination that could damage the functionality of the circuit.

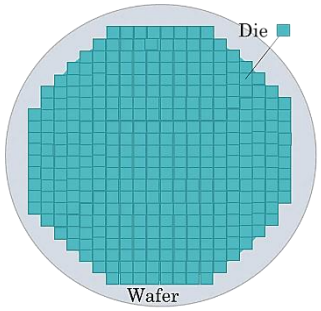

Figure I-12. Representative drawing of a die.

Complex technologies might have more than 40 layers, which implies more than 400 successive process steps. These steps can be segmented into different families [19,56,57,58].

- **Epitaxial growth.** It consists in growing a crystal of a material onto another material.
- **Ion Implantation or Doping.** To introduce chemical elements in the substratum material in order to obtain the right electrical properties (i.e., specific regions with positive or negative charge).
- **Thermal treatment.** By increasing the temperature of a substrate under controlled atmosphere in order to change its properties.
- **Deposition.** Thin films of different materials are deposited on the wafer through several processes, such as: Chemical Vapor Deposition (CVD), Physical Vapor Deposition (PVD), Plasma Enhanced Chemical Vapor Deposition (PECVD) and Metallization.
- **Lithography.** It is used to add patterns on the wafer. First, the wafer is coated with a film of photosensitive polymer. Then, the pattern is transferred from a photo mask onto the photosensitive polymer by projecting light through the mask and exposing the wafer using ultraviolet light. Finally, the polymerized sections of photoresist material are removed from the wafer to develop the pattern.
- **Etching.** With the etch processes, the areas defined by the patterns can be removed. Etching can be wet or dry. In wet etching, liquids are used such as acids, bases and solvents to chemically remove wafer surface material. In dry etching or plasma etching, the wafer surface is exposed to a plasma. Plasma etching is the most common etch process and since it is the object of study in thesis, details about this step will be developed in 3.
- **Planarization of the surface.** In order to achieve a flat layer, the wafer surface is polished. This is critical for the follow-on process steps (e.g. better linewidth control during photolithography) and can serve to increase device yields by removing

undesirable foreign material on the wafer surface. Usually by Chemical-Mechanical Polishing (CMP).

- **Cleaning.** It consists in removing any residue from the material surface.

There are two classes of processing steps in the manufacture of an integrated circuit: those concerning the implementation of active devices, the so-called "Front End of Line" (FEOL) and those related to the achievement of interconnections between these devices to get the expected logic function, known as "Back End of Line" (BEOL). Details about the FEOL and BEOL are introduced in the next sections.

2.2.1. Front End of Line (FEOL)

This thesis focuses on the FEOL. Therefore, we introduce the different processes performed during the wafer fabrication, which is characterized by its complexity and highly expensive processes. In order to design MOS transistors various successive steps are performed such as [29]:

- **Starting material**, called “substrate” or “well”. Consists of the selection of the type of wafer to be used, the CMP and cleaning of the wafer.
- **Shallow Trench Isolation (STI) module.** Creation of regions of dielectrics between regions of active areas. The regions of dielectrics, called STI, are not very deep trenches filled with SiO_2 in order to electrically isolate the transistors from each other.
- **Well module.** The “wells” are formed by creating n-type or p-type by means of implantation of Phosphorus (P) or Boron (B). The non-implanted areas are protected by a photoresist. This will allow the opposed conduction type respect to the transistor that will be created in this area.
- **Gate module.** The formation of the gate (N- or P-channel) which is the control electrode of the transistor.
- **Source/Drain module.** The Source as the Drain will receive the implantation N for a N-MOS transistor and P for a P-MOS. The non-implanted area, as it is the case for the STI, are protected by a photo-resist. The formation of the S/D take place in two parts. First, there is a Lightly Doped Drain (LDD) implantation, as a extension of the S/D. After that, the creation of “spacers”-explained below- is carried out before the second implantation. For the second implantation, the dose is incremented and the area is limited by the spacers. Here, the S/D regions themselves are created.
- **Spacers.** Two spacers are created on either side of the gate, allowing its alignment with the source/drain during the production and the limitation of the second implantation under the gate.
- **Siliciding.** This step is performed in order to reduce the contact resistance of the gate, source and drain.

After these steps, the transistors will be obtained as represented in Figure I-13. In order to perform these transistors, all the different fabrication processes explained before (such as deposition, lithography, etch, etc) are required. Specifications related to the etching of the trench for the different technologies studied in this thesis will be introduced at the beginning of each chapter.

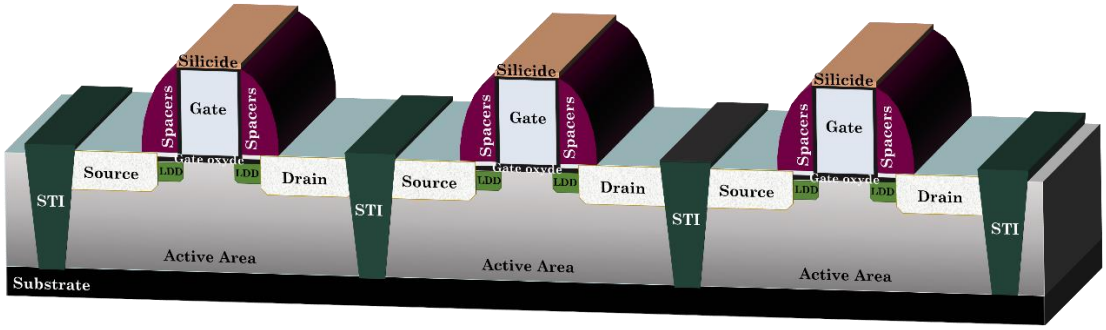

Figure I-13. Representation of MOS transistors at the end of the FEOL steps.

Major differences in the design of the FEOL are often due to the specific technology requirements.

2.2.2. Back End of Line (BEOL)

Once the various semiconductor devices have been created, they must be interconnected to form the desired electrical circuits. This occurs in a series of wafer processing steps called BEOL, which normally begins when the first layer of metal is deposited on the wafer. The BEOL will help to achieve the metal interconnections between the individual devices by creating interconnect wires, vias and dielectric structures. These interconnections are organized on several levels which are interconnected from each other by means of insulating trenches of a dielectric material. Current technologies use up to 12 levels of interconnections. Conventionally, aluminum (Al) metallization contact are used for these interconnections. However, higher performance BEOL are implemented using a Cu for the respective conducting and insulating materials, since the electrical conductivity of Cu is higher than the one of Al [58]. When the BEOL is finished, there is a “back-end process” also called “post-fab” since it is carried out not in the cleanroom.

2.3. The Role of Plasma Etching in CMOS Technology

Silicon-based CMOS technology has been the main force driving the progress of the microelectronics industry for over four decades. The remarkable decrease in design rule and increase in the number of components on an individual integrated circuit required a major change in the technology used to fabricate such circuits. By subsequent etching and deposition of patterns, the microelectronic devices like transistors and the interconnecting

lines are produced on a semiconductor substrate as it has been explained before. The main steps such as deposition, lithography and plasma etching, are sketched in Figure I-14.

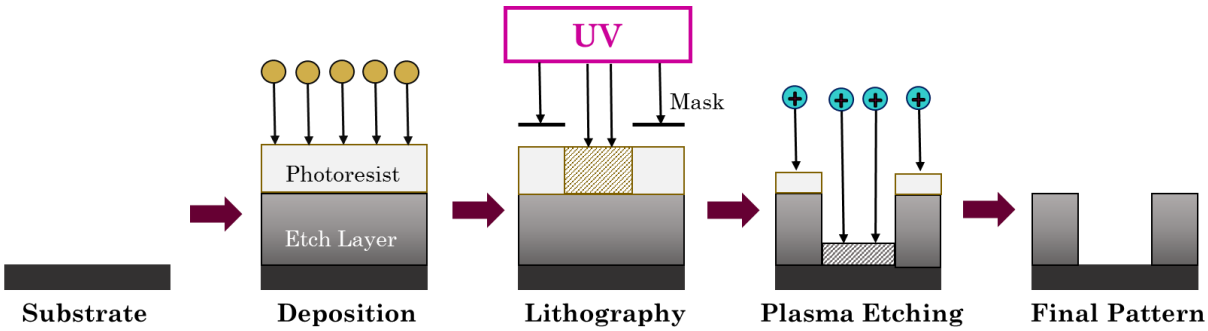

Figure I-14. Representation of the main microelectronics fabrication steps [Adapted from 59].

During the etching, the silicon is reached, as Figure 1-14 shows, this is why a good control of this process had to be developed. In the earliest days of large-scale integration, isotropic wet chemical etching was sufficient to produce the patterns required. As commercial pressures forced the industry to ever smaller design rules, the limitations of wet chemical etching became progressively less satisfactory and this is why dry etching or plasma etching became a technology essential to microelectronics circuit fabrication [60-61]. Figure I-15 illustrates the differences between wet and dry etching.

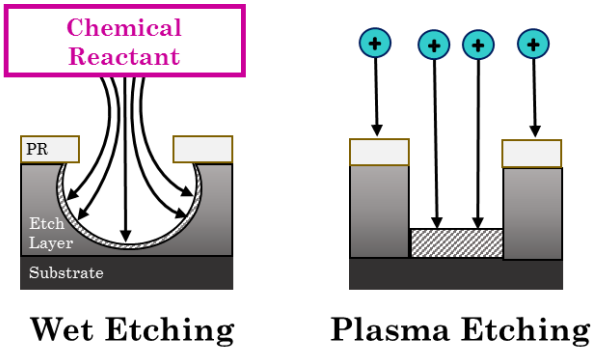

Figure I-15. Sketch of an isotropic wet etch process and an anisotropic dry etch process [Adapted from 59].

Nowadays, one of the principal challenges at the nanoscale faced by the semiconductor industry is the device fabrication [19] and the control of variations at the nanoscale [62-64]. To address this challenge, plasma etching is widely investigated [59,65,66,67]. Likewise, plasma etching is the object of this research so that an introduction to the plasma etching in microelectronic and its state-of-the-art will be presented in the next section.

3. PLASMA ETCHING

Plasma or dry etching of silicon plays a major role in semiconductor manufacturing. It consists in allowing the transfer of complex circuit patterns by photolithography to the silicon, silicon dioxide, and metals that build the integrated circuits.

3.1. Introduction

The first use of the term "Plasma" in literature is dated 1928 [68] when Irving Langmuir designates it as a partially ionized gas. More accurately, a plasma [69] is a gas containing charged and neutral species, including some or all of the following: electrons, positive ions, negative ions, atoms and molecules, that show a collective behavior. Plasma is one of the four fundamental states of matter, the other being solid, liquid and gas; but plasma has properties unlike those of the other states. Besides, it is the most abundant form of ordinary matter in the universe. The 99% is plasma such as the starts, the solar core, the aurora, etc. On earth, plasmas are used in domestic appliances like neon tubes; for energy production like fusion reactor and for surface treatments like depositing thin films and etching materials. Etching materials with plasma has become a key process for removing material from surface in CMOS manufacturing.

Much of the understanding of plasmas has come from the pursuit of controlled plasma etching processes for CMOS technology, where the plasma generation [70] requires the application of strong Radio Frequency (RF), under vacuum conditions. The main advantage of using dry etching against wet etching relies on the possibility that plasma etching offers of anisotropic etching (Figure I-15), which is highly preferable for smaller feature dimensions. Furthermore, anisotropic etching has the ability to etch with finer resolution and higher aspect ratio than isotropic etching. So, by the late 1970s, the microelectronics industry drives the transition from wet etching to plasma etching, and nowadays almost all the pattern-transfer processes are done by plasma etching. The possibility of anisotropic etching comes from the two approaches, physical and chemical, that this process implies. The physical part (3.3) can be accomplished by neutral, ion, electron or photon bombardment that assisted etching reactions of a surface exposed to a chemical etchant. It is anisotropic and non-selective. The chemical part (3.4) involves a chemical reaction between etchant gases to attack the silicon surface. It is spontaneous, isotropic and exhibits high selectively.

Coburn and Winters, in their classical experiment in 1979 [71] showed that plasma etching is the synergetic result of the combination between these two mechanisms; the ion bombardment and the neutral chemical reaction.

In the following sections, the main aspects of plasma etching will be discussed. The first one is about the basic properties of plasmas, since they are required for plasma etching processes. Then, the physical and chemical interactions at surfaces in contact with plasmas are discussed. Finally, the state-of-the-art in plasma etching is introduced.

3.2. Basic Plasma Properties

There are several textbooks that provide very comprehensive introductions to plasma physics [72-75]. In this section, the fundamental plasma discharge concepts which underlie the operation of plasma etching will be discussed.

To form and sustain, a plasma requires some energy source to produce the required ionization, the degree of ionization α is an important parameter of a plasma (I.1). The plasmas used in the semiconductor industry are weakly ionized plasma discharges because the degree of ionization is around 1 out of every 10,000 at most. The majority of the particles remain neutral, and only one ion and one electron exist for every 10,000 neutral particles [61]. The degree of ionization [76] of a plasma is defined as:

Degree of ionization: $$\alpha = \frac{n_i}{n_i + N_g} \quad \text{(I.1)}$$

where, n_i is the ion density (cm^{-3}), N_g is neutral species density (cm^{-3})

Therefore, if α is zero, then the gas is called neutral. However, if α = 1 then the plasma is completely ionized. The electron density (n_e) is related to this by the average charge state of the ions (Z) through (I.2.):

$$n_e = Z \cdot n_i \quad \text{(I.2)}$$

The electron density (n_e) and ion density (n_i) are substantially equal to one another, $n_i \approx n_e$, a condition commonly termed "quasi-neutrality" [77]. Because electrons are able to travel freely within the plasma, it has a conductive property. When a radiofrequency (RF) power is applied on a pair of electrodes in an etch chamber, electrons are accelerated by an electric field generated by the RF power, acquire kinetic energy, and collide with atoms and molecules to cause ionization, excitation, dissociation, etc (3.3.3). But even if in the RF electric field, the electrons are continuously accelerated, they have much smaller mass than atoms and so they can only transfer small amounts of energy in collisions. As a result, the different plasma species have different kinetic energies and thus different temperatures. This means that they are not in a thermodynamic equilibrium. Typically, one can only speak of temperature if the particles are in equilibrium between each other. However, it is possible to set a temperature for each of these species by making the approximation that the particles have an energy

distribution according to the Maxwell-Boltzmann distributions [78]. This means that there is a thermodynamic equilibrium within each specie.

Based on the relative temperatures of the electrons (T_e), ions (T_i) and the neutral gas (T_g), plasmas are classified as *thermal* or *non-thermal*. *Thermal* [79] plasmas have electrons and the heavy particles at the same temperature while that *non-thermal* [80] plasmas have the ions and neutrals at a much lower temperature (often near the ambient temperature), whereas electrons are much "hotter" (T_e>>T_g). Other definition based on the electronics temperature of a plasma (I.3), is referred to as being *hot* [81] if it is nearly fully ionized, or *cold* [82] if only a small fraction (for example 1%) of the gas molecules are ionized. In the literature, it can be also referred as *hot plasma* ($T>10^6$ K) and *cold plasma* ($T<10^6$ K). Plasmas utilized in semiconductor manufacturing are usually *cold plasmas* since only a small fraction of the gas molecules are ionized. Furthermore, for these plasmas T_e>>T_i.

Electronic temperature: $$T_e(eV) = \frac{k_B}{e} T_e(K) \quad \text{(I.3)}$$

where, k_B is the Boltzmann constant ($k_B = 1{,}38 \cdot 10^{-23}\, J.K^{-1}$)

e is the elementary charge ($e = 1{,}6 \cdot 10^{-19}\, C$)

As explained before, the electrons have much smaller mass than atoms and thereby they are much faster. Because of that, the flux to the walls of the electrons should be as well much bigger and thereby the plasma would not be neutral. To preserve its "quasi-neutrality", the plasma is protected by forming a load zone of positive space, called sheath. Due to this sheath, the plasma has higher potential (V_p) than the walls. The plasma is brought to a potential V_p>0 which will make that more electrons are retained in the plasma and more ions are accelerated to the walls. The sheath has a minimal thickness that is on the order of the Debye length (λ_D). The Debye length describes the distance over which an electrical disturbance is screened in a space charge as defined in (I.4).

Debye length: $$\lambda_D = \sqrt{\frac{\epsilon_0\, k_B\, T_e}{e^2 n_e}} \quad \text{(I.4)}$$

where, ϵ_0 is the electric permittivity of vacuum ($\epsilon_0 = 8{,}85 \cdot 10^{-12}\, A.s.V^{-1}K^{-1}$)

The main role of the sheath is to maintain the neutrality of the surface exposed to the plasma. Since the ions are attracted to the surface, they can bombard surfaces and etch the materials, and that is the principle which is used for etching processes. The result of the RF current flowing across a plasma sheath is the DC self-bias (V_{DC}). It increases with RF current and decreases with RF frequency. The DC voltage is created to repel electrons, therefore the higher the electron density and the higher the electron energy, the higher the modulus of the

DC voltage will be. The tendencies of the DC bias voltage can be predicted by modifying some plasma parameters (see 3.4.1).

3.3. Physics and Chemistry of Plasma Etching

Plasma etching uses chemistry to enhance rates and selectivity while keeping anisotropy properties of sputtering. This section deals with the basic phenomena of the plasma etching processes. An understanding of etching reactions in a plasma environment requires a knowledge of the three principal mechanisms: the chemical etching (3.3.1), the physical etching (3.3.2), and the ion-enhanced mechanism (3.3.3).

3.3.1. The chemical etching

The chemical etching involves a chemical reaction between the reactive species of the gas with the surface without ion bombardment. It is spontaneous, isotropic, exothermic and exhibits high selectively. The mechanisms of chemical etching can be divided into the four basic steps: reactive species generation, adsorption, volatile products creation and desorption. A simple example of chemical plasma etching [61,83,84,85] is Si etching using fluorine, which has a high etch rate even at room temperatures (see Figure I-16):

1. Generation. Start with inert molecular gas CF_4.
2. Adsorption. Make discharge to create reactive species:

$$CF_4^- + e^- \rightarrow CF_3 + F + e^-$$

3. Volatile products creation. Species reacts with material, yielding volatile product:

$$Si_{(solid)} + 4F_{(gas)} \rightarrow SiF_{4\,(gas)} \uparrow$$

4. Desorption. Pump away product. CF_4 does not react with Si. SiF_4 is volatile.

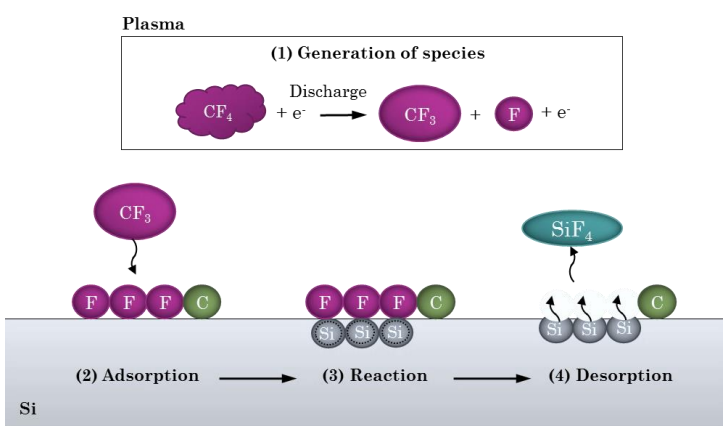

Figure I-16. Example of chemical etching process of silicon with CF_4 [Adapted from 61].

3.3.2. The physical Etching

The physical etching involves momentum from energetic ions to the surface atoms via commission cascade processes. This mechanism is non-selective, but allows directional anisotropy profiles. An example of the physical etching mechanism is shown in Figure I-17.

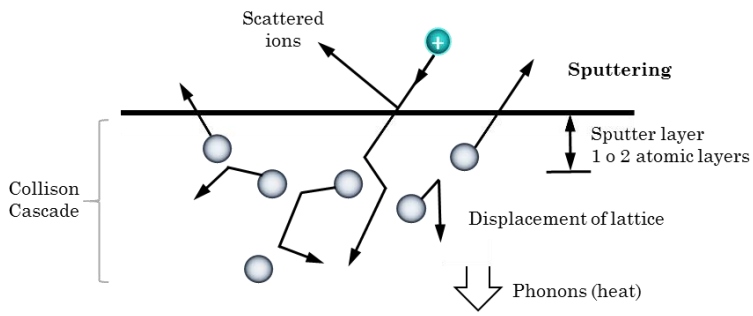

Figure I-17. Example of physical etching process [Adapted from 86].

The physical etching is also known as sputtering, this directional phenomenon that allows the anisotropy of etching profiles is the only mechanism leading directly to etching in physical etchings. This process is defined by the sputter yield Y_p (number of atoms ejected per incident ion) [86] which theoretically follows the relationship (I.5). The sputtering yield depends on the ion and target masses, the ion energy, the bonding energy of the target material and the crystal structure.

$$Y_p = A\,(\sqrt{E_i} - \sqrt{E_{th}}\,) \qquad \text{when } E_i > E_{th} \tag{I.5}$$

where, A is the proportionality factor,
E_i is the energy of the ions, and
E_{th} is the energy of the threshold.

While it is possible to remove material by a physical method such a sputtering, this is not acceptable for a process step since it is not selective and may introduce damage and impurities [87].

3.3.3. Ion-Enhanced Etching

When a surface is exposed to both chemically reactive neutral which can react with a surface to produce a volatile product and ion bombardment the combined ion and neutral fluxes often etch more rapidly than surfaces exposed to only the neutral bombardment [87].

This mechanism is a combination of both chemical and physical etching, where the reactive ions are directly involved in the chemical etching. Therefore, the kinetics of elementary steps of the chemical etching is accelerated by the presence of the ions. The typical processes that take place in the system together with the ion-enhanced etching are [70,87,88]:

1. Generation: Reactive species produced by ionization of etch gas atoms.

2. Formation of DC Bias for ion acceleration: Reactive species are transported by diffusion to the surface of the film being etched.

3. Diffusion: Diffusion of plasma-generated reactive intermediates from the bulk of the plasma to the surface of the material being etched.

4. Adsorption: Reactive species are absorbed onto the film surface.

5. Reaction: A chemical reaction occurs and volatile by-products are created.

6. Desorption: Volatile reaction by-products are desorbed from the surface.

7. Pumpout: Desorbed species are diffused into bulk of gas, and are pumped from the chamber.

A representation of this mechanism is shown in Figure I-18, including the name of each process.

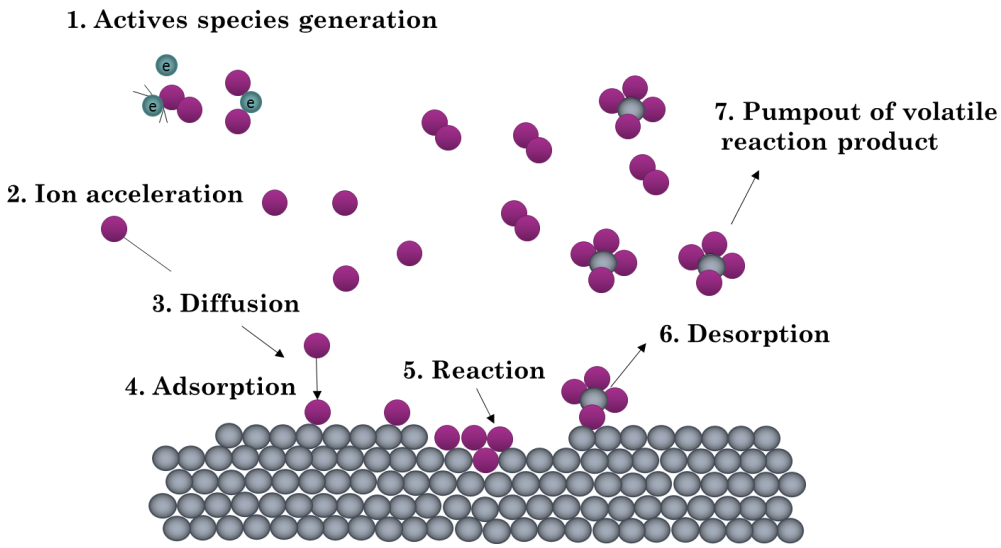

Figure I-18. Reaction steps taking place in the system during ion-enhanced etching [Adapted from 87].

This mechanism was introduced for the first time by Coburn and Winters, as mentioned before (3.1). In their classical experiment, whose results are represented in Figure I-19, the etching rate was monitored while XeF_2 and Ar^+ beams were turned on and off. It can be seen that the silicon etch rate increased by one order of magnitude when the ion beam was turned on. The etch rate of the combination of ions and chemical active species cannot be explained by the addition of the separate etch effects. This shows the importance of the ion/neutral synergy in plasma etching.

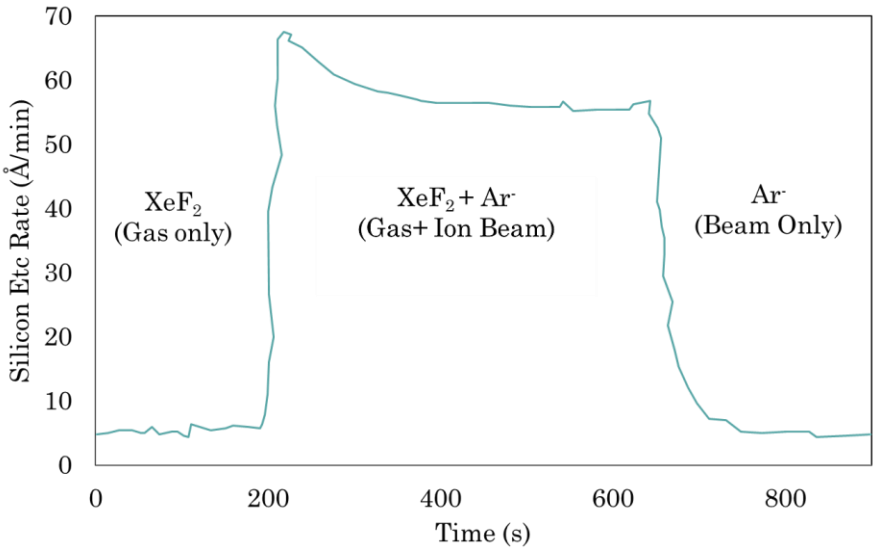

Figure I-19. Experiment showing the synergetic effect of ion-enhanced etch reactions. [Adapted from 71].

From physical to chemical processes, different etching systems can be found such as Sputter Etching, High Density Plasma Etching, Reactive Ion Etching, plasma etching and wet chemical etching [61]. In function of the selected process, the properties may change. A summary of the properties of these mechanisms is shown in Figure I-20.

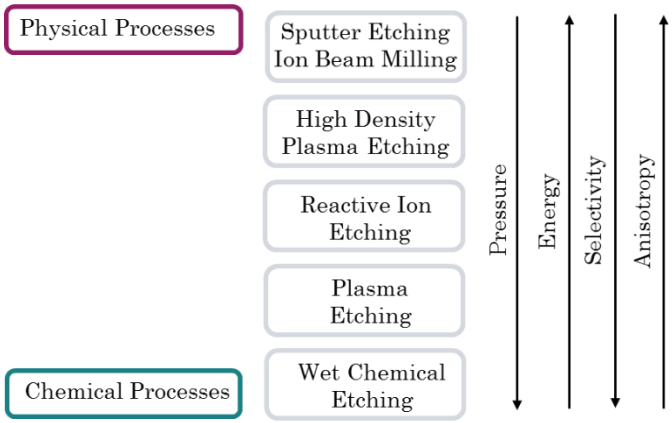

Figure I-20. Plasma etching mechanism by process.

This study is based on High Density Plasma Etching processes which take place into a Lam Research 2300 Versys, which is an improved ICP (Inductively Coupled Plasma) system. Even if this equipment will be described in Chapter II, Table I-4 summarizes some useful equations and orders of magnitude to describe a plasma.

Table I-4. useful equations and orders of magnitude to describe a plasma

Description	Definition	
Maxwellian velocity distribution function ($f(v_x)$)	$f(v_x) = \sqrt{\frac{m}{2\pi k_B T}} exp\left(-\frac{mv_x^2}{2k_B T}\right)$	(I.6)
Maxwellian electron energy distribution function ($f(E)$)	$f(E) = \frac{2}{\sqrt{\pi}} T^{-3/2}\sqrt{E} \cdot exp\left(-\frac{E}{k_B T}\right)$	(I.7)
Child-Langmuir, sheath thickness (d sheath) (if $eV_{DC} \gg k_B T_e$)	$d_{sheat} = \frac{\sqrt{2}}{3}\lambda_D \left(\frac{2eV_{DC}}{k_B T_e}\right)^{3/4}$	(I.8)
Thermal velocity ($\overline{V_e}$)	$\overline{V_e} = \sqrt{\frac{8k_B T_e}{\pi m}}$	(I.9)
Bohm velocity (U_B) [76]	$U_B = \sqrt{\frac{k_B T_e}{M_i}}$	(I.10)
Characteristic electron frequency (w_e)	$w_e = \sqrt{\frac{e^2 n_e}{\epsilon_0 m_e}}$	(I.11)
Characteristic ion frequency (w_i)	$w_i = \sqrt{\frac{q^2 n_i}{\epsilon_0 M_i}}$	(I.12)

electronic temperature **Te**~3eV [65,66] (1ev=11600K)
electron mass $\mathbf{m_e}$: $9{,}1.10^{-31}$kg
d sheath ≈ 0,74mm [65], ≈ 1mm [66]
electronic density **ne=ni**: ~10^{10} cm^{-3} [66], ~10^{11} cm^{-3} [65,66], ~10^{12}
Mi, q: ion mass and ion charge
Boltzmann constant $\boldsymbol{k_B} = 1{,}38 \cdot 10^{-23}\, J.K^{-1}$
elementary charge $\boldsymbol{e} = 1{,}6 \cdot 10^{-19}\, C$

3.4. Key Parameters in Plasma Etching

This section takes care of the main parameters involved in plasma etching processes.
The first part is dedicated to the influence of the plasma parameters (3.4.1) and the second one to the useful parameters that exist for the evaluation of the process performance (3.4.2).

3.4.1. Influence of Plasma Parameters

In general terms, the plasma etching recipe used to process a wafer in semiconductor manufacturing, can be divided into three main steps:

- The Breakthrough (BT), which starts etching the hard mask or anti-reflection layer.
- The Main Etch (ME), where profile and CD are the most two important concerns.
- The Over Etch (OE), where the most important factor is the selectivity to bottom layer.

In order to reach the goal settled down for each step some parameters involved in the process can be modified. Taking into account that the dimensions of the reactor are fixed, the DC Bias voltage can be influenced by the process parameters. As the DC voltage is created to repel electrons, therefore the higher the electron density and the higher the electron energy, the higher the modulus of the DC voltage will be. Using this reasoning, one is able to predict the tendencies of the DC bias voltage by modifying the following parameters [89]:

- **Power:** the influence of power is straightforward. An increase of power increases both the density and the energy of the free electrons. Therefore, the DC voltage becomes more negative with increasing power.

- **Pressure:** the pressure of the plasma does also influence the DC bias voltage. At higher pressure, electrons suffer more collisions, therefore they gain less energy between collisions. The electron energy decreases with pressure and the DC bias voltage becomes less negative with increasing pressure.

- **Gases and flows:** the electronegativity of used gases is a determining factor. When all other process parameters remain constant, the electronegativity of the gas will determine the DC voltage. Gases with low electronegativity, such as O_2, N_2 etc, have very negative DC bias voltages. Fluorine, chlorine and bromine containing gases are much more electronegative, thus, these gases decrease the density of the free electrons in the plasma (increasing the number of negative ions). F-plasmas are more electronegative than Cl-plasmas, which are more electronegative than Br-plasmas. The absolute flow of the gases does in general not affect the DC voltage. However, if a mixture of gases is used, the DC bias will be a monotonically increasing function of

the relative flows of the gases. On the other hand, small flows of electronegative gases do not influence the DC bias very much.

3.4.2. Parameters for Evaluating Plasma Etching Performance

High selectivity can be achieved with plasma etching; however, it is difficult to control the process. In order to verify the performance of each process some parameters should be taken into account [90-92]:

- **Etch rate:** is defined as the material thickness etched per unit time (Å/mn). It depends on the material as well as the chemistry and the etch power used. If the etch rate is too high, the process will be difficult to control.
- **Uniformity:** is the percentage variation of the etch rates across wafer. It is very important to control the uniformity within the wafer because it is very common to observe differences between the measures at the center and edge of the wafer (e.g. Figure I-21). These differences result in different electrical behaviors.

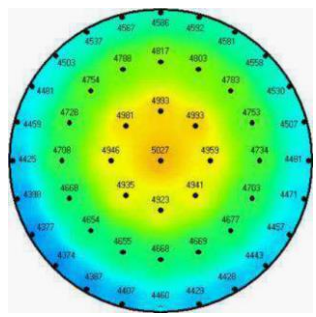

Figure I-21. Measure of uniformity [91].

- **Selectivity:** is the ratio of the etching rates of one material over the other. For example, the selectivity is the etch rate of the layer being etched to the etch rate of the mask. Etching with high selectivity is supposed to remove the selected layer entirely without harming the substrate and mask.
- **Isotropic/ Anisotropic:** etching that erodes material at a same etching rate in all directions is called Isotropic. Anisotropic etching refers to a directional etching, that means the etch rate is different in lateral and vertical direction. In plasma etching this is always perpendicular to the material and anisotropic, as explained before (See Figure I-15).
- **Microloading:** the behavior of the etching is highly dependent on the structures of the environment to be defined, this means if the structure is isolated or dense. The

concept of microloading refers to the difference in response to the process between the dense zones and the isolated areas.

- **Profiles:** the patterns obtained after etching can achieve different profiles as shown in Figure I-22. That depends on the process parameters such as chemistry, pressure, temperature, etc. It can influence the electrical behavior of the structure.

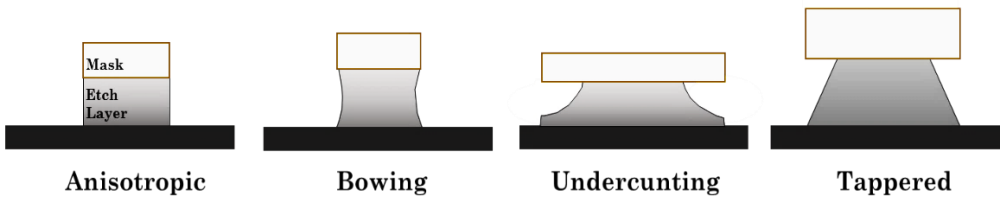

Figure 1-22. Plasma etching profiles [Adapted from 91].

- **Critical Dimensions (CD):** is the width of a pattern or the space between two patterns, as represented in Figure I-23. It is the most critical parameters of a device. The measures are performed with either CD-SEM or by scatterometry. Both of them will be explained in Chapter II.

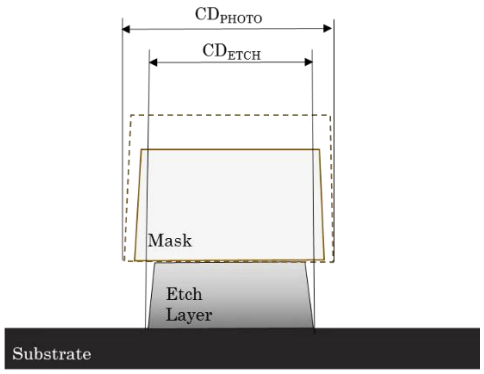

Figure 1-23. Representation of the CD post photolithography and etching [Adapted from 61].

- **CD bias:** is the difference between the CD measured after the etching, and the CD measure after the photolithography (the previous step before plasma etching). It allows to control the stability of the etching step regardless of photolithography. Is given by (1.13):

$$CD_{BIAS} = CD_{ETCH} - CD_{PHOTO} \tag{1.13}$$

3.5. State-of-the-art in Plasma Etching

Since the introduction of plasma etching processes into semiconductor manufacturing in the late 1960's and early 1970's [93,94], it should now be obvious that plasma etching is an incredibly complex technique and it takes some time before one is familiar with it. Although there was some discussion of profile control at the beginning, it was not until mid-1970's that plasma etching was able to eliminate the undercutting in the etching process [93].

At the beginning, most of the plasma etching work involved the use of halocarbon fedgases, being CF_4 the most common. An important paper, describing a method for etching SiO_2 selectively to Si by using a fluorine-deficient (polymerizing) chemistry, revolutionized the processes. For the first time, the *sidewall passivation* term was introduced. Fluorinated chemistries were known for having tendency to etch isotopically so that sidewall passivation was required in order to maintain an acceptable profile. Using the deposition of polymers as a passivation layer, the profile and selectivity could be controlled. There are two possible mechanisms for the formation of this passivation; by chemical reactions or by physical sputtering [94]. Chemical analysis using spectroscopy techniques are commonly used for revealing the composition of the passivation layer.

In the late 1970's some important etching studies were initiated. These studies confirmed the importance of the synergy between ion bombardment and the chemistry reactions during the plasma etching [71]. An important development of plasma etching equipment started by this time. The first method used for increasing the plasma density in single-wafer dry etching equipment was the magnetron RIE. This method had little margins in terms of wafer charging resulting from non-uniform plasma. Near the end of the 1980's system using inductively powered sources to generate higher density plasmas were successfully introduced. It was in 1985 that Hitachi commercialized the ECR plasma etching. The ECR etcher required a large magnetic coil to form a strong magnetic field, which made it difficult to have a compact etch chamber. The need for addressing this issue led to the development of the ICP. With a simple coil placed on top of the etch chamber it was possible to generate a high-density plasma by electromagnetic induction [61,95,96].

An important example of an ICP etcher was the transformer coupled plasma (TCP®) etcher launched by Lam Research in 1992 [93,95]. In this equipment, a DC_{BIAS} is created by applying RF power to the bottom electrode, then, the controllable DC_{BIAS} directs the ions normal to the wafer surface and therefore there is very little interaction between the top and the bottom electrical fields. The high energy efficiency creates a high density plasma where both ion energy and directionality are controlled by the power applied to the lower electrode [97]. Since this equipment is used for the development of this study, further information can be found in Chapter II.

The reactor walls can play important roles in the etching process, even if the plasma potential is low enough to eliminate wall sputtering as a source of contaminants [93]. The species of the plasma which diffuse away and interact with the reactor walls are not always susceptible to be cleaned. For instance, F-based chemistries are known for leaving contamination on the chamber, such as AlF_x, YF_x, etc, which have been widely investigated [66,67,98,99] but still highly difficult to eliminate. This is an important problem, not only because of the health of the equipment, but also because the surface of the reactor walls changing over time it might alter the plasma and the wafer surface by deposition of non-desired species over the wafer. Under these conditions, the reproducibility of the etching processes cannot be guaranteed. Several studies [65-67,99-102] have been carried out related to this subject. In Chapter IV, a deeper state-of-the-art related to this subject will be presented together with our results.

Nowadays, engineers are still looking for the most suitable process control of plasma etching in order to reach good reproducibility [62,103,104]. Because of the smaller dimensions this is still a big challenge, even more since any process variation can cause considerable fluctuation of the performance and the failure of the chip. For this reason, the control of the dispersion of the CD in plasma etching step is essential since it is extremely correlated to the electrical parameters of the transistor [105-108]. It is here, when process engineers need statistical tools. As we will see in Chapter V, in an industrial environment as STMicroelectronics, this control of the dimensions is pretty important in order to set regulation methods in place.

Due to the reduction of the dimensions, the high number of new materials introduced and the complexity of the process itself, plasma etching is still regarded as one of the most critical steps in IC manufacturing and this is why the research on this area it has not diminished.

4. OBJECTIVES

The **initial objective** of this thesis is to characterize and optimize the plasma etching process related to the new architecture developed in 2012 by STMicroelectronics, the eSTM. This structure has already been introduced (Figure 1-11). This would help for the enhancement and increase of our knowledge on the physical phenomena which happen during this process, which was not fully understood yet, especially the passivation during the etching of the vertical transistor. This would offer the possibility to optimize the etch process and get the best CD in terms of electrical results. The emphasis must be put on the characterization in order to get the maximum knowledge about the interactions taking place during the process inside the reactor walls, such as plasma-surface interactions and plasma-reactor wall interactions. Because plenty of new materials are introduced in semiconductor manufacturing, the study of the a-C:H (used as a mask for etching silicon during this study) has to be studied too, since it could influence the composition of the passivation layer.

Since the interactions between the plasma and the walls of reactors are responsible for a lack of reproducibility of the etching processes, this study also aims at the understanding of the cleaning of the reactor walls. As introduced in (3.5) the problem of the Fluorine has been shown in the reactor that is used for this study. As a new technology still in development, the study of the plasma-reactor wall interactions occurring in the case of the eSTM trench process was required.

The **second objective** of this thesis is to investigate the process drifts that occur during the first trench etching (STI), since the reproducibility of production processes generates serious concerns in making the component of the chips. Moreover, the reproducibility of the STI is critical for the following steps. As the eSTM is still in development stage, no-data about the drifts of this technology could be obtained yet. However, the first part -that one related to the STI/active- of the eSTM process fabrication is practically the same as the flash. Thus, the idea was to develop a model able to get the CD of the STI (flash) under control and based on that, set a similar model to control the STI of the eSTM technology. In this way, we will anticipate that everything is ready for switching to a production-mode when the day arrives.

"No amount of experimentation can prove me right; a single experiment can prove me wrong" (A. Einstein)

Chapter II

Experimental: Materials and Equipment

This chapter presents the main experimental techniques for the characterization of the plasma etching processes used in this work. It contains information about the tools, materials and characterization techniques. The plasma etching equipment and the plasma diagnostics techniques are introduced as well as the surface analysis characterization techniques, paying special attention to XPS characterization of thin films. Finally, the *Floating Sample Method* used to characterize the reactor walls will be introduced too.

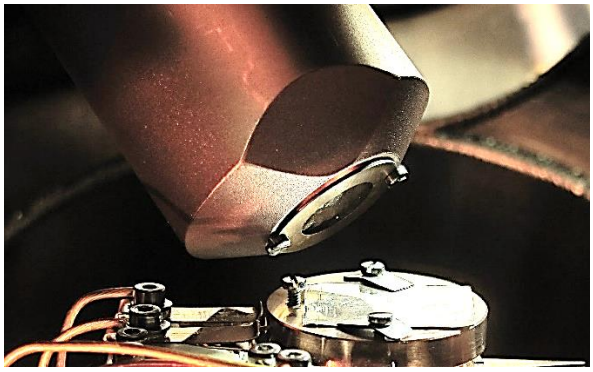

An inside view of an old-type XPS system [II].

All the experiments are carried out in a plasma reactor suited for 200mm wafer in STMicroelectronics Rousset. In addition, several diagnostic techniques are used to study the plasma-surface and the plasma-reactor wall interactions. Furthermore, since the use of different materials influences these interactions, the basic concepts of each tool and materials used will be discussed in this chapter.

1. MATERIALS

As dimensions decrease, extreme-UV photoresists are required. Photoresists as 193nm with low selectivity, demand a thick layer of *stack* to be used for successful pattern transfer [109]. In order to satisfy the continual need for shrinking CD, this *stack* changes for each technology depending on which are the most suitable materials and thicknesses. The different materials used as *stack* in this study are described below.

1.1. Stack

A classical semiconductor *stack* comprises a substrate, a semiconductor layer and a mask. For the work presented in the following chapters, the *stack* could be compound of a Photoresist, BARC, a-C:H, TEOS, NFARL, Nitride, SiO_2, the semiconductor layer and the substrate. In Chapter I we already introduced the properties of Silicon and SiO_2. Here, the properties of the rest of materials are briefly described.

- **Photoresist (PR).** A photoresist is a light-sensitive material used in the photolithography process to form a patterned coating on the surface to be etched. The PR are usually classified by their wavelengths in the UV spectrum. The PR used in this study is for 193nm lithography which have lower selectivity and a poor mechanical strength when compared to 248nm PR [109]. For this reason, a thick mask is needed. The PR can be positive (the exposed portion will be removed during development) or negative (the exposed portion will be retained during development). The resins used at STMicroelectronics are all positive. Their nature may vary; thickness, indices and viscosities are some of the parameters which have to be considered for reaching different critical dimensions.

- **Bottom Anti-Reflective Coating (BARC).** The BARC is an organic anti-reflective film applied before the PR in order to absorb light. It uses destructive interference to give little reflection at the PR/BARC interface. The main property of this material is to have a low coefficient of reflection. It prevents chemical interaction between the PR and the substrate and increases the CD control. In the absence of this layer, the light

used to react with the PR can expose an area of the PR intended to be masked being the cause of a CD variation. It can also increase depth of focus and reduce reflective notching [110]. This layer is also deposited by the photolitography workshop.

- **Hydrogenated Amorphous Carbon (a-C:H).** Also known as Ashable Hard Mask (AHM), is a diamond-like carbon film [111,112], hard, amorphous and with a significant fraction of sp^3-hybridized carbon atoms which contains a significant amount of hydrogen [111]. This material will serve as a mask for etching once the resin has been consumed. Typically, a-C:H films can be deposited by CVD, PECVD and ion beam deposition [112]. Depending on the processing technology used and the conditions of the process, the relative concentration of the film differs, but it can be characterized through the ratio of sp^2 to sp^3 hybridized bonds present in the material. In STMicroelectronics, a-C:H films are deposited by CVD and can be characterized experimentally comparing to the relative intensities of its spectroscopic peaks. Characterization of the a-C:H layer will be discussed in Chapter III.

- **Tetraethylorthosilicate (TEOS).** Prepared by alcoholysis of silicon tetrachloride is a tetrahedral molecule used as a precursor to silicon dioxide [113]. Note that the silicon oxide layer deposited by this technique is generally called TEOS, which is wrong from a chemical point of view [114]. Unlike the AHM which is a carbon-based mask, TEOS is an oxide-based material but it is also used as a hard-mask. Since it is an oxide, it will not disappear during the *strip* process that will be done at the end of the etching.

- **Nitrogen-Free Anti-Reflective Layer (NFARL).** It is a silicon-rich oxide with high etch selectivity to the a-C:H. Optical properties and etch characteristics of AHM and NFARL films make them well suited for integration into a spacer double patterning flow [115]. This is another anti-reflective layer but unlike the BARC; the NFARL material will tend to maintain a constant thickness regardless of the relief of the layer below. This is why it says to be *planarizing* and will tend to reduce inequalities of the relief.

- **Nitride.** Silicon nitride (Si_3N_4) is an amorphous material, similar to SiO_2 films, widely used as an oxide barrier in VLSI fabrication. It is usually used as an etch hard mask in STI applications [116]. Because of the thermal mismatch between silicon and Si_3N_4, silicon nitride is deposited onto Si with a thin oxide buffer layer, called *path oxide,* in order to prevent stress-induced damage at the interface at elevated temperature [58]. This is the last layer of hard-mask while etching the STI. Its main

function is to serve as a barrier layer during the polishing that will be carried out after etching by the CMP workshop. To take it out, wet etching using H_3PO_4 will be required.

The use of these materials is different for each goal and so the *stack* varies each time. The *stack* used for each case will be described in its respective chapter.

1.2. Photolithography Mask

The reticle used for this study was initially designed to conduct XPS studies at the STMicroelectronics site in Crolles. Figure II-1 shows the description of this mask, with the areas used for the characterization in this thesis. This is a reticle for 193nm photolithography.

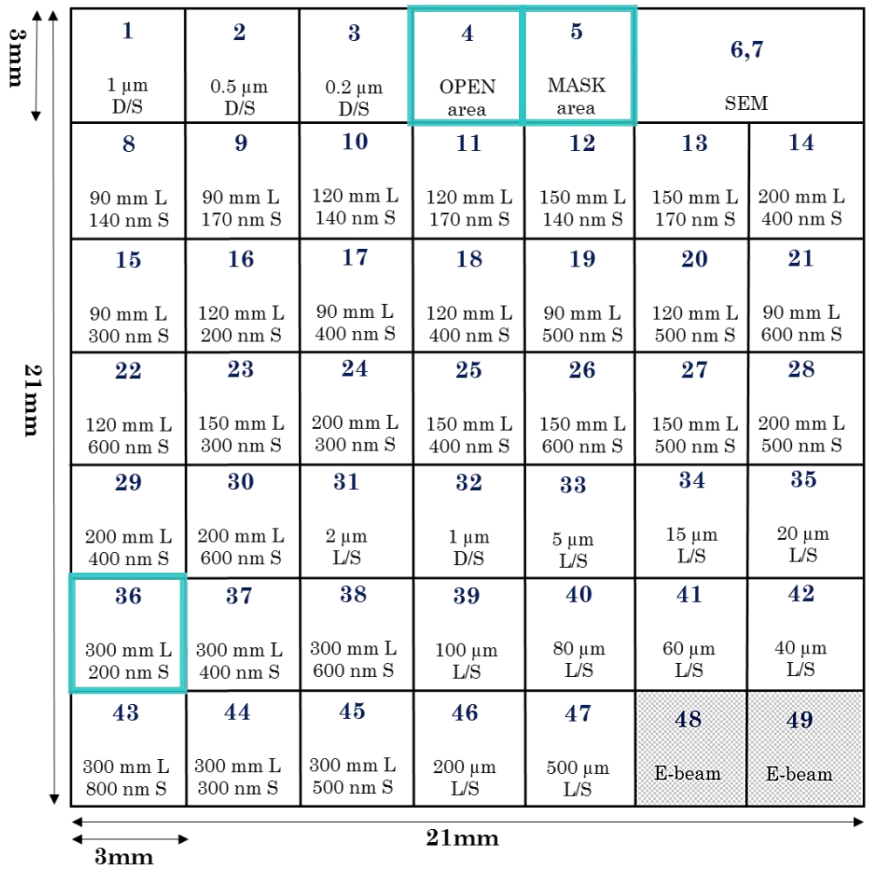

Figure II-1. Reticle mask for photolithography UV 193 nm used in this study.

The structures of the eSTM developed by STMicroelectronics, whose dimensions are 40x160 µm², are not adapted to carry out the first characterizations by XPS or TOF-SIMS with a high sensitivity. A prior analysis is necessary to determine the chemical composition of the passivation layer formed on the surfaces. Therefore, different sized structures, defined by a

lithographic mask specially designed for a similar study carried out in Crolles, are used as a first stage of the study presented in Chapter III. The advantage of this mask is that it has a plurality of width structures and different spaces such as the open area, the mask area and some others with shapes large enough to be characterized by using XPS and ARXPS. The reticle is made by 47 zones of approximately 3 x 3 mm² involving different-sized structures and a SEM observation area 3 × 6 mm². The characterization analysis is done through the zone numbers selected in Figure II-1 being the zones 4, 5 and 36. These areas are detailed in the following section 1.2.1. The dimensions of each of the zones being 3x3 mm² make XPS analysis able to be performed with a maximum probe size in order to obtain excellent detection sensitivity. This will be a first approach on the analysis that will be finally carried out over the real product.

1.2.1. Areas of Study

For the characterization of the eSTM structure, that will be discussed in Chapter III, we will talk about two steps; the one related to the etching of the **STI trench**, and the other one related to the **eSTM trench etch**. Further details about that will be given in Chapter III. A brief introduction of each area of the mask presented in Figure II-1 are presented as follows.

- **Area n°4:**

It is called "open area". It will be the “Silicon reference” for this study. It is not covered by chrome and so during the photolithography step, the resist is irradiated by the UV rays. Thus, the present resin on the silicon wafer is subjected to chemical modifications and after the development of the resin, it is removed from this area. This means that after the etching step, the area n°4 is completely composed of silicon, since the AHM will be totally consumed during the STI step. Area n°4 is therefore used as reference, allowing the characterization of the chemical composition of the silicon surface after each of the two etching steps (STI and trench). This chemistry will be later compared with the chemical compositions of the bottom trench (a priori silicon) of areas n°36 and n°46. Figure II-2 is a representation of the development of the stack from the start to the end of the etching step related to this area.

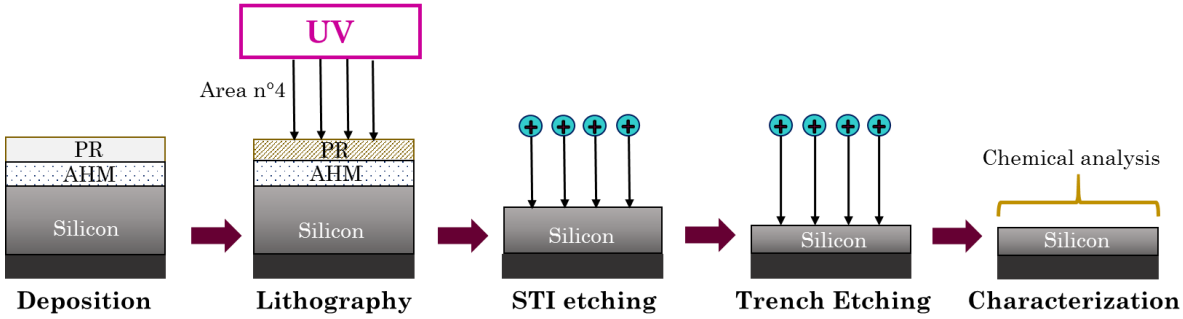

Figure II-2. Representation of the process of the ***Area n°4*** being totally exposed to the photolithography UV and resulting in the etching of a non-protected silicon.

- **Area n°5:**

It is called "mask area" ". It will be the "*Line*-reference" for this study. Unlike the "open area", the area n°5 is completely covered by chrome during the photolithography step, thus the resin is not irradiated by the UV rays, which does not cause chemical modification and so during the development of the resin, it remains on the original stack. As represented in Figure II-3, during the STI etching step, the resin is completely etched first, inducing a first contact to the AHM which will be partially consumed at the end of this step. During the trench etching, a part of the AHM will be consumed, but still remaining after the etch process. This is why area n°5 will be used as a reference for the *lines* (a priori AHM-based).

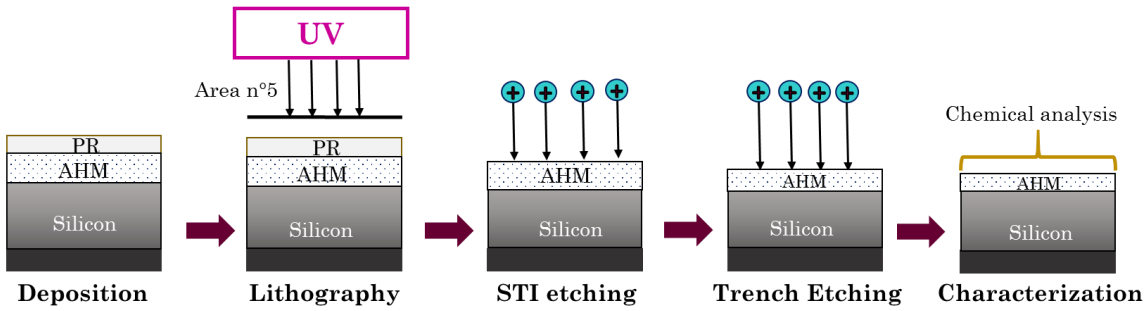

Figure II-3. Representation of the process of the ***Area n°5*** being totally covered by the mask during the UV photolithography and resulting in the etching of the AHM without reaching the silicon.

- **Area n°36:**

This area of the mask, contains alternating lines and spaces. The widths of the lines and spaces in this area are those closest to the eSTM dimensions with *lines* of 300nm and *spaces* of 200nm. It is on this area that we will achieve the XPS analyses to characterize the chemical composition of the passivation layer formed on the bottom and the sidewalls of the trenches created in the two etching processes that will be used as input for the real product characterization. Figure II-4 is a representation of the development of the stack from the start to the end of the etching step related to this area, with a final representation of the sample that will be characterized in Chapter III.

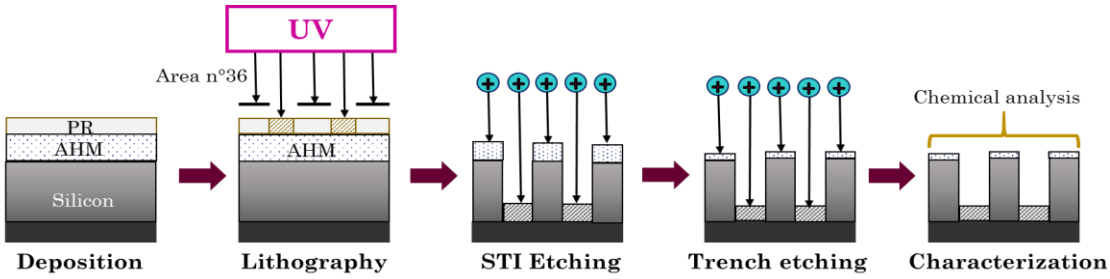

Figure II-4. Representation of the process of the ***Area n°36*** which lines and spaces does not measure the same being ***L=300nm S=200nm***.

2. PLASMA ETCH EQUIPMENT

Plasma etch equipment in STMicroelectronics are available from Lam Research. The experiments carried out in this PhD are done in a Lam Versys 2300 etch chamber designed for 200mm wafers system for sub-90 nm applications. Further details of this equipment are presented in 2.1.1. The equipment is available for both production and research experiments. The wafer handling and processing is controlled by software. In addition, this platform includes a new EPD (EndPoint Detection) system that will be introduced in 3.1.

2.1. The Etch Platform

With the aim of reducing cost and accelerate the process, the etching chambers are grouped on a platform composed of multiple chambers that contains the following parts (see Figure II-5)

- **Load lock**: in each *load lock* a cassette of 25 silicon wafers can be loaded, up to 3 *load locks* per equipment. Each cassette of 25 wafers will be called "*lot*" in this thesis.

- **Transfer robot:** a robot arm which recovers the wafers present on the loading ports to be etched.

- **Aligned system:** equipped with a laser that locates the notch of the silicon wafers that defines the orientation of the crystals so that they are always introduced into the etching chambers with the same orientation.

- **Two vacuum load locks:** the wafers are introduced before entering into the transfer chamber. Here, they are brought from atmospheric pressure to a vacuum pressure of about 90mTorr.

- **Vacuum transfer robot:** a robot arm which transfers wafers between the etch chambers and vacuum load lock. The wafer remained there briefly before being introduced into the appropriate etching chamber.

- **Chambers:** 3 chambers for the polysilicon etching processes and one more used for stripping, which removes resin used for masking during the etching.

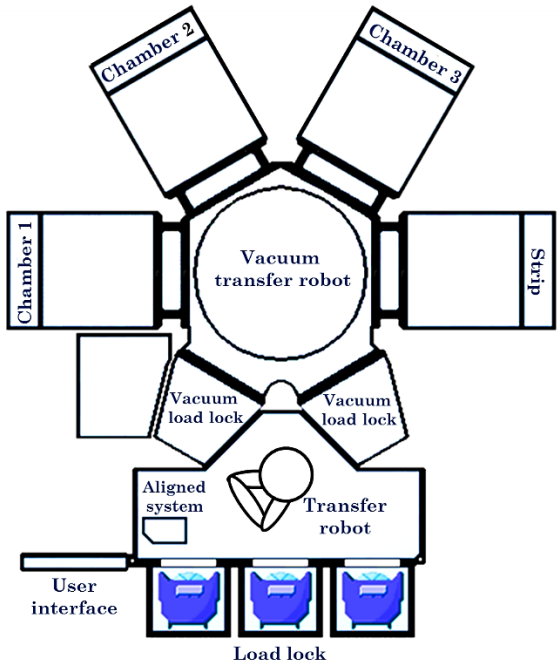

Figure II-5. Schematic representation of the LAM Versys etching platform.

2.1.1. Lam Versys 2300 Etch Chamber

The Versys 2300 etch chamber is a high density Transformer Coupled Plasma (TCP) source as we introduced in Chapter I. Based on the ICP source, Lam Research launched this equipment [93,95] where the plasma is generated by a planar ring shaped coil with multiple windings just like in a transformer [65]. This design is able to deliver a much higher plasma density compared to a standard chamber design. A schematic drawing of the etch chamber is given in Figure II-6.

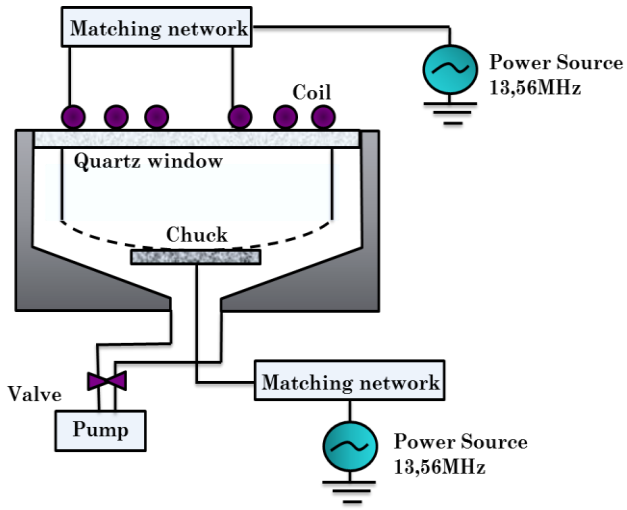

Figure II-6. Schematic representation of the etching platform LAM Versys [Adapted from 65].

As explained in Chapter I, the high energy efficiency creates a high density plasma where both ion energy and directionality are controlled by the power applied to the lower electrode [97]. Nowadays, this configuration is widely used, especially for highly selective processes where good anisotropy is required [65]. A capacitive couple source does not generate a high density plasma because a lot of power is used to accelerate ions (low density, high energy) unlike in a purely inductive coupled plasma where ions have little energy as most of the power is used for ionization (high density, low energy). In this TCP configuration, capacitive as inductive, the power is supplemented with a capacitive coupled RF source to control the ion energy. The biggest advantage is that the separation of RF coupling provides the opportunity of controlling the ion current (inductive TCP) independently of the control of ion energy (capacitive bias). In these capacitive tools the power is often delivered with multiple frequencies, allowing some independent control of ion density and energy. The different properties of the inductive coupling used in conductor etching are detailed below:

- High fractional ionization 10^{-3}-10^{-1} %.
- Low pressure from 1 to 80mTorr; High flow turbo pump.
- Requires high inductance between coil and plasma.
- Need some capacitive power to control energy (requires 2RF generators).
- Generates large RF current but low power is used for ion acceleration.
- Fine control of ion density and energy (useful for conductor etching).
- High plasma density 10^{11}-10^{13}/cm^3 → High fractional dissociation.
- Chamber wall collisions dominated → Sensitive to wall conditions.
- Without bias power field lines do not cross any sheath → No ion acceleration.

2.1.2. Process Etch and Chamber Conditioning

In this section, some important concepts for the plasma etching processes are presented such as the plasma recipe, the steps with variable time during etching processes and the chamber conditioning.

2.1.2.1. Example of a Plasma Etching Recipe

In Chapter I we divided a recipe into 3 steps: the BreakThrough (BT), the Main Etch (ME) and the Over Etch (OE). However, recipes are more complex than this due to the large number of steps that it contains. In order to understand how a recipe looks like, a simplified example is presented. Figure II-7 shows the representative diagram of the stack of material to be etched during the recipe and Figure II-8 presents the recipe itself.

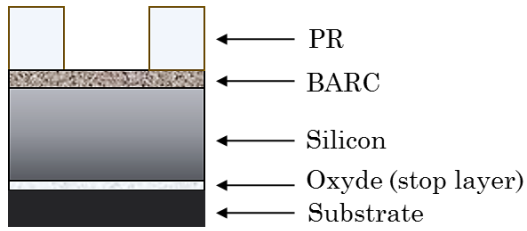

Figure II-7. Representation of the stack to be etched.

1	Parameter	1	2	3	4	5	6	7	8	9	10	11	12	13	14
2	Step description	STBL	EDP_BARC	STBL	BT	STBL	ME1	STBL	ME2	STBL	OE	Dechuck 1	Dechuck 2	Dechuck 3	Pins-Up
3	Pressure (mTorr)	10	5	10	5	9	9	11	11	60	60	5	5	5	5
4	TCP RF Power (w)	0	470	0	430	0	580	0	685	0	430	0	400	0	0
5	Bias RF Voltage (V)	0	350	0	315	0	170	0	180	0	120	0	0	0	0
6	Gas injection ratio	Equal	Equal	Equal	Equal	Equal	Equal	Equal	Equal	Equal	Equal	Center	Center	Center	Center
7	Cl2_150 (200.0sccm)	0	0	0	0	50	50	25	25	40	40	0	0	0	0
8	HBr_100 (98.0sccm)	75	75	0	0	0	0	0	0	0	0	0	0	0	0
9	HBr_100O (980.0sccm)	0	0	0	0	150	150	145	145	200	200	0	0	0	0
10	CF4_200 (199.0sccm)	0	0	100	100	0	0	0	0	0	0	0	0	0	0
11	He_500 (500.0sccm)	0	0	0	0	0	0	0	0	150	150	0	0	0	0
12	O2_20 (20.0sccm)	8.5	8.5	0	0	0	0	2.5	2.6	0	0	0	0	0	0
13	O2_20O (200.0sccm)	0	0	0	0	0	0	0	0	0	0	180	180	180	180
14	CH2F2_100 (100.0sccm)	25	25	0	0	17	17	0	0	0	0	0	0	0	0
15	Helium (torr)	8	8	8	8	8	8	8	8	8	8	0	0	0	0
16	Inner ESC Temp (degC)	62	62	62	62	62	62	62	62	62	62	60	60	60	60
17	Outner ESC Temp (degC)	56	56	56	56	56	56	56	56	56	56	60	60	60	60
18	Step type	Stab	EndPT	Stab	Time	Stab	EndPT	Stab	EndPT	Stab	Time	Time	Time	Dechuck	Time
19	Process Time (sec)	30	55	30	17	30	25	30	25	30	35	12	8	50	2
20	OverEtch (%)	0	0	0	0	0	0	0	0	0	0	0	0	0	0
21	Minimum Endpoint Time (sec)	0	20	0	0	0	0	0	0	0	0	0	0	0	0

Figure II-8. Recipe example for etching the stack presented before (Figure II-7).

The rows represent the process parameters and the columns correspond to the different steps of the process which are carried out one after the other. The process parameters are composed of:

- **Row 1, 2**: the numbers and names of the steps.
- **Row 3**: the desired pressure in the chamber for each step (in mTorr).
- **Rows 4, 5:** the RF power applied to the upper electrode (W) and the voltage between the two electrodes (V); respectively.
- **Row 6:** the injection mode of the gas in the chamber. It is possible to choose between "Equal", "Center" and "Edge".
- **Rows 7 to 14:** the different rates of gas to be sent to the chamber, in cm^3/min (or *sccm*). The theoretical maximum and the maximum measured flows are also indicated (for instance the row *"HBr_100 (98.0 sccm)"* the theoretical maximum flow is 100sccm, and the maximum measured flow is 98sccm).
- **Row 15:** Helium is sent under the wafer throughout the process in order to maintain it cool. This row corresponds to the set pressure of helium under the wafer (in Torr).
- **Rows 16 to 17:** the temperature of the ESC at the center (Inner) and edge (Outer) of the wafer (in ° C).
- **Row 18:** the type of step (five possible choices):

- Stab: in these stabilizing steps, the gas is sent to the chamber. But during these steps the plasma is not turned on (because there is no RF power), so there is not etching yet. The step ends when the required pressure, flow and temperature are reached. The time written as "Process Time"(row 19) is the maximum time allowed to achieve these instructions (usually 30 seconds). If after that time, the conditions are not achieved, the process will stop and an alert will be displayed on the machine. It is also possible to set a minimum time for the detection of the end of etching (row 21).
- Time**:** these are the classic steps of etching (with "fixed time"). The etching is carried out during the time indicated on row 19.
- EndPT: these are the steps to be etched with endpoints. The machine will perceive itself (by means of optical and interferometric systems) that it must stop the current etching and go to the next step. If the endpoint is not detected before the time indicated in row 19, the machine switches to *abort*.
- OverEtch: These are the "over-etching" steps, placed after the endpoints. They allow to continue etching after the endpoint detection (for instance, for the elimination of possible waste). The time of this OverEtch corresponds to a percentage of the endpoint time. The percentage is fixed in the line called "*OverEtch (%)*". If this line is not filled, the time will be the one written in row19.
- DeChuck: this step is the end of the process. It is the step when the wafer will be detached to be returned to the fout. The time specified in row 19 is the maximum time allowed for dechuck.

The order of the steps corresponds to the stack by layers. In this example (Figure II-8):

- The first layer to be etched is the BARC. The first two steps of the recipe are the stabilizing and etching steps of BARC.
- The next step is the Breakthrough (*BT*), which allows to pass through the eventual native oxide who was able to grow on the Polysilicon (since the Polysilicon etch chemistry is selective to the oxide).
- The etching of Polysilicon is then divided into three steps increasingly selective to oxide: ME1 and ME2 (for Main Etch) and OverEtch (OE). This sequence keeps the no degradation of the barrier layer while maintaining a relatively short time of process.
- Finally, the steps of *Dechuck* and *Pins-Up* are the steps where the wafer is removed from the holder and back into the “cassette”.

2.1.2.2. Steps with Variable Time

Etching processes are dependent on some process parameters that may vary from wafer to wafer and/or lot to lot, especially the time. There are three types of variable time steps:

- **Endpoint steps:** these are the steps where the end of the etching is detected automatically. Their time, thus, vary from wafer to wafer (because of thickness variations of the layers to be etched and etch rate variations).
- **Stabilization steps:** These steps end when all instructions (pressure, temperature and gas flow) are reached.
- **Run to Run (R2R) steps:** these are the steps where the etching times are calculated by control loops in order to compensate the etching rate variations, or the variability of photolithography. These times are updated automatically in the recipe while the lot starts to be processed. They are calculated in function of the CD measured after photolithography on the lot, and the etch rate of the etching machines.

2.1.2.3. Chamber Conditioning

In order to keep the chamber in the same conditions at the beginning of each new process, the WAC (Waferless Auto Clean) is used. It consists of recipes similar to the process recipe, with the difference that there is not wafer in the chamber. There are two types of WAC:

- **Conditioning:** it starts automatically before the passage of the first wafer of each lot. It can be used for both to bring the chamber to the right temperature and to clean the interior of the room.
- **Post-WAC:** after etching each wafer, it is launched in order to clean the chamber.

With the aim of use the most suitable WAC for each process, the recipe has to been well selected in function of the deposition by-product on the chamber after the process. In this thesis (Chapter IV) the optimization of the WAC process used for the eSTM will be shown.

3. DIAGNOSTIC TECHNIQUES

The diagnostic techniques used during this thesis were performed in-situ and ex-situ. The etch platform is equipped with *in-situ* diagnostic tools such as the End Point detection systems which allows the control of the etching and the plasma characterization. The other characterization techniques that will be introduced in this section are not *in-situ*. Some of them are anyway performed in the cleanroom (CDSEM used for CD control), others in the laboratory namely the physical characterization techniques (SEM and TEM, used for

morphological characterization of the patterns after etching) and the chemical characterization (XPS and ARXPS, used for the surface characterization) are carried out at *Cimpaca*. The characterization platform *Cimpaca* is a french mutualized laboratory supported by european, national and regional public funds.

3.1. End Point Detection Technique (EPD)

The etch platform LAM Versys is equipped with an End point detection system that combines the techniques of Optical Emission Spectroscopy (OES) and Light Signal Reflectometry (LSR). This is essential for the process in order to achieve the end of each material with good precision.

3.1.1. What is an Endpoint?

By using dry etching, the layers of the stack can be removed partially. The goal is to remove the layer in the unmasked areas without etching the next layer below. In order to achieve this goal several possibilities can be considered [117]:

- Use chemicals which etch the layer selectively, which means that some specific chemicals can etch one layer better than another one.
- Stop the etching by using a fixed time that can be calculated from the etch rate. However, this method is not very precise due to the variabilities of thickness that can be induced during the deposition process.
- Stop the etching after removal a certain thickness of material. This method requires a thickness measurement system in the plasma etcher and is the called EndPoint Detection.

Ideally in dry etching, the film must be removed completely with no damage or removal of the underlying film. Nevertheless, usually an over-etch is required in order to remove any remaining. Figure II-9 shows the difference between an ideally etched material versus one that has been over or under etched. Under-etch is characterized by not clearing out completely the film being etched, over-etch is characterized by clearing out the film completely and partially etching through the next film and ideal etch clears out only the film required [118].

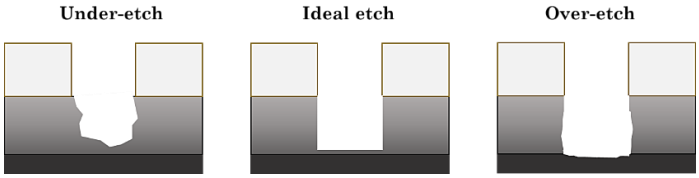

Figure II-9. Representation of the terminology used in endpoint detection. [Adapted from 118].

Endpoint detection is used to identify when the film being etched has reached the underlying film. This allows to identify which point of the process can be stopped, or changed to a more selective etching [118]. There are a variety of phenomena from which signals can be derived to mark the beginning and end of the process such as pressure change, bias change, Mass Spectrometry, Emission Spectroscopy, laser interferometry and reflectance [119]. When the power is on, the etchant concentration increases until etching starts. Then, the etchant concentration decreases while the reaction products accumulate to stable values. As the film clears, the etchant signal increases again and the product signal falls. Finally, at the endpoint, there is a third signal from the reactions and the substrate. These events are represented in Figure II-10.

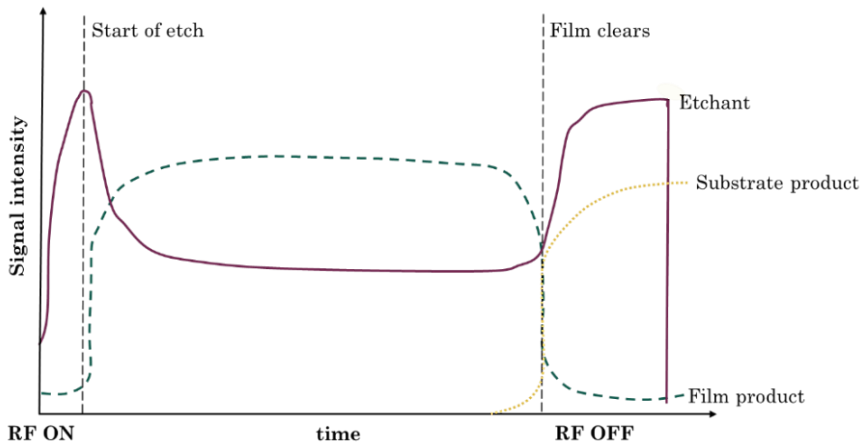

Figure II-10. Idealized schematics of the events that can be used for EPD [Adapted from 119].

The endpoint detection was probably the first system for controlling the etching process, being used even before SPC [120] and today several ways to detect the endpoint are provided for plasma etching available from almost all the manufacturers. In STMicroelectronics both LSR (Light Signal Reflectometry) as OES (Optical Emission Spectroscopy) systems are used to determine the endpoints. Further details about each technique are explained in the following sections.

3.1.2. Light Signal Reflectometry (LSR)

This technique is used to determine the remaining film thickness in real time by measuring the reflection of a monochromatic light beam. The beam is sent perpendicularly towards the substrate, so that the light is reflected by the different layers composing the stack due to the difference in the nature and the diffraction indexes of these layers. The reflected beam undergoes constructive and destructive interferences. These interferences depend on the material thickness and so the remaining material can be determined in real time. This technique is able to determine both the endpoint of a material at the interface with another material and to stop the etch process before reaching this interface.

3.1.2.1. Principle

Since Michelson, the father of visible-light interferometry, was awarded with the Nobel in physics in 1907 [121], interferometry-based techniques are one of the most important methods of experimental physics today [122]. LSR technique is based on this principle of interferometry. It relies on an external light source directed onto the sample which reflected light is detected and analyzed. Interferometry, in the strict sense, is the measurement of changes in the signal phase between two separate acquisitions, from the same ground target. The principle of reflectance interferometry used to determine the endpoints, implies that for different layer thicknesses, constructive or destructive interference occurs leading to a sinusoidal change in the signal intensity as the layer thickness reduces. It is possible to count the number of *fringes* (each period of the oscillation) in order to calculate the thickness etched [123,124].

Two different materials *A* and *B* are considered for an example. A is the material where the etching must be stopped. *B* is the material to be etched which optic index is *n* and thickness is *d*. If the monochromatic light is sent with a normal incidence towards these layers, the light will be reflected by the surface of *B* and the interface of *A*. Figure II-11 illustrates this example.

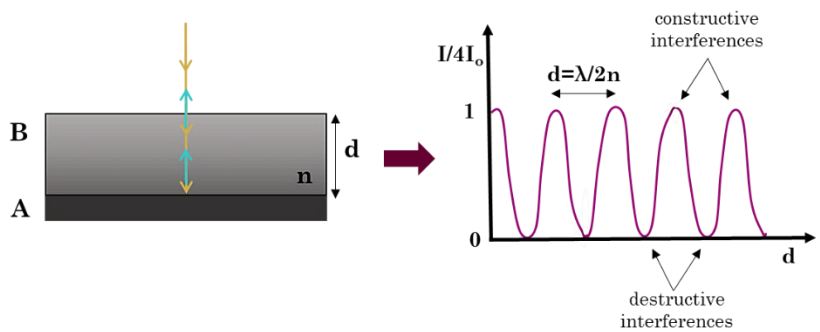

Figure II-11. Light reflection with normal incidence on a stack of 2 materials *A* and *B* [Adapted from 125,126].

The period of this function is d=λ/2n (λ is the light wavelength), which means that for each *fringe* of this function, a thickness of *B* equal to λ/2n has been etched. In this way, the thickness etched can be calculated when necessary just by counting the number of *fringes* as explained before. When the signal stops fluctuating, the etching will be finished.

3.1.2.2. End Point Detection by LSR

An example of EPD detection by the LSR technique is represented in Figure II-12, which is related to the partial etching of polysilicon during the 80nm gate process [125].

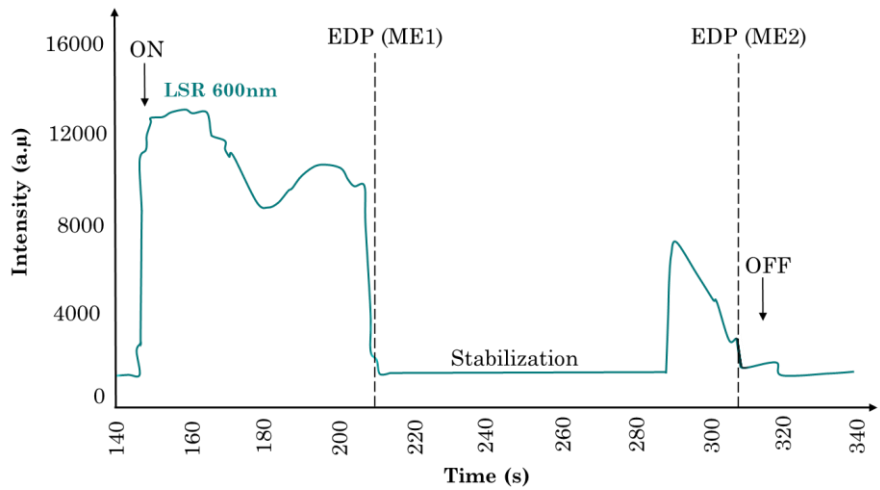

Figure II-12. Evolution of the polysilicon etching of 80nm by interferometry (LSR-600nm) [Adapted from 125].

In this example, the first EPD is detected for the ME1 when the first 60nm of polysilicon has been etched. The second EPD is detected when the remaining 20nm are reached.

3.1.3. Optical Emission Spectroscopy (OES)

This technique is based on the spectral analysis of the light emitted from the plasma that allows to identify the reactive species present in the gas during the etching process. In contrast to LSR technique, OES analyzes the light emitted from a plasma source to draw the interferences about the chemical and physical state of the process [127]. In the plasma phase, the molecules are excited due to the interactions of electrons and neutral species. While the relaxation process, when the light emission occurs, each excitation state emits a specific wavelength (λ) and thus, the molecules that compose the plasma phase can be determined by the analysis of the emission spectra [128]. Tables of spectral lines [129,130,131] and identification of molecular spectra [131,132] in conjunction with knowledge of the process chemistry are the relevant elements for the identification of the EPD and the spectral analysis.

3.1.3.1. Principle

The principle of operation of OES is based on the measurement of photons emitted when electrons move from an excited electronics state to a lower state [133].
The existence of discrete energy levels for electrons orbiting the hydrogen-like atoms nucleus is described in the Bohr model of the atom introduced in 1913 [134]. The electron is subjected to inelastic collisions which makes the electron drops from higher to lower energy levels. When that happens, a photon is released from the atom and the frequency of the emitted photon is proportional to the energy difference between the original and final electron energy

levels [135]. Basically, OES is used to deduce the gaseous species that exist in a plasma, the inelastic collisions which take place for a plasma glow discharge (see Figure II-13) such as [135]:

- Ionization: the atom, in a neutral state where all electrons are in the lowest orbits available, needs the ionization energy that is the energy required to remove the outermost electron in an atom or molecule in its ground electronic state.

- Excitation: occurs when the atom absorbs energy, as the ionization energy, and its electrons are excited to higher energy orbits.

- Relaxation: is the opposite process to excitation. Relaxation is the movement of an electron in an excited atom from a higher energy level to a lower one. Excited electrons fall from their unstable outer orbits and release energy in form of photons in the process.

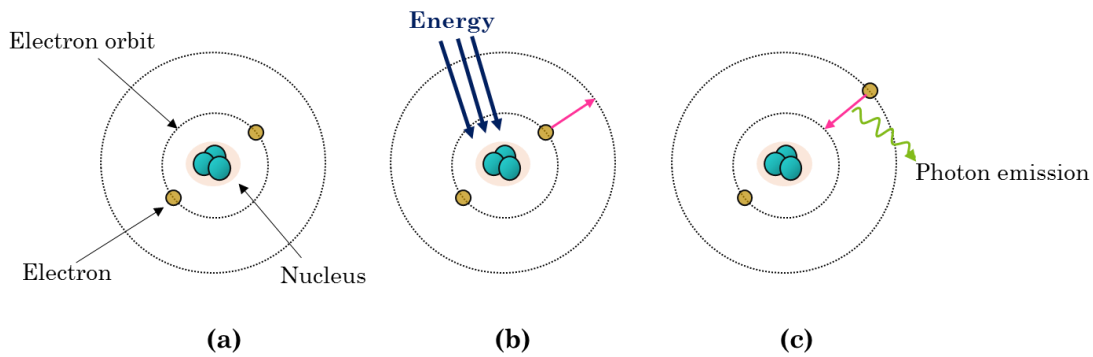

Figure II-13. Schematic of radioactive decay principle. Representation of ionization **(a)**, excitation **(b)** and relaxation and emission **(c)** process [adapted from 135].

The radioactive decay principle represented in Figure II-13, lies in the radiative decay of the excited species X* from the plasma where a photon with energy hυ is produced according to the process: X* = X + hυ. The photons emitted from excited atoms and ions are measured as they decay to lower electronic levels. Since each element has its characteristics wavelengths, the elements can be identified. The photons emitted from the excited species (atoms and ions) are separated by a diffraction grating according to their wavelength and reach the photon detection system [133].

3.1.3.2. Instrumentation

Spectrometers used for plasma diagnostics are in principle similar as UV-VIS spectrometers used in chemistry. The main difference is its much higher spectral resolution and in the case of emission spectrometry, there is no lamp inside the spectrometer. Optical prisms are used in older spectrometers, only. The OES used in this thesis (OES Plus on Flex45) is more stable than those older spectrometers by design, because there are no mirrors. The spectrometer is

mounted on the hoist arm. The process starts when the light is collected through a fused quartz window at the height of the plasma in the reactor. Then, a diffraction grating spreads out this incoming light into a spectrum. When the process ends, the wavelength spectrum shows the plasma composition. Figure II-14 outlines the OES sensor structure showing the three most important components: the entrance, the diffraction grating and the Charged Coupled Device (CCD). To generate an OES spectrum, the light emitted by the plasma is directed onto a dispersive element followed by a Charged-Couple Device (CCD). A spectrum is acquired every 100 milliseconds, which is equivalent to 10 Hz [136].

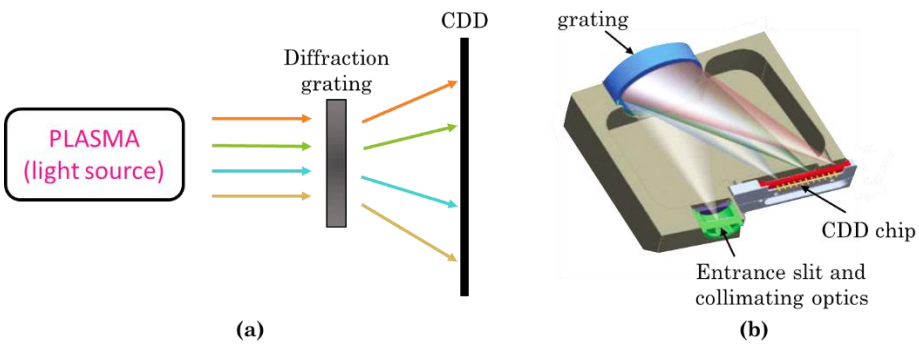

Figure II-14. Schematic of how the OES sensor works (a) and the spectrometer used from LAM (b).

The spectrometer has the following characteristics:

- Wavelength precision and stability of < +/- 1nm
- Unit to unit intensity matching < 20% (250-850nm)
- Second order diffraction < 1%

3.1.3.3. End Point Detection by OES

OES is another commonly method used for detecting endpoints during wafer processing. During the course of an etch process and the material transition, the composition of the plasma is modified, resulting in a change in the emission spectrum [127]. The basic principle of the OES endpoint system is to take advantage of these modifications in plasma chemistry when a layer in a film stack has completely cleared and a new layer is exposed during the etch process. In order to detect a material transition using OES, the first step is to determine which spectral regions show a change at the transition. Once the candidate regions have been selected, the EPD can be detected by monitoring the light intensity at the selected wavelengths.

An example of the SiO_2 etching with CO, whose representative wavelength is 484nm, is followed in Figure II-15. At the beginning, the intensity of the CO line increases, which is representative of the SiO_2 etching process, but when all the silicon oxide is consumed, the intensity of the CO line drops indicating the end of the process [125].

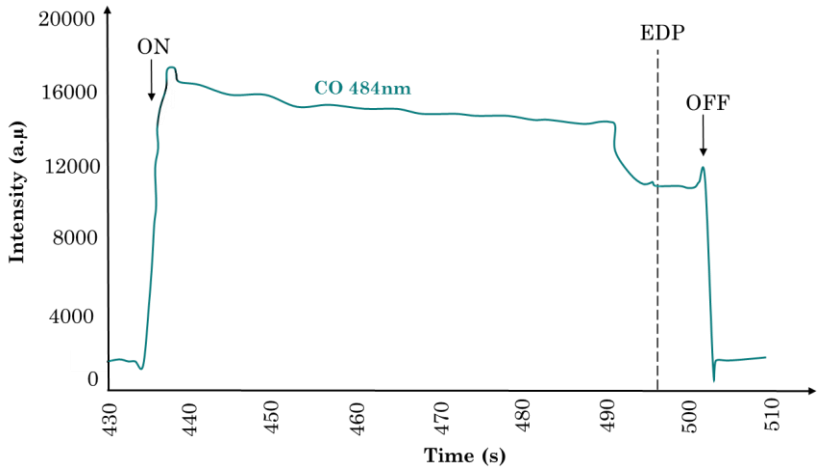

Figure II-15. Evolution of the CO line intensity (484nm) during a SiO_2 etching process in a CF_4/CH_2F_2 plasma [Adapted from 125,137].

The disadvantage of the OES as EPD system is its lack of precision: it helps to determine when the etching is complete but it is not able to know the remaining thickness in real time [126]. This is why LSR technique is used when stopping before the end of the layer is necessary. However, OES can be used to analyze the composition of the plasma as it is explained as follows.

3.1.3.4. Spectral Analysis

OES can be used not only for EPD but also for spectral analysis which enables the identification of the species involved in the plasma during the etch process. It is able to detect all the excited atoms and radicals emitted in the spectral regions between 200-900nm. The color of the global discharge is thus dependent on the feeding gases. In some cases, from the emission intensities of the excited species it is possible to obtain their concentration in the ground state, and this can be very useful in the formulation of the growth and etching mechanism [138].

An example of the spectral analysis is presented in Figure II-16. It is the study of the fluorocarbon-based chemistry ($CF_4/CH_2F_2/He$) which was performed during this thesis for the plasma diagnostic (Chapter III). By using OES, fluctuations in relative concentrations of plasma species have been monitored, including CF_2*, CH*, H*, and F*. The spectrum correspond to a silicon non-coated wafer.

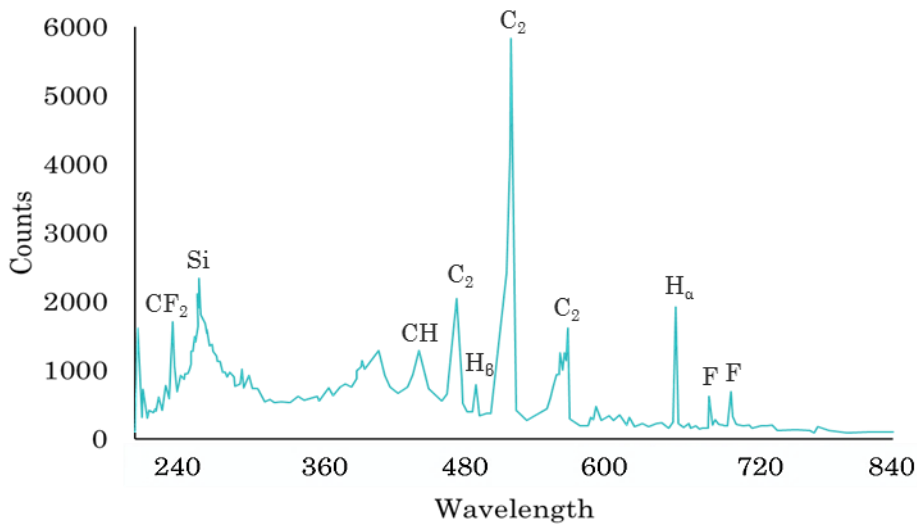

Figure II-16. Optical emission spectrum of F-based plasma over a silicon non-patterned wafer.

The presence of H is concluded by the two lines of the Balmer series for hydrogen at 656.3nm (H_α) and 486.2nm (H_β), being the H_α the strongest one. Several C_2 band system were also identified, represented by the Swan band (435nm-686nm) system at 516.7nm, 473.71nm, 563.55nm, with the 516.7nm as the most intensive line over the entire spectrum, for both cases. Swan bands are the most characteristics features of C_2 in all hydrocarbon spectra. The presence of F as an atom is observed with low intensity lines that appear at 703.7nm and 712.7nm, almost with the same intensity for both of them. However, the presence of F is shown at the beginning of the spectrum, by means of the presence of CF_2 radicals, even if these radicals are not as intense as C_2 lines, the dissociation coming from the CF_4 gas is confirmed.

3.2. Scatterometry

Two methods of CD measurement are used during manufacturing, namely -Scanning Electron Microscopy (3.5) and scatterometry [139]. The term scatterometry refers to optical methods of measuring critical dimensions using a grating test structure. The measures can be done in a spectroscopy ellipsometer as is the case in STMicroelectronics. The main challenge is to analyze the changes in the optical response that the grating structure imparts versus the response of a non-patterned film stack [140]. Scatterometry has many attributes common to other optical metrologies. It is simple and cheap, highly repeatable (good precision) and consistent with other methods (accurate) [141].

3.2.1. Principle

Scatterometry can be defined as the measurement and characterization of light diffracted from periodic structures [141]. The scattered or diffracted light pattern (*signature*) can be used for characterizing the details of the grating shape itself. Since the device is composed of periodic structures, the scattered light consists of distinct diffraction orders at angular locations specified by the following grating equation:

$$sin\,\theta_i + sin\,\theta_n = n\frac{\lambda}{d} \qquad \text{(II.1.) [141]}$$

where θ_i is the angle of incidence,
θ_n is the angular location of the n,
n is the diffraction order,
λ is the wavelength of incident light, and
d is the spatial period (*pitch*) of the structure.

In the most part of cases, the measurement is performed with an ellipsometer associated with a method of solving an inverse problem. For this purpose, two conditions must be satisfied: it is necessary to know the optical indices of the materials and the sample to be measured must be composed of periodic structures [142]. Basically, the principle of ellipsometry-based scatterometry is that light polarizes in-plane of reflection reflects differently than light polarized perpendicular to the reflection plane [140].

3.2.2. Instrumentation

Scatterometers are simple instruments that essentially consist of an illumination source, some focusing optics, perhaps a rotation stage and a detector. Usually, by using these instruments, one has access to the top CD, middle CD, lower CD and the angle between the pattern and the substrate surface [125]. The scatterometry principle of operation and the scatterometry measures that can be obtained are represented in Figure II-17.

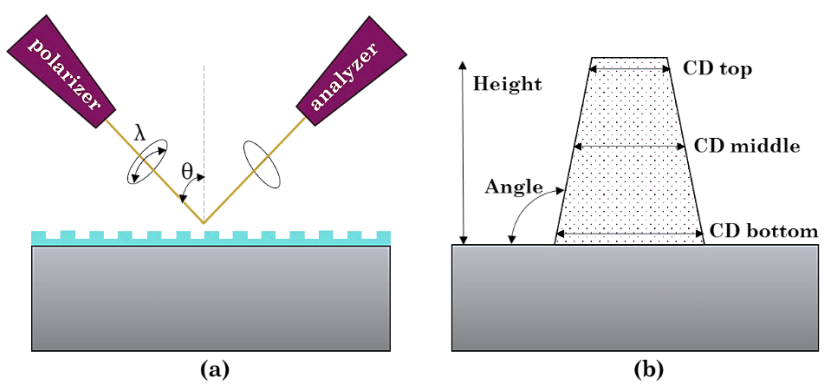

Figure II-17. Scatterometry operation (a) and measures (b) [Adapted from 125].

The main advantage of this technique compared to microscopy is that it is able to provide different geometrical information (thickness, CD) by performing a single measurement.

3.2.3. New Model for STI Measures

At the beginning of this thesis, in STMicroelectronics, there was not a scatterometry model available for the STI measurements. Since CD-SEM measures were not highly accurate at this stage, a scatterometry model able to perform these measures was required. Further details about this will be presented in Chapter V, where the R2R model will be introduced. Nevertheless, Figure II-18 confirms the better accuracy of scatterometry versus CD-SEM for the STI.

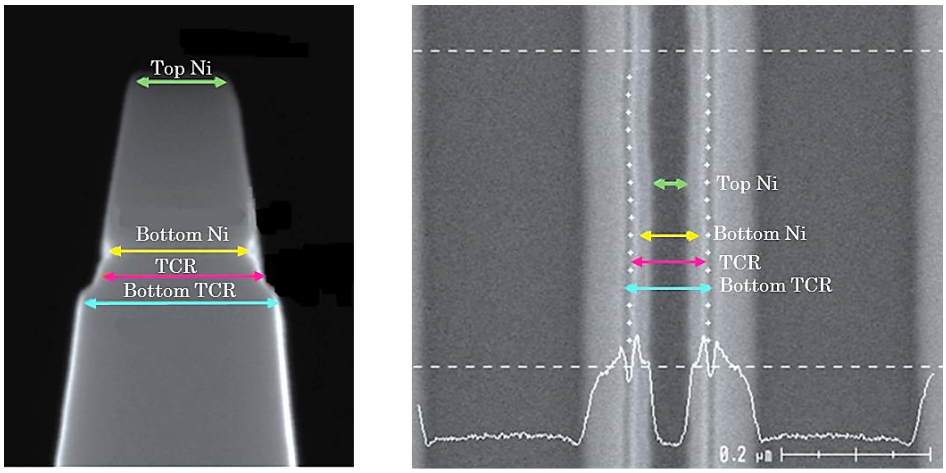

(a) **(b)**

Figure II-18. Scatterometry (a) vs CD-SEM (b) measures for the STI.

As it can be appreciated, by using CD-SEM, the measurement is hard due to the *top view* which complicates the decision about where the measures should be taken, making this technique unprecise for that purpose. However, the scatterometry model, using a *profile view*, simplifies that decision. Therefore, it is more convenient for the CD control of the STI.

The model was developed in collaboration with the metrology equipment. The major challenge for developing this model was the complexity of measuring the STI by using Scatterometry because of the stack after etch such as the line of shape and TCR (Top Corner Rounding). Until then, the only scatterometry measure available for the STI was the total height, and there was not scatterometry measures post the photolitography step. By developing this model, we did introduce not only the measure post-photolitography, but also all the informations about the different CDs, notably the CD at the TCR which is the most important since it is the most correlated with the electric performances of the final device. Furthermore, the model uses optic measures at the interfaces, unlike other models which measure CDs by using percentages of height from the ground. This makes the model even

more accurate. In Chapter V, explanations about why it was important to develop this model, will be presented. The models that will be cited for the development of the R2R model in Chapter V are represented in Figure II-19.

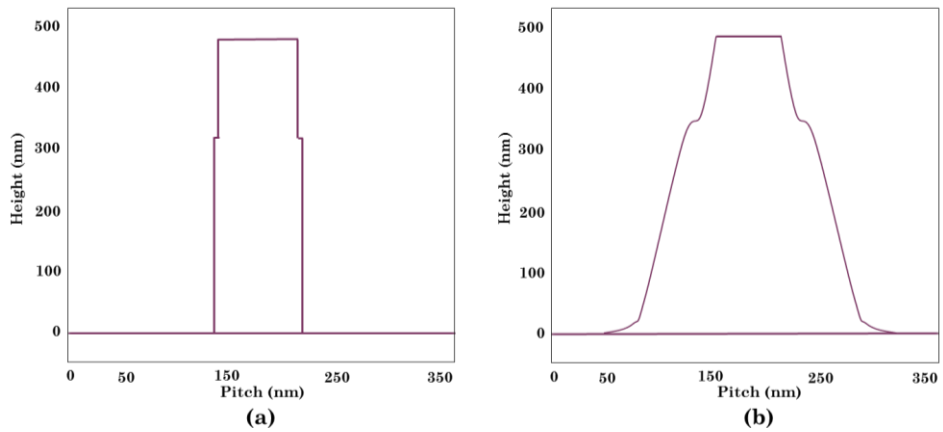

Figure II-19. Scatterometry model post photolithography (a) and post etching (b).

3.3. X-Ray Photoelectron Spectroscopy (XPS)

X-ray Photoelectron Spectroscopy (XPS) [143] is the most widely technique used for surface analysis. It can be applied to a broad range of materials and it provides chemical state information from the surface of the material being studied.

3.3.1. Principle

The existence of discrete energy levels for electrons orbiting the nucleus of H-like atoms, described in the Bohr model, it has been referred before in 3.1.3. So that matter is made of atoms, atoms are made of a nucleus and several electrons. XPS derives information on the elemental composition and specification of matter by evaluating the electronic structure of the atoms and/or ions residing within the surface of the sample [143].

XPS is based on the photoelectric effect, illustrated in Figure II-20. The basic principle of the photoelectric effect was enunciated by Einstein [144] in 1905. Knowing that each atom has core electron with its characteristic binding energy, and that conceptually, this binding energy is equal to the ionization energy of that electron. When an X-ray beam directs to the sample surface, the energy of the X-ray photon is absorbed completely by the core electron of an atom. If the photon energy (hv) is large enough, then the core electron will escape from the atom and emits out of the surface. The emitted electron with the kinetic energy of E_k is referred to as the photoelectron [145].

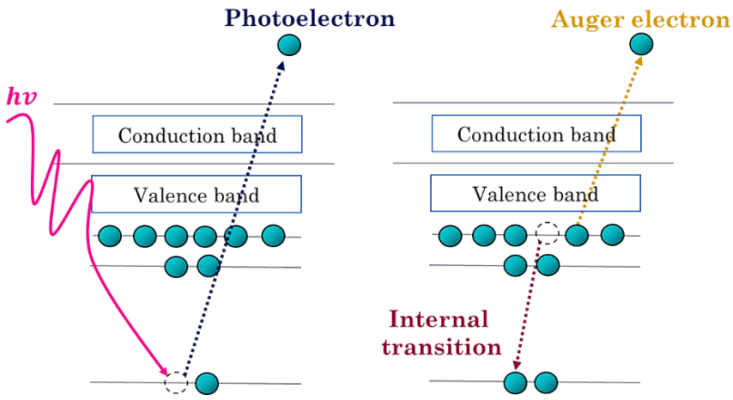

Figure II-21. Representation of the photoelectric effect [Adapted from 146].

According to the Einstein equation [144] for the photoelectric effect, the kinetic energy of the photoelectron was related through the X-ray energy to an atomic binding energy as:

$$E_K = hv - E_B \qquad \text{(II.2) [147,148]}$$

where hv: X-ray beam incident energy or photon energy,
E_K: Electron kinetic energy of the photoemitted electron, and
E_B: Electron binding energy of the core level.

Considering the photoemission process as sketched in Figure II-21; before the emission of the photoelectron, the total energy of the system is the energy of the X-ray hv plus the energy of the target atom in its initial state E_i. By following the emission of the photoelectron, the total energy of the system is the kinetic energy of the photoelectron E_K plus that of the ionized atom in its final state E_f. The total energies before and after photoemission, related to the Einstein's equation, can be seen as if the "binding energy" E_B of the electron is just the difference between the final and initial state energies of the target atom $E_f - E_i$ [148].

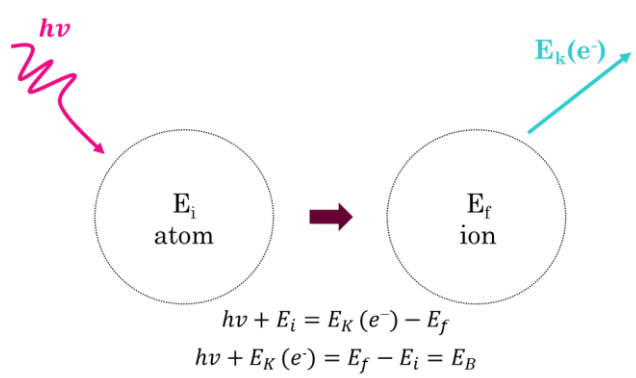

Figure II-21. Sketch of the photoemission process [Adapted from 148].

According to the photoelectron emitted (Figure II-20), some atoms could lack electrons in the internal layers from which photoelectrons have been released. To get over this ionized state, the atom can emit another photon or undergo an Auger transition. For the absorption of a photon carrying energy of hv, there is an equation (II.3) that enables to explain the energy balance, based on the principle of the conservation of energy as [149]:

$$hv = E_K + E_B + \emptyset_{Work\ function} \quad \text{(II.3) [149]}$$

where $\emptyset_{Work\ function}$: Energy required for an e^- to leave the material, dependent of both the spectrometer and the material.

3.3.2. Instrumentation

The XPS used for this thesis is a KRATOS AXIS NOVA from CIMPACA (Centre Intégré de Microélectronique Provence-Alpes-Côte d'Azur) characterization platform. The equipment is composed of a photoelectron extractor system along with an analyzer detector system, enable to generate spectra by their binding energies. The main characteristics of this XPS are:

- Pumping system to achieve ultra-high vacuum (10^{-8} to 10^{-10} Torr).
- Monochromatic X-Ray aluminum source (Al Kα =1486eV).
- Delay Line Detector system, used for both spectroscopy and imaging modes.
- Analyzer for separating the emitted electrons according to their kinetic energy and a counting system (associated with a computer acquisition).
- Ion gun for performing analysis cycles / abrasion in depth.
- Electron gun for the analysis of samples for electrical insulation.
- Non-fixed holder, with possibility of movement for analysis ARXPS (3.3.4).

3.3.3. Spectral Analysis

XPS analysis reveals which chemical elements are presented at the surface and it informs us about the chemical bound nature which exists between these elements [149] by measuring the kinetic energy of the ejected electrons from the analyzed surface. Thus, it is possible to determine their binding energy which depends on the analyzed element and its chemical environment. An appropriate data processing leads to the specimen elemental composition. The software used for analyzing the data collected during this thesis was *CasaXPS*. All the spectra analyzed during this thesis were obtained from cimpaca.

The analyzed depth is dependent on the ability of electrons for reaching the surface. Since the emitted photoelectrons undergo inelastic collisions within the material and lose some part of their energy, only some of them will have enough energy to reach the surface and be collected. Therefore, the XPS analysis comes from the surface's first 10nm [137].

An example of an a-C:H sample that has been etched by using F-based chemistry, is shown in Figure II-22.

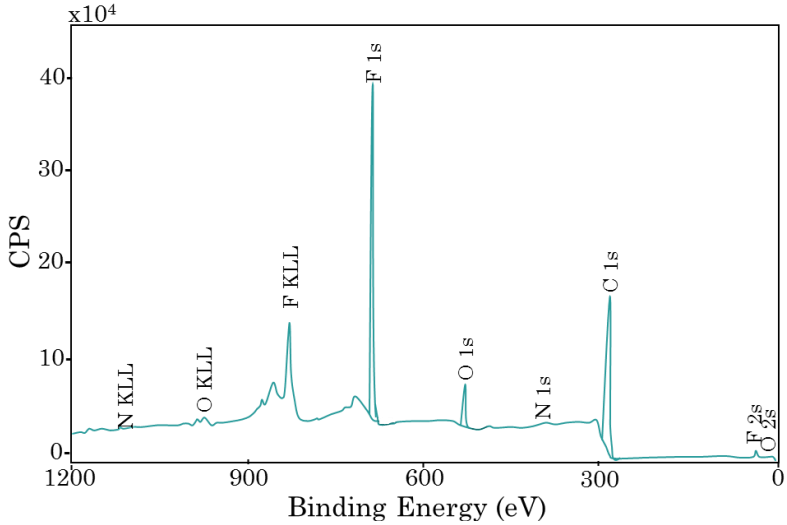

Figure II-22. XPS general spectrum of a-C:H surface etched with $CF_4/CH_2F_2/He$.

By counting these electrons versus their binding energy, the general spectrum shown in Figure II-22 is obtained. The peaks are indexed with the same name as the electronic layers where the photoelectrons come from. Each line corresponds to a given binding energy. Several tables have been set up to show which orbital is associated with each energy, even if in some cases there are several solutions.

For the semi-quantitative analysis, high energy resolution (<0.6eV) spectra are required. Figure II-23 shows the XPS spectrum of the carbon C1s from the same analysis as the spectrum at low resolution (Figure II-22).

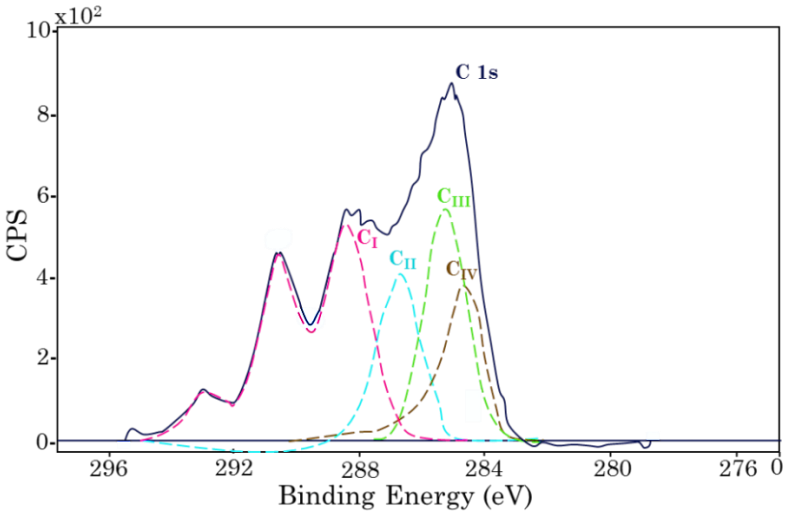

Figure II-23. XPS high-resolution spectrum of carbon C1s.

By subtraction of the continuous background by the semi-empirical method of Shirley [150], which attempts to use information about the spectrum to create a background sensitive to change in the data, each XPS peak can be decomposed into its different components. In Figure II-23, for example, the C1s envelope has been resolved into four components that correspond to the signals of four different chemical environments (C_I, C_{II}, C_{III} and C_{IV}). Unfortunately, by using XPS, the absolute concentrations of the different species presented in the analyzed surface cannot be determined. However, it is possible to determine the relative concentration of each element and therefore, to determine the total surface composition as an atomic percentage. In this thesis, the data treatment of the XPS spectra was carried out at cimpaca. Thus, in order to perform our analysis, we will present these results pre-treated such as they have been obtained. Further information about peak fitting in XPS can be found in [151,152,153].

3.3.4. Angle-Resolved XPS (ARXPS)

The Angle-Resolved X-Ray Photoelectron Spectroscopy (ARXPS) enables the analysis of the surface composition by varying the angle of analysis of the XPS, unlike standard XPS which characterizes the composition of flat surfaces. This is highly interesting for characterizing the Sidewall Passivation Layer (SPL) that protects the structures from lateral etching [59,66,67,125,126]. It is in function of the angle of the analysis that the photoelectrons coming from the *mask+bottom* or *mask+sidewalls* would be differentiated. Figure II-24 sketches how the sidewall passivation layers are analyzed by using ARXPS.

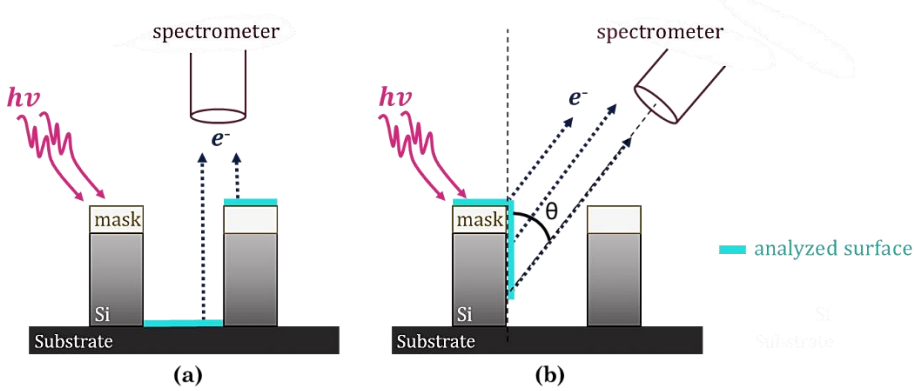

Figure II-24. Sketch of the ARXPS technique for analyzing the SPL [Adapted from 125,126].

However, not only by tilting the analyzer one can identify the contributions coming from the mask or the polysicon. For that purpose, we will use along with the ARXPS technique, the ***differential charging effect*** which takes place on the insulating analyzed surfaces due to the electron gun effect. In electron spectroscopy, the surface can be either positive or negative charged [154]. In fact, the photoelectrons coming from these insulating surfaces will see their

kinetic energy increase shifting the peak toward lower binding energies. Figure II-25 shows this effect.

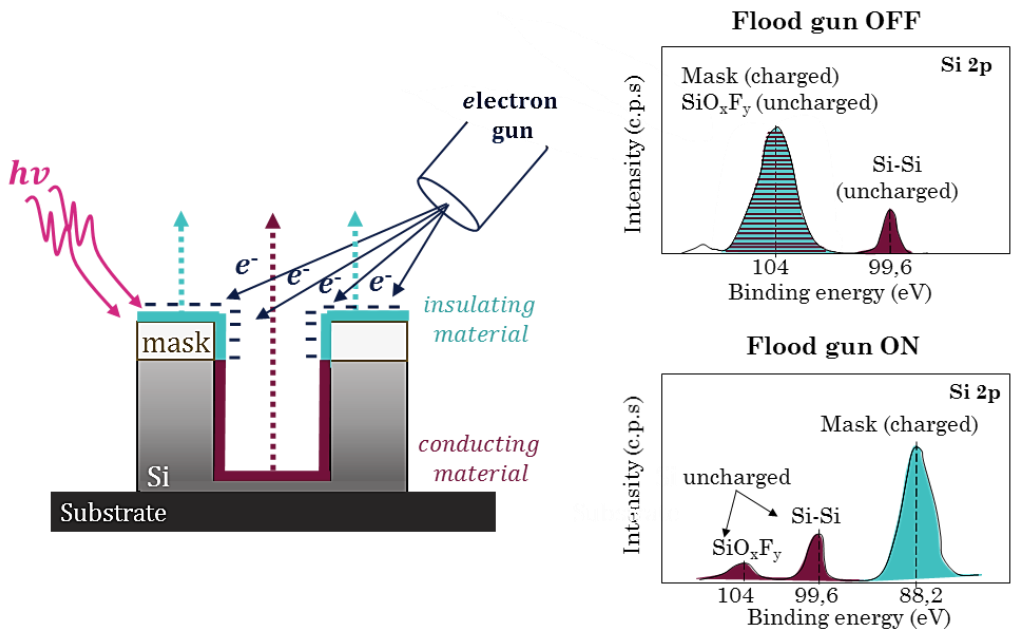

Figure II-25. Difference between a conductor and insulating material due to the electron gun influence [Adapted from 67].

As shown in this example, the contribution coming from the insulating surfaces can be separated from the ones coming from the conducting materials where the photoelectric peaks are not influenced by the electron flux. Here, the conducting material is the polysilicon and the insulating material is the mask. While the electron gun is OFF, the contribution of both materials overlap whereas that when the flux of electrons is turned ON, the mask contribution is clearly separated from the conducting material.
The sample surface acquires a positive potential which varies from several volts and the kinetic energies of the photoelectrons are decreased by the electronic field. This means that Fermi levels of the sample and the spectrometer are no longer in equilibrium [154].

For the development of this thesis, the analysis of passivation layers formed on the sidewalls with a a-C:H hard mask (Chapter III) are done by taking advantage of this method. Another method which profits the XPS analyses is the floating sample method, also used in this thesis.

3.3.5. Floating Sample Method

During plasma etching processes, some material layers are deposited on the chamber walls. Since these layers are source of shifts in the etch process, Joubert et al [155] developed the so-called “floating-sample” technique in order to analyze these deposits. By using XPS, these

layers can be analyzed in order to know their chemical composition. For that purpose, a floating sample is set on the top of a wafer where the layers deposited are identical to those deposited on the chamber walls. The principle of this technique is illustrated in Figure II-26.

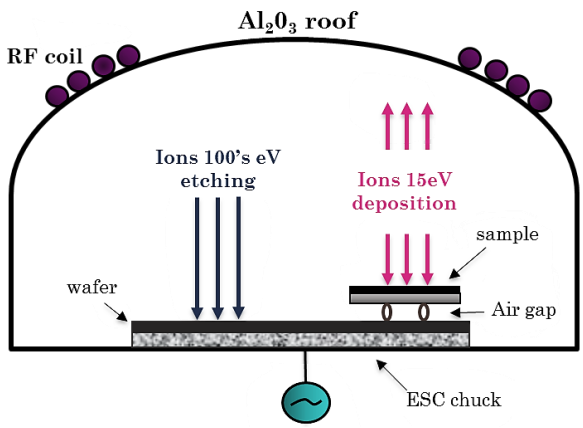

Figure II-26. Floating-sample technique setup for measuring the chamber wall deposition [Adapted from 156].

Providing that the air gap between the floating sample and the wafer is large enough, the sample will be electrically floating while the silicon wafer is RF biased [155]. The air gap acts as serial condenser whose capacitance is small compared with the sheath. The floating sample experiences absolutely the same condition as the reactor walls so that the same deposit will be formed. Unlike the standard etching, where the wafer is submitted to 100eV, the ion bombardment for the floating sample as the reactor walls is around 15eV, so that related to the deposition instead of etching.

In their studies [155, 156], the floating sample was transferred under vacuum to the XPS analyzer after the process. Thus, the chemical composition of the deposit formed on the sample could be analyzed quantitatively. In this thesis, an experimental study is conducted where different materials are sputtered in order to find out in which conditions the walls impact on the plasma composition. However, the transfer will not take place under vacuum since our XPS is not in-situ so that some contamination will be considered. The development and results of this procedure will be presented in Chapter IV.

The thickness of the air gap has to be calculated in order to prevent the DC biasing of the floating-sample that happens when the RF voltage applied between the electrode and the plasma, drops across the equivalent capacitance represented by the air gap [155]. The air gap thickness is calculated following the equations by Ramos and Joubert [66,155].

The RF amplitude on the floating-sample can be calculated since the two capacitances are in series by;

$$V_{sheath}^{RF} = \frac{C_{gap}}{C_{gap}+C_S} V^{RF} \quad \text{(II.4) [66,155]}$$

where V_{sheath}^{RF} is the power applied to the wafer,

C_{gap} is the equivalent capacitance of the air gap, and

C_S is the sheath capacitance.

C_{gap} and C_S are respectively given by;

$$C_{gap} = \varepsilon_0 \varepsilon_r S / d_{gap} \quad \text{(II.5) [66,155]}$$

$$C_s = \varepsilon_0 S / d_{sheath} \quad \text{(II.6) [66,155]}$$

where ε_0 is the permittivity of vacuum,

ε_r is the dielectric constant of the material below the floating-sample substrate, (being equal to 1 in the air gap case [155])

S is the area of the sample,

d_{gap} is the spacing between the sample and the wafer, and

d_{sheath} is the sheath thickness on the floating-sample.

Plasma physics distinguishes two types of sheath [66]. For the first case, the sheath thickness is calculated according to the Child-Langmuir law (I.8) which can be applicable when $V_{sheath}^{DC} \gg T_e$. For the second case, the sheath thickness is calculated according to the Debye length (I.4), which is applicable when $V_{sheath}^{DC} \approx V_p$. The two cases can be considered respectively the upper and lower limit for self-bias but in fact, the floating-sample technique is between them. The result of our calculations can be found in Chapter IV.

3.4. Scanning Electron Microscopy (SEM)

The Scanning Electron Microscope (SEM) operates on the same basic principles as the light microscope but uses electrons instead of light. What one can see with a light microscope is limited by the wavelength of light. SEM uses electrons as "light source" and their much lower wavelength make possible to get a good resolution [157]. Therefore, the resolution is much higher than an optical microscope being in the order of nanometers but the images are obtained in black and white. In order to obtain all the information that SEM can provide, it is necessary an understanding of the major modes of microscopy and the electron beam parameters that affect them [158,159].

During the measure, a focused electron beam is scanned across the sample while secondary electrons emitted from the sample are collected. The orientation of the surface features is highly influent respect to the number of electrons emitted which creates variations in the contrast of the image. The electron probe of a SEM is scanned horizontally across the sample into two perpendicular (x and y) directions. The *x-scan* is relatively fast unlike the y-scan which is much slower [160]. In this work, a S-4800 FE-SEM from Hitachi was used for all the morphological cross section analysis.

3.5. CD-Scanning Electron Microscopy (CDSEM)

The CD-SEM (Critical Dimension-Scanning Electron Microscopy) used for controlling the CD [58], is a top view SEM, as it was introduced before (3.2). The images are automatically analyzed with detection algorithms. The objective is to determine the characteristic dimension of the structure. This dimension is called *critical dimension*, denoted by the following CD, and depends on the geometry analyzed [142]. The interest of this technique is that it allows measuring a large number of patterns in a short period of time. Therefore, it is one of the most used metrology techniques in the microelectronic industry [137]. For instance, for a transistor in top view represented by a polycrystalline silicon rectangle, the critical dimension will be the width of the rectangle.

3.6. Transmission Electron Microscopy (TEM)

It was invented soon before the SEM and is used as well for morphological characterization. Whereas the conventional SEM scans horizontally across the sample in two perpendicular directions, TEM uses a stationary incident beam [160]. The TEM allows us to measure the dimensions obtained after etching with a sub manometer scale resolution. In this technique, an electron beam is focalized normal to the sample and by the help of magnetic lenses, the electrons transmitted or diffracted by the sample are focalized in the plane of the image. Therefore, high resolution images can be obtained but the preparation of the samples is long and difficult. As well as SEM, to obtain all the information that TEM can provide, it is necessary an understanding of the major modes of microscopy and the electron beam parameters [161,162]. In this work, a CM 200-T from FEI was used for all the TEM analysis.

4. SUMMARY

In this chapter, the etching platforms, diagnostic tools and the methods used for the characterization of the etching process during this thesis, have been defined. In the chapters that follow, we will outline how we used these tools and we will present the studies and analyzes performed during this thesis.

"It was almost as incredible as if you fired a 15-inch shell at a piece of tissue paper and it came back to hit you" (E. Rutherford)

Chapter III

eSTM: Characterization and Process Optimization

This chapter shows the characterization and optimization of the eSTM process. Firstly, the characterization of the different parts that interact during the process etch are discussed. Therefore, the diagnostics of the plasma itself and the composition of the surface layer being etched are studied, paying attention to the determination of the chemical composition of the passivation layer. Secondly, in order to optimize the CD performances, a model is proposed by using DOE. This model is able to predict and control the CD by establishing the units for the most important parameters. Finally, the conclusions of this chapter are discussed.

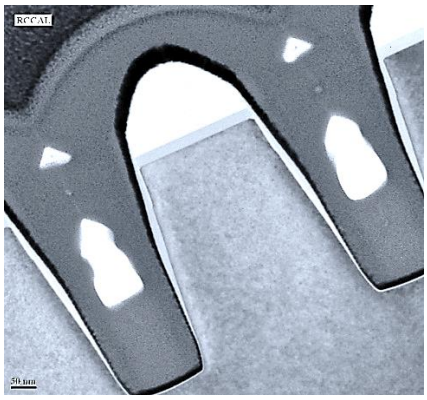

TEM profile of the eSTM of this thesis.

As it has been introduced in Chapter I, the eSTM aims at having the advantages of consumption and isolation from the EEPROM, due to its selection transistor, plus the advantage of the Flash by reducing its size.

The chapter is organized as follows. Firstly, an introduction based on the literature review is presented followed by the experimental details related to the eSTM fabrication process and the etching specifications. Secondly, the characterization of the plasma and the wafer surface interactions are discussed, followed by the optimization of the CD developing a model by means of DOE. Finally, the conclusions of this study conclude this chapter.

1. INTRODUCTION

Besides the information of the eSTM introduced in Chapter I, this section seeks to increase the knowledge related to the state-of-the-art of this memory as well as the plasma etching challenges that has been faced for developing this structure (Figure I-11).

1.1. Embedded Select Trench Memory (eSTM)

Recently, demands for a higher density e-NVM (embedded Non-Volatile Memory) are increasing. At the same time, high performances of the cell are also currently requested since cell performances can be a speed limitation. The eSTM is a new disruptive NVM architecture for ultra-low power application developed at STMicroelectronics Rousset site. Table III-1 summarizes the targets of this cell.

Table III-1. Targets of the eSTM structure.

Item	Specifications
Cell size	<0.1 μm^2
Consumption during programing/erasing	<10 nA/cell
Cycling	500 Kcyc
Retention	10 years 85°C
Programming/erasing speed	<1ms

The main objectives during the development of the eSTM cell were:

- To integrate the selection transistor for reducing power consumption.
- To have a quite simple manufacturing process that approximates the one of the Flash.
- To maintain a cell size close to that of a floating gate transistor.

In literature, one memory cell respects the first two criteria: the **2T cell** (2 transistors), so this was our starting point.

1.1.1. The Starting Point: The 2T cell

The 2T cell [169,170], represented in Figure III-1, counted with a selection transistor. This cell was particularly easy to perform with a standard CMOS process flow.

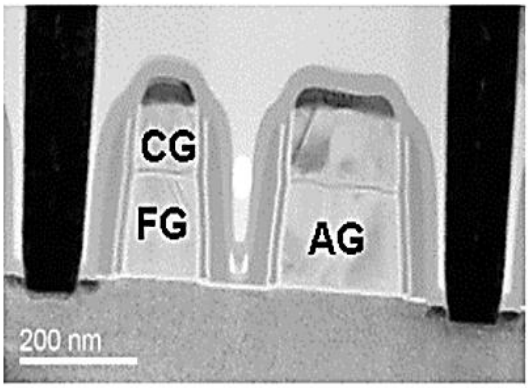

Figure III-1. TEM cross-section of the two-transistor cell in 90nm technology node [169], where CG is the Control Gate, FG the Floating Gate and AG the Access Gate.

One of the most important points in 2T-cells for eVNM applications is how to sustain or increase cell performance while cell size must be continually shrinking [170]. This disadvantage of size is due to the two transistors which are used for only one memory. It was therefore essential to find a solution able to reduce the size of this cell. Therefore, it was necessary to perform a new memory architecture. For the eSTM, the size of the cell was reduced by integrating a polysilicon vertical transistor but the process of integration of this transistor was pretty complicated. Before going into details of the process flow needed for obtaining the deep trench of the eSTM, it was important to search in literature if other polysilicon trenches had been already used.

1.1.2. Literature Review of the Polysilicon Vertical Trenches

In the literature, deep trenches are used in various ways such as *insulators*, *inductors*, *DRAM capacitors* or *floating gate transistors*.

1.1.2.1. Polysilicon Trenches Used as Insulators:

For the good performance of the IC, it is important to keep the structures isolated between them. However, with the decrease of technological nodes, the structures are getting closer and closer, increasing negative effects as leaks. In order to reduce these effects, polysilicon

deep trenches have been used to improve the insulation of the structures [171-173]. In 2004, A. Watson and S. Voltman [171] demonstrated the influence and improvement of Deep Trench (DT) isolation and Sub-collector on the Latchup Robustness in BiCMOS Silicon Germanium Technology. As a result, significant improvements of latchup robustness were demonstrated with the trench structure, which implied an advance in the understanding of the influence of deep trench on CMOS latchup robustness. Figure III-2.c shows the Latchup Structure with the Deep Trench and Sub-collector. A. T. Tilke et al [172] presented in 2006 a novel buried integration for compact cell design with Deep Trench Isolation (DTI). In their paper, they reported the working principle of the novel buried bitline cell where a novel deep trench isolation module was added to shallow trench isolation. In 2007 [173], they outlined an even more aggressive shrink was feasible by using a self-aligned STI-on-DTI concept used for the integration of an embedded flash memory in a high-performance CMOS logic process. The schematic layout of the eFlash array with DTI are shown in Figure III-2.a as well as the TEM cross-sectional micrographs of the DTI/STI in Figure III-2.b.

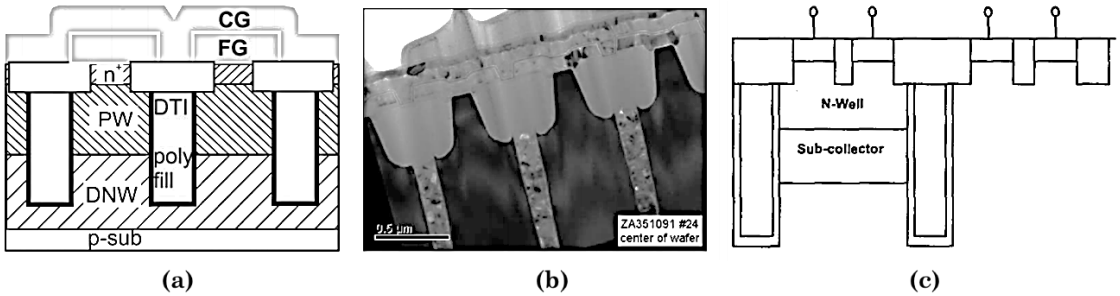

Figure III-2. Two different application of polysilicon trenches used for transistors insulation. a) schematic layout of the eFlash array with DTI [173], b) the TEM cross-sectional of the DTI/STI [173] and c) polysilicon trench used as insulating ring to surround the structure [171].

The first application [173] was used for the integration of an embedded flash memory in a high-performance CMOS logic process. Here, the DTI was placed between the two memory transistors below the STI. The dimensions of the DTI were 1.5 to 3µm depth and a length of 160 to 180nm fully filled with polysilicon. In the second application [171], the polysilicon trench was used as insulating ring to surround the structure. The length was not specified but the depths of the trench varied between 1 and 6µm. In both cases, the presence of a polysilicon trench was used to improve the device performance.

1.1.2.2. Polysilicon Trenches Used as Inductors:

Another possibility was to use the polysilicon trenches in order to improve the performance of the inductors. In 2006, H-L. Tu [174], showed that the deep-trench-mesh pattern significantly improves the inductor performance with higher resonant frequency and higher peak in broadband response. The integration of these deep trenches improved the inductors

in two ways; increasing the resonant frequency by decreasing the capacity coupling and/or increasing the quality by reducing the resistive losses. Figure III-3 shows the necessary steps followed for performing a deep trench.

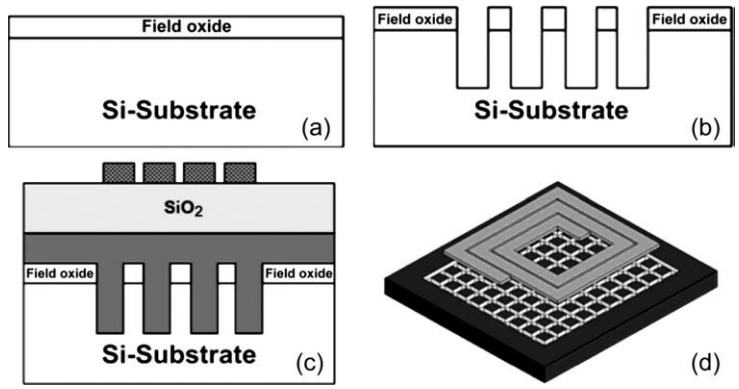

Figure III-3. Steps for improving an inductance by integrating polysilicon lines [174], where a) Standard substrate, b) Deep trenches substrate, c) Side view of inductor of deep trenches and d) Mesh-like deep trenches beneath the inductor.

1.1.2.3. Polysilicon Trenches Used as Capacitors for DRAM:

Another use of the polysilicon deep trenches was as trench-capacitor in volatile DRAM memories as described by H. Sunami in 2008 [175]. In this paper, the author described the circumstances of invention and development of the trench-capacitor DRAM cell. The invention of the trench-capacitor DRAM was patented in 1975 but the first trial development was presented in 1982 in I-Mbit DRAM era. Those volatile memories were composed of a transistor and a capacitance. Figure III-4.a presents the different approaches that have been provided in order to improve both the performances and the size of the cell. Figure III-4.b shows a deep polysilicon trench used as buried capacitor.

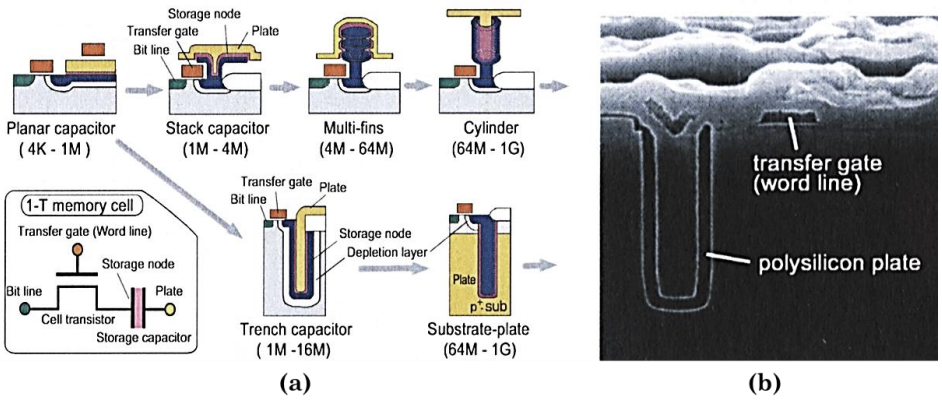

Figure III-4. a) Major advancement in DRAM cell innovation and b) First I-Mbit DRAM with trench capacitor [175].

1.1.2.4. Polysilicon Trenches used as Floating Gate Transistor:

In literature, the deep trench has been also used as floating gate [176-178]. In 2004, D. Lee et al [176] presented the structural and electrical characteristics of the latest generation of a self-aligned split-gate NOR memory incorporating a vertical floating-gate channel. Their results demonstrated the continued scalability of the SuperFlash cell for high-density, high-speed applications. Two years later, H. Van Tran et al [177] showed an experimental 0.11um 4.5F² 1.8V multilevel 1Mb vertical floating gate split gate source side injection (SSI) test vehicle for Giga-bit NOR flash memory for the first time. In 2007, B. Chem [178] exposed the highly reliable Low Power SoC throughout the three generations of SuperFlash embedded memory.

The cell structure, the process sequence and the final trench [176-177], whose dimensions were 200nm depth and 280nm longer, are represented in Figure III-5. The polysilicon, deposited after the oxide (the tunnel oxide), is etched to obtain the spacers which will be the floating gate of the memory.

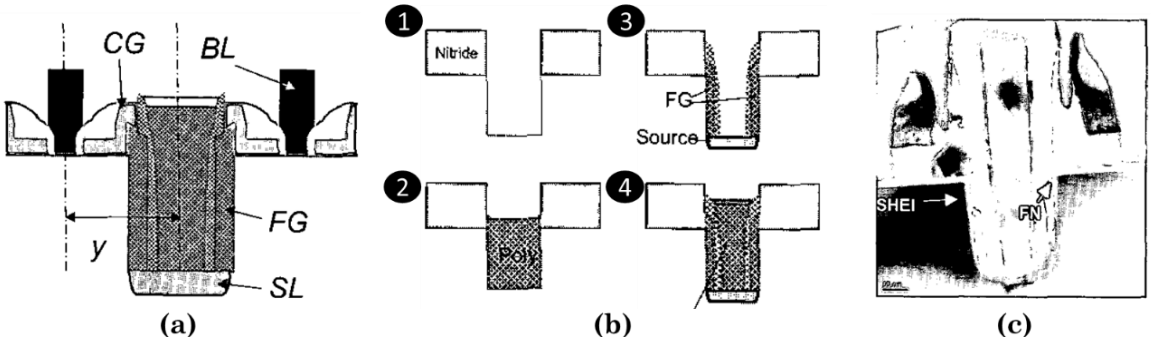

Figure III-5. a) cell structure, b) process sequence where *(1) is the trench post etch, (2) the polysilicon deposition, (3) polysilicon etch for creating the spacers and (4) oxide deposition* and c) is the profile of the final trench [176].

So far, different kinds of polysilicon trenches has been used in literature. In this research, the architecture of the eSTM uses the polysilicon trench as vertical transistor.

1.1.3. The Polysilicon Trench of the eSTM: The Vertical Transistor

As we introduced in 1.1.1. the starting point for the eSTM architecture development was the 2T cell. Apart from its size, this cell was a very interesting memory since its manufacturing process was compatible with the CMOS process. In order to reduce its size, its two selection transistors have been merged into a single vertical transistor reaching the size of a flash for this new cell. The polysicon trench of the eSTM is, hence, used as vertical transistor as shown in Figure III-6. This made the manufacturing process more complex but still compatible with CMOS process as for the flash. This manufacturing process will be detailed in section 2.

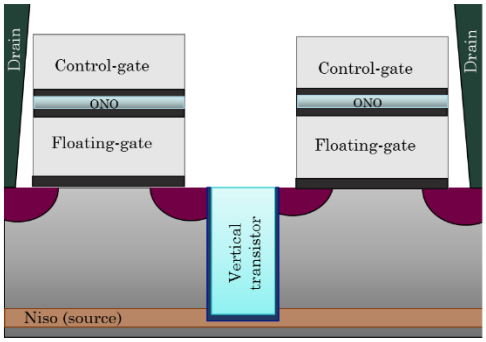

Figure III-6. Polysilicon trench used as vertical transistor for the eSTM.

This structure, developed by STMicroelectronics in 2012 [53,54], uses the polysilicon trench as vertical transistor. The Niso serves to isolate the transistors from the substrate and as source line allowing earn a contact. Two floating gate transistors are located on both sides of the vertical transistor. The polysilicon trench, whose characterization and process optimization are the purpose of this chapter, requires a width of 150nm and a depth of 450nm in order to reach the Niso. A perspective of the trench is represented in Figure III-7 together with a SEM cross-section of its profile.

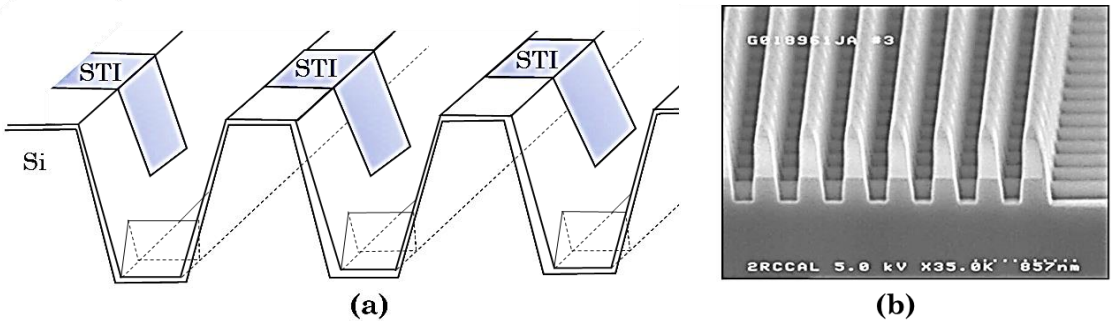

Figure III-7. a) Schematic representation of the trench after etching and b) SEM cross-section.

Since the good integration of this trench is critical for the cell performance, the step of plasma etching needs to be carefully studied in order to perform a required and reliable trench. For that purpose, some plasma etching considerations have been taken into account and the literature review related to this subject is presented in the next section.

1.2. Plasma Etching Considerations

The dimensional control is very important for the realization of small structures. However, the speed of etching remains a secondary aspect since the thicknesses of the layers used are thin and the most important thing to consider is the plasma chemistry used.

In the previous section, the polysilicon trench was named as *deep trench*, from a standpoint of plasma etching; this changes. *Deep trench*, in plasma etching, refers to an attack of several tens to hundreds of silicon's microns, which is not the case of the nanometric dimensions required for performing CMOS transistors as explained in the previous section. For *deep silicon trenches* there are different methods such as Bosch™, cryogenic or STiGer™, among others [67]. However, within the framework of this thesis, for an etch of 700nm as is required for the eSTM trench, the importance relies in knowing the plasma chemical considerations as well as the factors involved for a directional and selective etching. It is therefore presented, in this section, an analysis of considerations of the etch directionality and etch selectivity as well as a review of the literature on plasma chemistries used for polysilicon trenches.

1.2.1. Pure Plasma Chemistries

A large variety of fluorine, chlorine, bromine, hydrogen and oxygen based plasmas mixed with gas additives are used in semiconductor industry. The chemistry used varies depending on the material used. During the etching of the eSTM trench, two materials must be considered; Si and SiO_2. As sketched in Figure III-7, the eSTM trench is composed of polysilicon alternating with the silicon dioxide of the STI. If remembering the STI process, it involves the etching of a pattern of trenches in the silicon and depositing one dielectric material (SiO_2) to fill the trenches. Table III-2 summarizes the reactive gases used for those materials.

Table III-2. Reactive gases used for Si and SiO_2.

Material	Reactive Chemistries
Si	CF_4/O_2, BCl_3 [70], CCl_4, CF_3Br [70,184], $SiCl_4$ [183,184] Hl [179], BCl_3/Cl_2 [180,183], Br_2/SF_6 [181, 183] SF_6, HBr, Cl_2, NF_3 [70, 179, 180, 182], CF_4 [179, 183,184] BCl_3/Cl_2 [180, 181], $HBr/Cl_2/O_2$, HBr/O_2 [180, 181, 183] SF_6, Cl_2 [70, 179, 180, 182, 183, 184], Br_2 [184]
SiO_2	CF_4 [182,183,184], CHF_3 [179, 182,184] C_3F_8, C_5F_8 [180, 182, 183,184], C_2F_6 [179, 180, 182, 183,184] F_4/H_2, CHF_3/C_2F_6, CHF_3/CO_2 [70], CCl_2F_2 [181,183] C_4F_8, SF_6, NF_3 [179], CHF_3/CF_4, CHF_3/O_2, CH_3CHF_2 [181] CF_4/O_2, $CF_4/CHF_3/Ar$, C_4F_8/CO, CH_2F_2 [180]

The most used chemistries for etching silicon are hydrogen- and halogen-based plasmas (F, Cl, Br) due to their high etch rates. Whereas F-based plasmas are generally used for isotropic etching, Cl- and Br-based plasmas are primarily used to achieve anisotropic etch profiles [88]. Generally, plasmas with large amounts of F atoms generation will etch Si faster than plasmas that contain large amount of Cl or Br, but profile control is harder to achieve, due to

the fast-isotropic etching by F atoms. For the case of etching silicon oxide, as for other dielectrics etching, the most used chemistries are fluorocarbon and hydrofluorocarbon usually with some additives [182]. To etch, chemical bonds need to be broken, so reactions that lead to bond stronger than Si-Si will etch silicon, and reactions that lead to bond stronger than Si-O will etch SiO_2. F-, Cl- and Br-based plasmas will etch the silicon because Si-halogens bonds are stronger than Si-Si bonds, however, only Si-F is stronger than Si-O bond and thus only F is preferred to etch SiO_2. Nevertheless, because of the ion bombardment, SiO_2 slightly etched in Cl- and Br-plasmas [185]. A brief introduction to some pure plasma chemistries such as F-, Cl-, Br-plasmas, are presented here:

- **Fluorine-based Plasmas**

  Fluorine plasma with silicon, as silicon dioxide, proceeds spontaneously without ion bombardment, inducing high etch rates and profiles nearly isotropic. Often, chlorofluorocarbons (CFC) are used to produce polymers deposition in parallel with the etching process and polymerization occurs simultaneously. Adding Hydrogen causes HF to form and the F/C ratio to drop, leading to more polymerization and less etching [183].

- **Chlorine-based Plasmas**

  Si and SiO_2 are not etched spontaneously at room temperature by Cl atoms making only ion-induced possible which is useful for etch directionality [186]. Chlorine atoms chemisorb on Si and form an ordered Cl monolayer which is barely influenced by temperature and will “inhibit” etching.

- **Bromine-based Plasmas**

  The low spontaneous etch rate of Si and SiO_2 with Br atoms, by creating a Br monolayer, has received considerable interest in RIE [187]. Including HBr in plasma the gas mix results in an improved etch profile. There are less undercut, more vertical sidewalls, and flatter trench bottoms, which are really important for high aspect ratio trenches. It is highly used since it makes the profile more anisotropic than when using Cl_2 alone being besides very selective [180].

Usually when selecting the chemistry, noble gases (typically Ar or He) are considered because they stabilize and homogenize plasmas that otherwise constrict or oscillate in the reactor. Furthermore, the “inert” addition can enhance anisotropic etching due to its effect on the sheath potentials [184]. For instance, Br-containing plasmas have tendency to form localized discharges under normal RIE processes conditions, which can be mitigated by diluting the HBr. Helium has been demonstrated to be effective for this purpose [188].

However, the chemistry selection requires some other criteria besides the nature of the materials being etched. Between these other criteria, the etch directionality and the etch selectivity are explained as follows.

1.2.2. Etch Directionality in RIE

Etch directionality is due to directed energy input into an etching reaction at a surface and can be accomplished by neutral, ion, electron or photon bombardment of a surface exposed to a chemical etchant [70,88].

1.2.2.1. Fluorine- vs Chlorine- vs Bromine-based Plasmas

Etching can be accomplished using F-, Cl-, and Br-based chemistries, which in all the cases, generate volatile etch products such as SiF_4, $SiCl_4$ and $SiBr_4$, respectively. In order to get a good directional etching, F-based is not the most suitable choice, since it results normally in a large undercut of the masking layer, indicating a large chemical etch rate [70]. As explained before, Chlorine and Bromine-based chemistry are primarily used for anisotropic etching profiles. Etch directionality can be explained by the fact that Si and SiO_2 are not spontaneously etched by Cl and Br atoms [186]. Furthermore, the F-C bond is stronger than the Cl-C or Br-C bond, so the electron impact dissociation of the mixed halocarbons produces especially Cl or Br atoms and the etching characteristics using these discharges are Cl- or Br- like. In both cases, for Cl- as Br-plasmas processes, a vertical sidewall inherently appears and helps therefore the vertical etching [185].

1.2.2.2. Etch Directionality Through Sidewall Passivation

The anisotropy control can be also obtained by the formation of a passivation layer on the sidewall which protects it from spontaneous etching reactions [179], as shown in Figure III-8. The formation of the sidewall passivation decreases the lateral etch rate compared to the etching where no sidewall passivation occurs. Hence, these sidewalls passivation are the key to achieve directionality etch.

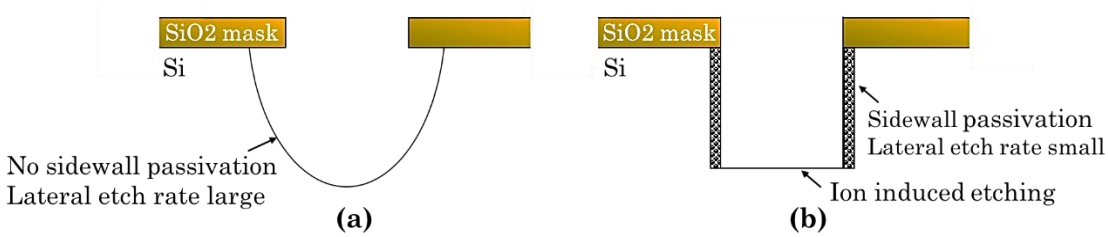

Figure III-8. Schematic of etching profiles a) without sidewall passivation and b) with the passivation [Adapted from 70].

The passivation prevents the sidewalls of the trenches of being exposed to ion bombardment and they will be covered by the etch-inhibiting film and prevents mask undercutting. The bottom of the trench which is exposed to ion bombardment is free from passivating film and etching reaction can proceed [70]. This is why sidewall passivation makes possible to achieve directionality. In addition, passivation of the sidewalls is observed for most reactive chemistries. It uses as precursor erosion and redeposition of masking material or formation of etch products with low volatility and redeposition. On the other hand, the presence of these passivation changes the etch rate, mask selectivity, etc. Thus, the control of the composition and the formation of the passivation layer is highly important for controlling the trench profile. This is why an important part of this thesis is related to the analysis of the passivation composition formed during the eSTM trench (3.2).

1.2.3. Etch Selectivity in RIE

Pattern transfers require that a substrate material would be preferentially etched with respect to the masking layer but also to other materials. A partially selective process can usually be improved by controlling the temperature or by using additives. For instance, the selectivity for F atoms etching Si over SiO_2 decreases exponentially with temperature [184]. Hence, selective-controlled materials etching is an essential part of plasma chemistry selection.

1.2.4. Literature Review on the Mechanistic Studies of Si and SiO_2 Etching

Since the eSTM trench, object of study in this chapter, implies the etching of Si and SiO_2 (STI), a brief state-of-the-art looking for the mechanistic studies of mixed plasmas chemistries used for etching those materials in the literature, is provided in this section. In most cases, a specific gas mixture or *"recipe"* is created for etching, taking into account the materials and the effect of the additives. Certain insights as the effect of the oxygen, hydrogen, nitrogen or other gas additions should be considered when creating the recipe [88,70,182]. Beyond this, some examples from the literature where mixed plasma chemistries have already been studied for etching Si as SiO_2 are presented.

1.2.4.1. Literature Review of Si and SiO_2 Etching in Fluorocarbon Plasmas

It is well known that F atoms are responsible for etching SiO_2 at room temperature unlike Cl, Br and H do not react with this material. Even if slowly, F atoms react with SiO_2 under these conditions. Furthermore, ion bombardment greatly accelerates this process. However, to satisfy the constraints of selectivity between SiO_2 and other materials (such as Si, Si_3N_4…) strongly polymerizing chemistries are required. This is why **Fluorocarbon plasmas** are used for selective etching of SiO_2. By using fluorocarbon plasmas, neutral CF_x radicals and

ions bombard surfaces and lead to the formation of a fluorocarbon film. It passivates the wafer surface by polymeric deposition, which is the most important aspect of etching SiO_2 in fluorocarbon-based plasmas [182]. This process is a competition between the deposition of the passivation film and the etching itself as represented in Figure III-9.

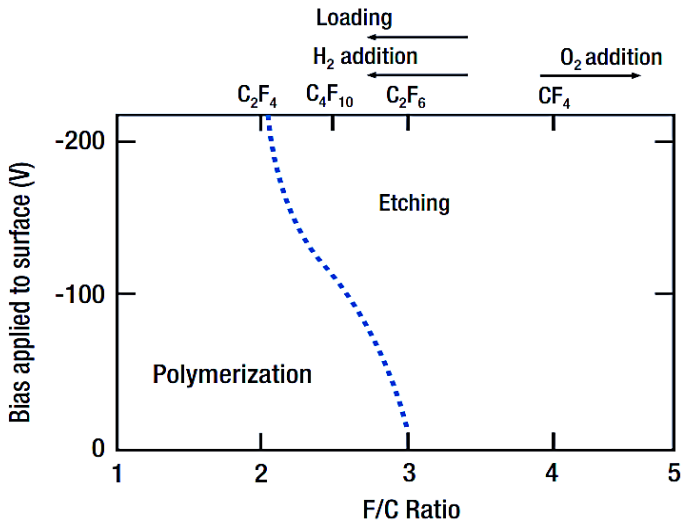

Figure III-9. The influence of F/C ratio and electrode bias voltage on etching and polymerization processes in a fluorocarbon discharge. [189,190].

Figure III-9 summarizes the study of the etching mechanism by using fluorocarbon plasmas which were extensively described by E. Hay et all in 1980 [190]. Unlike processes that rely on a sidewall film to suppress etching, the fluorocarbon film supplies reactants that are activated by ion bombardment. The film also improves selectivity toward etching of Si. If the deposition rate is too fast, then the film continues to thick and no etching occurs [182]. The polymerization has several origins; the passivating species may come from the gas phase (by deposition of etching products or by condensation of the species on the gas phase) or from the redeposition of species sprayed from the bottom of the trenches. Oehrlein et al have extensively studied these etching mechanisms for SiO_2 in fluorocarbon plasmas [191-194]. They have identified three distinct etch regimes mechanisms for SiO_2 (see Figure III-10.a) and have named them as: the fluorocarbon film deposition regime, the fluorocarbon suppression regime and the oxide sputtering regime. They also explained that the deposition rate of the fluorocarbon film depends on gas composition and self-bias voltage, as E. Kay et all. Under conditions when the etching rate for the fluorocarbon film is much slower than the deposition rate, a thick film grows and no etching occurs. If conditions are such that the film etching rate is much greater than the deposition rate, then little if any film will form on Si or SiO_2 [194]. Figure III-10.b shows the results of their study related to the deposition and etching rates of the film deposited in fluorocarbon plasmas for different feed gases as a function of the DC-bias voltage and hence ion bombardment energy.

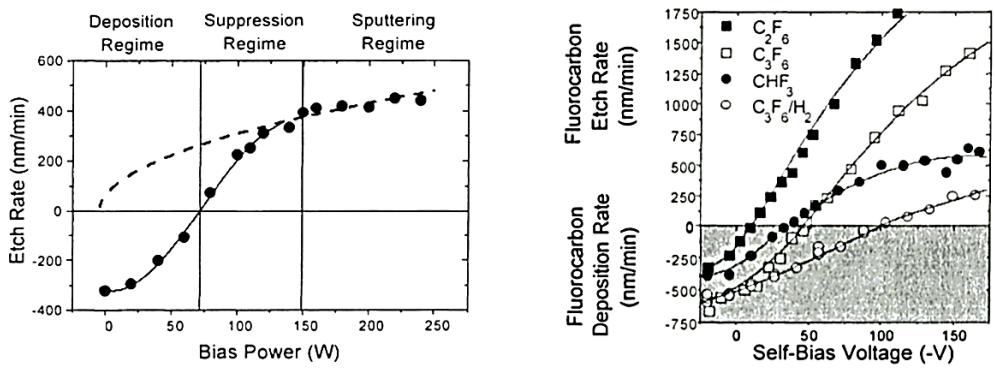

(a) **(b)**

Figure III-10. a) SiO_2 etch rate as a function of RF bias power level (40sccm CHF_3, 10mTorr operating pressure, 1400W inductive power) b) Fluorocarbon etch rates as a function of self-bias voltage at 6mT operating pressure in 1400W discharges fed with fluorocarbon plasmas [194].

In parallel to these studies, Coburn started to investigate the formation of these fluorocarbon films on Si and SiO_2 in CF_4/H_2 plasmas [195], where more carbon deposition was observed on the Si surface relative to the SiO_2 surface as hydrogen was added to the CF_4 plasma. He attributed the high selectivity of etching SiO_2 over Si to this difference in film thickness formed on Si and SiO_2. After Coburn, **the role of hydrogen** on the etching process has been extensively investigated in the literature. Standaert et al [196] reported the etching of silicon through a thick fluorocarbon layer for silicon etching in CHF_3, C_3F_6, C_2F_6 and C_3F_6/H_2 plasmas. By studying the role of H_2 they saw a change in the refractive index of the thick passively deposited fluorocarbon layer, where it was concluded that the composition of the fluorocarbon layer changes upon hydrogen addition. The H in the layer suppresses the F flux towards the silicon interface by the formation of volatile HF in the steady state fluorocarbon layer. This results in a thicker fluorocarbon layer and the suppression of the silicon etch rate. Roland et all [196] also studied the role of the fluorocarbon layer while proposing a new high density plasma SiO_2 etching process based on CHF_3/CH_4 mixture. They demonstrated that adding CH_4 to CHF_3, the SiO_2/Si selectivity improves considerably, through the formation of a thick fluorocarbon layer on Si. During the study, they were focused on the understanding of the deposition of this layer on the SiO_2 which played an important role in the etching mechanism and the role of neutral species such as C_xH_y and $C_xH_yF_z$ were pointed out for the fluorocarbon deposition mechanism. In summary, etching performances can be modified by using hydrofluorocarbons with F/C ratio less than 3, such as CHF_3 and CH_2F_2, to increase the selectivity [119]. Hyun-Kyu et al [197] showed that the addition of CH_2F_2 enhanced the production of fluorocarbon films by reactive C-F species, resulting in more fluorocarbon films deposited on the photoresist layer and the sidewalls compared to the CH_2F_2 being absent.

This finally led to drastic improvements in the critical dimension loss and the profiles. Figure III-11 shows the trench profile manipulation by decreasing the F/C ratio when inducing H_2.

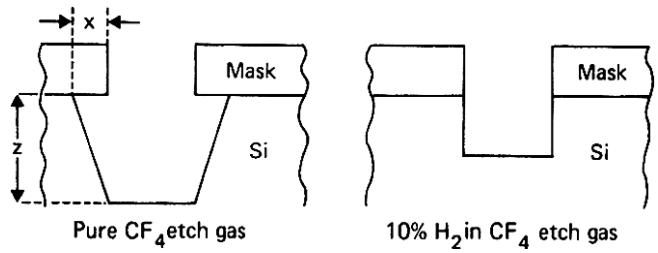

Figure III-11. Trench profile manipulation of the F:C ratio through hydrogen introduction [119].

The addition of amounts of O_2 is also known to play an important role in the mixed gases by increaseasing dramatically the F-atom density, thus etch rate in the discharge as it was described by D'Agostino et al [198]. Mogab and co-workers also presented the effect of oxygen additions to CF_4 plasmas for etching SiO_2 and Si [199]. They showed that for SiO_2, the variation in etching rate with O_2 is accounted by a proportional variation in F, the active etchant. As for the silicon, the etching occurs by a reaction with F atoms. Other gas additives have also been studied in the literature. **Noble gases** such as argon and helium have been added, as explained before, to stabilize plasmas. Xi Li and co-workers presented in 2002, the effect of Ar and O_2 additives on SiO_2 etching in C_4F_8-based plasmas [200]. They did a comparative gas-phase study of C_4F_8, C_4F_8/O_2 and C_4F_8/Ar plasmas. When a strong reduction of the fluorine content of the fluorocarbon steady-state layer, an increase in the thickness was seen. This was observed when up to 90% Ar was added to C_4F_8, coinciding with an increase of the Si/SiO_2 etching selectivity. They explained this change in the fluorocarbon surface chemistry by the strongly increased ion/neutral flux ratio characteristic of Ar-rich C_4F_8/Ar gas mixtures. Later, they presented their study about the characteristics of C_4F_8 plasmas with **Ar, Ne and He additives** for SiO_2 etching [201]. With their conditions (600W and 20mTorr), Ar addition gives rise to the largest ion current density, and He to the smallest ion current density. Fluorocarbon deposition rates on unbiased Si substrates were measured and was greater for C_4F_8 discharges with Ne or He additives than when Ar was added. Zhang and Kushner [202], in their study of the surface reactions during C_2F_6 plasmas etching SiO_2, developed a surface reaction mechanism for fluorocarbon plasmas. The mechanism describes the polymerization process as resulting from neutral sticking, ion sputtering, F atom etching, and low-energy ion assisted deposition. The etch mechanism is a multistep passivation process which results in consumption of both the polymer and the wafer, as represented in Figure III-12. The major steps in the mechanism proposed in their study were as follows. Polymer layers grow on the SiO_2 surface by C_xF_y deposition. Low-energy ion bombardment activates polymer surface sites while ion sputtering (F atom etching) and ion assisted polymer–wafer interactions consume the polymer. A steady state thickness of the polymer

may be reached as a balance of its deposition and consumption. SiO_2 etching results from a polymer–wafer interaction which consumes both the SiO_2 wafer and the polymer. Chemisorption on SiO_2 sites from either the polymer or directly from the plasma produces SiF_xCO_2 which dissociates to SiF_x sites upon ion bombardment or F atom interaction. The SiF_x species are then removed by either ion chemical sputtering or F atom etching. The polymer passivation layer limits mass diffusion and dissipates energy. Thus, the rates of reactions involving energy transfer or species diffusion through the polymer, depend on the polymer thickness [202].

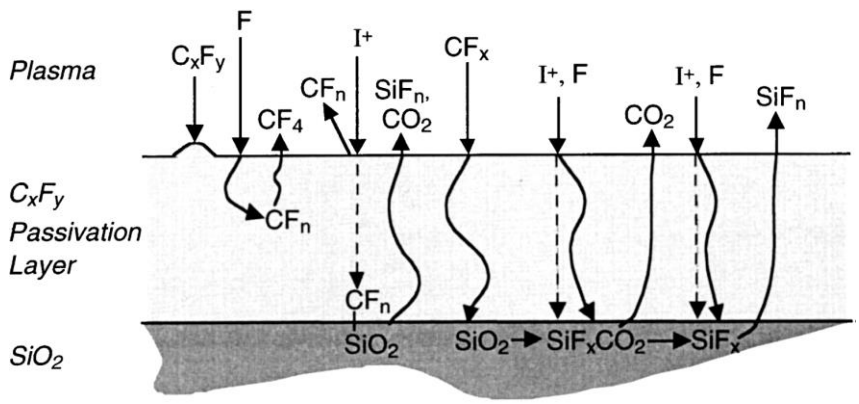

Figure III-12. Schematic of the surface reaction mechanism for fluorocarbon etching of SiO_2. I^+ represents ion species, the dashed lines represent energy transfers through the polymer layer and the curved lines represent species diffusion through the polymer [202].

So far, numerous studies of etching Si and SiO_2 in fluorocarbon plasmas can be found in literature. Here, some examples showed up that when using C_xF_y radicals as the precursors, a fluorocarbon passivation film is formed. Furthermore, this etching is conditioned by the F/C ratio which is strongly influenced by the bias power. When including some additives in the plasma, the chemistry turns about a more selective one and the etch profile becomes much more anisotropic.

1.2.4.2. Literature Review of Poly-Si Etching in Halogen Plasmas

When etching only Poly-Si, several gas combinations are used in RIE reactors to produce vertical trench sidewalls. These etch chemistries have evolved from F to Cl to Br. Furthermore, the chemical etching of Si by halogen atoms at room temperature follows this trend (F>Cl>Br), but the dopant type and level highly affects the Cl and Br reactivity [182]. When etching with fluorocarbon plasmas, the mechanism related to the passivation are identical to those described above for the SiO_2 etching (1.2.3.a). **SF_6 plasmas** have been extensively studied for etching vertical profiles, but it is always necessary to include an additive since, alone, they cannot etch anisotropically. Gomez et al [203], explained that the anisotropy cannot be reached without adding O_2 when etching with SF_6 plasmas. They

explained that increasing the SF_6/O_2 ratio in the feed gas increases the F/O ratio in the plasma and so the sidewall passivation by O atoms cannot keep up with the chemical etching by F atoms. As the F-to-O ratio is decreased, effective sidewall passivation by O_2 results in nearly vertical sidewalls. The temperature plays still an important role in these processes. One year later, they studied the **$SF_6/O_2/Cl_2$** plasmas [204], in order to increase the vertical etching rate by creating volatiles species such as $SiCl_4$ besides the SiF_4. In this case, the passivation layer created was SiO_xCl_y. Hwang et al [205], were the first interested in the use of Br for etching silicon, since it does not generate a chemical etching. In 2005, Gomez et al [204], taking advantage of this, used the HBr in complement to the gas mixture SF_6/O_2. They found out that by using **$SF_6/O_2/HBr$** the H_2 molecules coming from the dissociation of the HBr were able to modified the F-/O ratio of the plasma and the etch kinetics. This is because H_2 causes a reduction of the F concentration in the gas phase of the plasma. However, in terms of selectivity (Si/SiO_2), Cl_2, HBr, or their mixture are better choices when vertical or near vertical walls are desired. Nevertheless, when using Cl or Br there is no deposition layer (*passivation*) on the sidewalls, but profile control and loading are easier to achieve than by using F due to the fast isotropic etching by F-atoms. In order to improve the anisotropy of the process when etching with Cl_2 and/or HBr is necessary to add a ***passivating component***. **The role of O_2 addition** is therefore highly important. When etching with SF_6 the O_2 is needed for controlling the anisotropy of the process by creating thin SiO_xF_y layers. When etching with Cl_2 and/or HBr, O_2 is required for reaching vertical trenches with the help of the sidewall passivation. Without this addition, neither Cl_2 nor HBr could generate this layer. Mainly, the O_2 addition contributes to the sidewall passivation but also improves selectivity to underlying oxygen-containing layers such as SiO_2 [182]. Furthermore, the O_2 addition has also an impact on the profile in function of the mask [179]. With a resist mask, stronger mask charging and sidewalls attack (foot removal). With a hardmask, higher ion flux and availability of O_2 for creating SiO_xBr_y/ SiO_xCl_y formation.. This is sketched in Figure III-13.

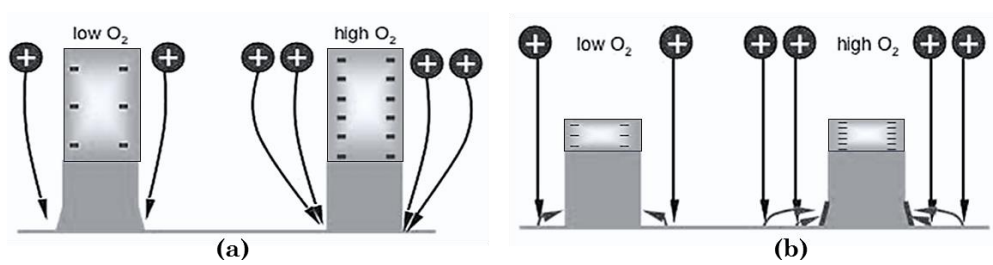

Figure III-13. Effect of the O_2 when using a resist mask (a) and a hardmask (b) [179].

Chang et al [206], studied the effect of O_2 addition, microwave power and RF power for a high selective etching of polysilicon with the three halogen-bearing plasmas (SF_6, Cl_2, and HBr). They found out that the maximum etching rate and selectivity in the three cases occurred at concentrations where oxygen was added; about 7.5% for SF_6 plasmas, 5% for Cl_2 plasmas and 3% for HBr plasmas. Furthermore, they observed that the selectivity to oxide was related to

the amount of silicon halides that were produced during poly-si etching and the electrically polarized level of these products when they adsorb on the oxide surface. They concluded that the selectivity on oxide is approximately infinite for the HBr system. In their study, they proposed the HBr gaseous system for satisfying the VLSI applications since it exhibited excellent etching characteristics. In contrast with the SF_6 gaseous system that obtained the lowest selectivity and anisotropy among the three gaseous systems studied. Several studies have been carried out for the etching of Si with **Cl-based** plasmas obtaining good results, as the one of Schwartz and Schaible [207] who studied the etching of Si using Cl/Ar RIE. In their study, the use of Cl_2 resulted in very directional profiles. When etching silicon using **Cl_2/O_2** and even **$Cl_2/O_2/HBr$** plasmas leads to SiO_xCl_y-like passivation on the sidewalls. Typically, a composition gradient is presented: the surface layer is more Cl-, H- and Br-rich, while the bulk layer is more oxidized [208]. Recently, the use of **Br chemistry** has received considerable interest in RIE. Bestwick et al [188], studied the characteristics of Si and SiO_2 etching in HBr reactive ion etching plasmas by measuring etch rates, optical emission, cross-sectional analysis, and XPS analysis. They found that the reaction layer on silicon due to HBr reactive ion etching is typically very thin, of the order of 1 monolayer thick. Fukasawa and co-workers [209], characterized the structural and electrical properties of **HBr/O_2** plasma damage to the Si-substrate. They saw that in the case of HBr/O_2 plasma-induce damage, H generates the deep damage layer and ion-enhanced diffusion of oxygen causes the thick surface oxidation. Etching with HBr implies low etch rate and the formation of residues on the wafer and the chamber walls. But, as Chang et al proposed [206], the HBr gaseous system exhibited excellent etching characteristics. Some of the most important reasons for moving to HBr are its better selectivity, more isotropic profile, and mainly less formation of micro-trenching. Vyvoda et al [211], studied extensively the effects of plasma conditions on the shapes of features etched in Cl_2 and HBr plasmas. Figure III-14 shows the evolution of the microtrenching in time by using Cl and HBr. As it can be seen, even if with the time both systems have been improved, microtrenching is much worse when using Cl_2 than HBr.

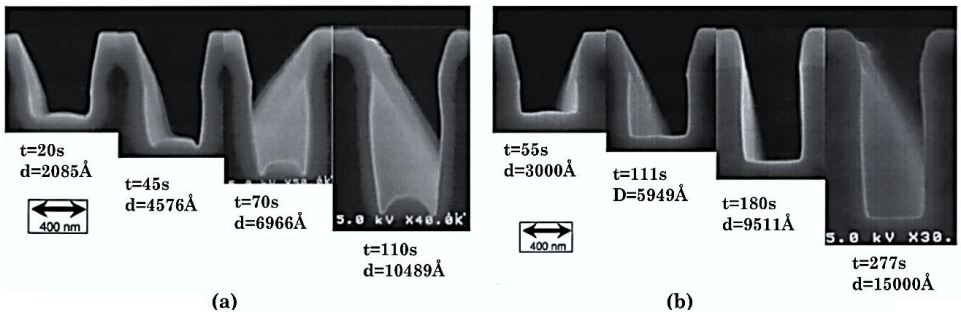

Figure III-14. Microtrenching evolution in time for Cl-plasmas (a) and HBr-plasmas (b) [210,211].

In their study [211], they observed microtrenching formations under certain plasma conditions and they proposed that it could be reduced by using higher bias powers. When a

HBr plasma was used instead of Cl_2, the etching rate decreased by 50%, but the etching profiles were more vertical and the trench bottoms were flat. They found as well, some isolated lines etched in the HBr plasma, which revealed broad but shallow microtrenches near the edges of the line. However, the microtrenching was much worse for Cl_2 than HBr plasmas.

Hence, experimental results from different studies, confirm that the use of halogen gases are useful plasma sources for Si etching applications. Mainly, Cl_2 and HBr are highly recommendable when vertical trenches are targeted. Being the Cl_2 more suitable when high etch rate is necessary and HBr when really small features are sought, since it is able to reach more isotropic profile without microtrenching formation. Furthermore, it is the most selective when adding O_2. The experimental details as well as the selected chemistry used during this study will be detailed in next section.

2. EXPERIMENTAL APPROACH

Besides the information of the eSTM introduced in Chapter I and 1.1.3, this section seeks to increase the knowledge related to the experimental details that would be necessary for the understanding of the rest of the chapter; the characterization and optimization of the process etch. For that purpose, the technology and the specifications of the etching process will be presented in this part.

2.1. Fabrication Process

The operation of the eSTM cell is identical to a NOR Flash with a selection transistor. This new technology, the eSTM, is based on another technology already in production at STMicroelectronics, the M10+. However, some constraints are linked to the process of realization of the vertical transistor, since it is completely new. The fabrication of the cell consists of a succession of steps, similar to the Flash but with additional steps that are explained as follows.

2.1.1. The Necessary Steps for Reaching the eSTM Trench

The eSTM trench after etching was sketched together with a SEM section in Figure III-7. Here, the main steps for performing this trench are represented in Figure III-15. These steps share the standard flash steps. Once the active/STI are defined, the STI is filled with SiO_2. Then, a perpendicular trench to the active lines is created. To do this, a hardmask is required. This hardmask will allow the etching of the active/STI areas while protecting those other areas that should not be etched. Details about this hardmask are described in 2.2.1. When

the photolithography step ends with the masking and photolithography, the etching of the eSTM trench starts. The etching process, that will be explained in details in the following sections, could be divided into 2 main etch steps. The first one consists in etching the Si together with the SiO_2 (STI). The second one is the final one since will reach the required dimensions for the eSTM trench into the silicon (7000Å). Afterwards, the trench will be filled with polysilicon. Since this study is based on the characterization and optimization of the plasma etching process involved for the creation of this trench, further details about the following steps are not necessary. However, specifications about the process etch will be presented in 2.2.

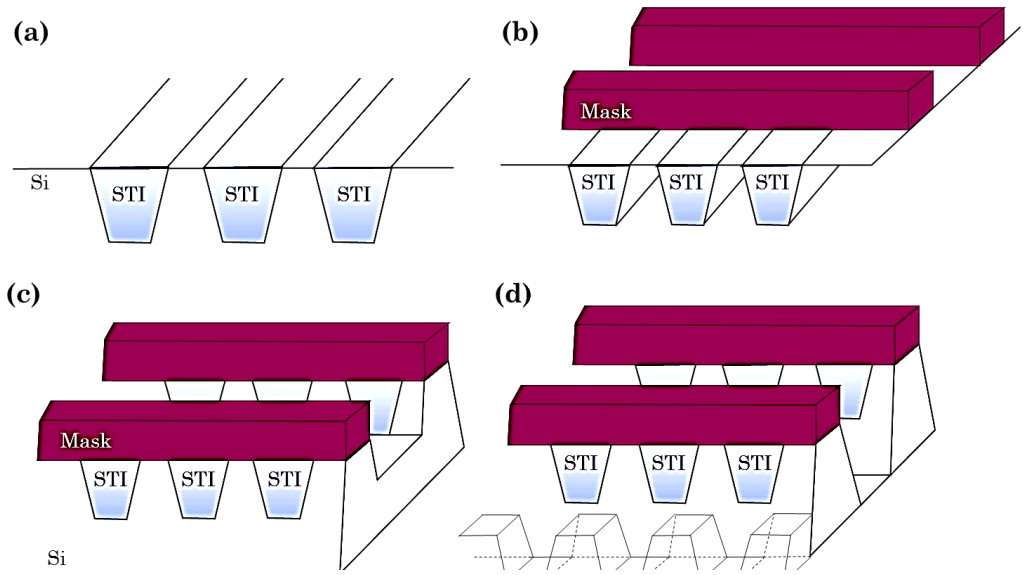

Figure III-15. Schematic representation of the main steps for performing the eSTM trench. a) starting from the standard flash active/STI, b) masking and photolithography, c) etching the first part of the trench and d) final etching step for reaching the eSTM trench.

The residues of polysicon of the Figure III-15.d are due to the chemistry used for etching that will be explained in the following section.

2.1.2. The Selected Chemistry for the eSTM Trench

In order to choose the suitable chemistry for etching the trench of the eSTM, two main steps have been considered. The first step required the etching of SiO_2 of the STI together with the silicon of the trench. The second step starts when the STI ends and just the silicon needs to be etched. Figure III-16 schematizes the two main steps of the trench. For the first step (Si/SiO_2), the selected chemistry was $CF_4/CH_2F_2/He$; whereas that for the second step (Si), the selected chemistry was $HBr/O_2/He$. The decision was based on the needs of each process. The first step required a strongly reactive chemistry since it was necessary to etch both Si

and SiO_2 at the same time. The second step required a highly selective chemistry. Based on these requirements and with the background of the literature for etching Si and SiO_2 presented previously in 1.2.4, an F-based chemistry was the most suitable in terms of reactivity for the first step as a Br-based was the adequate for performing a selective *deep* vertical trench. In the first step, we chose CF_4 as main gas but etching together with CH_2F_2. By adding CH_2F_2 gas, the production of fluorocarbon films by reactive C-F species is enhanced, as explained before. Even the etch selectivity to photoresist was also enhanced in the presence of CH_2F_2 due to hydrogen atoms as well as reactive C-F species. In the second step, the HBr was selected because of its selectivity. Moreover, by adding O_2, the passivation on the sidewalls occurs easily. However, during the first chemistry (F-based) there is a difference between the etch rate of Si and SiO_2 that leads to the *residues* represented in Figure III-15.d and Figure III-16.b. These residues are just peaks of silicon.

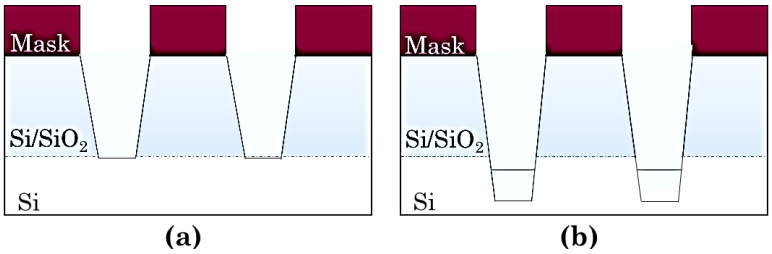

Figure III-16. Scheme of the two main etch steps of the eSTM trench a) firs step; Si/SiO_2 etching and b) second step; polysilicon etching.

During the first step, the F-atoms are able to etch the complete STI (450nm) but only 78nm of silicon. Therefore, it can be observed (Figure III-17) that the depth of the trench is not identical between a cross-section along the active (450nm) and along the STI (700nm).

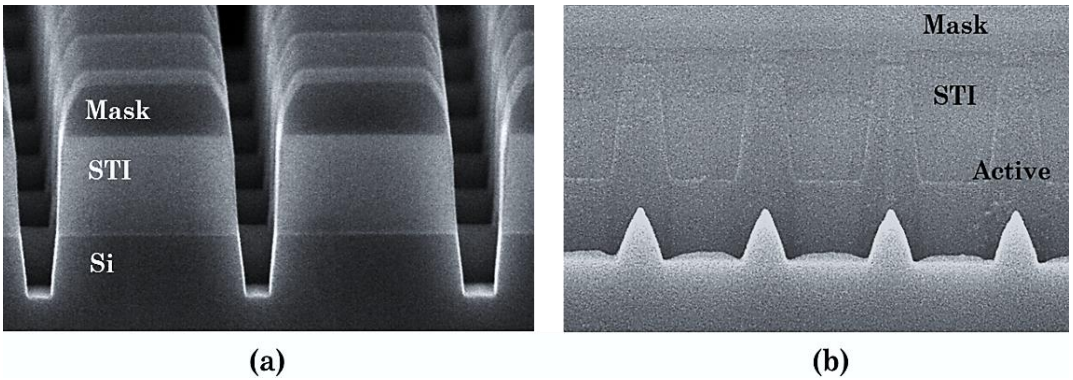

Figure III-17. SEM cross-section of the eSTM. a) Perpendicular to the trench, b) Parallel to the trench. The silicon peaks can be seen in both images.

2.2. Specifications

In this part, the stack composition will be described followed by the etching specifications of the recipe. Finally, a physical characterization of all the steps of the recipe will be performed.

2.2.1. Stack

As explained before, a hardmask is necessary for the etching of the eSTM trench. The required stack for this process is represented in Figure III-18.

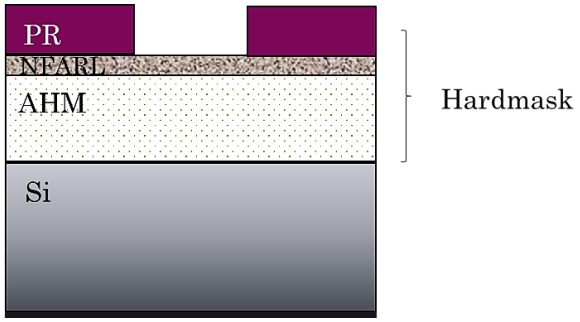

Figure III-18. Required stack for the etching of the eSTM trench.

The silicon part, represented in Figure III-18 as Si, included the Si as the SiO_2. The harmask is composed of NFARL and AHM. Those materials were already introduced in Chapter II. The PR, which is deposited during the photolithography step, measured 3750Å. NFARL and AHM, both of them deposited by PECVD, measured 275Å and 4000Å respectively. Due to the required depth for the trench (7000Å), a high resolution PR is necessary. The PR used has a wavelength of 193nm. In addition, NFARL and AHM were mandatory to protect the areas that should not be etched until reaching the end of the trench. NFARL is used for controlling the CD whereas that the AHM is used to protect the covered areas from the implantation. Besides, since the AHM is C-based material (a-C:H), it can be easily removed after the etching process. Usually, the BARC is situated between the NFARL and PR, but for this process in order to avoid another layer to be etched, the BARC have been replaced by HMDS (Hexamethyldisilazane). The HMDS is as the BARC an antireflective material but it does not impact the etching process.

2.2.2. Etching Specifications

The *recipe* used for etching the eSTM trench is sketched in Figure III-19. It is composed of 5 etching steps. This 5 steps are the etching of the NFARL, the etching of the AHM, the over-etch of the AHM, the first main step (Si/SiO_2) and the second main step (Si) which is the final one. As explained previously, the etch rate of the SiO_2 during the step four of this recipe, it

is much faster than for etching Si. However, during the final step, the Si etch rate increases strongly by using the Br-plasma.

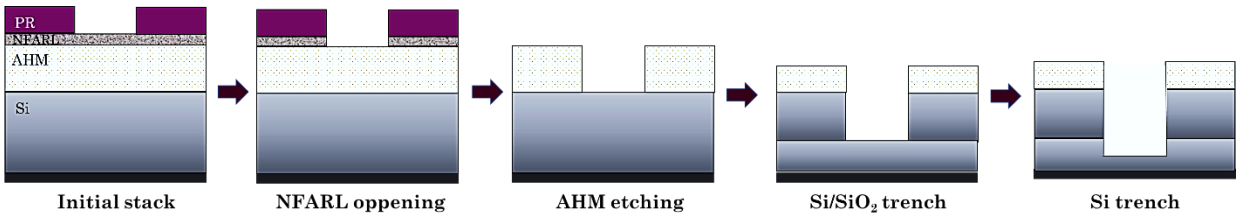

Figure III-19. Schematic representation of the five etching steps of the eSTM trench.

Here, the AHM overetch step is not represented, since it is somehow included on the AHM step. During this overetch the chemistry used is the same, the goal is to "clean" the residues of AHM that could remain after the main etch of this material. Henceforth, we could refer to the fourth step (Si/SiO_2) as STI trench and to the final one (Poly-Si) as eSTM trench. The chemistry used during the NFARL step, $CF_4/CH_2F_2/He$, is only responsible for the NFARL opening. A F-based chemistry was required since the NFARL is kind of oxide-type material. Then, the AHM which is C-based material is etched with $Cl_2/HBr/O_2$. This chemistry is selective and it is just directed to etch the AHM. The following layer is the STI, but first, just after the etching of the AHM which takes 50sec we perform an overetch of 29% of time in order to eliminate the possible residuals of AHM that can remain on the sidewalls. During the overetch the etching is lateral. There is no risk of etching the following layer (Si/SiO_2). After having etched the hardmask, the first main step starts, the STI trench. As explained before, during this step, the etching rate of SiO_2 is faster than for Si (3780Å/min vs 840Å/min, respectively) but since it is F-based ($CF_4/CH_2F_2/He$) and so that non selective, it is able to etch both even with different rates. Finally, the etch of the eSTM trench, which is Br-based (HBr/O_2), etch the silicon deeply and vertically but being at the same time strongly selective respect to the SiO_2. The etch rate of the Si etching during this step is 3015Å/min. The temperature is constant during all the recipe (Inner/Outer: 60/60°C). The specifications of this recipe for each step are summarized in Table III-3.

Table III-3. Etching specifications for each step.

Parameter	NFARL	AHM	AHM OE	STI	eSTM
Pressure (mTorr)	**15**	**5**	**5**	**7,5**	**30**
TCP RF Power (W)	**445**	**800**	**800**	**1130**	**1000**
Bias RF Voltage (V)	**135**	**400**	**400**	**275**	**360**
Process time (s)	**28**	**50**	**0**	**70**	**76**
OverEtch (%)	0	0	**29**	0	0
Cl_2 (200sccm)	0	**20**	**20**	0	0
HBr (1000sccm)	0	**150**	**150**	0	**450**
CF_4 (200sccm)	**40**	0	0	**105**	0
He (500sccm)	**250**	0	0	**270**	0
O_2 (20sccm)	0	0	0	0	**10**
O_2 (200sccm)	0	**100**	**100**	0	0
CH_2F_2 (100sccm)	**15**	0	0	**75**	0

2.2.3. Morphological Study of each Step

In order to get an idea of the morphology and the dimensions of each step of the process, a physical study was performed. The SEM cross-sectional images are shown in Figure III-20.

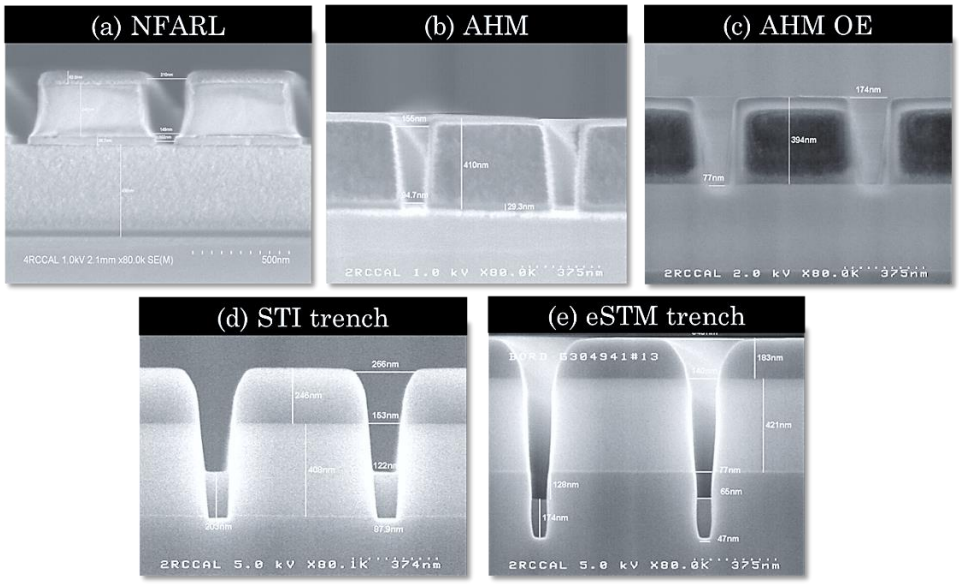

Figure III-20. SEM cross-section of the etching steps of the eSTM trench with the AHM mask. a) NFARL, b) AHM, c) AHM OE, d) Si/SiO_2 trench, e) Poly-Si trench.

As it can be noted, the CD changed continuously, being at the end of the process (STI trench to eSTM trench) where less differences occur. The variability from one wafer to another plays also a role in those changes. It can be appreciated as well, in Figure III-20.d (the STI trench) and Figure III-20.e (the eSTM trench) the residues of silicon that have been previously mentioned.
A similar study was performed at the end of the chapter for the optimization of the process, trying to be more representative of what happens just after each step. Thus, without considering the AHM.

3. CHARACTERIZATION

The aim of this section is to characterize the etch process of the eSTM trench since it is a completely new process at STMicroelectronics. The methods used for this study are OES and XPS. Spectroscopy techniques have been widely used for plasma process monitoring and control. By using these two methods we could understand the reactions that are taking place during the etch process. OES is used in order to know the species in the plasma and XPS to analyze the chemical composition of the sidewalls; the passivation layer. The idea was to increase our knowledge about the plasma-surface interactions.

With OES, a simple study looking for the species identification during the final trench was performed. With XPS, we have monitored the two main steps of the etch process; the STI trench and the eSTM trench. For that purpose, specific analyses have been performed as they will be explained in each subsection (3.1. and 3.2.) where the particularities of each study will be developed. Furthermore, the study of the AHM is necessary for the understanding of the process, so it has been taken into account for the characterization of the process.

3.1. Plasma Diagnostics

The first part of the characterization is related to the identification of the species that are active through the plasma while etching the trench. As it has been established in Chapter II (3.1.3.), OES is one of the most extensively used diagnostic technique for in-situ plasma monitoring [127,128,133]. The majority of optical emissions in etching plasmas is a result of electron impact excitation. Most atomic and diatomic species can be monitored by OES, but due to the complexity of the excitation mechanism, OES is usually a qualitative technique. Only excited species in plasmas are detected and so the observed spectrum gives information about the excited-state density and does not directly reflect the ground-state population profile [213].

In this section, spectra that have been taken during the process are analyzed looking for the element identification. The goal was to have a basic idea of the species involved in the plasma-

phase to facilitate the understanding of the plasma-surface interactions (3.2.). No species density or quantification of them are studied.

3.1.1. Background

3.1.1.1. Mechanisms for Optical Emission

Plasma-induced emission can result from several different excitation processes [212], such as electron impact excitation (III.1), electron impact dissociation (III.2) or chemiluminescence recombination (III.3). Where A and B are atoms or molecules, AB and BC are radicals or molecules, the asterisk (*) indicates the excited emitting species, and e^- (+ M) may be either a neutral species, a negative ion, an electron plus a third body (M), or a surface [213].

$$A + e^- \rightarrow A^* + e^- \quad \text{(III.1)}$$

$$AB + e^- \rightarrow A^* + B + e^- \quad \text{(III.2)}$$

$$A + BC \rightarrow AB^* + C \quad \text{(III.3)}$$

Lineshape measurements can distinguish process (III.1) from all others. Since the electron mass is small compared to atomic or molecular masses, the velocity distribution of the emitting species formed in reaction (III.1) is the same as the ground state, which is in turn equilibrated with the gas temperature.

3.1.1.2. Literature Review on Plasma Etching Diagnostics by Using OES

Optical emission during plasma processing may come from neutral or ionized atoms, radicals, or molecules that have been electronically excited. This type of emission has been critically reviewed by Donnelly [212], Herman [213] and Dreyfus [214]. It was first used in an etching application by Harshbager et al [215], both to probe and control the etching of with CF_4/O_2 in parallel plate plasma. They studied the spectroscopic analysis of optical emission during RF plasma etching to gain a better understanding of the plasma chemistry involved in those systems. They identified F, O, Si and CO emissions and showed that F and Si emissions exhibited a maximum as a function of O_2 addition to CF_4. The F* and O* emission decreased greatly when a silicon wafer was introduced because these atoms were consumed during etching; while the CO bands were unaffected. Jung et al [216] studied the molecular emission of CF_4 in low pressure ICP. The analysis of the spectra showed the CF radical but the other CF_x radicals were not seen, whereas strong C and C_2 emissions, dissociation products of CF_4 gas, were observed. Hansen and Engeln [217] also studied the detection of hydrocarbon radicals during plasma etching processes. Since then, many similar studies have been conducted on etching species [218-220]. Besides, some other studies by using OES have been extensively developed as well. Dreyfus et all [214], in 1985, discussed between other optical techniques, the OES with actinometry, proposing the advantage to be able to quantify the

species. The same year, Shabushnig et al [221], summarized the applications of OES to semiconductor processing. Their idea was to present several examples serving as a brief introduction to both chemists and process engineers. Some years later, G. Gifford [222] also described the applications of OES in plasma manufacturing system. In his study, he explained that to properly identify a specific chemical species in complex gas mixture, the OES analyses must be performed with a high resolution equipment. He illustrated how a high resolution spectrum from OES should be (Figure III-21). Hershkowitz and Breun [223], pointed out that plasma processing diagnostics play two different roles- characterization and control. The goal of plasma characterization is related to establish connections of data with external parameters and to verify models. The goal of control diagnostics is to make noninvasive in situ measurements of relevant processing parameters.

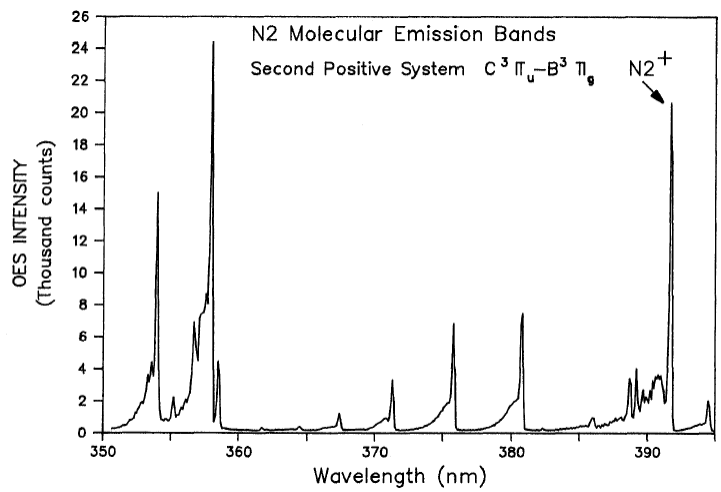

Figure III-21. High resolution OES spectrum of nitrogen plasma [222].

Using OES for a slightly different purpose, in 1996, Ino and co-workers [224] studied how to enhance the chamber cleaning in-situ by evaluating extracted plasma parameters obtained with OES. At the end of their study, they confirmed the accuracy of the technique with a RF-plasma direct probing method and by ion current measurements. Not far from this, Miwa and Kawabata [225] used OES for in-situ quantification of the deposition amount in a Poly-Si etch chamber. In this study, they described an attempt to estimate the deposition amount. They found out that the quantity of the deposition increased as a function of cumulative etched wafers in the etch chamber. In addition to all these uses, optical emission can be used to detect tool and process malfunction in plasmas used for etching and other processes by monitoring emission from discharge-excited impurities. This was explained by Selwyn [226] with several examples such as N_2 emission at 337.1 nm, which can indicate an air leak; OH emission at 306.4 nm indicating dissociation of water vapor or CO emission at 483.5 nm can indicate residual photoresist on the surface.

3.1.1.3. Representative Emission Lines

Table III-4 compiles a selection of emission lines detected in OES obtained from literature by different research groups and companies[1].

Table III-4. Representative emission lines of some species from literature.

Species	λ (nm)
Si	212,41; 220,79; 221,08; 243,51; 250,69; 251,61; 251,43; 251,29; 390,55 [216] 288,2 [118,227,228]; 251,5; 288,08; 390,48 [238]; 504,1; 505,5; 634,7; 637,1 [228]
O	777; 843 [70,88]; 777,2 [118,227,228]; 777,38; 844,7 [118,228]; 844,6 [65] 615,6; 615,7; 615,8; 645,6 [228]; 437; 497; 502; 533; 544; 605 [241]
F	704 [70,88]; 703,7 [65,118,227,228]; 677; 683; 686; 687; 690; 691; 697 [241] 683,4; 685,6; 690,9 [228,232,233]; 634,8 [228]; 712,8 [118,227,228]; 685,4 [118,227]
Br	834,37 [65,228,230]; 827,5 [218]; 470; 479; 570; 576; 588 [241]; 440; 450 [240] 827,24; 780,30; 793,87; 751,30; 734,85; 844,66[228]; 656 [230]; *460-480* [239]
H	656 [70,88,217,230,241]; 653,3; 410; 486,2 [228,229]; 656,5 [118,217,227,228] 486 [228,241]; 434 [228,231,241]; 486,1 [118,217,224,227,228]; 434,1 [229]
He	706 [225]
C	247,86 [228,229,216]; 248 [241]; 283,7; 426,7; 732,6 [228]; 597,36 [216]
C_2	516,5 [228,234]; 410; 563,55 [229]; 473,71 [229,234] 471,52; 496,76; 468,48; 467,86; 466,87 [234]
N_2	337 [70,88,227]; 315,9; 337,1 [228]
H_2	600 [229]
CN	387 [70,88, 227,228]; 289,8; 304,2 [228]; 410; 388 [229]
CO	484 [70,88]; 483,5 [227,228,224]; 519,8 [227,228] 292,5; 302,8; 313,8; 325,3; 482,5 [228]; 431,4; 520; *432-434* [231]
CH	431,4 [217,231,229]; 388,9 [217,229] 432,3; 438,5; 430; 390; 314; 387,13; 388 [229]
OH	309 [70,88]; 308,9 [227,228]; 281,1; 306,4 [228]; 306 [216]
CF	202,5; 209,7; 210; 213; 247; 240; *220-320* [216]
CF_2	251,9 [227,228]; 600; 202,5; 209,7; 210; 213 [216] *250-350* [232]; *470-720* [235,236]; *220-320* [216]
CF_3	*255-275* [237]; *220-320* [216]
CH_2	216 [229]
CH_3	537,5 [229]
SiF	440 [70,88, 228,227]; 440,1 [228] 436,82; 440,05; 443,02; 446,20 [224]; 777 [70,88,118,228,227]
SiBr	290 [132]; 308 [225]
SiF_2	390,15; 395,46 [224]

[1]LAM Research [228], which provides the hardware specifications with the equipment.

The emission lines from this table are a collection from the literature. The series are signaled in blue italic. These wavelengths will be used in 3.3.3. for the analysis of our spectra. However, there are numerous tables for identifying all the rest of species if necessary [129,130,131]. This selection from the literature is based on the emission lines that may be involved in our process and so it will be useful for the following part.

3.1.2. Experimental

3.1.2.1. Experimental Set-up

Specifications about all the equipment used for this thesis, were introduced in Chapter II. The experimental set-up for this study includes:

- The plasma reactor: 200mm *VERSYS STAR* from LAM Research (Chapter II. 2.1.1.)
- The OES spectrometer: *OES Plus on Flex45* (Chapter II. 3.1.3.2.)

The spectrometer is mounted on the plasma equipment as it can be seen in Figure III-22. In that way, emissions from the plasma can be collected by the equipment. Emissions from 220-900nm are collected with this equipment.

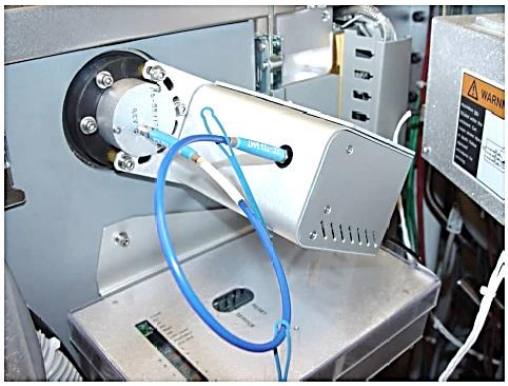

Figure III-22. OES equipment used for this study.

3.1.2.2. Substrates

The substrate was a patterned wafer where all the etching process steps for reaching the eSTM trench have been performed. The final step, where the eSTM trench is etched has been monitored in order to be analyzed. With the aim of analyzing the optical emissions during the etching of the eSTM trench, we performed, additionally, some previous analyses carried out across a typical silicon wafer and across a silicon wafer with a coating layer of amorphous hydrogenated carbon (AHM). This will enable us to understand how the chemistry employed to etch impacts different surfaces. Furthermore, we could differentiate the Si and AHM

contribution to the spectrum of the eSTM etching. A schematic representation of the substrates is shown in Figure III-23.

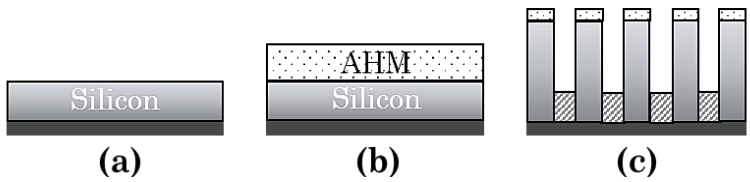

Figure III-23. Schematic representation of the substrates uses during this study a) full silicon wafer non patterned, b) full silicon wafer with a AHM(a-C:H) deposition of 4000Å non patterned and c) patterned wafer during the process etching of the eSTM trench.

3.1.2.3. Chemistry Considerations

We have monitored the two etch processes. They are related to the STI trench and the eSTM trench. As it has been introduced in previous sections; the first process, related to the STI trench, uses F-based plasmas ($CF_4/CH_2F_2/He$). The second one, related to the eSTM trench, uses Br-based plasmas (HBr/O_2). However, the eSTM trench is performed just after the STI trench, so F-based considerations might be needed for the analysis. Therefore, the second etch process is performed using the two steps, the first one with CF_4/CH_2F_2 as in the first etch process, followed by a second step using HBr/O_2, to finalize this process. This is summarized in Table III-5, where Run#1 would be the conditions for the STI trench study, and Run#2 would be the conditions for the eSTM trench study, as explained, Br-based chemistry but preceded by a F-based chemistry.

Table III-5. Experimental gases set for the spectral analysis.

Run #	Gas flow (sccm)				
	CF_4 (200sccm)	CH_2F_2 (100sccm)	He (500sccm)	HBr (1000sccm)	O_2 (20sccm)
1	105	75	270		
2*	105	75	270		
				450	10

*The Run#2 is composed of 2step, the first one which is the same as the first run followed by the second one: HBr/O_2.

During the plasma diagnostic study, the first process (Run#1) will be referred to F-based chemistry and the second one (Run#2) to Br-based chemistry as it will be focused on the second step (HBr/O_2).

3.1.3. Results

The results are presented in two parts. The first part is performed with non-patterned wafers. The goal of this part is to identify the different behavior of each material during the etching process. The two chemistries (F-based and Br-based) are regarded in order to see the influence of each one. The second part is dedicated to the analysis of the patterned wafer which is the spectrum monitored during the real etching of the eSTM trench.

Identification of species was made by comparing observed spectral lines with compiled list of known lines. All the references for the wavelength used during this section can be found in Table III-4.

3.1.3.1. Influence of the Chemistry over Different Materials: AHM and Si

The two main chemistries employed for reaching the eSTM trench are studied in this part. Firstly, the F-based chemistry related to the STI trench step, where both AHM (mask) and Silicon are involved. Secondly, the Br-based chemistry related to the eSTM trench, where these two materials are still involved after being exposed to the F-based chemistry in the previous step. Thus, this section is organized in function of the chemistry used, in that way the different behaviors of the material can be shown under the same conditions. It must be remembered that those studies were performed over non-patterned wafers, and so the only interactions considered were the interactions plasma-surface of the material being studied each time. No interaction with other materials were considered. It should be noticed that the background of the spectra is not always flat since the noise, offset, and baseline filtering methods were not used here. The goal is to have an idea about the species present in the plasma and not to quantify them.

- **F-based Plasma**

First, we studied the fluorocarbon-based chemistry ($CF_4/CH_2F_2/He$). By using OES we monitored fluctuations in relative concentrations of plasma species, including CF_x*, CH*, H*, and F* analyzed on deposited a-C:H film as well as over silicon non-coated wafer. The optical emission spectra of F-based plasma are shown in Figure III-24 and Figure III-25. It has been taken as example in Chapter II, 3.1.3.4, the emission spectrum for F-based plasma etching a silicon sample, this example corresponds to Figure III-25, whose study is developed here.

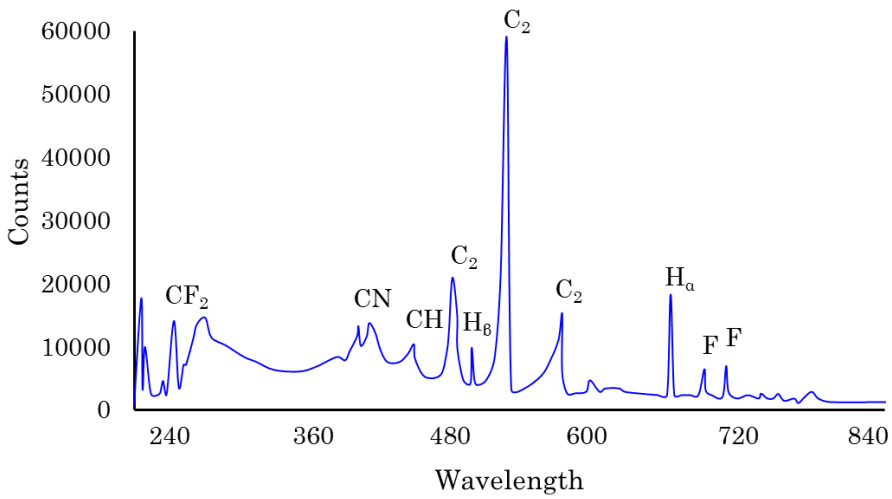

Figure III-24. Emission spectrum for F-based plasma etching an a-C:H sample, representative of the interactions between the plasma and the mask (AHM).

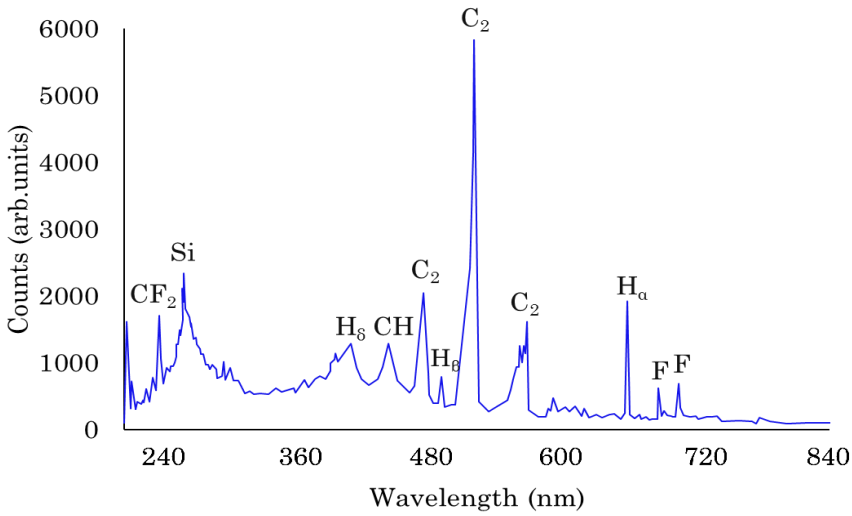

Figure III-25. Emission spectrum for F-based plasma etching a silicon sample, representative of the interactions between the plasma and the trench during the STI etching step.

Both spectra showed almost the same composition, with a strong response due to hydrocarbon radicals. The main difference was due to the Si signal at the beginning of the second spectrum (Figure III-25), which was missing for the a-C:H one, since there was no silicon. This signal could be also a CF_2 line. Since in the a-C:H spectrum this signal was missed, the Si emission was more probable but still the CF_2 could be hidden by Si. CH* lines appeared at 390nm for the AHM spectrum and 431.4nm for both of them. CH bands are usually produced in electrical discharges where carbon and hydrogen are present [229]. The presence of H was concluded by the three lines of the Balmer series for hydrogen at H_α (656.5nm), H_β (486.1nm) and H_δ (410nm), being the H_α the strongest one in both spectra. H_γ (434 nm) was difficult to

identify due to the CH band at 431.4nm, but it should be present since the other three lines were detected. Several C_2 band system were also identified, represented by the Swan band (435-686nm) system at 473.71nm, 516.5nm, 563.55nm, with the one at 516.5nm as the most intensive line over the entire spectrum for both cases. Swan bands are the most characteristic features of C_2 in all hydrocarbon spectrums.

The presence of F as an atom was also observed, but as slight sign in comparison to all the rest of species detected. These small lines of F appeared at 683.4 and 703.7nm, almost with the same intensity for both of them. Moreover, the presence of F was shown at the beginning of the spectrum, by means of the CF_2 emission line at 251.9nm. CF_3 radicals were also in that range between 255-275nm. When CF_4 gas is introduced into the plasma, various species containing F can be produced by dissociation. The most common species are CF, CF_2 and CF_3 radicals [216]. Here, the presence of F*, CF_2* and C_2 lines proved that the dissociation coming from the CF_4 gas was taking place.

- **Br-based Plasma**

For the second case, where the bromine-based chemistry was analyzed, which chemistry is composed by HBr/O_2, preceded by the first chemistry ($CF_4/CH_2F_2/He$), we have monitored mainly Br*, O* and F*. When etching the silicon sample, the presence of Si was detected at the beginning of the spectrum, not being presented over the a-C:H sample. The optical emission spectra of bromine-based plasma are shown in Figure III-26 and Figure III-27.

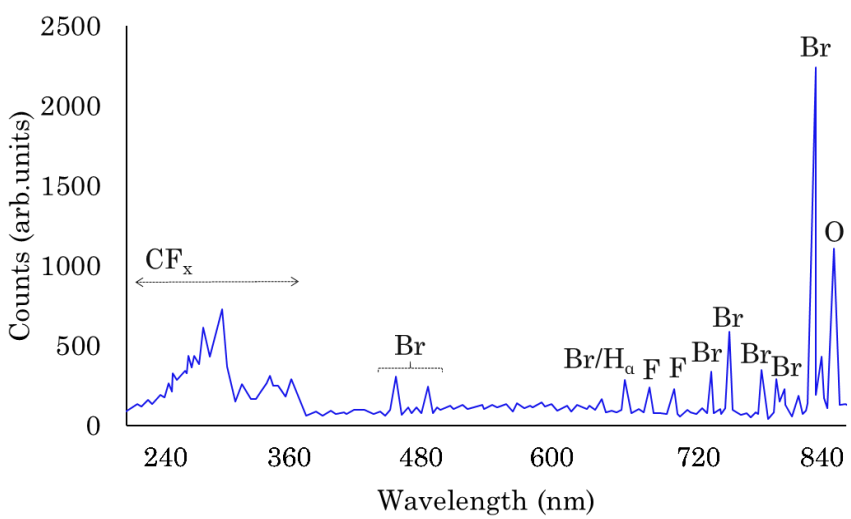

Figure III-26. Emission spectrum for Br-based plasma etching an a-C:H sample, representative of the interactions between the plasma and the mask (AHM).

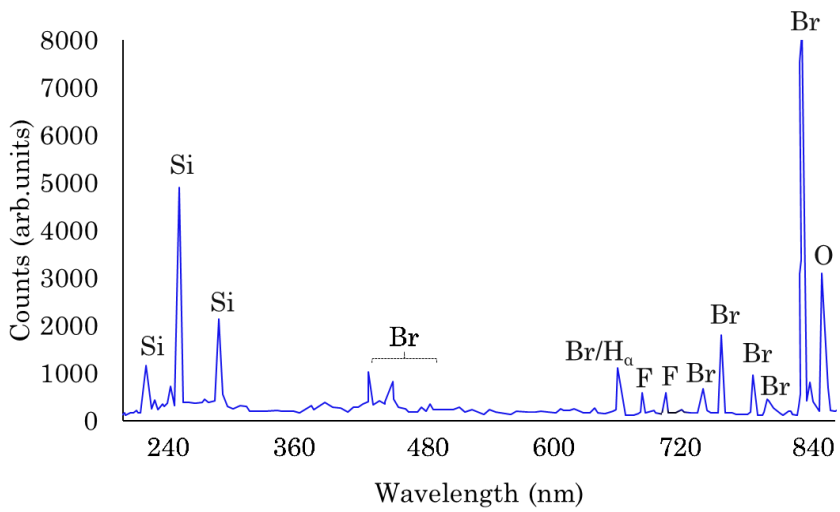

Figure III-27. Emission spectrum for Br -based plasma etching a silicon sample, representative of the interactions between the plasma and the trench during the eSTM etching step.

The presence of Br, which was the most present specie over both spectra, was detected at 450nm, 479nm, 734.85nm, 751.30; 780,30nm, 793.87nm and 834.37nm, being this one the most intensive line over the whole spectra. This region is usually used for oxygen detection too, which can be hidden for some of those Br species in this study. However, it was easy to detect its presence at the end of both spectra with the representative intensity line at 844.7nm. Other species which have in common those spectra with those where the F-plasma was used are Fluorine and Hydrogen. Fluorine is detected at 683.4nm and 703.7nm, as well as the spectra studied before by using F-plasmas. The presence of H was not confirmed in these spectra. An emission line was detected at 656.5nm, corresponding to the H_α but it could be also due to bromine [230]. In any case, the absence of the other lines from the Balmer series suggests that hydrogen concentration was small compared to the previous spectra where F-based plasma were used. The leading difference between these two spectra is located at the beginning of them. The presence of Si at 212.41nm, 251.61nm and 288.2nm for the silicon wafer, was easily recognized on the second spectra. Being the line at 251.61nm the second most important contribution of this spectrum, after the Br line at 834.37nm.

3.1.3.2. eSTM Optical Emission Study

Until now, we described the spectra of wafers non patterned, for both a-C:H and silicon materials that were specifically prepared for the study. In this section, a standard wafer (eSTM) was used to be monitored during the etching of the eSTM trench. Therefore, the bromine-based chemistry was analyzed (HBr/O_2, preceded by the first chemistry $CF_4/CH_2F_2/He$). The species presented on the plasma during the STI trench were also monitored, but some of them were in saturation (from 360nm to 600nm). Beyond this range, H_α at 656.5nm and the F lines at 683.4nm and 703.7nm were shown. For the eSTM trench,

we monitored mainly Br*, O* and F*. The optical emission spectra of the eSTM trench etching with bromine-based plasma is shown in Figure III-28.

As happened during the previous analysis, the contribution of the first etch step ($CF_4/CH_2F_2/He$) remains during the second step (HBr/O_2). This was concluded for the presence of CF_x*, CH*, H*, and F*, that could not come from the second chemistry but from the first one. CF_x* and CH* lines were not identified, but several peaks were seen in their regions. That would be related to influence of the F-based chemistry over the mask, since the CH is representative of the a-C:H film presence. Other feature of the first step was the strong presence of hydrogen. The four lines of the Balmer series for hydrogen at H_α (656.5nm), H_β (486.1nm), H_γ (434nm) and H_δ (410nm) were detected during the eSTM process. The line at 656.5nm (H_α) could be also representative of Br. Nevertheless, even if the Br could be detected at this wavelength, the presence of H was confirmed due to the presence of the others lines of the Balmer series. F* atoms were also detected at 683.4 and 703.7nm as in all the previous spectra. In this spectrum, other line could be associated to F at 634.8nm, but that one could be also related to Si. The Si-line was also present at the beginning of this spectrum at 288.2nm. However, the species identified at the beginning of the spectrum are just indicatives because with the strong background is difficult to confirm them. This is the case of CF_x, CH, Si, H_δ and H_γ.

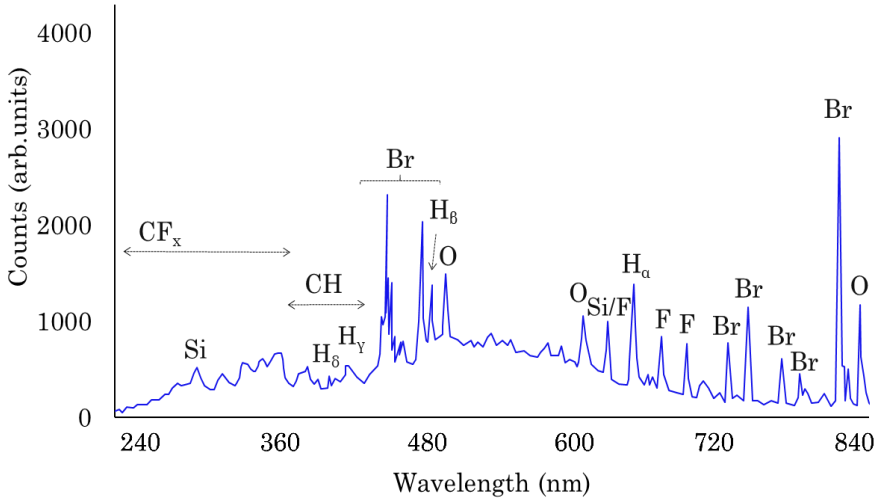

Figure III-28. Emission spectrum for Br -based plasma etching the Poly-Si trench patterned with the AHM mask during the eSTM etching step.

The signature of the second chemistry in this spectrum was determined by the detection of Br* and O*. Bromine was detected at the same wavelengths as it was detected before for the AHM and Si-wafer. Also the O* was detected at the end of the spectrum as for the previous spectra, but with two additional lines in this case which were detected at 497 and 615.6nm.

3.1.4. Summary

This section presented the study of spectrographic test performed in order to improve the understanding of the species present within various plasmas. The light emitted by the plasma, which is investigated using OES, was analyzed in the 220-840nm range. With the different optical emission systems studied, the understanding of the species that interfere on the etching process of the eSTM trench was described based on the contributions from both the chemistry (F-based and Br-based plasmas) and the materials (AHM and silicon). The main species detected were CF_x*, CH*, H*, and F* for the first chemistry and Br*, O* and F* for the second one. The a-C:H film (mask) produced both CH and C_2 radicals during the F-based plasma etching. Hydrogen Balmer emission lines were very intense in the F-based plasmas (for AHM and Si) as for the eSTM trench etching. During the first etching ($CF_4/CH_2F_2/He$) the presence of H_α was clearly detected. For the Br-based plasma spectra, this line at 656.6nm, could be rather associated to the Br. This is the case of the AHM and Si spectra during the Br-plasma etching, as we concluded because of the absence of H_β and H_δ. Nevertheless, for the eSTM etching, we associated this line to H_α since other lines of this serie were detected. It is remarkably interesting the presence of F in all the spectra, even during the second chemistry. This F could remain from the first chemistry as it could be just still present on the gas lines. In any case, it is something to keep in mind while analyzing the surface and the composition of the coating deposited on the reactor walls.

Since it was a qualitative analysis, those studies were performed to have an idea about how the spectra looked like, the species that were involved during the process and the reaction with each material. Those analyses were not used to deduce the concentration of the species, but rather to define the plasma process state and to identify meaningful wavelengths of the OES signal for those different etching. In addition to these analyses, another study was performed for improving the understanding of the process etch related to the wafer surface composition. This study is presented as follows in the next section.

3.2. Surface Characterization

In the previous section we had characterized the plasma itself with the aim of understanding the species presented in the gas phase as an input to better understand the plasma-surface interactions that takes place during the eSTM trench etching. It is, therefore, essential for this understanding to characterize the Sidewall Passivation Layer (SPL) and the elements that compose this layer. Thus, the goal of this section is to characterize the chemical composition of the sidewalls after the etching process. Based on the method introduced in Chapter II (3.3.3.4.), we wanted to develop a similar protocol at STMicroelectronics Rousset to have the possibility of studying the SPL.

However, as explained by Hershkowitz and Breun [242], industrial processing tools manufacturers have resisted to the use of in situ diagnostics and most of the tools are not equipped with diagnostics, since they are not designed for diagnostic uses. This is the case of STMicroelectronics, where ex-situ XPS analysis have been performed, since there was no other possibility. By taking into account the limitations of the ex-situ analyses, several analyses have been performed in collaboration with the cimpaca platform for developing this protocol and characterize the eSTM trench passivation.

3.2.1. Background

During the etching, anisotropy control is obtained by the formation of a passivation layer which is formed on the sidewalls and it protects them from spontaneous etching reactions. In the order to investigate the composition of the sidewall passivation layer, XPS analyses were performed. The passivation is function of the mask material, the etch chemistry and the plasma processing conditions. Since the critical dimensions are directly dependent on the passivation layer thickness, the control of the sidewall passivation is essential. Hence, the formation mechanisms and the composition of these layers should be understood. As explained in Chapter II (3.3.3.), the chemical composition of the SPL is usually studied by XPS [243-256].

3.2.1.1. Mechanisms for Sidewall Passivation Layer Formation

A balance between continuous deposition and etching produces a specific etch slope. This slope depends on the passivation. Depending on the plasma etching conditions, there are different mechanisms (see Figure III-29) for sidewall passivation layer (SPL) formation [179]:

- Mask etch products sputtered into the plasma gas phase by energetic ion bombardment and they are deposited on the sidewalls.
- Dissociation of the feed gas stock leading to the condensation of some molecules or atoms.
- Etch by products dissociation in the gas phase creating the formation of partially volatile or non-volatile etch by products on the sidewalls.
- Direct line of sight deposition of non-volatile etch by -products.

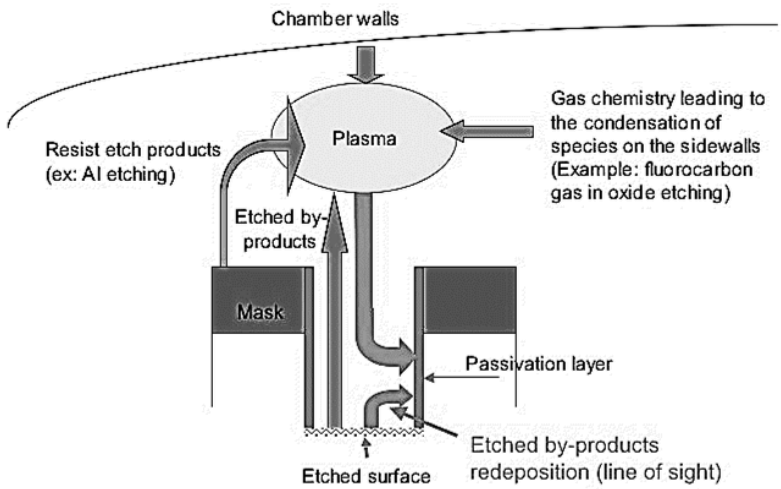

Figure III-29. Sidewall passivation layer formation mechanisms [179].

The development of plasma etch processes requires a good comprehension of the passivation layer formation mechanisms which are key parameters to control the critical dimensions.

3.2.1.2. Literature Review on Surface Characterization by Using XPS

XPS analyses after plasma processing analyzed the kinetic energy of electrons that are ejected from the atoms in the sample when the sample is irradiated with a beam of x-rays for determining the elements present in the sample. In 1967, Siegbahn published a comprehensive study of XPS [257], bringing instant recognition of the utility of XPS, which he referred to as ESCA (Electron Spectroscopy for Chemical Analysis). To acknowledge his extensive efforts to develop XPS, Siegbahn received the Nobel Prize for Physics in 1981. Since that time, the use of XPS analyses for understanding the sidewall passivation layer created during the plasma etching processes has been largely studied.

In 1988, Oehrlein et al [255] studied for the first time the silicon trenches formed by RIE using XPS. They proposed a powerful approach to the surface characterization of semiconductor microstructures by analyzing the silicon sidewall passivation for a SF_6/O_2 etching process. This approach was based on the geometrical shadowing of the incident X-Ray beam (ARXPS) and the electrostatic charging of insulating portions. Based on this method, at the *Laboratoire des Technologies de la Microelectronique* (LTM) in Grenoble (France), the ***Chemical Topography Analysis*** method was developed [249-254].

In 1989, Bestwick and Oehrlein [188] studied the composition and thickness of reaction layers on silicon surfaces resulting from exposure to HBr RIE plasmas. The results that they obtained indicated that silicon etching by bromine occurs only in the presence of ion bombardment. The two factors that lead them to that conclusion were the relative involatility

of silicon bromides and the relative difficulty with which bromine penetrates the surface to react with the underlying silicon. Cheng et al [245] also studied the HBr and Cl_2 coverage on Si surfaces etched in mixed HBr/Cl_2 plasmas. For that, they used XPS and in-situ, real-time, pulsed laser-induced thermal desorption. In their results, they showed up that HBr plasmas etch Si more slowly than Cl_2 plasmas because less halogen is available on the surface for the formation of volatile $SiBr_x$ products in ion bombardment-stimulated reactions.

In 1996, Bell et al published a group of studies related to the polysilicon gate etching in high density plasmas related with different XPS investigations [251-254]. In these studies, they investigated the silicon trenches by using Cl-based chemistry, the sidewall passivation of Si-trenches with an oxide hard mask and the difference between using photoresist and oxide masks. In their experiments, they used the geometrical shadowing of photoelectrons and electrostatic charging of insulating portions to differentiate the XPS peaks resulting from insulating photoresist surfaces from those conducting silicon surfaces, as shown in Figure III-30.

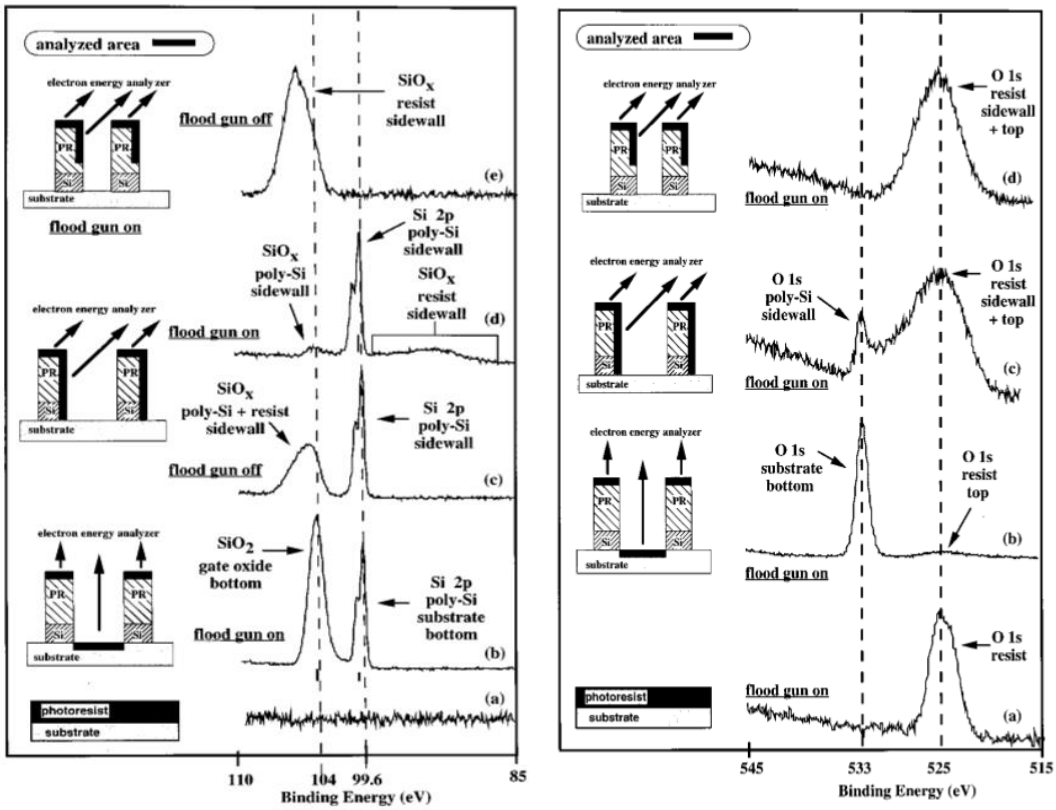

Figure III-30. XPS spectra recorded by Bell et all. Si 2p on the left and O 1s on the right [251].

Desvoivres et al [249] also studied the sidewall passivation films formed during gate etch processes by using XPS. Their studies, performed for HBr, Cl_2 and O_2 based chemistry,

showed that the sidewall passivation films SiX_xO_y (X=Br, Cl, x+2y ≤ 4) were formed during the main step of the process and become oxidized at the early stage of the overetch step leading to an oxidelike layer after halogen desorption. They also studied different chemistries such as HBr/O_2, $HBr/Cl_2/O_2$ and Cl_2/O_2. When comparing them, a high SiO_x percentage was detected for the HBr/O_2 chemistry which indicated that a relative thicker passivation layer was formed with respect to the chlorine-based chemistries. They observed SiO_xBr_y on the sidewalls for the HBr/O_2 chemistry and SiO_xCl_y for the chlorine-based plasmas. Besides, they observed that the SiO_x percentage increased with the overetch step, while bromine concentration decreased, showing that bromine atoms are substituted by oxygen atoms when analyzing the HBr/O_2 chemistry. Related to that, they also investigated the impact of air exposure on the chemical composition of the passivation layer. The results were similar to those obtained when increasing the overetch time. A strong increment in the oxygen concentration in the layer, while bromine desorbs under air exposure. Even more, no bromine was detected in the passivation layer when the wafer was exposed to the air. Vallier et al [250] used as well the chemical topography analysis using XPS based on the photoelectron shadowing effect together with the differential charging of insulating vs. conductive materials under a low energy gun. They showed the same results as Desvoivres, so that the oxygen concentration in the passivation layer increases as a function of the overetch time, while bromine concentration decreases, showing that the bromine atoms are substituted by oxygen atoms. Furthermore, the Si-Si percentage decreased as a function of the overetch time, so the photoelectrons were screened by the passivation layer, as shown in Figure III-31. From those observations, they concluded that the substitution of bromine by oxygen increased in the passivation layer as a function of the overetch time. Thus, leading the SPL to its densification.

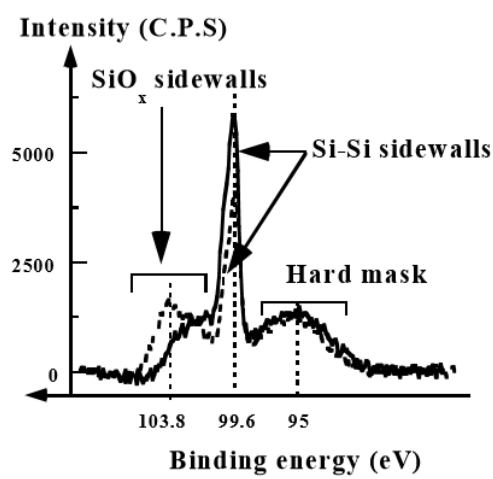

Figure III-31. Si 2p energy region recorded by XPS for HBr/O_2 chemistry. The plain line is the spectrum recorded after the main etch, and the dotted line after the final process (main etch+overetch) [250].

In any case, the passivation layer thickness seems to be strongly dependent on the oxygen concentration in the gas phase. Higher oxygen concentrations in the gas phase lead to thicker passivation layers. Also, when etching with a F-based plasma, the oxygen plays an important role. Passivation mechanisms have been also proposed for the F-based plasmas [67,85,259]. For instance, Avertin [67], proposed the SiO_xF_y layer formation for a SF_6/O_2 plasma (Figure III-32).

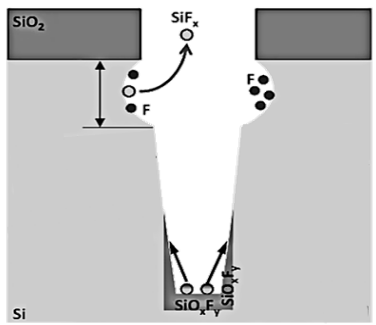

Figure III-32. Formation of the SiO_xF_y passivation over a Si-sample with $SF_6/O_2/HBr$ [67].

3.2.2. Experimental

3.2.2.1. Experimental Set-up

Specifications about all the equipment used for this thesis, were introduced in Chapter II. The experimental set-up for this study includes:

- The plasma reactor: 200mm *VERSYS STAR* from LAM Research (Chapter II. 2.1.1.)
- The XPS equipment: *KRATOS AXIS NOVA* (Chapter II. 3.3.2.)

The equipment where all the analyses were performed is part of the CIMPACA characterization platform. It counts with a monochromatic X-Ray aluminum source (Al K_α =1486eV) and a non-fixed holder so it is able to perform ARXPS analysis (Chapter II. 3.3.4.) as it can be seen in Figure III-33.

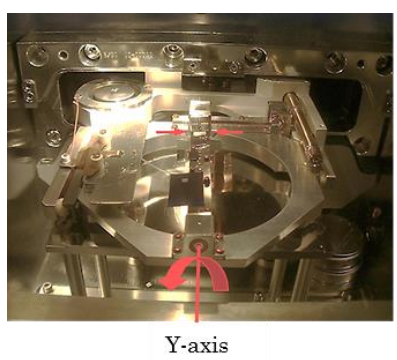

Figure III-33. Sample Platen for ARXPS used in this thesis. Entire strip (indicated between red arrows on the right) rotates about the Y-axis.

Furthermore, by the chemical topography analysis method, a pattern of lines and trenches can be analyzed by using ARXPS, so that some signals are shadowed by adjacent lines. Then, the signal from the mask can be identified thanks to a technique of differential charging: an electron flood gun charges dielectric materials and shifts their peak positions (binding energies) in the XPS spectra. Several studies have been done related to this method [59,67,125,258, 249-255].

For the ARXPS analyses, the sample was always analyzed at 0° and X°, by tilting the holder. The angle of analysis (X°) was calculated based on the SEM measures that determined the dimensions of the patterned features. Furthermore, the charging compensation was applied to both positions. The protocol used for the samples analyzed on this thesis is sketched in Figure III-34.

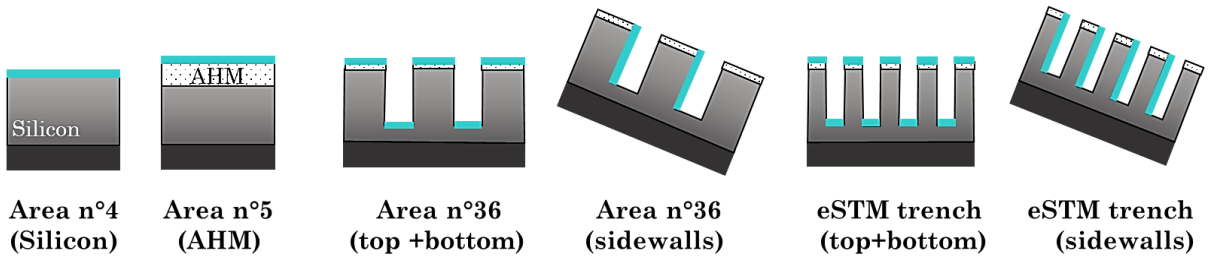

Figure III-34. Samples studied by using XPS. The blue lines correspond to the analyzed part. The area n°36 and the eSTM trench are analyzed by using the flood gun on/off in each position.

The area n°36 and the real product were studied by performing the chemical topography analysis (ARXPS + differential charging effect). However, when analyzing the eSTM trench SiO_2 was included to the analysis since it was present on the sidewalls as the material used to filled the STI. To differentiate these parts, the floating sample method was used.

3.2.2.2. Substrates

With the aim of analyzing the sidewall passivation of the eSTM trench after the etching process, additional analyses were required since such a small dimension were never before characterized at STMicroelectronics Rousset. Thus, some previous analyses were carried out by using the photolithography mask presented in Chapter II. In that chapter, we presented three areas (Chapter II. 3.1.1.2.). Areas 4 and 5, the *open-area* and *mask-area*, were used as representation of the reactions between the plasma and two different materials; the silicon and the hydrogenated amorphous carbon (AHM mask). This enabled us to understand how the chemistry employed to etch impacted different surfaces. The other area of the photolithography mask studied before analyzing the eSTM trench on the real product, was the area n°36. This area was easier to characterize than the eSTM trench, not only because

it had bigger dimensions but also because it was only composed of polysilicon. Thus, it was used to develop the protocol for to the real product (the eSTM trench). Finally, the eSTM trench was studied by using the chemical topography analysis and the floating sample method (see Figure III-34).

3.2.2.3. Chemistry Considerations

We have performed XPS analyses after the two etch processes related to the STI trench and the eSTM trench. Details about these processes have already been explained previously in this chapter (3.1.2.3.).

3.2.3. Results

The results are presented in three parts. The first part (3.2.3.1.) is related to the study performed with non-patterned wafers in order to identify the different composition of each material after the etching process. The passivation of the a-C:H (area n°5), representative of the mask during the process, and over silicon (area n°4), representative of the Si-trench, are discussed in this part. The second part (3.2.3.2.) is dedicated to the analysis of the patterned area n°36 which have bigger dimension than the eSTM trench. This study was performed by studying the contributions of areas n°4 and 5 first, and afterwards by using ARXPS analyses in order to develop the protocol of characterization for the eSTM trench. Finally, the analysis of the real product, the eSTM trench, are presented in the third part (3.2.3.3.).
For all these analyses, the two chemistries (F-based and Br-based) are regarded in order to see the influence of each one with respect to the chemical composition of the wafer surface.

3.2.3.1. Influence of the Chemistry over Different Materials: AHM and Si

The two main chemistries employed for reaching the eSTM trench are studied in this part. The F-based and the Br-based chemistry, where the AHM and Si materials are involved. For the Br-step, the samples were previously exposed to the F-based chemistry, as it has been explained in 3.1.2.3. Thus, this section is also organized in function of the chemistry used, in that way the different behaviors of the material can be shown under the same conditions. All these studies were performed over non-patterned wafers, and so the only interactions to be considered were the interactions plasma-surface of the material being studied each time. The goal was to have a global idea about the chemical composition presented over the wafer surface after etching each material.

- **F-based Plasma**

First, we studied the fluorocarbon-based chemistry ($CF_4/CH_2F_2/He$). From the survey spectra of the areas n°4 and n°5, the chemical composition was identified. This chemical composition is represented in Figure III-35.

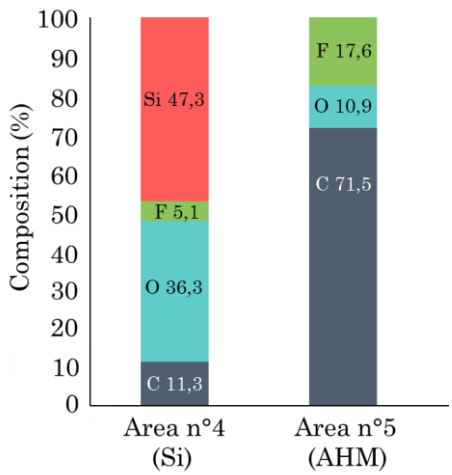

Figure III-35. Chemical composition after the first etching (F-plasma) of the areas n°4 and n°5 representatives of the silicon and the AHM, respectively.

C 1s, O 1s, F 1s and Si 2p were detected by using XPS. All the elements were presented in all the samples except for the area n°5 (AHM), where no silicon was detected. Areas n°4 and n°5 have a strong contribution of the material analyzed. Area n°4 is mainly composed of silicon whereas area n°5 is mainly composed of carbon, as the material analyzed were silicon and amorphous carbon, respectively.

The composition of area n°4 (Si) was ranked as Si > O > C > F. The Silicon was mainly Si-Si with a part of it linked to the oxygen which was detected in the Si 2s peak at 103.2eV and at 532.7eV on the O 1s peak. Moreover, the O-Si contribution to the O 1s peak was the main contribution, followed by H-O-H at 533.4eV. Part of the C contributions were linked to F, with a clear contribution F-C to the F 1s peak at 686.6eV. This means that this part was coming from the chemistry employed during this etching (CF-based). However, a big part of the C 1s peak was also due to the hydrocarbon contamination (C-C/C-H contribution) of the sample which was exposed to the air after the etching process, before the XPS analysis. The composition of area n°5 (AHM) was ranked as C > F > O. The C 1s peak counted with the clear signature of the AHM material, as revealed with the presence of the Csp^2 (284.2eV) and Csp^3 (284.8eV) contributions, the rest of the contributions to this peak were linked to the chemistry (C-F) and to the air contamination (C-C/C-H). Furthermore, the main contribution to the F 1s peak, as happened with the area n°4, was the F-C that appeared here at 687.9eV and 686.9eV. This verified the chemistry contribution also for this analysis. The oxygen in this case was not linked to the Si, which besides was not present in this analysis, but to the

C. The O-C contribution to the O 1s peak appeared at 532.4eV being the most important contribution to this peak followed by O=C (533.8eV) and 0-H (531.1eV). From these analyses, the area n°4 was mainly composed of Si as well as the area n°5 was manly composed of C, both of them with a superficial layer highly fluorinated and oxidized. Area n°4 mainly oxidized while area n°5 mainly fluorinated.

- **Br-based Plasma**

The XPS study for the second case was related to the bromine-based chemistry, which is composed by HBr/O_2, preceded by the first chemistry ($CF_4/CH_2F_2/He$). The chemical composition obtained from the spectra of the areas n°5 and n°4 is shown in Figure III-36.

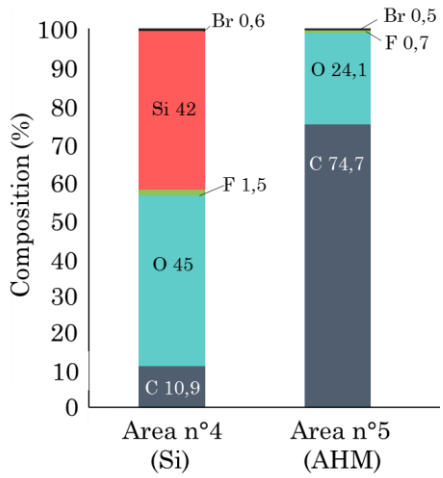

Figure III-36. Chemical composition after the second etching (Br-plasma) of the areas n°4 and n°5 representatives of the silicon and the AHM, respectively.

As for the first chemistry studied before, C 1s, O 1s, F 1s and Si 2p were detected during the second chemistry. Moreover, some traces of Br 3d were also presented this time. As happened before, all the elements were presented in all the samples except for area n°5 (AHM) where no silicon was detected. The explanation was the same as before, areas n°4 and n°5 had a strong contribution of the material analyzed. Area n°4 was mainly composed of silicon whereas area n°5 was mainly composed of carbon, as the material analyzed were silicon and amorphous carbon, respectively.

The composition of area n°4 (Si) was ranked as O > Si > C > F > Br. Even if the silicon was still mainly Si-Si, a stronger contribution than for the first chemistry was detected in the Si 2s peak related to the SiO_2 contribution. Also the O-Si contribution to the O 1s peak was here more important than for the first study, followed by the H-O-H contribution at 533.4eV. The presence of fluorine, remaining from the first chemistry, was still linked to C, as it can be deduced from the F-C contribution to the F 1s peak at 686.6eV. The composition of area n°5

(AHM) was ranked as C > O > F > Br. The C 1s peak counted as before with the signature of the AHM material, as revealed with the presence of the Csp^2 (284.2eV) and Csp^3 (284.8eV) contributions. Furthermore, since the presence of oxygen increased, the C-O and C=O contributions were detected both on the C 1s and the O 1s peaks. Being the C-O contribution at 532.4eV, the most important for the O 1s peak. Fluorine and Bromine traces were also detected, each one issued of each chemistry used (F- and Br-based plasmas). This verified the chemistry contribution also for these analyses.

From these analyses, the area n°4 was mainly composed of O and Si while area n°5 was manly composed of C. The chemical composition after the second chemistry was not far from the results obtained after the first chemistry except for the Br traces detection. Furthermore, a strong raise of the oxygen contribution was clearly appreciated. This increment was due to the chemistry (HBr/O_2). Thus, the SiO_2 passivation over the area n°4 (Si) was thicker and the Si-O contribution was more significant than before. The consequences of this oxygen increment when analyzing the area n°5 (AHM) were the same, a passivation layer strongly oxidized with several links between the oxygen and the carbon (O-C, O=C).

3.2.3.2. XPS Analysis of the Area n°36: Protocol Development

The two main chemistries employed for reaching the eSTM trench are also discussed in this part, where both AHM (mask) and Silicon are involved. However, this study was performed over a patterned wafer, the area n°36, which dimensions were bigger than the real eSTM trench. This structure had lines of 300nm and spaces of 200nm, as it has been already introduced in Chapter II (1.2.1.).

The area n°36 was studied in two ways. First, after having analyzed the areas n°4 (Si) and n°5 (AHM), we analyzed the area n°36. The idea was to use the contribution of these two areas (n°4 and n°5) to the area n°36 in order to deduce the part related to the mask and to the sidewalls. Secondly, by using the ARXPS we only analyzed the sidewalls and mask without taking into account the bottom contribution, and then by using the differential charging effect we deleted the contribution related to the AHM to finally understand just the sidewall passivation of the silicon trench.

- **F-based Plasma**

First, we studied the fluorocarbon-based chemistry ($CF_4/CH_2F_2/He$). The chemical composition from the survey spectra obtained by using XPS is shown in Figure III-37.

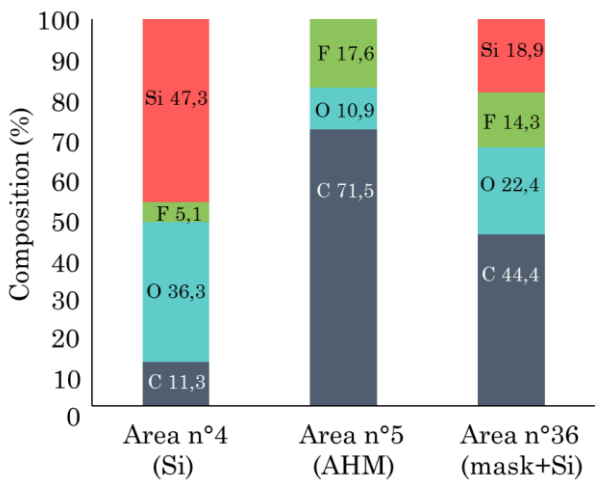

Figure III-37. Chemical composition of the of the areas n°4, n°5 and n°36 after the F-plasma etching.

The composition of area n°36 was ranked as C > O > Si > F. The Silicon was mainly Si-Si with a part of it linked to the oxygen which was detected in the Si 2s peak at 103.7eV and at 533.1eV on the O 1s peak. The C was linked to the F as represented with the F-C contribution to the F 1s peak at 686eV. But the main part of C was the C-C/C-H which appears at 285.5eV on the C 1s peak.

Concerning the previous analysis (area n°4 and n°5), almost all the elements were in the middle of the two studied areas. For the area n°36, more C (44.4%) than area n°4 (11.4%) but less than area n°5 (71.5%) was detected. Also the fluorine was in the middle of the other two areas. However, area n°36 was closer to area n°5 in fluorine composition. The contribution of oxygen was more important for area n°4 (36.3%) than n°5 (10.9%), being the area n°36 in between (22.4%). But the composition of the O 1s peak was closer to that of the area n°4 (Si), being the O-Si (533.1eV) the most important contribution whereas that for the area n°5 (AHM) was O-C. Since the Si was not detected for the AHM study, this could only be correlated to the Si part of the sample. Nevertheless, the contribution of Si to the chemical composition of area n°36 (18.9%) was lower than for the area n°4 (47.3%). The most important contribution to the Si 2p peak for the area n°4 was the Si-Si contribution. When analyzing the high resolution peak Si 2p for the area n°36, the most important contribution was still the Si-Si. However, the Si-O contribution was stronger than for area n°4, with the presence of SiO_2 at 103.7eV. This was not surprising when seeing the percentage of Si and O for both areas. Area n°4 had 47.3% Si and 36.3% O while area n°36 hasd18.9% Si and 22.4% O. Being the contribution of oxygen more important to that of silicon, a high Si-O contribution was expected as it was verified with these results for the area n°36.

From that first analysis based on studying the contributions of the AHM and Si samples, we concluded that the area n°36 has similar compositions to the other areas. We found out a

good agreement in area n°36 between the two materials previously studied. Based on the contributions of each peak we could say that those of F and C were closer to the area n°5 (AHM) while those of O and Si were closer to area n°4 (Si). However, with this analysis was difficult to conclude that the sidewalls were only composed of Si and O. Therefore, a second analysis was performed; the ***ARXPS + differential charging effect***. The high resolution spectra of the area n°36 by using ARXPS at 45° for the peaks F 1s, O 1s, C 1s and Si 2p are shown in Figure III-38. These spectra were obtained with and without the charge compensation, so that with the flood gun ON and OFF.

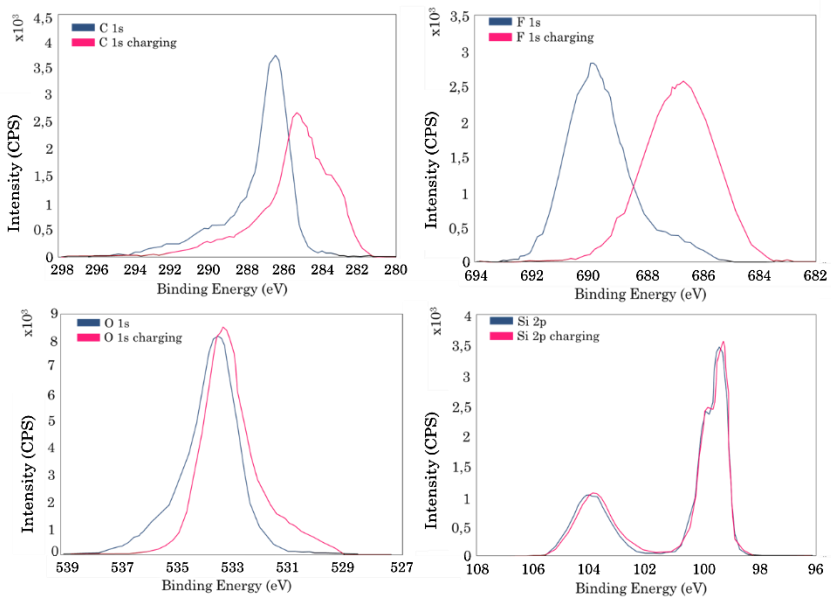

Figure III-38. XPS spectra area n°36 after the STI trench etching (F-based chemistry).

In Figure III-38, the peaks that looked affected by the differential charging effect were C 1s and F 1s. Thus, these peaks were related to the AHM. The O 1s also experimented a little effect. The Si 2p did not change when applying the charge compensation. The hypothesis that we took from that, was that the sidewalls were mainly composed of Si and O. However, the chemical composition for this area n°36 (Figure III-37) was 44.4% C, 22.4% O, 14.3% F and 18.9%Si. C 1s was the main contributor to this composition and it was mainly presented on the mask. However, since a small part of C was linked to F, some C could be also presented on the sidewalls. The silicon was completely on the sidewalls as well as the oxygen with just a little part affected by the charging effect that could be attributed to the mask.

From the two analyses, the *contribution of areas n°4 and n°5* plus the *ARXPS with charging effect*, we could say that after the first chemistry, the silicon sidewalls of the area n°36 were mainly oxidized with a fluorinated contribution that could be related to this layer or due to polymer formation on the sidewalls (C_xF_y) which is, in any case, coming from the chemistry.

- **Br-based Plasma**

The chemical composition obtained from the XPS survey spectrum for the Br-based plasma is shown in Figure III-39. This analysis was performed after the second chemistry etching, where the bromine-based chemistry was analyzed.

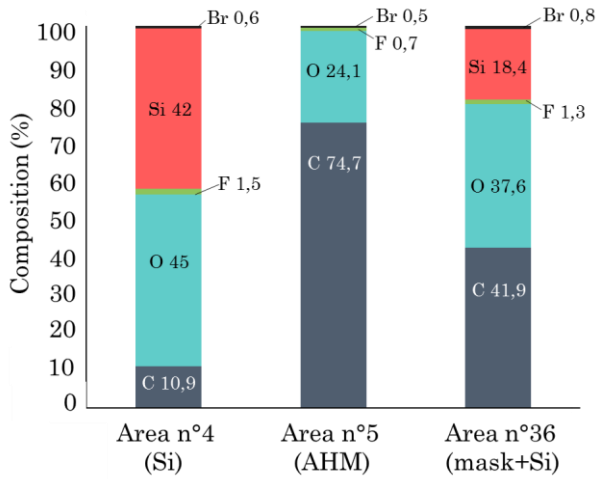

Figure III-39. Chemical composition of the areas n°4, n°5 and n°36 after the Br-plasma etching.

The composition of area n°36 was ranked as C > O > Si > F > Br. Actually, it was really close to the chemical composition after the first chemistry with some traces of bromine coming from the chemistry. Moreover, this time there was more percentage of oxygen 37.6%, compared to the previous analysis where it was 22,4%. This increment of the oxygen contribution was linked to the chemistry employed (HBr/O_2) as happened before with areas n°4 and n°5, where the oxygen was notably more important after the second chemistry. The main contribution when analyzing the high resolution peak for O 1s was O-Si (531.1eV). The C 1s was the main contributor to this composition. It was mainly composed of C-C/C-H that could be linked to the AHM mask as well as the air exposition. Furthermore, some C-F links were found when analyzing the C 1s peak at 287.2eV. This link was confirmed on the F 1s peak at 688eV (F-C). The Si 2p, as before, was mainly composed of Si-Si and Si-O.

Concerning the previous analyses (area n°4 and n°5), the area n°36 had more C (41.9%) than area n°4 (10.9%) but less than area n°5 (74.7%). The fluorine was closer to the area n°4, but still all the areas showed low F composition, which was normal since no fluorine was used during the second etch. The F contribution was remaining from the first chemistry. The oxygen was more present for area n°4 (45%) than n°5 (24.1%), being the area n°36 in between (37.6%). However, the composition of the O 1s peak was closer to that of the area n°4 (Si) since the O-Si (531.1eV) was the most important contribution whereas that for the area n°5 (AHM) was O-C. Since the Si was not detected for the AHM study, this could only come from

the Si part of the sample. Nevertheless, the contribution of Si to the chemical composition of area n°36 (18.4%) was lower than for the area n°4 (42%). Bromine was also detected but in really low percentage as for the other areas (n°4 and n°5).

From that second analysis based on studying the contributions of the AHM and Si samples, we concluded that the area n°36 after the second chemistry (HBr/O_2) had similar compositions to the other areas. Based on the contributions of each peak we could say that those of F and C were closer to the area n°5 (AHM) while those of O and Si were closer to the area n°4 (Si). However, based on this analysis, it was difficult to conclude that the sidewalls were only composed of Si and O. Therefore, the ***chemical topography analyses*** were also performed for this study. The high resolution spectra of the area n°36 by using ARXPS at 30° for the peaks F 1s, O 1s, C 1s, Br 3d and Si 2p are shown in Figure III-40. These spectra were obtained with and without the charge compensation, so that with the flood gun ON and OFF.

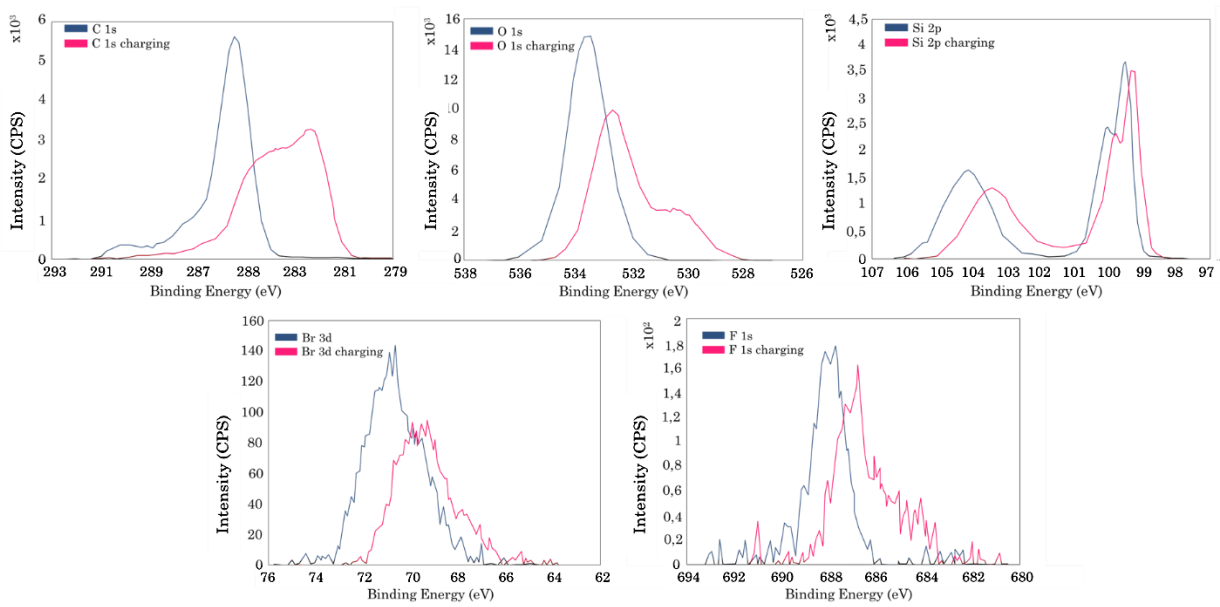

Figure III-40. XPS spectra area n°36 after the eSTM trench etching (Br-based chemistry).

In Figure III-40, all the peaks looked somehow affected by the charging effect, mainly the C 1s. Also the O 1s experienced an important effect, but a part of it was still related to the sidewalls since it did not experiment any change. The Si 2p changed as well when applying the charge compensation. However, the Si-Si contribution was almost not affected by this effect. The most important change was related to the Si-O contribution, indicating that some SiO_x passivation was also presented on the mask sidewalls. Bromine and fluorine shared contributions with AHM and Si, being the more important part of bromine related to the Si and the most important part of F related to the AHM. The hypothesis that we took from that, was that the sidewalls were mainly composed of Si, O, Br and some F. However, the chemical

composition for area n°36 (Figure III-33) was 41.9% C, 37.6% O, 18.4%Si, 1.3% F and 0.8%Br. Being the C 1s the main contributor to this composition, mainly presented on the mask respect to these analyses. The Si-Si part of the silicon was completely on the sidewalls as well as some Si-O-Br and Si-O-F, since all these elements (Si, O, Br and F) have kept a part of them that was not affected when applying the charge compensation.

From the two analyses, the *contribution of areas n°4 and n°5* plus the *ARXPS with charging effect*, we could say that after the second chemistry, the silicon sidewalls of the area n°36 were mainly oxidized with a brominated contribution to this layer which was related to the chemistry and some fluorinated contribution remaining from the first chemistry.

3.2.3.3. Sidewall Passivation Study of the eSTM Trench

Until now, the idea was not to have a final conclusion about the passivation layers studied but to develop the protocol that it could be applied to the real product. However, this product counted with a supplementary difficulty to the small dimensions which was the STI trench. The STI trench, as explained before, is filled by SiO_2. Thus, in this part, the study was performed taking into account that the trench was not only composed of polysilicon (as it was the case of area n°36) but of Si/SiO_2.

The final protocol was based on the ARXPS with the differential charge effect. The contribution of areas n°4 and n°5 was not considered since it did not provide any further information. Furthermore, by using ARXPS we could eliminate the bottom contribution keeping only the mask and the sidewalls contributions. Then, by using the differential charge effect, it was easier to dissociate the mask from the Si sidewalls since only the isolated materials are affected by this effect (the AHM in our case). With this protocol, we could analyze the sidewall passivation of the eSTM trench which was the final goal of this study. Nevertheless, by using XPS ex-situ we had some limitations: the passivation layer could be not completely representative of the passivation after the etching due to the air exposition which increased the O and C contributions to the layer. Furthermore, the desorption of some products together with the oxidation of the passivation layer would not be well controlled, as it has been studied for other groups [67]. Therefore, the goal was to have an idea of the passivation composition but mainly to know the differences between the center and the edge of the wafer. For that purpose, ***ARXPS analyses with and without charge effect*** have been performed on the center and the edge of the wafer. Then, to differentiate the Si-passivation from the SiO_2-passivation, since the trench of composed of Si/SiO_2, the ***floating sample method*** was used. These floating sample studies were performed only for the second chemistry since it was the final one and so that the representative of the real passivation after the etching process. However, the first chemistry has been also analyzed in order to

have an idea of the layer created after the first etch with ARXPS and the differential charge effect.

- **F-based Plasma**

First, we studied the fluorocarbon-based chemistry ($CF_4/CH_2F_2/He$). The chemical composition obtained from the XPS survey spectra are shown in Figure III-41. The analyses were performed on the center and edge of the wafer at 0° and 30°, where 0° was mainly representative of the AHM top and Si bottom, and the 30° of the sidewalls of the trench and the AHM.

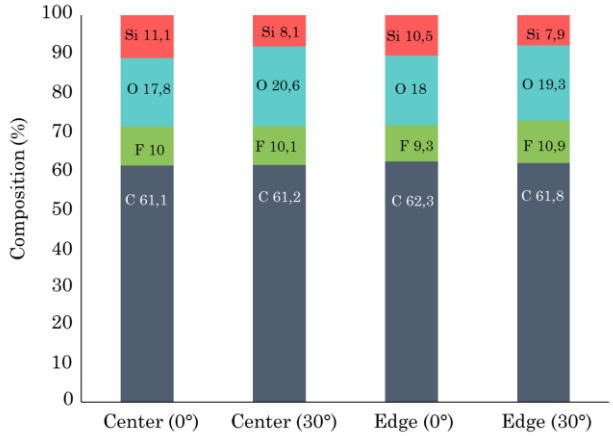

Figure III-41. Chemical composition in function of the tilt (0°/30°) and the position (center/edge).

The elements detected during these analyses were C 1s, F 1s, O 1s and Si 2p. In all the cases, the C 1s was the maximum contributor followed by the O 1s. Being the oxygen more presented on the sidewalls than the bottom, whereas the carbon was almost completely constant for all the situations. For the analysis performed at 0°, more silicon than fluorine was detected whereas that for the analysis performed at 30° was the opposite. Furthermore, the fluorine concentration increased at the edge when analyzing at 30° (10.1% center vs 10.9% edge). The silicon was less presented on the sidewalls (30°). This was normal since at 0° we were analyzing the bottom, were the passivation was less thick and more silicon should be detected. At 30°, the sidewalls having thicker passivation allowed less Si signal to be detected. The main differences were related to the Si 2p peak being 7.9% the lowest percentage (edge-30°) and 11.1% the highest one (center-0°). The chemical composition relative to the Si 2p in function of the tilt and the position is shown in Figure III-42.

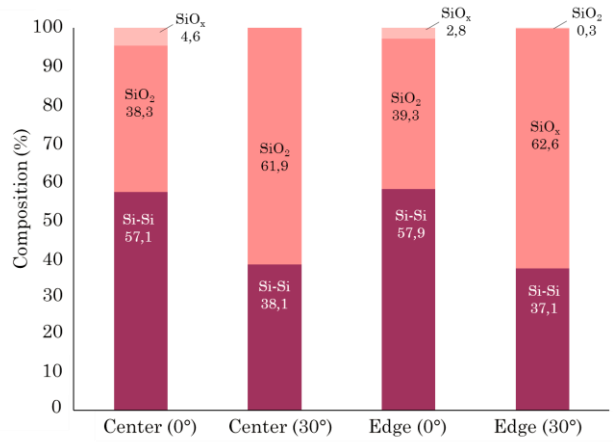

Figure III-42. Chemical composition relative to the Si 2p in function of the tilt and the position.

From the results of Figure III-42, the main contributions were the Si 2p peak were Si-Si and Si-O, being the last one presented as silicon dioxide (SiO_2) and silicon sub-oxides (SiO_x). When analyzing at 0°, the silicon was mainly elementary silicon (Si-Si) with some contribution of Si-O in its form SiO_2 and SiO_x. However, at 30° the silicon was strongly oxidized and almost completely SiO_2, with a contribution of Si-Si about 37-38% in both the center and the edge. That means that the sidewall passivation of the trench was mainly SiO_2. But it should be considered that here there was also the STI trench which composition was SiO_2. Furthermore, these analyses were not only related to the eSTM trench but also to the AHM. The differential charge compensation was used to dissociate the part related to the AHM from that one related to the eSTM trench at 30°. The results are shown in Figure III-43.

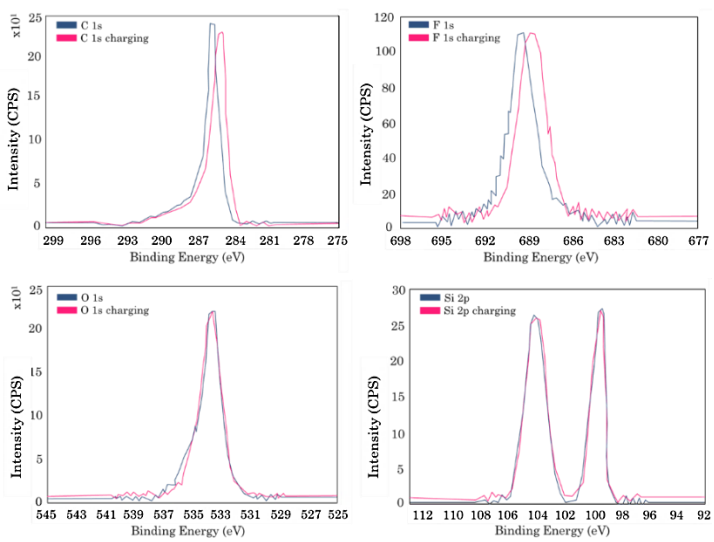

Figure III-43. XPS spectra with and without charge compensation after the first chemistry at 30°.

The spectra of the Figure III-43 were performed at 30° and at the center. All the spectra were analyzed showing the same behavior. All the peaks were almost not affected by the differential charging effect except the C 1s and some part of the F 1s that could be linked to

the AHM. The O 1s and the Si 2p practically did not change with the charge compensation, mainly the Si 2p, which does not move at all. The conclusion was that the sidewall passivation of the trench was mainly composed of F, O and Si. Being the Si mainly oxidized in its form SiO_2 and having bigger contribution of O than F. Thus, the passivation of the trench sidewalls was more oxidized than fluorinated and moreover the fluorination was more pronounced on the edge than the center. The presence of polymers type C_xF_y was also considered, due to the high contribution of C 1s which is linked to F. In any case, the presence of F, could be due to a deposition coming from the reactor walls which was also exposed to this F-based chemistry and so that a F-passivation could happen also on the walls. This will be studied in the next chapter (Chapter IV).

- **Br-based Plasma**

The chemical composition obtained from the XPS survey spectra for the Br-based plasma step are shown in Figure III-44. These analyses were performed after the second chemistry etching (HBr/O_2) and on the center and edge of the wafer at 0° and 30°. As before, the 0° is mainly representative of the AHM top and Si bottom, and the 30° of the sidewalls of the trench and the AHM.

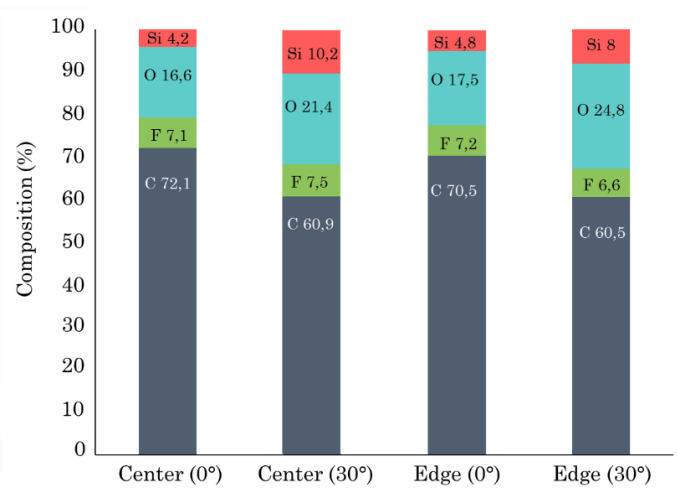

Figure III-44. Chemical composition in function of the tilt (0°/30°) and the position (center/edge).

The elements detected during this analysis were C 1s, F 1s, O 1s and Si 2p. Some traces of bromine were detected as well, but in such small contribution that it was not possible to quantify them. In all the cases, the C 1s was the maximum contributor followed by the O 1s, as happened before for the first chemistry. Being the oxygen more presented at 30° than 0°, thus, on the trench sidewalls. Unlike the oxygen, the carbon was more present at 0° than 30°, corresponding to the AHM top and the Si bottom. The behavior of the silicon was the same as the oxygen, being more present on the sidewalls than the bottom of the trench. However,

no big differences were appreciated between the passivation at the centers and the edges. Furthermore, the contributions related to the Si 2p peak presented the same behavior, being the passivation more similar in terms of tilt than due to its position on the wafer. The chemical composition relative to this peak is shown in Figure III-45.

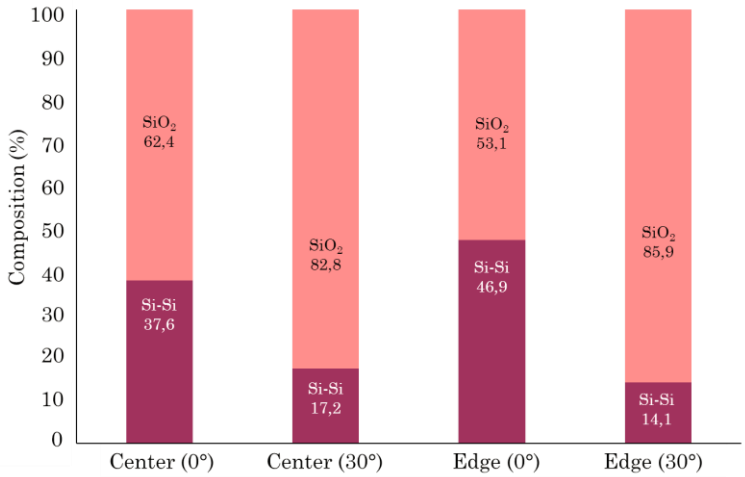

Figure III-45. Chemical composition relative to the Si 2p in function of the tilt and the position.

When analyzing the Si 2p peak, no sub-oxides were detected, just Si-Si and SiO_2 contributions fitted the peak. For the analysis after the first chemistry, the silicon was mainly Si-Si at 0° with some contribution of Si-O (SiO_2 and SiO_x) and strongly oxidized (almost completely SiO_2) at 30° with a contribution of Si-Si about 37-38%. After the second chemistry, the contributions were the same for all the samples in terms of proportion, being ranked as Si-O > Si-Si, for a Si-O completely in form SiO_2. However, at 30° the samples were much more oxidized than those at 0°. This means that the sidewall of the trench was much more oxidized than the bottom of the trench. Nevertheless, as before, it should be considered that the trench had also the STI, composed of SiO_2.

In order to identify the part related to the STI and the one related to the polysilicon trench, the floating method were used. Nevertheless, before using the floating sample method, the part related to the AHM had to be dissociated from that one related to the eSTM trench. For that, the differential charging effect was used which results are shown in Figure III-46. These spectra were performed at 30° and at the center.

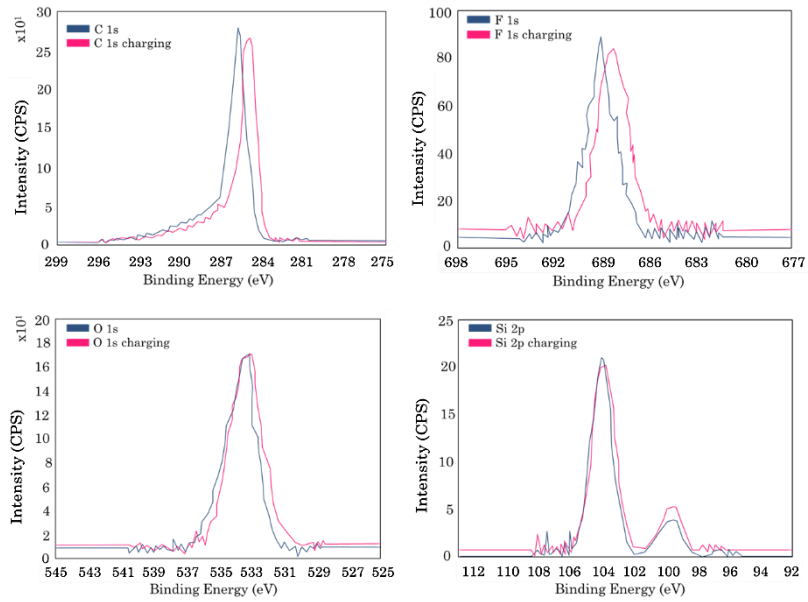

Figure III-46. XPS spectra with and without charge compensation after the second chemistry at 30°.

Carbon and fluorine were affected by the charging effect. This could mean that the mask was mainly composed of C and F. However, a part of F could be still linked to the sidewalls as well, since the effect was so small that it was difficult to properly appreciate it. The O 1s and the Si 2p practically did not change due to the charge compensation, mainly the Si 2p which did not move at all. The conclusion was that the sidewall passivation of the trench was mainly composed of O and Si with some fluorinated contribution remaining from the first chemistry. Being the Si mainly oxidized, if the passivation layer could be in form SiO_xF_y, the "x" should be significantly higher than "y".

<u>Floating sample analyses:</u>

Trying to better understand the composition of the sidewalls, the floating sample analyses were carried out. For performing these analyses, the floating samples were a Si-sample and a SiO_2-sample being representatives of the eSTM trench related to the Si-trench and the STI-trench (SiO_2). The small samples were placed on the top of a standard process wafer. After the process, these small samples, were analyzed by using XPS. These results are shown in Figure III-47.

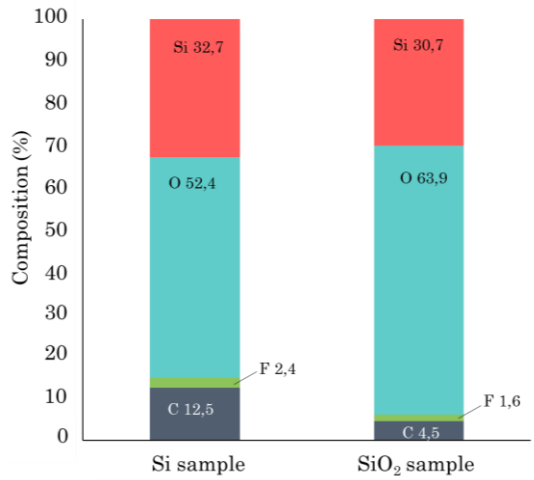

Figure III-47. Chemical composition of the Si and SiO_2 samples representative of the eSTM trench.

The elements detected during these analyses were C 1s, F 1s, O 1s and Si 2p. Some traces of bromine were detected as well, but as in previous analyses, they were such small that it was not possible to quantify them. For both samples, Si and SiO_2, the O 1s was the main contributor followed by the Si 2p. The lowest contribution to the chemical composition were the bromine and fluorine. However, the fluorine was quantified being more important for the Si sample (2.4%) than for the SiO_2 sample (1.6%). Also the carbon was more present over the Si sample than over the SiO_2. The oxygen, even if it was the main contributor in both analyses, it was more presented over the SiO_2 (63.9%) sample than the Si sample (52.4%). Both samples were ranked as O > Si > C > F > Br. The detailed composition of the most important peaks (O, Si, C) are summarized in Table III-6.

Table III-6. Composition of the peaks C 1s, O 1s and Si 2p for the Si and SiO_2 samples.

	C 1s					O 1s		Si 2p	
	CC-CH	COH	C=O	C=C	COOH	O-C	O-Si	Si-Si	$SiO_x + SiO_xF_y$
Si sample	8.8%	2%	0.6%	0.6%	0.5%	3.7%	48.7%	14%	18.7%
SiO_2 sample	3.7%	0.4%	0.2%	0.1%	0.1%	0.8%	63.1%	0%	30.7%

The chemical compositions of each peak are expressed respect to the contribution envelope peak to the total (Figure III-43)

The most important contribution to the C 1s peak was in both samples the CC-CH, followed by COH. The other three contributions (C=O, C=C and COOH) were also the same but did not follow the same order of importance for each sample. Anyway, even the contribution of the three together was not bigger than 2% of the total in any case, being 1.7% for the Si sample and 0.4% for the SiO_2 sample. The Si 2p was difficult to analyze. Only the Si-Si contribution was evident for the Si sample being 14%. No Si-Si was detected for the SiO_2 sample, which was not surprising since no elementary silicon was expected when analyzing the silicon dioxide. The other components of the Si 2p peak, the Si-O contribution presented in both samples, was named as $SiO_x + SiO_xF_y$ since it was not possible to identify the

components linked to the O and/or to the F. Furthermore, neither the F 1s peak or O 1s peak were possible to be decomposed. For the O 1s peak, the part linked to the carbon (O-C) being 3.7% for the silicon and 0.8% for the SiO_2, was subtracted from the total percentage of oxygen. Thus, the oxygen linked to the silicon (O-Si) was 48.7% for the Si sample and 63.1% for the SiO_2 sample.

From that analyses we could conclude that a heterogeneous layer SiO_xF_y, with x and y variables, was presented on the two samples after the final trench etching. The value of x and y was unknown, however, in order to compare the samples between them, we had calculated the ratio of O and F respect to this layer. The values of these reports are shown in Table III-7.

Table III-7. Oxygen and fluorine ratio respect to the SiO_xF_y layer.

	F 1s	O-Si	SiO_xF_y	F/ SiO_xF_y*	Si-O/ SiO_xF_y
Si sample	2.4	48.7	18.7	0.13	2.6
SiO_2 sample	1.6	63.1	30.7	0.05	2.1

*This is the value of the ratio of the atomic concentration of fluorine divided by the atomic concentration SiO_xF_y.

From the results presented in Table III-7, we concluded that the passivation layer over the Si sample was more oxidized and fluorinated than the SiO_2 sample.

The floating sample analyses led us to the same conclusion as before. A SiO_xF_y passivation mainly oxidized, was detected over both the STI part (SiO_2) and the Si part of the eSTM trench after the final etching. Since Bromine was used to etch the last part of the trench, some bromine was expected (SiO_xBr_y). However, it was impossible to quantified the bromine signal in our experiments. Although it had always been detected when analyzing after the final chemistry, it was not able to be quantified. This phenomenon had already been studied by others authors and explained based on the ease of Br to be replaced by F and O atoms [67].

3.2.4. Discussion

The etching process of the eSTM trench is sensitive to several parameters which allow the anisotropic etching of the trench. The surface characterization by means of XPS with the different substrates, helped us understanding the composition of the passivation layer of the eSTM trench. The main elements detected were C 1s, F 1s, O 1s and Si 2p for both chemistries, with some traces of Br 3d detected after the second chemistry (HBr/O_2). Several analyses were performed in order to develop the protocol and better understand the mechanism of passivation of the eSTM trench, since the dimensions were highly small compared to the features studied in the literature. This is also because the XPS works at lower resolution

since more information is coming from the lines and spaces of the device studied which complicates the analyses. First, we analyzed the reactions taking place over a Si and an AHM samples. Then, by using the contribution of the information taken during these analyses, we could understand easier the passivation of the area n°36 and the eSTM trench. The goal was to know the chemical composition of the eSTM trench. However, we did analyze the passivation created also after the first chemistry. For the eSTM trench, during the first chemistry, the main contributors to the passivation were C, F, O and Si. Being the silicon mainly oxidized in its form SiO_2 and having bigger contribution of O than F. The fluorinated contribution, even if smaller than the oxidized one, was more detected on the edge than the center. As hypothesis, we associated this effect to the influence of the reactor walls, since some F-passivation is also expected on the reactor walls during the process when using a F-based chemistry.

For us, it was really difficult, to identify the parts coming from the mask and those coming from the silicon sidewalls, since in all our analyses, the differential charging effect was not highly pronounced. In Babaud [125], for instance, the differential charging effect was bigger and so the results more evident, as it is shown in Figure III-48.

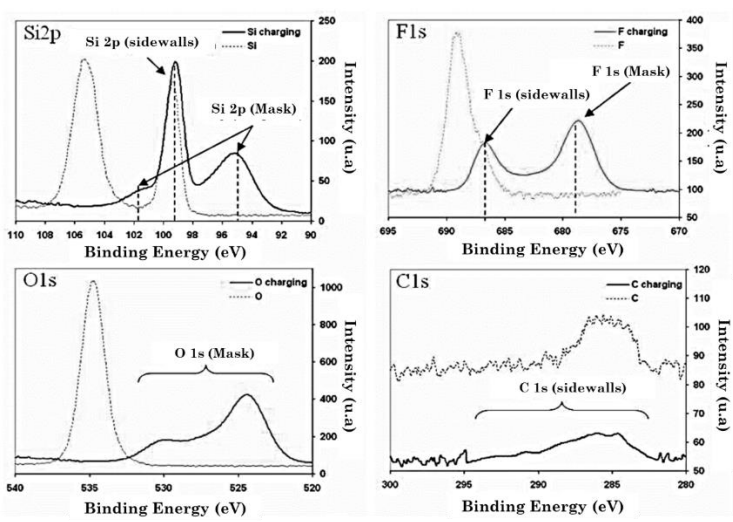

Figure III-48. Differential charging effect where the impact can be clearly appreciated [125].

When analyzing the passivation after the second chemistry, it was mainly composed of O and Si. However, still with some fluorinated contribution remaining from the first step. Based on the literature, the passivation layer when etching with HBr should be SiO_xBr_y. In our case, the passivation was more SiO_xF_y, even if some contributions of Br were detected, they were too small to be quantified. Actually, since our analyses were performed ex-situ, the bromine desorbs due to the air exposition, as it has been explained in section 3.2.1.2. Furthermore, in literature [249,250] is extensively studied the fact that the oxygen addition to HBr-based

chemistries as well as air exposure, induces some effect on the silicon sidewalls passivation films: bromine desorption occurs and the films oxidizes, leading to the densification of the SPL. Avertin [67], also saw this phenomenon during his studies for a $SF_6/HBr/O_2$ plasma. He explained that the bromine, being not detected, was easily replaced by F or O and so that it was difficult to detect Br on the surfaces. Since our analyses were performed ex-situ, due to the industrial limitations, the passivation studied was subjected to these factors. Furthermore, we did not only expose the samples to the air, but also we added oxygen to the HBr-chemistry. However, these analyses allowed us to have an idea of the plasma-surface mechanism that take place during the eSTM process. Furthermore, those studies were used to develop the protocol of the chemical topography analyses and the floating sample method at STMicroelectronics.

With a SiO_xF_y passivation on the sidewalls, we wanted to differentiate the STI (SiO_2) part of the trench to the eSTM trench itself (Poly-Si). For that purpose, we used the floating sample technique. This method, is mainly used to simulate the reactor walls, however, some studies have employed it for analyzing the sidewalls passivation [67,125,260]. From these studies, we know that the floating sample is not as accurate for analyzing the passivation as it is for characterizing the reactor walls deposition. In fact, the walls of the reactor as a floating sample are bombarded by ions at normal incidence with an energy equal to the plasma potential whereas the sidewalls of the structures are bombarded by ions of grazing incidence with an energy set by the power of polarization of the substrate. The technique of the floating sample therefore, allows the access to information about the presence of a re-deposition of the gaseous phase, which may optionally be formed on the sidewalls of the etched structures. In any case, the use of this method was not isolated. Instead, it allowed us to confirm the conclusion given before, a SiO_xF_y passivation mainly oxidized, is detected over both the STI part (SiO_2) and the Si part of the eSTM trench after the final etching. However, the main use of the floating sample method in this thesis was related to the characterization of the reactor walls. Those studies will be presented in Chapter IV.

In any case, the creation of the sidewall passivation layer is a combination of complex mechanisms and its absence has disastrous consequences for the etching profile and the critical dimensions. In our case, some problems were faced as the difficulty of doing the analysis ex-situ together with the low effect induced by the differential charging effect. However, the aim of these analyses was to characterize the passivation, which is related to the CD. But in order to keep the CD under control, several parameters have to be taken into account. The following part is related to the study of these parameters influence respect to the CD.

4. OPTIMIZATION

Nowadays, RIE is one of the most widely used pattern-transfer processes in semiconductor manufacturing, which becomes increasingly challenging due to the complexity of the process itself together with the decrease in feature dimension as it has been explained in Chapter I. Furthermore, the Critical Dimension is highly influenced by the RIE of silicon in the CMOS technology. This CD has to be well-controlled, as explained before, since it is one of the most important parameters for the electrical results. However, the RIE process involves lot of parameters which makes highly complicated the understanding of the process. Before we characterized the process by studying the influence of the gases on the passivation layer which is highly related to the CD. The objective of this part, was to describe and evaluate the parameters which take place during the process in order to select the most important in terms of CD variations for the eSTM trench. Thus, we could optimize the performance of the cell by improving the eSTM trench CD in terms of electrical results. For this purpose, some experiments were carried out to finally propose an analytical model developed using DOE. The final objective was to have a model adapted to the process such that it can even predict the CD anytime we need an industrial change.

4.1. Background

The first use of the term “Design of Experiment” in literature is introduced by Ronald A. Fisher. To study the process stability, the concept of variance is rendered. R. Fisher firstly introduced the term variance in 1918 [262] and developed the subdivision of sums of squares, which is now known as the Analysis of Variance (ANOVA). In 1935, Fisher [263] further proposed the fundamental concept of the design of experiments which then has been widely applied and extended in every aspect. Meanwhile, Fisher also completed the key elements to the theoretical groundwork in both ANOVA and DOE. His first ANOVA application was published in 1921 [263]. The synergy between mathematical and statistical techniques in DOE provides the precious process insights and the optimal result through experimental runs. Wang et al [264] pointed out that ANOVA helps to optimize the effect of each factor versus the objective function. Furthermore, DOE methods are very useful in analyzing the complex multi-parameters processes [271-273], as the systematic relationship between the adjustable inputs, i.e., the factors, and the response outputs, i.e., the measurements, will be analyzed and extracted in an attempt to determine the optimal process performance.

The most used statistical techniques to optimize the required output parameters are Factorial Method, Taguchi Method and Response Surface Method (RSM) [274]. However, there are other options. Saltelli named a few such as the Sensitivity Analysis (SA) [265] and "One Factor At a Time" (OFAT) approaches [268]. His definition of the term sensitivity

analysis is the study of how the uncertainty in the output of a mathematical model or system (numerical or otherwise) can be apportioned to different sources of uncertainty in its inputs [265]. He also pointed out that the sensitivity analysis is valuable for the determination of some physical parameters embedded into a complex model from experimental determination of observables that are further down-stream in the model. One of the most common and simplest methodologies that could be implemented for the sensitivity analysis is via an elementary "One Factor At a Time" (OFAT) approach [268]. This derivative-based method was conceived and defined as a local measure of the effect of a given input on a given output. The system derivative is denoted $S_j=\partial Y_j/\partial X_j$, where Y is the output of interest and X an input factor as explained by Rabitz and Turanyi [266-267].

As explained in previous chapters, the number of parameters involved in the etching plasmas is important and therefore the analysis of the mechanisms and interactions involved in these plasmas become complex. Both, experimental strategies and response surface methodologies, help to optimize the organization of experimental tests to obtain the maximum information with minimum experiences. When using DOE, understanding the experience plans is based on two key concepts; the experimental space and the mathematical modeling of the studied variables. Compared to those other experimental strategies, RSM is intended to predict the response with a good quality all over the experimental domain [275]. Factorial designs are widely used to investigate the joint effects of the factors on a response variable. A factorial design is an experimental strategy in which design variables are varied together, instead of one-at-a-time [276]. If the number of combinations in a factorial design is too high to be logistically feasible, it will be called **fractional factorial design** [277], in which some of the possible combinations are eliminated. A major use of these designs is in screening experiments. These fractional factorial designs are among the most widely used kind of designs in industry. The other factorial designs are **full factorial designs**. A very important case of the full factorial design is that one where each of the k factors has only two levels [277]. Since each replicate of these designs has exactly 2^k experimental trials or runs, they are usually called 2^k factorial designs. These designs are one of the subject of this section and therefore some concepts related to them are presented as follows. The understanding of these designs resides in two main notions: the experimental design and the mathematical formulation.

- **The Experimental Design**

In a factorial design the influences of all experimental variables, factors, and interaction effects on the response or responses are investigated. If the combinations of k factors are investigated at two levels, a factorial design will consist of 2^k experiments [278]. In the experimental layout, the actual process parameter settings are replaced by - 1 and + 1. In

this way the size of the experimental domain has been settled. The level of the factors may be arbitrarily called "low" and "high". These two levels can be quantitative or qualitative [277]. An experiment with two variables would be represented as in Figure III-49.

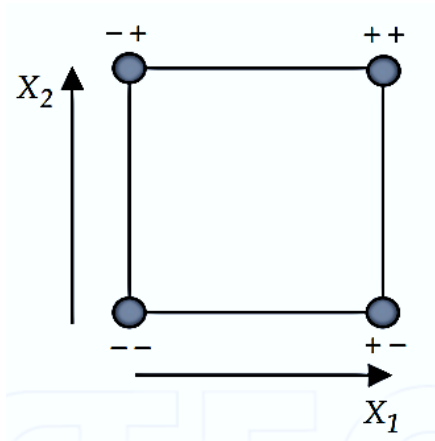

Figure III-49. The experiment in a design with two variables [278].

- **The Mathematical Formulation**

The outcome of an experiment is dependent on the experimental conditions. This means that the result can be described as a function based on the experimental variables (see III.4).

$$y = f(x) + residual \qquad \text{(III.4)}$$

The f(x) is approximated by a polynomial function and represents a good description of the relationship between the experimental variables and the responses within a limited experimental domain [278]. There are several types of polynomial models. The simplest one contains only linear terms and describes only the linear relationship between the experimental variables and the responses (III.5). The next level of polynomial models contains additional terms that describe the interaction between different experimental variables (III.6). The next level of polynomial models can be used to determine an optimum (maximum or minimum). Quadratic terms have to be introduced in this model to determine non-linear relationships between the experimental variables and responses (III.7).

$$y = b_0 + b_1x_1 + b_2x_2 + residual \qquad \text{(III.5)}$$

$$y = b_0 + b_1x_1 + b_2x_2 + b_{12}x_1x_2 + residual \qquad \text{(III.6)}$$

$$y = b_0 + b_1x_1 + b_2x_2 + b_{11}x_1^2 + b_{22}x_2^2 + b_{12}x_1x_2 + residual \qquad \text{(III.7)}$$

The polynomial functions described above contain a number of unknown parameters (b_0, b_1, b_2, etc.) to be determined. The residual is related to the lack of fit.

For the different models different types of experimental designs are needed. However, the main steps for designing an experiment are always the same [270]: Statement of the problem, formulation of hypothesis, experimental design choice, performing the experiment, statistical analysis of the data and modeling, optimization and verification of the results.

4.2. Experiments

The equipment used in this study is the 200mm VERSYS STAR from Lam Research introduced in Chapter II (2.1.1.). The specifications about the process have also been already introduced in this chapter (2.2.) as well as the stack (2.2.1.) and the etching specifications (2.2.2.). In Figure III-19, the etching specifications were sketched. This is, the etch definition from the initial stack, which comes from the photolithography step, to the silicon trench (eSTM) reached after etching. This process definition does not require a long recipe in terms of steps. However, the complexity of the process increases with the huge number of parameters required. There were 10 main parameters involved in the recipe used for this study, such as pressure, temperature, TCP, BIAS and gas flows. Several gases are needed in order to cover the necessity of etching each layer. For instance, as it has been explained before, while etching the Si/SiO_2, the selected chemistry is F-based whereas that for the Silicon etching is Br-based.

To begin designing a set of necessary experiments, it was critical to know the most important factors (inputs) related to the outputs, i.e., the CD in this study. Given that the process under study involves 10 parameters in each of the 4 steps, the reduction of the number of inputs was mandatory even all they are suspected to be key factors. A factorial design could be proposed but since the study was carried out in an industrial environment (STMicroelectronics), the RIE process was conducted on the basis of “lot”. One “lot” is a set of 25 wafers to be processed within an etching chamber. Therefore, the first desired constraint due to industrial limitation was imposed by the company: the number of experiments was expected not to exceed 25 in order to avoid the variability that can be induced from the lot-to-lot effect. There were two goals in this research: the first one was to find out the factors and steps with the biggest influences in terms of final CD in order to build up a mathematical model with the significant "process window"; the second goal was to be able to predict the CD with the model such that it enables to adjust the CD when needed (ex: for electrics performances, morphology, etc.). These aims will be satisfied by choosing the suitable factors to perform the DOE modelling and by evaluating the model.

For the whole study, the final CD was measured on the top of the trench by using CDSEM online. Figure III-50 shows the standard CD after etching indicating where the CD, that we target to optimized, had to be measured. The SEM images are taken after removing the mask.

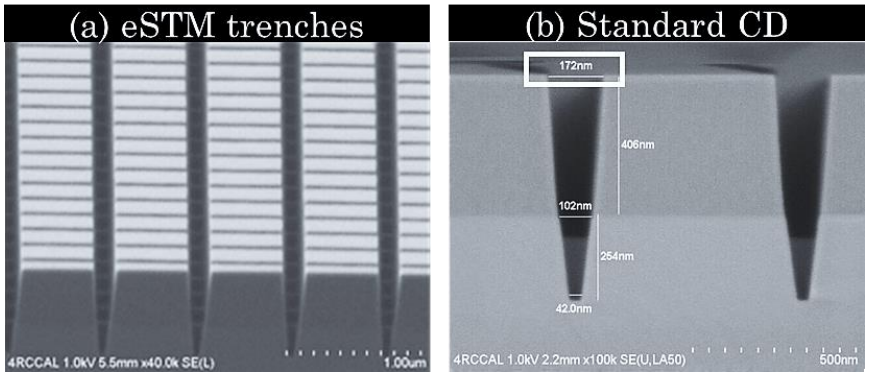

Figure III-50.SEM images of the eSTM trenches appearance and the CD measured at the top.

4.2.1. Choice of the Factors

In order to reduce the number of factors, several experiments were performed. Since the majority of inputs came from the recipe parameters, experiments related to the process sensitivity were done. After knowing the most important parameters, further experiments were executed to find out the most influential steps concerning the CD. These experiments, related to the steps sensitivity, were performed in two stages. First, a partitioning was done in order to know the most important steps by analyzing the influence of each layer with respect to the final CD. However, there were still too many inputs left to start the DOE analysis. Hence, another experiment was finally carried out to correlate the most influential parameters with the most important steps by doing other process sensitivity analysis for each of the selected parameters. These preliminary experiments were very essential for factor screening, i.e., identifying the correct set of process variables to be included in the DOE study. The resulting choice of key factors shows high adequacy for the experimental design. In the following sub-sections, these preliminary tests are explained respectively.

4.2.1.1. Identification of Most Influential Parameters and Steps

As mentioned before, Saltelli [265], defined the term Sensitivity Analysis (SA) as a study of how the uncertainty in the output of a mathematical model or system can be apportioned to different sources of uncertainty in its inputs. In our study, the sensibility analysis used is an OFAT screening test, which consist in changing one parameter of the recipe at a time in order to exploring what the model did with the new value. In these analyses the baseline value was kept constant. The factors were moved away from the baseline only once (or twice) and the baseline was not changed throughout the analysis. Saltelli called this approach "Elementary

OAT", or EOAT [268]. The existence of interactions is initially ignored. We assume that there are no interactions between steps since the chemistry used was selective. Thus, this study was used as a screening stage before the DOE analysis.

- **Process Sensitivity Analysis**

To perform the process sensibility, it was necessary to check the hardware variabilities of the tool configuration such that the chamber matching capability and the key sub-system with largest contribution to the CD variability could be understood in advance. Table III-8 shows the hardware variabilities from Lam Research related to the RIE equipment used in this study.

Table III-8. Hardware variabilities for 2300 VERSYS system.

Hardware Sub-system	Intrinsic HW variability (3σ)
TCP RF Power & Delivery	± 1.5% [w]
Bias RF Power & Delivery (voltage mode)	± 3.0% [volts]
Vacuum & Pressure	± 3.6% [mTorr]
Gas Delivery	± 3.4% sccm
Temperature Control (TCP Window)	± 5.0 °C
ESC Temperature (Wafer Temperature)	± 1.5 °C (at 250W Bias Power)

The parameters involved in the process under study were the pressure, the TCP Power, the Gas Flows, the BIAS Voltage and the ESC Temperature. For each one of them, two variations were performed. Normally, these variations should be done as Add/Subtract following the Lam Research recommendations. However, in our case some modifications of these suggestions were required for some parameters as it is shown in Table III-9.

Table III-9. Hardware variabilities for 2300 VERSYS system.

Process parameters	Variation for Sensitivity Analysis
Pressure	Add/Add → +10%/+20%
TCP power	Subtract/Subtract → -10%/-20%
Gas flows	Add/Subtract → ±15%
Bias voltage	Add/Subtract → ±10%
ESC temperature	Add/Subtract → ±5%

There were two cases where the recommendations of Add/Subtract had to be changed. The two parameters under modifications were the Pressure and the TCP Power. For the case of the pressure, it was not possible to do Add/Subtract since in some steps of the recipe we need to use too many gases. Thus, we were obliged to do Add/Add because we could not even turn

on the plasma for these steps if we would decrease the pressure. The case of the TCP Power was in the opposite way. In some steps, almost the maximum power of the equipment was reached. For instance, while etching the Si trench, the TCP Power was already close to 1200w. This is the reason why we could only do Subtract/Subtract. For the rest of parameters, we followed the Add/Subtract recommendations by doing ±10% for the BIAS Voltage, ±5% for the ESC Temperature and ±15% for the gases flows. The gases involved on this study were Cl_2, HBr, CF4, He, O_2 (at 20sccm and 200sccm) and CH_2F_2. The total number of experiments required to perform the EOAT were 20, as the numbers of parameters were 10. The results of this process sensitivity analysis regarding the CD expected variation are shown in Figure III-51.

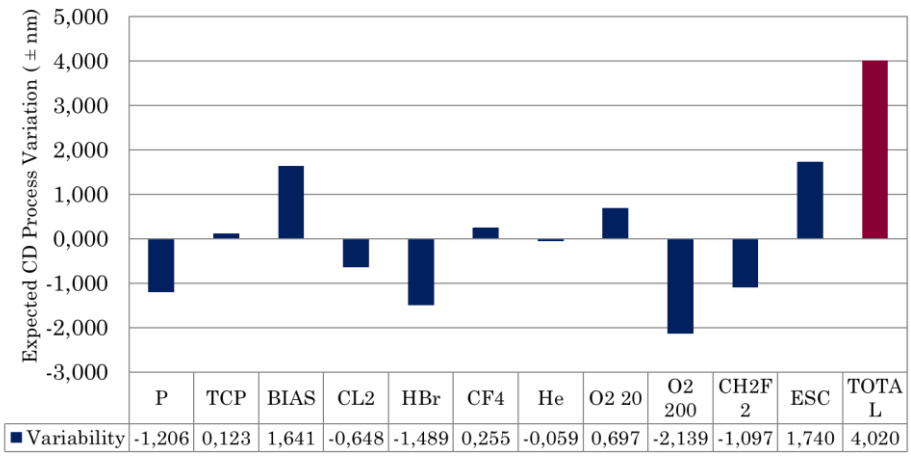

Figure III-51.CD expected process variation from the process sensitivity analysis.

As shown in Figure III-51, the high sensitivity was related to the O_2 (200sccm), the ESC Temperature, the BIAS Voltage, the HBr, the Pressure and the CH_2F_2. There were still too many parameters to be used for the next sensitivity analysis even if the partitioning will identify the most important steps. The total expected CD variation (III.8) as well as the worst case CD variation (III.9) are calculated as follows.

$$Expected = \sqrt{\sum_i R_{x_i}^2 \left(\frac{df}{dx_i}\right)^2} \quad \text{(III.8)}$$

$$Worst\ Case = \sum_i R_{x_i} \left(\frac{df}{dx_i}\right) \quad \text{(III.9)}$$

The expected CD variation was ±4.02nm while the CD variation in the worst case could be magnified to ±11.1nm.

- **Step Partitioning**

As explained before, a "partitioning" consist on etching one wafer per each step. By stopping the process after each step, each wafer is representative of one of the steps. After identifying the key process parameters, the following stage was on the step partitioning to find out the most important steps by analyzing the influence of each layer with respect to the final CD. The measures performed by SEM (Figure III-52) and the results of this partitioning are presented in Table III-10.

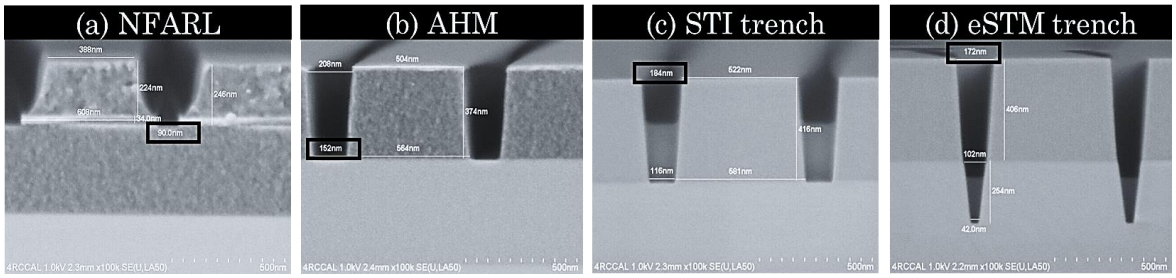

Figure III-52.SEM images of the etching partitioning for the eSTM trench process.

Table III-10. Step partitioning in relation to CD.

Step	CD variation	Δ CD*
PHOTOLITOGRAPHY	Starting CD: 100nm	-
NFARL	100nm → 90nm	10nm
AHM	90nm → 152nm	62nm
STI	152nm → 184nm	32nm
Si trench	184nm → 172nm	12nm

*Absolute values

In Table III-10, it can be appreciated that the CD was changing from one step to another. The differences between two consecutive steps were calculated to study the source of variation in terms of steps. According to Table III-10, the steps which induce the most CD variation were the AHM and the STI. In particular, the AHM step which induced 62nm of CD variation which increased the CD from 90nm after the NFARL opening to 152nm after the AHM etching.

The measurements were taken by online CDSEM and verified by SEM profiles, which further confirm that these measurements had small variability. However, the wafer-to-wafer variability could always appear during the experiments. Repeating the analysis several times led to the same results and verified that the AHM and STI were the most influential steps.

4.2.1.2. Key Factors Selection for DOE Analysis

With the identification of the most influential parameters and steps, the most influential parameters (O_2 rate flow, the ESC Temperature, the BIAS Voltage, the HBr, the Pressure and the CH_2F_2 rate flow) were then correlated with the most important steps (AHM and STI trench). To select the design factors for DOE, two new sensitivity analyses were carried out. The first analysis was to evaluate the effects of the influential parameters during the AHM etching step and the other one was to study the impacts of the same parameters during the STI trench etching step. The results for the two analysis are shown in Figure III-53 and Figure III-54.

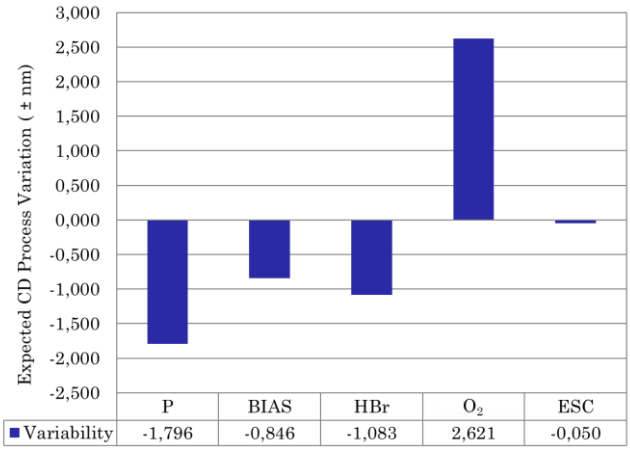

Figure III-53. CD variation for the AHM etching step.

The effects of the parameters during the AHM etching on the final eSTM trench CD were ranked as: O_2 > P > HBr > BIAS > ESC. The contributions of the ranked parameters to the variability occurred in this step were 41%, 28%, 17%, 13% and 1%, respectively.

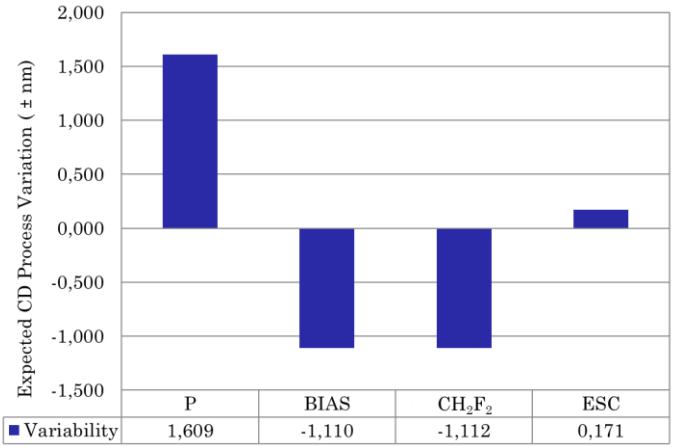

Figure III-54. CD variation for the STI trench etching step.

The effects of the parameters during the STI trench etching on the final eSTM trench CD were ranked as: P > BIAS > CH_2F_2 > ESC. The contributions of the ranked parameters to the variability occurred in this step were 40%, 28%, 28% and 4%, respectively.

As a result, the input factors for the DOE were O_2 (AHM), P (AHM), P (STI trench), BIAS (STI trench) and CH_2F_2 (STI trench). Considering that these five control factors were the most critical parameters/steps related to the final CD of the eSTM trench, a response surface model was built to take into account the main effects and the interactions among the key parameters. The model must be capable of predicting/optimizing the CD through fine-tuning the parameters.

4.2.2. Design of Experiments

The software *Design Expert* proposed several DOE models. The one used for this study was a response surface D-Optimal. It used discrete factors with any number of levels. The construction of the experimental design is often easy and simply selected from matrices already published. But it is important that the plan suits to the study and not the reverse.

4.2.2.1. Experimental Design

To study the main effects and all the interactions of the selected factors, the ideal design matrix is surely based on the full factorial design. Given the 5 factors with 3 levels, the full factorial design will require 243 wafers. However, only 21 runs were indispensable to study the full quadratic model. With the constraint of using only one lot, i.e., 25 wafers, the number of experiments was reduced to 21 in order to evaluate the main effects and all the second order interactions. Three additional experiments at the center of the design space, called replicates, were added in order to study the repeatability and robustness of design [269]. To avoid the first wafer effect and to have the stable chamber condition, total 24 experimental wafers are processed and their CD's of the silicon trench, i.e., the response of the DOE model, were measured after the process. Replicates are not the same that repeated measurements on the same experimental unit. Replicating a run means including the same set of processing conditions more than once during the experiment. There are two reasons for replication: to increases the precision of estimates of effects and to give additional information on background process variation [269]. The requirements to be respected for performing a good experiment are randomization of experiments to improve statistical tests, replication or center point repetition for experimental error estimation and maximization of the accuracy of measurements [270]. Table III-11 summarizes the design levels of the 5 selected parameters. The 24 experiments (21 trails with 3 replicates) were generated based on D-Optimal criteria where level 0, i.e., S_A, S_B, S_C, S_D, and S_E, indicates the standard setting for the five factors.

Table III-11. Selected factors and designated levels.

Step	Parameters	-1	0	+1	Variations
AHM	O_2	S_A-10	S_A	S_A+10	20sccm
	P	S_B-0,5	S_B	S_B+0,5	1mTorr
STI trench	P	S_C-0,75	S_C	S_C+0,75	1,5mTorr
	BIAS	S_D-27,5	S_D	S_D+27,5	55V
	CH_2F_2	S_E-7,5	S_E	S_E+7,5	15sccm

This DOE was carried out through the AHM and STI trench steps, since the two steps were evaluated as the most important ones. However, the CD was always measured at the top of the final eSTM trench, which was therefore the final CD. No interaction between the steps take place since the chemistry changes for each step and it is selective to etch the target material. Therefore, it was expected to see only the interactions among the parameters within the same step.

4.2.2.2. Execution of Experiments

Table III-12 summarizes the test performed during the DOE study made in random order. *Design Expert* automatically randomizes the order of the experimental runs. There are two reasons for randomization: it reduces the risk of unanticipated sources of variation affecting the estimates of effects and it helps to meet the assumptions of the statistical methods used in analyzing experimental data [269].

Table III-12. D-Optimal design matrix.

Run	A (sccm)	B (mTorr)	C (mTorr)	D (V)	E (sccm)
1	0	0	0	0	0
2	+1	-1	-1	0	-1
3	-1	+1	-1	0	+1
4	-1	+1	+1	-1	-1
5	-1	0	+1	-1	0
6	-1	0	-1	+1	0
7	0	0	-1	-1	+1
8	+1	+1	0	-1	+1
9	0	0	0	0	0
10	-1	+1	+1	+1	0
11	0	+1	+1	+1	+1
12	+1	-1	+1	0	+1
13	0	+1	-1	+1	-1
14	-1	-1	+1	0	-1
15	0	0	0	0	0
16	-1	0	+1	-1	+1
17	+1	-1	+1	+1	-1
18	-1	0	-1	-1	-1
19	+1	+1	+1	+1	-1
20	-1	-1	+1	-1	0
21	-1	-1	0	+1	+1
22	+1	0	-1	+1	+1
23	+1	+1	-1	-1	0
24	+1	0	+1	-1	-1

4.3. Results

By conducting all the 24 experimental runs and collecting the process responses, i.e., the final trench CD, the response surface models were built and evaluated using the *Design Expert* software. The best model was then selected and analyzed in the following.

4.3.1. DOE Analysis

From all the models proposed by *Design Expert*, ANOVA suggested the one that suited the best to the experiments. The ANOVA summaries for different types of models are listed in Table III-13.

Table III-13. Analysis of variance (ANOVA) for three estimated models.

Source	Sequential p-value	Lack of Fit p-value	Adjusted R-Squared	Predicted R-Squared
Linear	<0.0001	0.9031	0.9756	0.9651
2FI	0.9006	0.7268	0.9639	0.8216
Quadratic	0.7268	-	0.9508	-

As can be seen in Table III-13, a linear model would be sufficiently good as it outperforms the other two types of models. Therefore, the linear model was decided. To further evaluate the effect significance of the process parameters, ANOVA was again performed within the linear model and summarized in Table III-14.

Table III-14. ANOVA for the Linear Response Surface model.

Source	Sequential p-value	Degrees of freedom	Mean Square	F-value	p-value Prob > F
Model[a]	1498.64	5	299.73	184.60	<0.0001
A	1069.28	1	1069.28	658.55	<0.0001
B	260.28	1	260.28	160.30	<0.0001
C	18.34	1	18.34	11.30	0.0035
D	30.78	1	30.78	18.96	0.0004
E	84.42	1	84.42	51.99	<0.0001
Residual	29.23	18	1.62	-	-
Lack of Fit[b]	19.42	15	1.29	0.40	0.9031
Pure Error	9.81	3	3.27		
Cor Total	1527.87	23			

[a] Significant/ [b] Not significant

Apparently the linear model was significant with the extremely small p-value (<0.0001). The Model F-value of 184.60 implies that the model was significant. Furthermore, the five main effects resulted from the key parameters were all significant as well. The insignificant lack of fit for this model undoubtedly confirmed the significance of the linear model. The statistical results related to this model are shown in Table III-15.

Table III-15. Statistical results evaluated by ANOVA.

Std.Dev	1.27	**R-Squared**	0.9809
Mean	133.31	**Adj R-Squared**	0.9756
C.V. %	0.74	**Pred R-Squared**	0.9651
PRESS	53.37	**Adeq Precision**	46.622

The Predicted R-Squared of 0.9651 was in reasonable agreement with the Adjusted R-Squared of 0.9756; i.e., the difference was less than 0.2. The Adequate Precision measures the signal to noise ratio. A ratio greater than 4 is desirable. Our ratio of 46.622 indicates an adequate signal. Therefore, we can conclude that this model can be used to navigate the design space. The linear model can be expressed as (III.10) in terms of the 5 factors and the intercept term.

$$\mathrm{CD} = +172.67 - 7.88 \cdot \mathrm{A} - 3.95 \cdot \mathrm{B} - 1.01 \cdot \mathrm{C} + 1.36 \cdot \mathrm{D} - 2.32 \cdot \mathrm{E} \qquad \text{(III.10)}$$

The CD model in (III.10) was built in terms of coded levels, i.e., - 1 and +1, with respect to the baseline settings. Equation (III.10) is useful for identifying the relative impact of the factors by comparing the coefficients. Figure III-55 shows a Pareto diagram which standardizes the effects of the 5 design factors to the variability of the final CD of the eSTM trench.

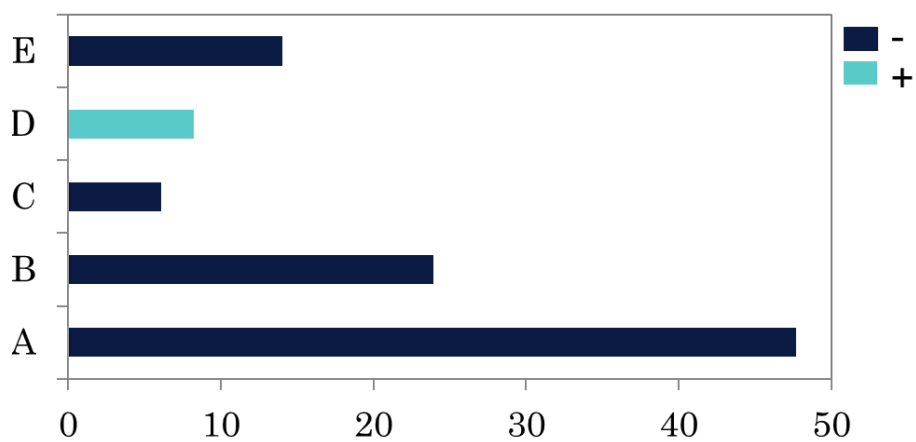

Figure III-55. Pareto diagram of the standardized effects studied with respect to the final CD variation.

The Pareto diagram in Figure III-55 shows that the biggest impact on the final CD variation actually came from the factor A, i.e., the mass flow of the O_2 during the AHM etching. The pressure during the AHM etching step (factor B) and the mass flow of CH_2F_2 during the STI trench etching (factor E) had as well a significant effect but less important than the O_2 during the AHM etching. The Bias voltage (factor D) and the pressure (factor C) during the etching of the STI trench, despite significant, were the least important. Figure III-56 displays the factor effects over the final CD of the silicon trench within the practical process window. The estimated effects of all the five factors were: 0.79nm/sccm (A), -9.35nm/mTorr (B), 0.02nm/mTorr (C), 0.01nm/V (D), and -0.22nm/sccm (E). Furthermore, each factor plays a different role through the process.

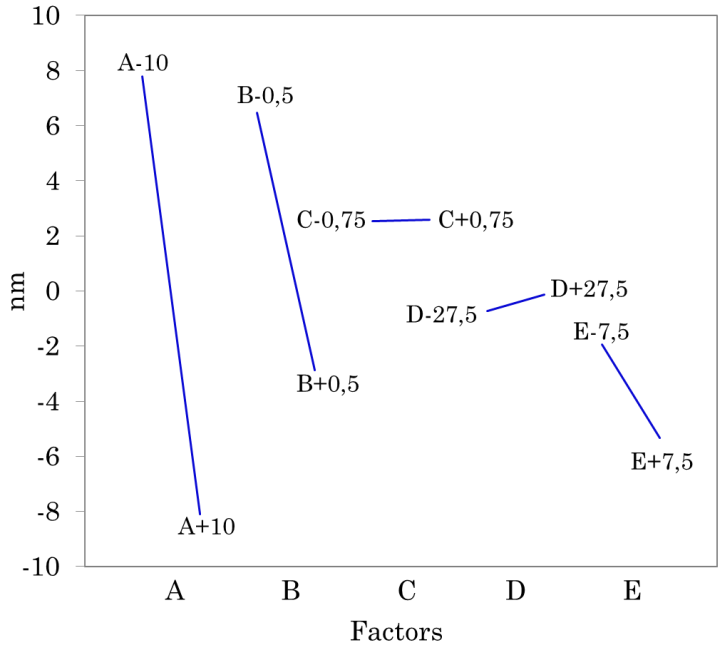

Figure III-56. Factor effects over the final CD with the practical process window.

The gases flow as was the case of the factor A (O_2_AHM) and E (CH_2F_2_ STI trench) were related to the plasma chemistry. By increasing or reducing a gas, we could see impacted the CD dimensions due to the passivation effect. Both of these gases, O_2 and CH_2F_2, were used to passivate. For instance, the CD of the AHM was extremely important since it was used as a mask for its following steps. The CD coming out of this step would be directly influenced for the next steps and, therefore, affect the final CD. The O_2 plays a role to the lateral etching and the passivation of the AHM as well as happened with the flow of CH_2F_2 during the STI trench etching. Increasing the flow rate induced an augmentation of the C:F ratio and affects the CD because of its strong polymerizing behavior. In order to keep a good isotropic etching, it should be highly controlled. A similar behavior happened when increasing the Bias voltage (factor D), which was related to the STI trench. With the increasing Bias voltage, the CD would increase accordingly due to the effect of the sidewalls passivation. The pressure as was the case of the factors B (P_AHM) and C (P_ STI trench) was related to the gas phase. By increasing the pressure, the lateral etching increased as well, and thus the CD became lower. The effect of the pressure was less significant when etching the STI trench than when etching the AHM.

4.3.2. Predictions and Validation

To easily explain and utilize the CD model, the -1 and +1 levels in (III.10) were restored to their real values in each factor and the model was rebuilt as shown in (III.11). The factor effects in (III.11) could not be compared directly as the coefficients were now scale sensitive. However, this model was more straightforward to predict the real CD values using the real

factor settings without any encoding. The initial recipe could be then optimized with the desired CD such that the best electrical performance of the IC can be achieved.

$$CD = +315.614 - 0.788 \cdot A - 7.896 \cdot B - 1.341 \cdot C + 0.049 \cdot D - 0.309 \cdot E \qquad \text{(III.11)}$$

A comparison of experimental and predicted results for the different answers of the DOE is represented in Figure III-57.

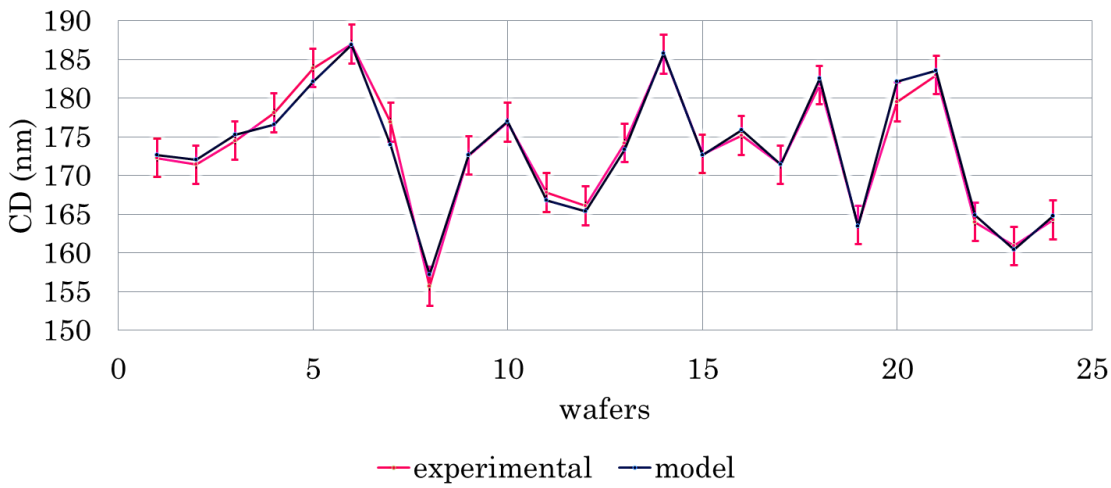

Figure III-57. Comparison between experimental and calculated CD values.

To verify that the model worked for making predictions, some complementary wafer was processed and the corresponding responses were collected. As can be seen in Figure III-57, the predicted and the real CD measurements for these testing runs were highly matched. It did not only prove the significance of the model in (III.10) and (III.11), but also confirms the applicability of this response surface model.

4.3.3. Further Details

Taking advantage of the experiments performed, further analyses were carried out over some of these experimental wafers.

4.3.3.1. Physical Analyses

The wafers with the lowest and highest CD, were used to perform physical analyses, such as SEM and TEM. Figure III-58 shows the SEM analysis of these wafers.

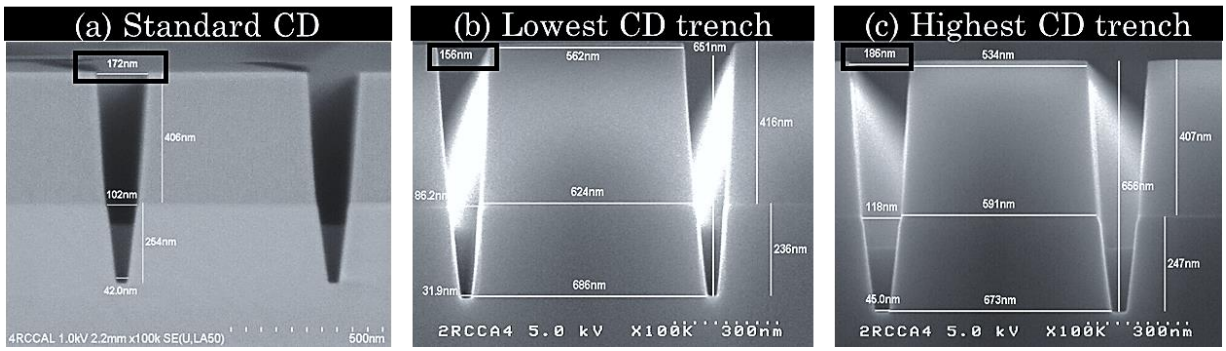

Figure III-58. SEM images of a standard CD of the eSTM trench compared to the lowest and highest CD obtained during the DOE.

With the results shown in Figure III-58, we could verify the measures taken online by CDSEM, so the accuracy of measurements was confirmed. Table III-17 summarizes the comparison of the CDSEM and SEM measures for the wafer with highest and lowest CD.

Table III-17. Comparison of CDSEM and SEM measures.

Wafer CD	SEM	CDSEM
Highest	186nm	187nm
Lowest	156nm	155,7nm

Figure III-59 shows the TEM analysis of these wafers with the measurement of the sidewall passivation at the top and at the bottom of the trench.

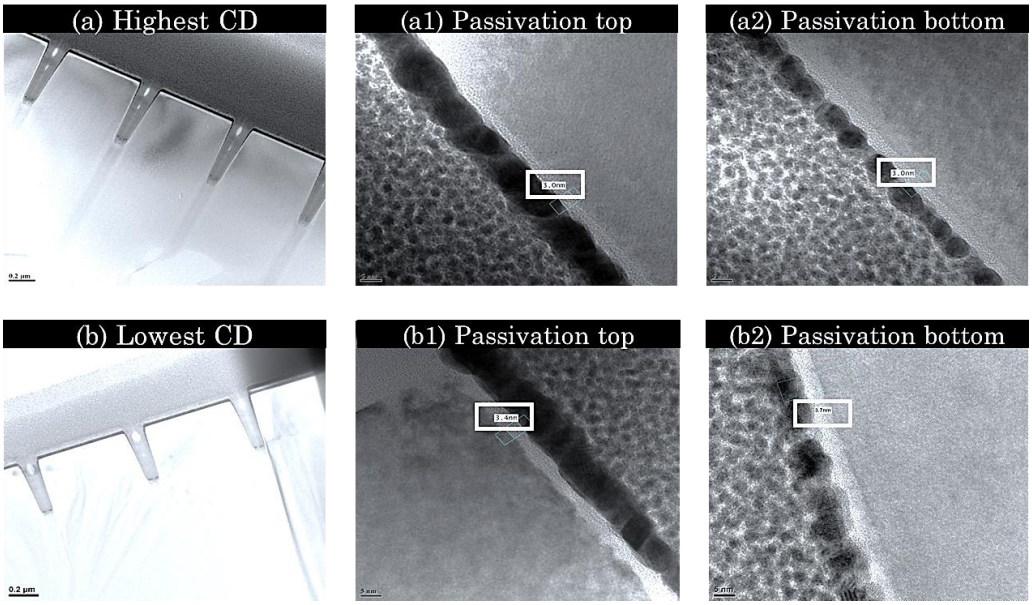

Figure III-59. TEM images of the passivation at the top and bottom of the eSTM trench for the wafer with highest (a) and with lowest CD (b).

It can be appreciated that the passivation top and bottom of the trench with lowest CD was thicker than that created at the top and bottom of the wafer with highest CD. 3.4nm/3.7nm for the lowest CD wafer and 3.0nm/3.0nm for the highest CD wafer. That verified that the lowest CD was due to an increment of the passivation layer due to the effect of the studied parameters.

4.3.3.2. Electrical Analyses

With the validated confidence of the CD model, electrical analyses were done to study the electrical properties of the experimental wafers. During the wafer testing, which is performed before a wafer is sent to die preparation, all individual integrated circuits of the wafer were tested for functional defects by applying special test patterns to them. During those tests, it was concluded that the wafers with lower CD's did have less scatter. Based on the engineering knowledge, it was also known that the wafers with lower CD's usually have better reliability.

4.4. Summary and Industrialization

To study the physical behavior in the Reactive Ion Etching (RIE) process in relation to the final trench CD measurements, a practical study was done in this research and two objectives were accomplished. The first one was to identify the key factors and steps with the largest influences on the final CD. The DOE analysis was performed and the final CD was modelled with the representative "process windows" significantly. The second goal was therefore to use the designed model to predict the CD such that it enables reaching the desired CD for better product performances (ex: electrics, morphology, etc.).

The physical characterization verified that when there was a thicker passivation, the CD was lower, since we were measuring the trench (the space). The electrical characterization of the wafers allowed us to choose the best CD in terms of electrical performances.

For the industrialization, the selected CD was lower than the standard CD of the eSTM trench (172nm). There is one electrical parameter (HBIN60) that is critical for us. This parameter is related to the electrical results. The lower it is, the better the reliability of the cell. This critical parameter was not even present over the wafer no.12 in the DOE study, which had the CD measurement equal to 166nm (see Figure III-60). It is therefore regarded as the optimal CD of the eSTM trench. To put this model in real practice, the selected CD should be lower than the actual CD of the eSTM trench (172nm), which was settled down to be at 166nm.

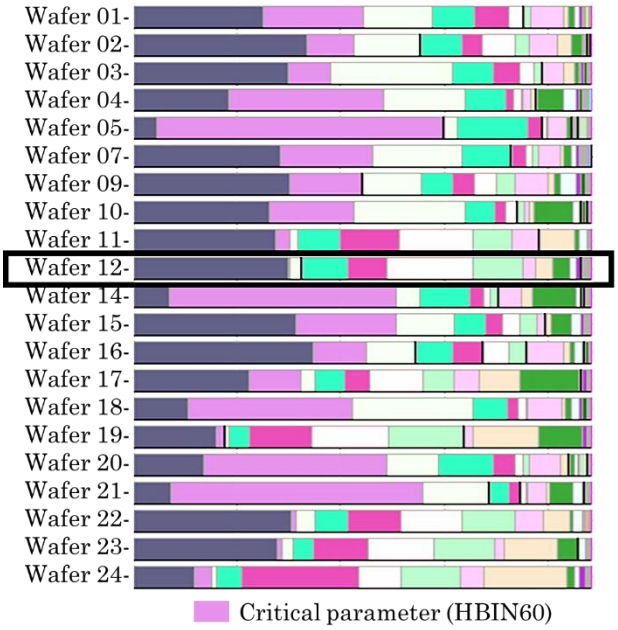

Figure III-60. Electrical results of the experimental wafers.

To obtain the desired CD from the designed model, there could be up to 100 solutions of the parameter settings. In order to have an executable recipe, the setting choices were based on the plasma considerations and the limitations of the equipment. Several tests were carried out to validate this new recipe and ensure its successful process.

5. CONCLUSION

This chapter shows the characterization and optimization of the eSTM process. First, the characterization of the different parts that interact during the process etch were discussed. Therefore, the diagnostics of the plasma itself by using OES and the composition of the surface layer being etched by XPS were studied. In a second stage, for reducing the CD with the aim of optimizing the electrical results, a model was proposed by using DOE; being able to predict and so that control the CD by establishing the units for the most important parameters.

Once the plasma and the chemical composition of the SPL were characterized, we could explain the formation of a SiO_xF_y passivation layer which is mainly oxidized due to the influence of the oxygen in the chemistry and the air exposure. This is also the reason why the bromine desorbs together with the ease of being replaced by F and O. The characterization of the plasma as the sidewall passivation was important for the development of the process since it was a totally new process which needed to be characterize but also

because we could develop the chemical topography analysis at ST Microelectronics Rousset. Thus, the protocol it can be nowadays used for characterizing others samples.

The final goal of this chapter was to reduce the CD in order to get better performance related to the electrical results. In order to keep the CD under control, several parameters were taken into account. Some studies were performed in order to find out the factors and steps with the biggest influence in terms of final CD. With that, we improved our knowledge of the process and obtained a mathematical model with the representative "process window". The model proposed by means of DOE was able to predict the CD such that it allow us to change the CD as long as it will be required for any reason as it has been demonstrated by changing the target CD of the technology from 172nm to 166nm. We decided to reduce the CD based on the electrical results, since the wafers with lower CD were those with better performance respect to the electrical results. Therefore, it was demonstrated that the eSTM trench CD can be achieved with the model presented in this chapter.

"A careful analysis of the process of observation in atomic physics has shown that the subatomic particles have no meaning as isolated entities, but can only be understood as interconnections between the preparation of an experiment and the subsequent measurement" (E. Schrödinger)

Chapter IV

Plasma-Reactor Wall Interactions: The Fluorine Problem

This chapter presents the experimental analyses carried out for the characterization of the reactor walls used in this work. It contains information on the process and the characterization technique used, the *Floating Sample Method*. The analyses were focused on the fluorine problem, a well know issue in plasma reactors which use F-based plasmas. Finally, a new strategy for cleaning the reactor is proposed.

Image of the floating sample performed during this thesis.

During plasma etching processes, there are plasma-surface interactions, as explained in the previous chapter but also the plasma-reactor wall interactions. Due to the differences on the energy of the ion bombardment and the chemical composition of the reactor walls respect to the wafer surface, the effects are completely different. In this chapter, the reactions taking place on the reactor walls during the eSTM trench process are studied.

The chapter is organized as follows. Firstly, an introduction based on the literature review is presented followed by the experimental details related to the process and cleaning. Secondly, the characterization of the coatings deposited on the walls and the optimization of the cleaning strategy are discussed. Finally, the conclusions of this study conclude this chapter.

1. LITERATURE REVIEW

Organic or mineral layers are deposited on the chamber walls during the plasma etching processes [155]. These layers can produce large and uncontrolled shifts in the etch process so that should be well controlled and properly cleaned. However, the chemical nature of these layers, even if it is largely studied [66, 155, 279-286], remains poorly understood in industries, due to the lack of in-situ diagnostics available to monitor the reactor walls. In this section, we present a state-of-the-art about the studies carried out related to this subject as well as an introduction to the fluorine contamination problem.

1.1. Influence of Reactor Wall Conditions on Etch Processes

Controlling the stability of plasma processes becomes a major issue as the dimensions of the gates shrink at each new generation. Among the different reasons leading in controlling the feature dimensions, the chemical composition of the coating formed on the reactor walls is one of the most important [155]. During the etching of successive wafers, the wall surfaces exposed to the plasma will change progressively. As result, the etching characteristics of the plasma changes. The coating layers formed on the reactor walls have been studied by several authors for different plasmas chemistries.

Schaepkens et al [279], studied the influence of the reactor wall conditions in high density fluorocarbon plasma etch processes. They saw that the reactor wall temperature was an important parameter, since it could reduce the loss of fluorocarbon species from the plasma to the walls as the wall temperature increased. They even proposed a model describing the time dependence of the reactor wall temperature. Some years later, Joubert et al [155] proposed a method for monitoring the chamber walls coating deposited during plasma processes. This technique, which has already been introduced in Chapter II (3.3.5.), is the so-

called *floating sample* or *air gap*. They validated the technique during silicon gate etching in $HBr/Cl_2/O_2$ plasmas, which are known to deposit silicon oxychloride layers on the chamber walls. They also studied the influence of CF_4 addition in the plasma. They observed that CF_4 addition severely decreased the deposition rate of $SiOCl_x$ species on the chamber walls.
Xu et al [280] also showed that the chemical nature of coatings on the chamber walls can change by varying the CF_4/O_2 ratio in the $HBr/Cl_2/CF_4$ chemistry. When the chambers were exposed to low CF_4/O_2 ratios, they were covered by $SiOCl_x$ oxide-like films whereas that for a CF_4/O_2 ratio of 4:1, the Al_2O_3 chamber walls was kept free from deposition. They also appreciated that for higher ratios, the chamber walls were coated with carbon-like films. Cunge et al [281] also remarked this phenomenon of enhancement by the recombination rate of Br atoms with CF_4 addition and resist etching in $HBr/Cl_2/O_2$ plasmas. They explained that the recombination coefficient of Br atoms on organic polymer surfaces (C_xF_y or C_xCl_y) is much larger than on SiO_2-like surfaces (SiO_xCl_y). In another study, Cunge et al [282] measured the absolute concentrations of $SiCl_x$ radicals by broad band UV adsorption spectroscopy for $HBr/Cl_2/O_2$ processes at different O_2 gas flow rates and RF powers in the plasma. They saw that the oxidation by O atoms of $SiCl_x$ species chemisorbed on the layer leaded to the irreversible incorporation of silicon on the chamber walls by forming a silicon oxychloride film on the reactor surface. They represented the silicon lifecycle and the deposition mechanism of the SiO_xCl_y layer on the reactor as it is shown in Figure IV-1.

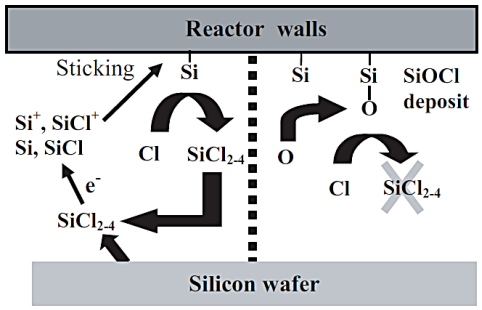

Figure IV-1. Schematic of the silicon lifecycle and deposition mechanism of the SiO_xCl_y layer on the reactor walls. The left part without O_2 and the right with O_2 added [282].

There are also several studies related to the fluorinated mechanism of reactor walls irradiated by high density F-based plasmas. Miwa et al [283] studied the contribution of F-based plasmas to Al_2O_3 and Y_2O_3 reactor walls. For both of them, when the surface of the reactor was bombarded by high-flux positive ions of a CF_4/O_2 plasma, the walls were significantly fluorinated. Ramos et al [284] saw the same problem; F-based chemistries leaved AlF_x species on the reactor walls being their reactor walls composed of Al_2O_3. Moreover, the mass-production factories reactor walls are composed of Al_2O_3 and Y_2O_3 inner walls which have problems in significant erosion and particle generation when they are immersed in fluorine-based plasmas [283]. Furthermore, this problem is accentuated due to the fact that

most of the cleaning strategies use also F-containing plasmas. This fluorine problem have been largely studied due to the importance of maintaining stable plasma processing conditions.

1.2. Contamination: The Fluorine Problem

Joubert et al [155] already saw a significant AlF component at 75.9eV in the Al 2p peak when developing the floating sample technique. This component was observed for O_2 flows larger or equal to 5sccm demonstrating that a fluorine-rich interference layer was formed on the Al_2O_3 surface of the reactor on which the $SiOCl_x$ film grew.

Ramos et al [284] delved more on this topic when studying the wafer to wafer reproducibility which is a major challenge in etching processes. The periodic dry cleaning of the reactor that they studied which was F-based is one of the most common strategy nowadays to ensure process repeatability. However, as mentioned before, this kind of cleaning based on fluorine, left AlF_x species on the reactor walls as they observed, and several groups confirmed [156, 283-287]. Ramos et al explained that during a SF_6/O_2 WAC (Wafer-less Auto Clean) the Al_2O_3 roof was simultaneously fluorinated and sputtered. Thus, releasing non-volatile AlF_x species in the plasma, which were redeposited on all other surfaces exposed to the plasma. Hence, the reactor cleaning plasma left residues on the reactor walls on its own. This accumulation of an AlF_3 deposited on the chamber walls from the process and the cleaning is at the origin of process drifts. In other study of this group [285], they exposed the presence of an $AlOF_x$ layer formed as well due to the fluorination of the Al_2O_3 reactor wall. In this work, they verified that this layer can flake off when it becomes too thick, as they said in their first study. They also explained that the AlF_x layer increased when the F-based plasma duration increased, as shown in Figure IV-2.

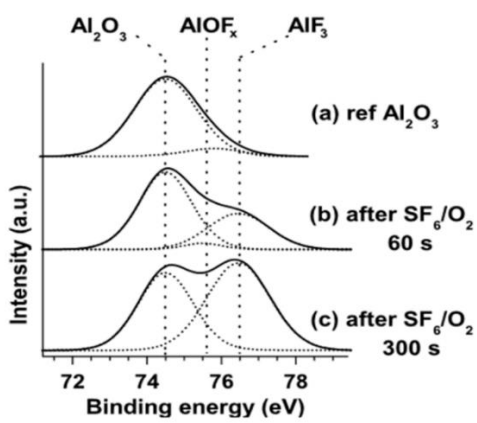

Figure IV-2. Al 2p XPS spectra from the floating Al_2O_3 sample before and after exposure to different SF_6/O_2 cleaning plasmas [285].

They concluded that the formation of AlF_x coatings is inescapable in any inductively coupled reactor containing Al_2O_3-covered parts. Furthermore, the problem was not only related to the reactor with Al_2O_3 walls, but also to the others.

Miwa et al [283], studied two kind of reactors, one with walls made of Al_2O_3 and another one made of Y_2O_3. Both surfaces, Al_2O_3 and Y_2O_3, were fluorinated after being exposed by F atoms. They explained that the key step in the fluorination process was the decomposition of the Al-O (or Y-O) bonding on the ceramic surface by reactions with carbon in fluorocarbon deposits. Once the metal-oxide bonding was decomposed, the progress of fluorination was inevitable. Ramos [66] also studied the behavior of Y_2O_3 surfaces when they were exposed to F-based plasmas. Their results confirmed those of Miwa. The concentration of fluorine in his results showed that the surfaces of the reactor walls composed of Y_2O_3 turned into a YF_x surface after exposure to the fluorinated plasma. He concluded, that we can expect the same types of problems with a Y_2O_3 reactor and an Al_2O_3 reactor. However, the Y_2O_3 is known to be a more stable compound than Al_2O_3. Actually, Miwa et al [283] said that even if fluorinated as well as the Al_2O_3, the Y_2O_3 surfaces were less contaminated when they were irradiated by the same plasma. In order to provide more stable CD performances, these F-based depositions on chamber walls need to be reduced. Several cleaning strategies propositions showed up due to this concern [156, 286-288], as it will be explained later in this chapter (4.1.).

2. PROCESS AND CLEANING CONSIDERATIONS

The **process** of the eSTM trench has already been introduced in Chapter III (2.1.). The same steps for reaching the eSTM as well as the selected chemistry for each one of them being those F- and Br-based plasmas are used for this study.
The **cleaning**, performed after each wafer, was the so-called WAC (Wafer-less Auto Clean) [289]. It is a periodic dry cleaning of the reactor in which a protective cover wafer for the electrostatic chuck is not necessary. WAC is the most common strategy to ensure process repeatability which is a major challenge in etching processes. It removes deposition from the chamber walls which ensures that the chamber is maintained in a clean state in order to improve process performance in the equipment. It also improves productivity, minimizes drifts associated with changing chamber conditions and enables application mixing an insitu processing capability in the tool [289].

LAM Research considers two possibilities when selecting the WAC. When etching with fluorocarbon based chemistries, it deposits C_xF_y polymers. When etching with $HBr/Cl_2/O_2$ chemistries, the deposits are silicon oxi halides-like films or “glassy” depositions (SiO_zCl_x and SiO_zBr_x). Thus, the WAC used for processes where F- and Br-based chemistries are employed

should clean both deposits, C_xF_y and SiO_zCl_x/ SiO_zBr_x. The most widely used WAC for that purpose uses SF_6/O_2 chemistry [156,283,284,286,289].

The WAC used in our experiment uses this SF_6/O_2 chemistry. It is composed of two main cleaning steps. The clean 1 (F-based), is used for cleaning the "glassy" deposition; the silicon oxi-halides. The clean 2 (O-based), is used for cleaning the C_xF_y polymers deposition. However, since the clean 1 uses also O_2, some C-containing deposits are etched during this step too. Since the eSTM is a new technology still in development, the WAC was taken from other technology where also F- and Br-plasmas were used. That WAC implied 30s for the clean 1 and 35s for the clean 2 (30_35). A schematic representation of the WAC operation process used in our study is shown in Figure IV-3.

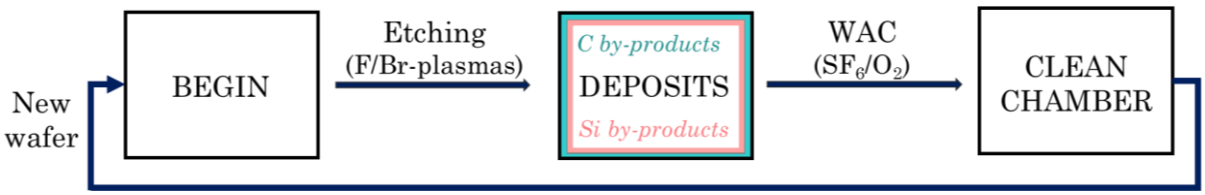

Figure IV-3. Principle of the WAC used for cleaning the C- and Si-by products.

Concerned about the fluorine problem introduced in the previous section, which is not only related to the process but also to the WAC because also uses F-based plasmas, we wanted to characterize the coating deposited during the process and during the WAC on the reactor walls. The goal of analyzing the fluorination produced during the process and during the WAC, was to reduce it by keeping the reactor as free of fluorine as possible.

3. CHARACTERIZATION

This section is related to the characterization of the reactor walls coatings formed during the etching process of the eSTM trench.

3.1. State-of-the-art

The study of the plasma-wall interactions is difficult due to the lack of diagnostic methods to monitor the chemical nature of the films formed on the reactor walls during the etching. Therefore, a state-of-the-art seeking the possible techniques existing for characterizing the coatings deposited on the chamber walls was required in order to select the way that best meet the conditions of this study.

The first study of the coating deposited during the silicon etching by Cl_2/O_2 plasmas on the reactor walls, was developed by Zau et al [290] in 1992. In their study, they fixed a gold sample on the surface which was analyzed later by Auger Electron Spectroscopy (AES). They saw that the oxychloride film, formed by reaction between the etching products and the added O_2, passivated the interior etcher surfaces against Cl surface recombination and the composition. Thus, the reactor walls conditioning was similar to the sidewalls passivation being SiO_xCl_y.

In 2001, Godfrey et al [291] proposed a new diagnostic method for monitoring the reactor walls. This one was based on Multiple Total Internal Reflection Fourier Transform InfraRed (MTIR-FTIR) spectroscopy. They used it to detect etch products and the films deposited on the reactor walls during Cl_2 plasma etching of Si, to determine the effectiveness of a SF_6 plasma to clean films deposited on the walls and to monitor wafer-to-wafer etching reproducibility. The technique consisted of a FTIR spectrometer and a box with all the necessary optical components to direct the infrared radiation to and from an Internal Reflection Crystal (IRC) that was mounted on the inside wall of the plasma reactor. The optical box was attached to the exterior of the plasma reactor wall and held the IRC just inside the reactor together with a series of mirrors. The bigger trapezoidal IRC was directly exposed to the plasma and simulated a portion of the reactor walls. The spectra collected as a function of time during their experiment was used to analyze the bonds formed on the IRC surface and so that the chemical composition of the coatings can be determined. Ullal et al [292] also used this method to monitor the films formed on the reactor walls. In their results, the silicon oxychloride film etching proceeded by incorporation of F, which also abstracted and replaced the Cl atoms in the film. If the SF_6 plasma was not maintained for a sufficiently long period to remove all the deposits, the F incorporated into the film was infiltrated into the gas phase during the subsequent etch processes. They explained that this residual F can have undesirable effects on the etching performance and the wafer-to-wafer reproducibility.

Some years later, Miwa et al [225] studied the deposition on the etch chamber using OES. They obtained relative quantity of deposition in the etch chamber from the ratio of optical emission intensity of SiBr to He in the plasma. Based on the results of relative quantity of deposition depending on cumulative etched wafers in the chamber, they estimated a mechanism of particle occurrence from the deposition on the chamber. They explained that the SiBr density in the plasma might be proportional to the Si contained in the deposition. Thus, they could estimate the deposition amount by determining the SiBr density from the optical emission.

In 2004, Joubert et al [155] proposed the floating sample method, already introduced in this thesis. This method is the most widely used method for characterizing the reactor walls

composition since it allows the quantitative analysis of the coatings chemical composition without requiring any specific equipment, by using a sample electrically floating on top of a standard wafer where the same deposit as on the reactor walls is formed. By transferring the wafer carrying the electrically floating sample into the XPS analysis chamber, the chemical composition can be determined.

Ramos et al [284] studied the plasma-reactor wall interactions in advanced gate etching processes by using two techniques. Firstly, the floating sample developed by Joubert et al [155]. Secondly, another technique already presented by Cunge et al [293]. This new method was based on the detection of Cl_2 by laser absorption allowing to determine whether the reactor has been correctly cleaned before processing a new wafer, which was no easy to characterize before. The goal of their diagnostic technique was to prevent process drifts and thus the waste of expensive wafers. This method was performed without wafer using laser absorption spectroscopy in a reference Cl_2-based plasma. They showed up that the advantage of using their method lies in the possibility of measuring within a few seconds the Cl_2 density in the steady-state plasma, which is highly sensitive to the reactor walls' coating.

In this research, we wanted to characterize the coatings on the reactor walls of the industrial reactor of ST Microelectronics Rousset, where all our experiments were carried out and until now the coatings on the reactor have never been characterized before. Due to industrial constraints, we decided to use the floating sample method since it allowed us to characterize the reactor walls, without opening the chamber and therefore, without contaminating it. Furthermore, we wanted to develop this protocol at the company so that it could be used for the process engineers in order to characterize any other equipment as needed.

3.2. Experimental

Specifications about all the equipment used for this thesis, were introduced in Chapter II. The experimental set-up for this study includes:

- The plasma reactor: 200mm *VERSYS STAR* from LAM Research (Chapter II. 2.1.1.)
- The XPS equipment: *KRATOS AXIS NOVA* (Chapter II. 3.3.2.)

The analyses were performed by using the floating sample method developed by Joubert et al [155]. The samples were fixed on the wafers, but separated from it by a thick air gap calculated for each process. *Kapton* adhesive rolls were used to create the air gap between the wafer and the sample. As mentioned before (Chapter II. 3.3.5.), when the RF biasing voltage is applied to the wafer, if the air gap is thick enough, it prevents the DC-biasing of the sample. The wafer holding the sample is etched under regular conditions while the

sample is electrically floating, and so the same deposits grows on the sample and the reactor walls [155].

The experimental protocol used in this research consisted into analyze the deposits created during the etch of the STI (F-based chemistry), the one created during the eSTM trench etching and the one created during the WAC. The value of the plasma parameters, such as the Boltzmann constant (k_B), the elementary charge (e) and the electric permittivity of vacuum($\in_0$), have already been presented in Chapter I (3.2. and 3.3.). However, there are some others that need to be introduced. For instance, the electronic density (ne) which in our case was 10^{11} cm^{-3}. Furthermore, there are specific parameters for each process (STI and eSTM) as summarizes in Table IV-1.

Table IV-1. Specific plasma operating conditions for each step (STI and eSTM).

Parameters	**Steps**	
	STI (F-plasma)	eSTM (Br-plasma)
Time	70s	76s
Pressure	7.5mTorr	30mTorr
Electronic temperature	3eV	2eV
Bias RF voltage	275v	360v

According to the equations introduced in Chapter I (Debye length (I.4) and Child-Langmuir sheat (I.8)) we can calculate the air gap needed. With a Debye length of 0.04mm for the STI step and 0.03mm for the eSTM step, the calculated air gap required for simulating the F-based step (STI) was 1mm and 1.3mm for simulating the Br-based step (eSTM). For analyzing the deposits created during the WAC, no space was required since there is no bias applied. Thus, the piece of silicon with the Y_2O_3 deposition was directly mounted on the wafer support. Another consideration was taken into account related to the characteristics of our process. The maximum time of each process step had to be at most 30 seconds to avoid temperature problems on the floating sample. Our process times were 70s for the first step and 76s for the second one. Thus, the steps were divided into several steps to not pass the maximum time advised.

Since this research was performed in an industrial reactor, several precautions were taken into account. For instance, the processes were always carried out between two TXRF (Total Reflection X-Ray Fluorescence) analyses in order to see that no contamination happened between them and also that the chambers were in the same conditions before/after the experiments. Furthermore, the Preventive Maintenance (PM) of the equipment was performed always after the second TXRF in order to be sure that the equipment was totally cleaned.

3.2.1. Substrates

The chamber walls are made of Al_2O_3 but coated with Y_2O_3 since LAM discovered that this compound is more stable than Al_2O_3. For analyzing the walls of the chamber by using the floating sample method, Y_2O_3 samples were essential. Our samples were deposited on silicon by ion sputtering with xenon at Université de Poitiers (CNRS). The thickness was about 200nm.

3.3. Results

The information that we had about the samples was just related to the deposition process, as explained before. Thus, the first analysis was performed over a Y_2O_3 sample to have it as a reference. The characterization of their composition was carried out by XPS and the results are shown in Figure IV-4. The sample was mainly composed of oxygen (39.1%), carbon (36.4%) and yttrium (23.2%). However, some traces of fluorine were also detected (0.2%) and most surprising; molybdenum (1.1%). We could not have further information about the molybdenum origin. In this study, we decided to not consider its presence which was detected in all the samples since it was not related to our process.

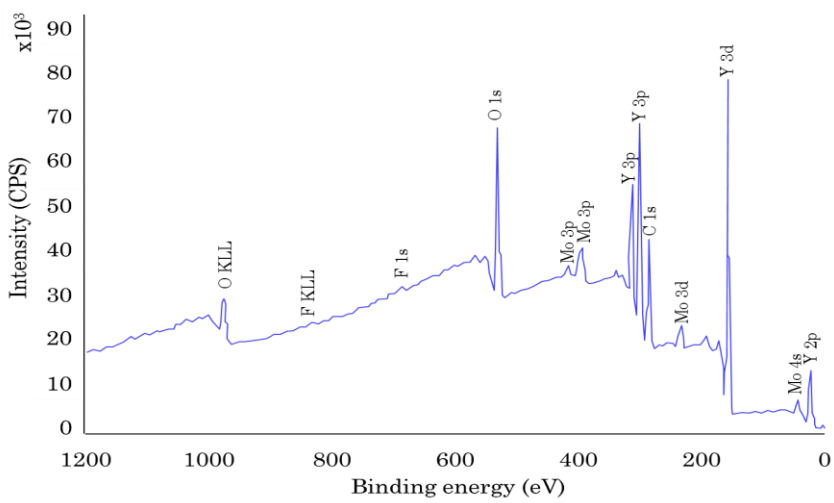

Figure IV-4. XPS survey spectrum of the Y_2O_3 sample used as reference for our study.

Avoiding the molybdenum presence, which is indeed very low, the composition of the reference was mainly Y atoms linked to O atoms (Y-O) and O atoms linked to Y atoms (O-Y). Actually, this was the expected composition for a Y_2O_3 sample. However, the sample presented as well some traces of fluorine and in particular an important carbon contribution, coming probably from the air contamination. Those contaminations (F and C) disappeared quickly during the first seconds that the sample is exposed to the plasma.

The first thing we wanted to study was the process influence on the reactor walls. This process, extensively explained in this thesis, is the one related to the eSTM trench. Thus, analyses about the influence of the STI step (F-based chemistry) and the eSTM step (Br-based chemistry) on the reactor walls were performed. The results, by using the floating sample method, are shown in Figure IV-5. From these results, we concluded that the presence of fluorine was the most important contribution for both processes, after the F-chemistry (STI step) and the Br-chemistry (eSTM step). Both compositions were pretty similar except for the presence of bromine over the sample related to the eSTM which was clearly coming from the chemistry (0.7%). The carbon was linked to the F (CF_x) with a contribution of the air contamination (CC:CH). However, no silicon was detected in any sample, only few traces during the eSTM step not even quantifiable. This was really surprising since from the eSTM step (HBr/O_2) some "glassy" depositions were expected on the reactor walls.

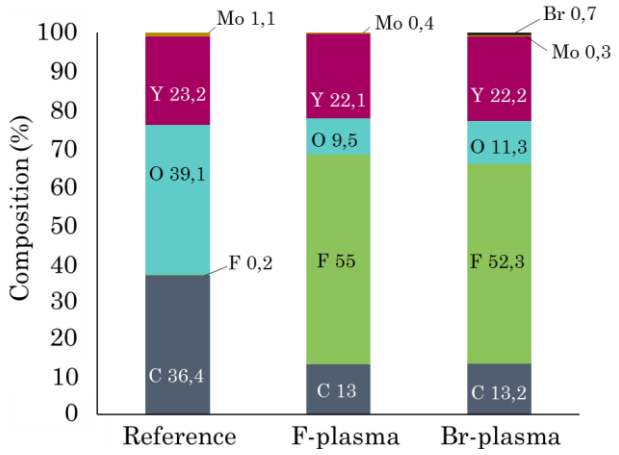

Figure IV-5. Chemical composition of the STI (F-plasma) and eSTM (Br-plasma) steps compared to the Y_2O_3 reference.

Trying to understand if the absence of silicon was due to the process or to the Y_2O_3 sample used, we decided to perform the same analysis on a Al_2O_3 sample. The reactor counts also with this material on its composition even if it is covered with a Y_2O_3 coating. The results when using the Al_2O_3 sample were similar to those obtained with the Y_2O_3 sample. Less than 2% of silicon was detected for the Al_2O_3 sample. Still too low compared with the percentage expected during a silicon etching step with HBr. In any case, we were always able to detect the composition of the sample (Y_2O_3) which means that the coating thickness was less than 10nm which is the range of detection of the XPS. The reduction of O atoms was explained by the incorporation of fluorine. The Y atoms were less linked to O atoms (Y-O) and more linked to F (Y-F) since its presence was more important after the process. Thus, after the process, the yttrium is mainly linked to the fluorine in the form YF_x.

Still concerned about the fluorine problem, we characterized also the coatings deposited on the reactor walls during the WAC, which is intended to clean the coatings (see Figure IV-3) from one process to another. The result is shown in Figure IV-6 compared with the Y_2O_3 reference.

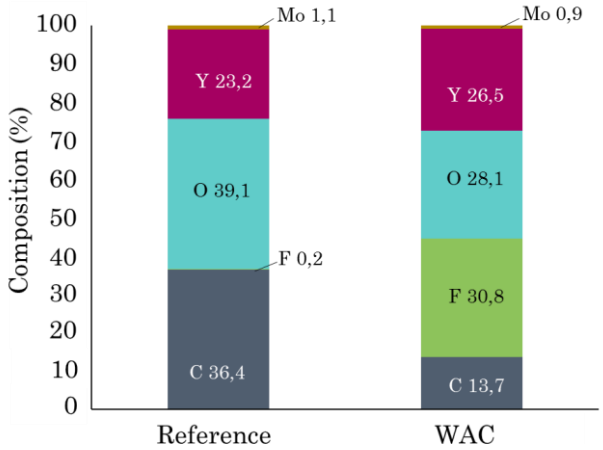

Figure IV-6. Chemical composition of the WAC (SF_6/O_2 plasma) compared to the Y_2O_3 reference.

Since the WAC was also F-based (SF_6/O_2), and knowing from the literature that these kind of plasma also leaves F-contamination on the reactor walls, we wanted to know if the coatings were more or less fluorinated than the process (STI and eSTM steps). Since the pressure used during the WAC is higher than those used during the processes, it is supposed to reduce these F-containing formations. From the results shown in Figure IV-6, we could see that the presence of fluorine after the WAC was still very disturbing, compared to the reference. Respect to the previous analyses, we saw a reduction of fluorine which before was 55% and 52.3% for the STI and the eSTM steps, respectively.

After the WAC, the Y atoms were more linked to O atoms than F atoms, even if the YF_x formation existed (Y-F). All the contributions related to the Y 3d peak can be observed in Figure IV-7, where the composition of the Y peak is represented for the reference (Y_2O_3), the STI process (F-based chemistry), the eSTM process (Br-based chemistry) and the WAC (SF_6/O_2 plasma).

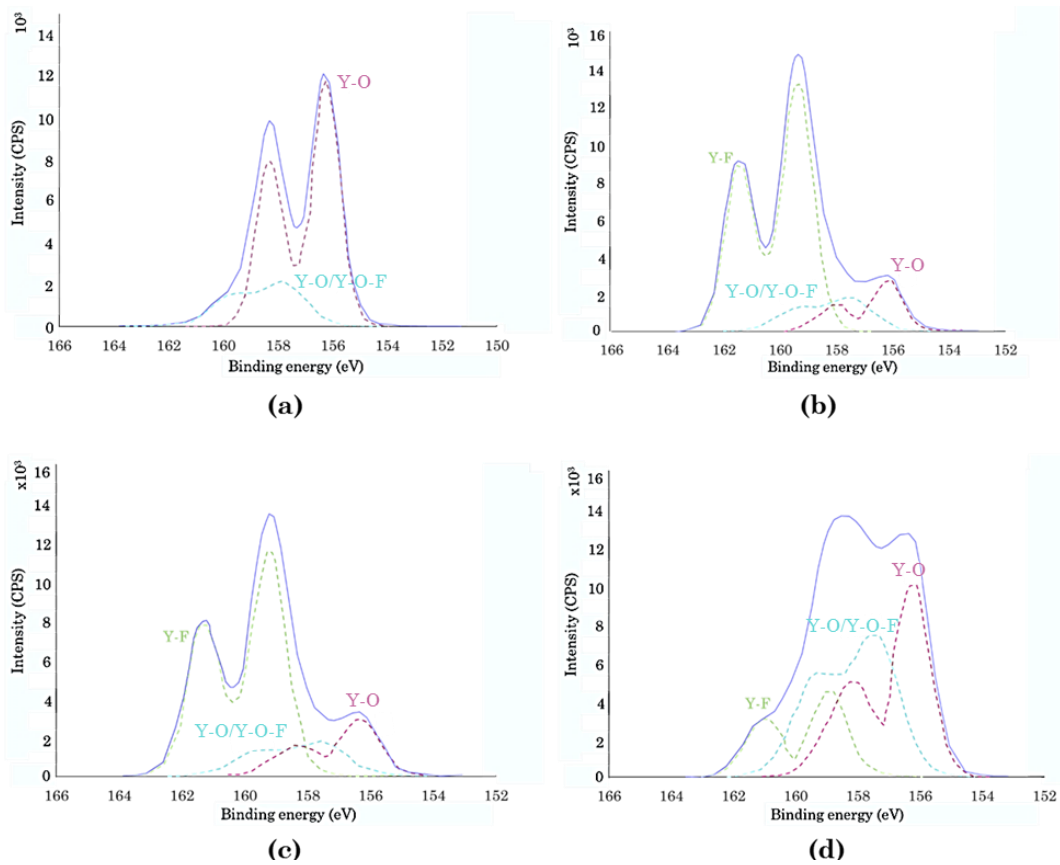

Figure IV-7. Y 3d spectra for the reference (a), the STI step (b), the eSTM step (c) and the WAC (d).

It can be appreciated, from Figure IV-7, that in all the analyses the Y-F contribution was present, except for the reference, where the yttrium was in its metal form and linked to the oxygen atoms.

After analyzing the process and the WAC influences on the reactor walls, all them affected by the fluorine problem, we needed to find a solution in order to improve the situation.

4. OPTIMIZATION

This section is related to the optimization of the cleaning strategy used nowadays at ST Microelectronics Rousset for the eSTM technology.

4.1. State-of-the-art

A brief state-of-the-art seeking the possible techniques existing for cleaning the coatings deposited on the chamber walls was done in order to select the best strategy for ST Microelectronics Rousset, since all these analyses were performed in its industrial reactor.

In 1998, Schaepkens et al [279], studied the influence of reactor wall conditions on etch processes in inductively coupled fluorocarbon plasmas. In their results, they showed that the loss of fluorocarbon species from the plasma to the walls was reduced as the wall temperature increased. Therefore, if the walls have a temperature higher than a certain feedgas chemistry dependent value, no net deposition will happen.

Smith and James [287] patented a method for removing PECVD residues of fluorinated plasma using in-situ H_2 plasma. This method for cleaning the chamber was related to the PECVD processes. Miwa et al [286] used the same principle for modifying the fluorinated Al_2O_3 surface in plasma etching processes. In their study, they irradiated H_2 and O_2 plasmas on fluorinated Al_2O_3 samples which was prepared by exposing the sample to an SF_6/O_2 plasma. The effects of the H_2 plasma irradiation were the reduction of the AlO_xF_y and AlF_x bonding components but it induced Al-OH bonding. For removing these Al-OH bonding they used sequential irradiation of O_2 plasmas after the H_2 plasma irradiation. However, the sample after being exposed to H_2 and O_2 plasmas increased the level of peroxidation and surface roughness.

Another widely used approach, was the one employed by Cunge et al [156]. They proposed a new chamber walls conditioning to improve the stability of plasma processes by getting rid of AlF particles. The chamber conditioning was achieved by coating the reactor walls between wafers with a carbon-rich polymer. The cleaning of the chamber was achieved in two steps. A first one used to remove the deposit formed on the carbon layer by using SF_6 plasmas followed by the carbon coating using O_2 plasmas. With their strategy, the etching process would always start under the same conditions. The carbon-coated chamber and the Al_2O_3 reactor walls would be only exposed to O atoms. The principle of conditioning is shown in Figure IV-8.

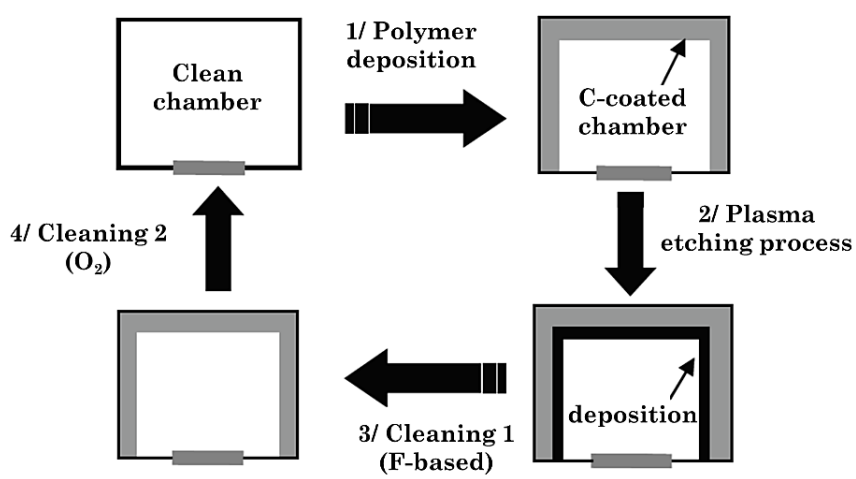

Figure IV-8. Principle of the strategy of coating by using a carbon-rich film [66].

Ramos et al [285], proposed to clean the aluminum fluoride coatings from plasma reactor walls in $SiCl_4/Cl_2$ plasmas. They remembered that by cleaning the reactor in fluorine chemistries, as SF_6, AlF_x and YF_x formations are inevitable, and so they proposed to clean it in $SiCl_4/Cl_2$ plasmas, restoring the Al_2O_3 or Y_2O_3 walls before processing the next wafer. Their results verified that the use of this chemistry was good enough. Furthermore, $SiCl_4$-based plasma chemistries also removed other metal fluorides, such as HfF_x and more generally metallic oxides from the reactor walls.

Other alternatives, as the one proposed by Abdolahad et al [288] exit. They used a fluorine-free high-resolution selective plasma etching of silicon-oxide on silicon substrates. Of course, if there is a way for etching without using F-based chemistries, no fluorine contamination will happen.

In our case, the first option was to put in place a strategy similar to the conditioning strategy developed by Cunge [156]. However, for economic reasons, we could not put it in place and the industrials decided to keep using the WAC. In any case, the optimization of the recipe was required in order to get the one that matched the best with our recipe. The goal was also to reduce the fluorine time exposition in order to reduce the YF_x formations. The strategy followed then, was to optimize the WAC. By optimizing the WAC, more repeatable conditions can be achieved which is essential as CD size continues to shrink.

4.2. Strategy

After deciding to continue using the WAC for cleaning the reactor walls, we employed a strategy based on 4 steps for improving it.

- Step 1: time definition for clean 1 (SF_6/O_2) by using the iteration method.
- Step 2: time definition for clean 2 (O_2) by using the endpoint detection method.
- Step 3: New WAC cleanliness verification methodology.
- Step 4: Floating sample method for verifying the optimization.

Due to the LAM restrictions related to the WAC, the clean 1 cannot be lower that 12s and the clean 2 cannot be lower than 30s. So that the minimum WAC would be 12_30s. This strategy is explained as follow.

4.2.1. Protocol

The protocol followed consisted on recording the optical emission of 5 production wafers. Two WAC's were performed after each one. The first one, was the one that we wanted to test. The second one, was a reference WAC, which times for clean 1 and clean 2 were longer (60_60) than the standard WAC (30_35) in order to be used as chamber clean reference.

- Step 1: time definition for clean 1 (SF_6/O_2) by using the iteration method

In order to define the time for clean 1, the recorded traces for 703nm (F) were compared with the chamber clean reference (60_60). The trace which overlap with the reference was the good one. Several references are needed to confirm the results are not due to the variability of the process. Five WAC times were tried for clean 1. These times were 25s, 20s, 15s, 10s and the standard one which is 30s. Even knowing that the LAM restrictions do not allow a clean 1 lower than 12s, we wanted to test it in order to see if 10s would be already enough. Since we knew, from the previous analyses, that there were not many "glassy" deposits to be cleaned.

- Step 2: time definition for clean 2 (O_2) by using the endpoint detection method

Once the time for clean 1 was defined, we ran a WAC with the optimal time selected for clean 1, and 60s for clean 2. Then, the endpoints of the clean 2 were evaluated by using the 516nm (C) line. The optimized time for clean 2 must be equal to the endpoint plus 30% of this endpoint.

- Step 3: New WAC cleanliness verification methodology

A long WAC and a clean reference (WAC 60_60) was required to be sure that the chamber was cleaned. We processed a standard wafer with the new optimized WAC, selected with the optimal times for steps 1 and 2. After that, a new chamber clean reference WAC was used for comparing its traces related to the 703nm (F) and to verify if the traces overlap. That would confirm that the WAC was successful.

- Step 4: Floating sample method for verifying the optimization

After verifying that the WAC was the good one by using OES, we used the floating sample method for comparing if the fluorine deposition was reduced with this new WAC compared with the previous one.

The results of these experiments are shown in the next part.

4.3. Results

The results related to the step 1, the time definition for clean 1 (SF_6/O_2) by using the iteration method, are shown in Figure IV-9 and Figure IV-10.

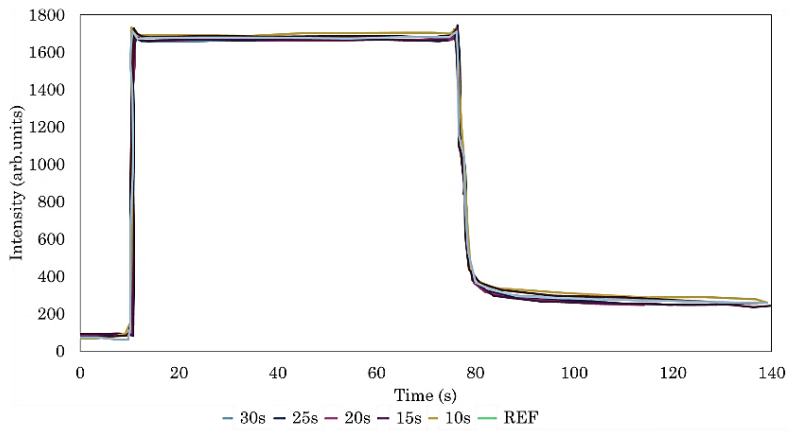

Figure IV-9. Time definition for clean 1 (SF_6/O_2) by using the iteration method.

In Figure IV-9 all the lines overlap. In order to clarify this, a zoom between 10 and 26s is shown in Figure IV-10, where it can be easily appreciated the fact that even when using a clean 1 of 10s, the chamber was already well cleaned.

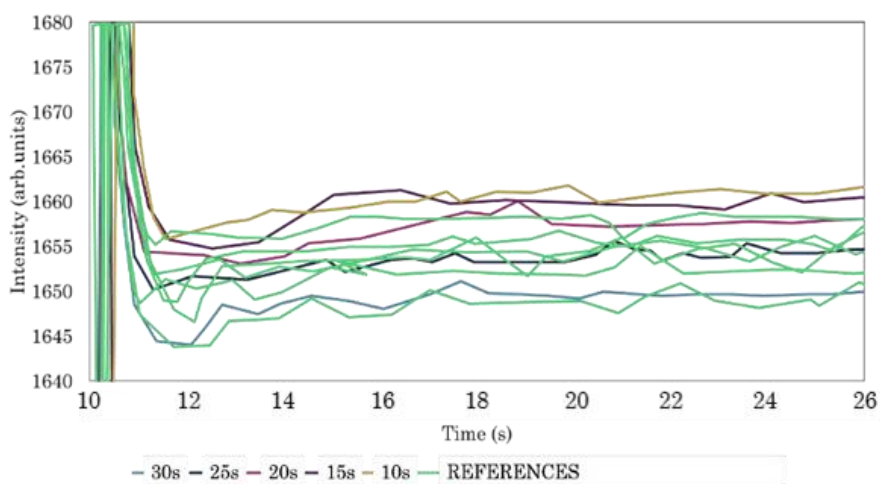

Figure IV-10. Zoom of Figure IV-9 between 0s and 40s with more references.

In Figure IV-10 more references were introduced in order to confirm that the variation was due to the equipment and not to the WAC time. By introducing these references, it was easy to see that the tests were mixed between them and the only difference was the variability of the equipment itself. Therefore, the chamber was always clean. Furthermore, for considering a real variation it should be around 250a.u., here, the scale was set between 1640a.u. and 1680a.u and moreover, the different times employed did not respect any logic, the variation between them is totally arbitrary which confirmed that it was associated to the variability and not to the process time. Thus, even at 10s, the clean 1 was enough. This matched with the analyses performed by using the floating sample, when we saw the influence of the process on the reactor walls. The absence of silicon when using the Y_2O_3 sample or the low

presence of it when using the Al_2O_3 sample, was therefore, confirmed with these experiments due to the fact that already at 10s the chamber is totally cleaned of "glassy" depositions. However, we set the time for clean 1 at 12s, which was the minimum recommended by LAM.

Once the time for clean 1 was selected (12s), we analyzed the 516nm line related to the carbon by running a WAC 12_35. The result of this second step of the protocol, related to the time definition for clean 2 (O_2) by using the endpoint detection method, is shown in Figure IV-11.

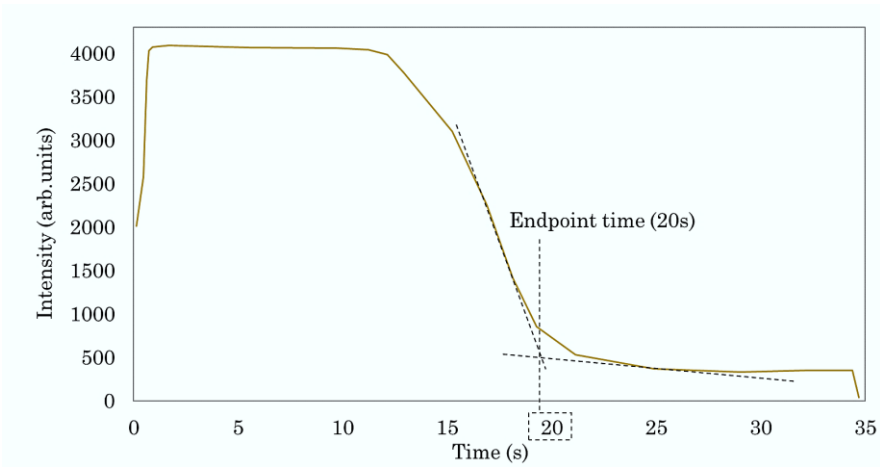

Figure IV-11. Time definition for clean 2 (O_2) using the *endpoint detection method* for line 516nm (C).

As it can be appreciated from Figure IV-11, the endpoint time was set at 20s. However, a 30% overetch is mandatory in order to be sure that we totally cleaned all the C-polymers. Thus, the optimized time for clean 2 was 26s, with the overetch included. Therefore, our optimized WAC was 12_26s, where 12s were needed for clean 1 and 26s for clean 2. Furthermore, during the clean 1 (SF_6/O_2) at the same time that the "glassy" depositions are cleaned by SF_6, the O_2 etch the C-polymers too. Since we reduced the time for clean 1, the clean 2 could not be reduced that much since more C-polymers (CF_x) than "glassy" depositions were founded in the analyses.

The step 3 was related to the verification of the WAC, which was successfully validated. However, even if the WAC was already optimized for the eSTM process, where few "glassy" depositions were involved on the process etch, we wanted to see how the fluorine contamination was affected by this reduction of time for the clean 1 (from 30s to 12s). For that purpose, we used the floating sample for characterizing the coating deposited during the new WAC (12_26s) and to compare it with the previous one (30_35s), as explained in the protocol (step 4). Furthermore, since we wanted to reduce the fluorine as much as possible, we characterized also the new WAC by increasing its pressure (from 60mTorr to 85mTorr). Because the number of molecules is proportional to the pressure of the system, and the mean free path (λ) is dependent on the number of molecules; under too high pressure the λ is too

short and so the electrons and ions cannot build up the necessary speed for ionizing collisions, thereby less is the Y_2O_3 attack and lower the YF_x formations. Figure IV-12 shows the chemical composition of the floating sample representatives of the coatings deposited on the reactor walls during the old WAC (30_35s) not optimized, the new WAC (12_26s) and the new WAC with high pressure (12_26s at 85mTorr).

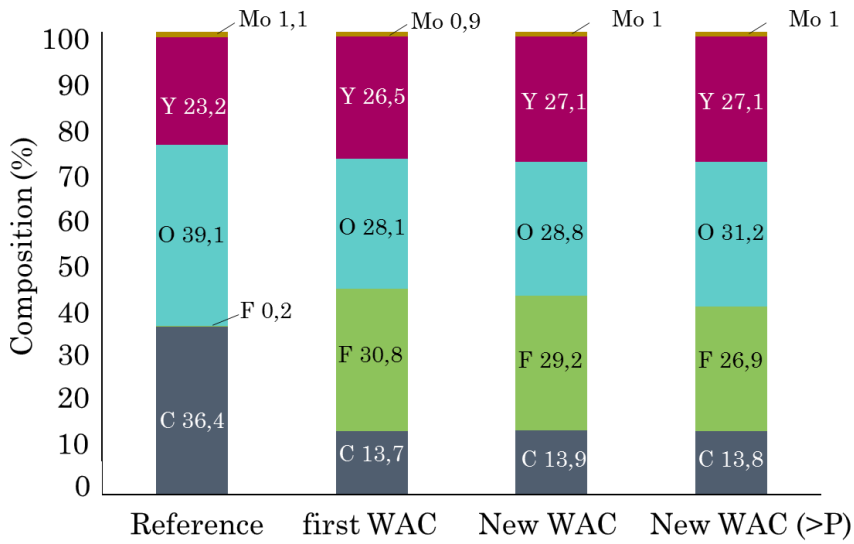

Figure IV-12. Chemical composition of the first WAC, new WAC and new WAC (high pressure) compared to the Y_2O_3 reference.

From the results shown in Figure IV-12, we verified that the reduction of fluorine was related to the reduction of time (new WAC) and implemented when increasing the pressure (new WAC high pressure). For the standard and new WAC, the pressure employed was 60mTorr whereas that for the new WAC (>P) we used 85mTorr, which is the maximum allowed by LAM Research. Due to the results obtained with the floating sample analyses, the optimal WAC which is nowadays in production is the new WAC with high pressure (85mTorr). Thus, the time for clean 1 is 12s at 85mTorr and the clean 2 is 26s.

5. CONCLUSIONS

This chapter shows the characterization and optimization of the plasma-wall interactions taking place during the eSTM process. The characterization of the plasma-reactor wall interactions was studied based on the analyses of the coatings deposited on the reactor walls. These analyses were performed by using the floating sample method and analyzed by XPS. Furthermore, the analyses of the influence of the WAC was also studied since the chemistry employed used also fluorine, which was the source of contamination during both, the process

and the cleaning. Of course, these analyses were performed ex-situ, since there was no other possibility, as happened for the analyses of Chapter III. Therefore, some contamination must be taken into account. However, in this part, more than going into details of the composition of the coatings, we were concerned about the fluorine problem and the YF_x formations. The fluorine was more present during the process than during the WAC, since the time of exposition to the F-chemistry was lower during the cleaning than during the process. However, it was highly present in all the analyses.

In order to reduce the problem of the fluorine contamination, a state-of-the-art looking for some possible strategies was done. However, due to industrial limitations, the only strategy possible for us was to optimize the WAC. Due to the low presence of "glassy" depositions, nothing when analyzing the coatings by using a Y_2O_3 sample and less than 2% when using an Al_2O_3 sample, the first clean step (clean 1) could be reduce 18s. Thus, the time for the clean 1 was modified to12s. The time for clean 2 was reduced to 26s. With this new WAC, we optimized the cleaning for the eSTM process, but we also reduced the total WAC time from 65s to 38s. Having this, a positive impact for the production line.

However, related to the fluorine problem, we could not do something else than reducing the clean 1, the one which uses SF_6, and increasing the pressure. With the new WAC at 85mTorr during 12s for clean 1 (F-based step), we reduced the percentage of fluorine on the coatings from 30.8% for the first WAC to 26.9% for the optimized one.

In summary, the goal of this chapter was to study the plasma-reactor wall interactions, we did understand that for the eSTM process more CF_x polymers are deposited on the chamber than SiO_xBr_y or SiO_xF_y as expected. By optimizing the WAC, we did reduce the YF_x formations, but still, some new strategies must be considered in order to completely avoid this formations, since as long as we continue using a F-based chemistry, they will be always present on the reactor walls. For the moment, further analyses must be performed in ST Microelectronics Rousset in order to see how important is the presence of the F-based coatings on the reactor walls for the process reproducibility in order to see if some other strategies, as for instance the conditioning explaining before (4.1.), should be put in place.

"A great deal of my work is just playing with equations and seeing what they give" (P.A.M. Dirac)

Chapter V

STI: Plasma Etch Process Control for Critical Dimensions

In this chapter, a process control solution is proposed in order to reduce the etch process variability for the critical dimensions of the STI trench. Tight controls of these dimensions are required for the suitable running of the transistors since CD variations are directly linked to processor speed and transistor performance. In this research, a fully plasma etch study is carried out looking for sources of variability throughout the STI etch process with the aim of set a Run-to-Run (R2R) controller able to optimize the CD for reaching better manufacturing yields.

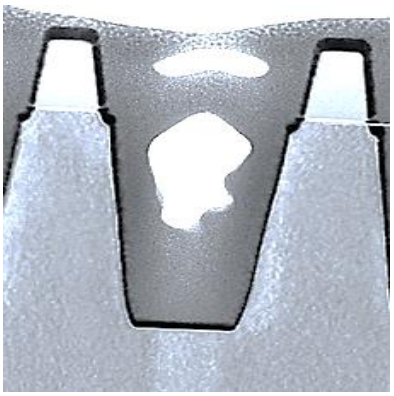

TEM profile of the STI trench of this thesis.

As feature size continues to decrease, process control has become essential for controlling profile and CD uniformity across the wafer [294]. To reduce the process variability related to the CD of the STI after etching, process control solutions have been performed based on a technology in production at STMicroelectronics. For confidentiality reasons this technology will be referred as follow as M10+. Since the etching process of the STI is the same for both technologies, M10+ and eSTM, these solutions can be applied to both technologies. However, since the eSTM is still in development, we needed the historical data of the M10+ to propose the adequate solution.

The chapter is organized as follows. Firstly, an introduction based on the STI and the definition of some process control concepts is presented, followed by the experimental details related to the etching process and the industrial context. Secondly, the characterization of the source of variation during the STI etching and the optimization of the CD drift are discussed. Finally, the conclusions of this study conclude this chapter.

1. INTRODUCTION

Since the size of the memory cell decreases and the packing density increases, it is becoming vital to ensure that each bit is electrically isolated from each other. Failure to electrically isolate the device core, can make difficult to program and erase the memory cell and to create reliability issues as a result of static-charge loss [295]. The goal of the study presented in this chapter was to control the CD of the STI in order to avoid these problems.

1.1. The STI Process

The STI process is considered a highly critical manufacturing step because it constrains all subsequent patterning layers by defining the active regions for the electrical structures [295]. It is the preferred isolation used on CMOS processes nodes of sub-0.5µm technology because it completely avoids the bird's beak shape characteristic compared to the LOCOS, which is the traditionally isolation technique [296]. The STI is created early during the semiconductor device fabrication process, before the transistors formation. The price for saving space with STI is the larger number of different process steps, as shown in Figure V-1, which are:

a) etching of the silicon substrate.
b) etching and under etching of the oxide pad.
c) a thermal oxide in the trench is grown, the so-called *liner oxide*.
d) the trench is filled with a deposited oxide.
e) the excessive oxide deposited is removed with chemical mechanical planarization.

f) the nitride mask is removed.

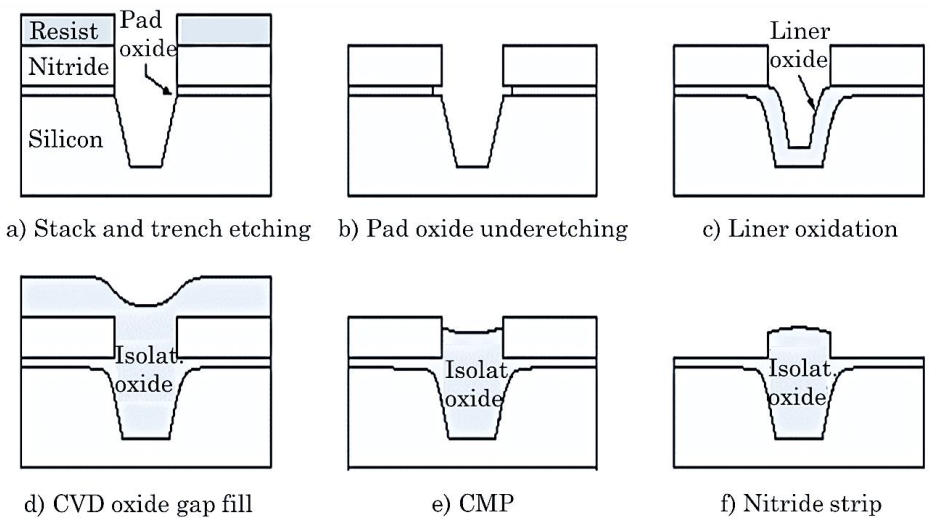

a) Stack and trench etching b) Pad oxide underetching c) Liner oxidation

d) CVD oxide gap fill e) CMP f) Nitride strip

Figure V-1. Steps in a typical STI process flow [296].

All these steps are usually required for creating the STI. Due to the number of steps and the processes involved, it is difficult to control the CD. Advanced Process Controls (APC) are employed in semiconductor industries for controlling the variability that can be induced during these steps.

1.2. Process Variation

All manufacturing and measurement processes exhibit variation by nature. When we sample the wafer after a process and take its measurement, such as the critical dimensions, we observe that the values are fluctuating. This is called **variability**, which can be also defined as the collection of observed values distributed around a location value.
There are different types of variations. One classification could be related to the Production Process Characterization (PPC) such as [297]:

- **Controlled variation:** When the variation is characterized by a stable and consistent pattern of variation over time. It will be random in nature and will be exhibited by a uniform fluctuation at a constant level.

- **Uncontrolled variation:** When the variation is characterized by a pattern of variation that changes over time and hence is unpredictable.

These concepts of controlled and uncontrolled variations are important for determining the variability of a process. It will be stable only if it runs in a consistent and predictable manner. This means that the average process value is constant over time and thus the variability is

controlled. On the other hand, if the variation is uncontrolled, either the process average or the process variation is changing [297].

1.2.1. Measures of Variation

An important aspect of a descriptive study of the variable is numerically measuring the extent of variation around the center. Two data sets of the same variable may exhibit similar center positions but have significantly different variability behavior. Two of the most frequently used measures of variation are the range and the standard deviation [298].

- **Range:**

The range is obtained by computing the difference between the largest and the smallest observed values of the variable in a data set:

$$\text{Range} = \text{Max} - \text{Min}. \tag{V.1.}$$

By using the range, a great deal of information is ignored, since only the largest and smallest values of the variable are considered. The other observed values are disregarded. The range can only increase, never decrease, when additional observations are included in the data set. Thus, the range is overly sensitive to the sample size.

- **Standard Deviation:**

The standard deviation is the most frequently used measure of variability. It is considered as the average of the absolute deviations of observed values from the center of the variable in question. For a variable x, the standard deviation (S_x), is:

$$S_x = \sqrt{\frac{\sum_{i=1}^{n}(x_i - \bar{x})^2}{n-1}} \tag{V.2.}$$

The standard deviation is always a positive number ($S_x \geq 0$), which is defined using the mean ($\bar{x}$) of the variable x. For that reason, it is the preferred measure of variation when the mean is used as the measure of center (i.e., in the case of a symmetric distribution). However, the standard deviation is used more often, through its square, called ***variance*** ($\boldsymbol{S_x^2}$) and expressed as:

$$S_x^2 = \frac{\sum_{i=1}^{n}(x_i - \bar{x})^2}{n-1} \tag{V.3.}$$

The standard deviation satisfies the basic criterion for a measure of variation. However, the standard deviation does have its drawbacks. For instance, its values can be strongly affected by a few extreme observations [298].

1.3. Process Control in Semiconductor Manufacturing

Traditionally, process variation is monitored through implementing Statistical Process Control (SPC) charts on the critical product characteristics. As in the complex manufacturing environment in IC fabrication, the framework of Advanced Process Control (APC) is defined and developed in a much bigger extent. With the advancement of modern IT systems, a full spectrum snapshot can be taken while the fab is running and stored in different databases according to the data properties. In the following, the evolution of process control techniques is introduced.

1.3.1. Statistical Process Control (SPC)

Statistical Process Control is used as an analytical decision making tool which allows practitioners to see when a process is working correctly and when it is not. Since the variation is present in any processes, it is necessary to identify when the variation is natural and when it needs to be controlled [299]. The idea was originated in the 1920s at Bell Laboratories. Dr. Walter Shewart developed the concept of control with respect to the variation, and came up with **SPC Charts** providing a simple way to determine if the process is under control or not. Today, this approach is widely used in semiconductor manufacturing facilities around the world.

It is a technique in which the process output is monitored in order to detect an out of control observation. A process is considered out of control if the output variance can be attributed to an assignable cause. This cause can be compensated by manipulating one or several process input variables [300]. SPC is used as an industry-standard methodology for measuring and controlling the product/process quality during manufacturing. The data are then plotted on a SPC control chart with pre-determined limits. These control charts are the essential tools to achieve a rational management of the production process.

- **<u>SPC Charts</u>**

Control chart is one of the primary techniques in SPC to show the variation of measurement over the time period the process is being monitored. A process is in control or not depends on the variance of the process output over time. Control charts illustrate and compare the process variation against upper and lower control limits to see if it falls into a normal region. There are usually two kinds of limits expressed in an SPC chart; ***specification limits***,

determined by the client's needs, and ***control limits***, determined by the capability of the process.

• ***Specification limits***: denoted by "LSL" and "USL" for Lower and Upper Specification limits. These are the strict limits that shall not be crossed, because there is a risk of malfunction.

• ***Control limits*** denoted by "LCL" and "UCL" for Lower and Upper Control Limits.

The control limits create a confident region indicating that everything is working as expected when the output falls within it. Any variation observed within the region will be concluded as a common cause, i.e., the natural variation, which is expected as part of the process. If the output falls outside the region, as the point "A" in Figure V-2, an assignable cause should be investigated to identify the source of the product variation. Therefore, corresponding changes in the process settings should be performed in order to fix the issue.

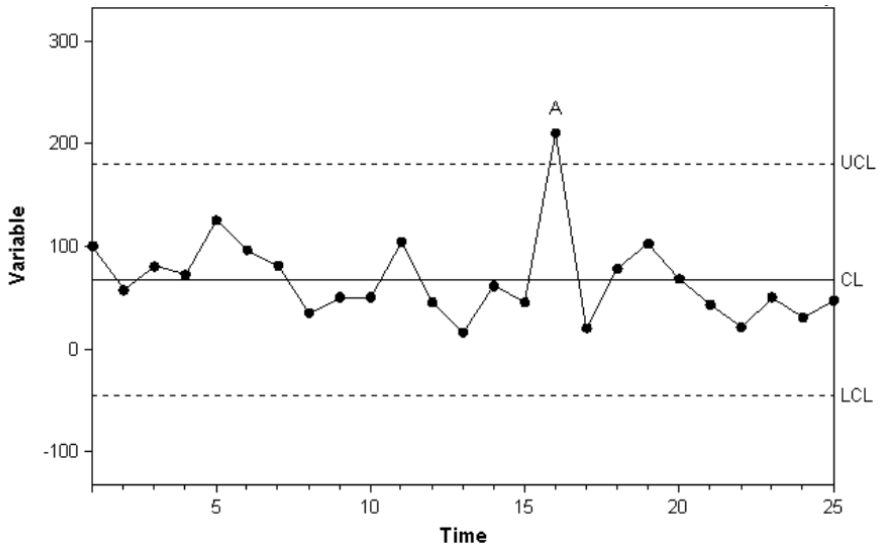

Figure V-2. SPC chart where the value "A" is out of the UCL [299].

1.3.2. Advanced Process Control (APC)

The APC concept evolved the SPC in which process or product data are analyzed to see if the process is deviating from the statistical norms. SPC techniques can only detect a small class of process deviations, and generally cannot tell what caused the deviations or how to correct them. However, APC, as a comprehensive framework, uses measurements of important process variables to incorporate a feedback loop into the control strategy. APC has included critical IT systems and statistical algorithms to study the variability transmission from the

output variable to certain controllable input variables. Two main modules are commonly addressed in a APC framework [300-302]:

- **Fault Detection and Classification (FDC)**

FDC involves monitoring the behavior of the manufacturing equipment during operation and detecting events that might affect the quality of the product. The importance of FDC mainly resides in increasing the equipment utilization while maintaining the product quality by extracting key features and patterns from the huge amount of real-time process data.

- **Run-to-Run (R2R)**

R2R is a type of discrete process control which includes wafer-to-wafer and batch-to-batch control in an attempt to reduce output variability [300]. The product recipe is modified between "runs" in order to minimize process drift and shift. Moyne [303] said that nowadays this is the main form of process tuning implemented as standard process and equipment control solution in the industry.

The first R2R controls system was proposed in the early 1990s when the results of Semi-tech-funded projects showed that the thickness of wafers in a CMP process could be controlled by modelling the process physics and making adjustments before the start of each run. Today, R2R control is used throughout the factory and has been even extended to support "inter-process control", or control across multiple process types [301].
R2R control solutions are process-centric and can be categorized as ***feedforward (FF)*** and ***feedback (FB)*** controls. FF and FB can be further augmented to inter-process control solutions, such as the CD control between lithography and etch operations. Once the throughout the key process operations can be effectively tightened, the device performance at the end will be surely enhanced. The structure of a typical R2R control solution is shown in Figure V-3.

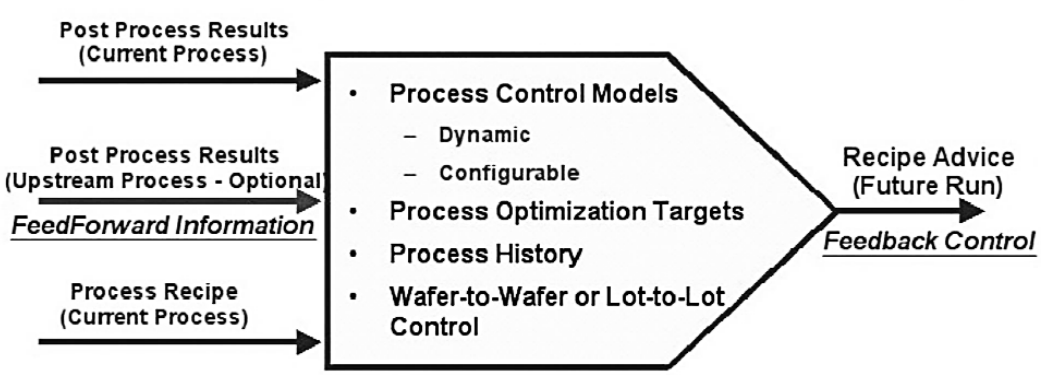

Figure V-3. Input/output R2R structure [303].

Campbell et al [300] did a comparison of R2R control algorithms and they classified them as: EWMA Controller, Predictor-corrector controllers and model predictive control. Ning et al [304] classified them such as EWMA Gradual Mode (GM), time-based EWMA (GMt), Knowledge-based Interactive R2R Controllers (KIRC) and Optimizing Adaptive Quality Controllers (OAQC). Others R2R classifications from literature can be seen as Single Input/Single Output (SISO), Multiple Input/Multiple Output (MIMO), Lot-Level control, Wafer-level control or Within Wafer control.

In this chapter, the R2R controller developed for controlling the CD of the STI during the plasma etching process is discussed. Modelling details are presented in section 4.2.

2. EXPERIMENTAL

As introduced before in 1.2, the STI is considered as a highly critical manufacturing step. Moreover, when it is used as a base of a complex process such as the eSTM, the limits (CD) have to be really well defined in order to avoid electrical problems. The STI process is performed at the beginning of the process *flow*. The etch process definition required for the STI formation, takes into account from the stack deposition, until the measure of the STI trenches performed during the etching. In order to understand the study performed for controlling the CD of the STI, some experimental concepts need to be introduced before. Thus, the necessary stack and the etching specifications related to this process are presented in this part.

2.1. Stack

As well as for the etching of the eSTM trench, a hardmask is also necessary when etching the STI trench since the dimensions are quite small. The required stack for this process is represented in Figure V-4.

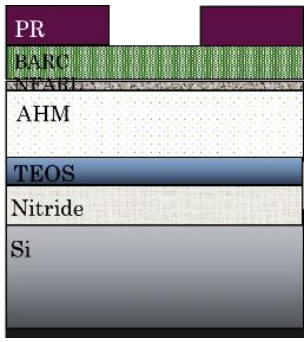

Figure V-4. Required stack for the etching of the STI trench.

The required mask for reaching the STI trench is composed of NFARL, AHM, TEOS and nitride. These materials were already introduced in Chapter II. The PR and the BARC, deposited during the photolithography step, measure 1900Å and 820Å, respectively. The NFARL and AHM, both of them deposited by PECVD, measure 275Å and 2000Å. The thickness of the TEOS is 490Å and 1200Å for the nitride. The nitride will remain after the plasma etching process for protecting the features during the CMP process and it will be removed later. There is also a thin layer of SACOX (sacrificial oxide) between the nitride and silicon layers.

2.2. Etching Specifications

The most important steps required for the process definition of the STI trench are sketched in Figure V-5.

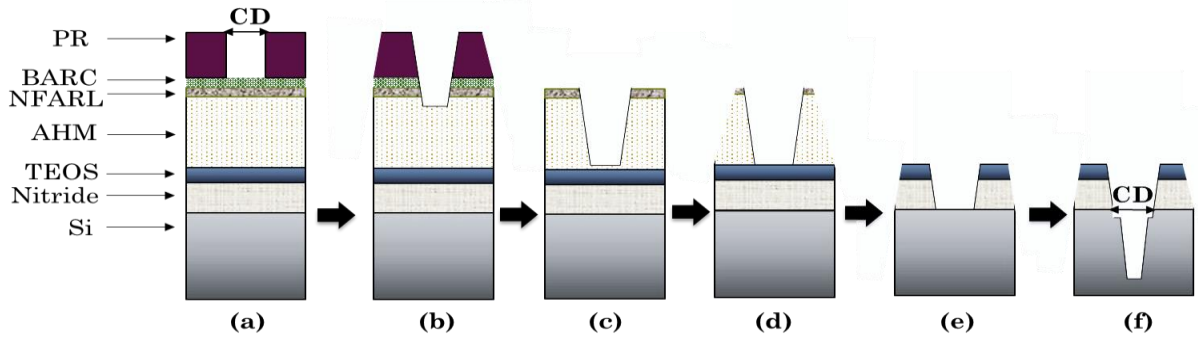

Figure V-5. Schematic representation of the main etching steps required for reaching the STI trench: Initial stack (a), BARC and NFARL etching (b), AHM etching (c), AHM overetch (d), TEOS/Nitride/Breakthrough and stripping AHM (e), TCR and STI trench (f).

In Figure V-5, the first CD (a) is representative of the CD after the photolitography step, which is our input CD. The last CD (f), is the CD that will be the case of study during this thesis, which is the CD of the STI trench after the etching process.

This huge stack and the complexity of the plasma etch process itself are directly responsible of the CD drifts. The recipe counts with 32 steps, including stabilization and transitions steps. However, it could be summarized with 8 main steps, where 5 of these steps require EPD systems and therefore also an overetch. Since the goal of this chapter is to study the variations on the CD after etching from a process control point of view, no great specifications related to the chemistry or the others parameters are required. However, it is important to underline, which of these steps are using EPD. They are BARC, NFARL, AHM, Strip, TEOS, nitride, and the final etching of the STI trench. All these layers are etched in two step; the EPD followed by the overetch. As explained for the eSTM process, the goal of the overetch is

to "clean" the residuals of the target material after the EPD etching. Therefore, the unique steps that are performed without EPD systems but in fixed time are the BreakThrough (BT), the TCR (Top Corner Rounding) and the final etching of the trench. The BT is used to open the silicon to be sure that the next step starts really etching the silicon.

The chemistry used during each step, is only responsible of the etching of this step since it is selective to the others, as it has been already explained in previous chapters.

2.3. Industrial Context

As it has been introduced in Chapter II, during the time that this study was developed at STMicroelectronics Rousset, there was not scatterometry model available for the STI measures. All the measures, before/after etching of the CD were performed by using CDSEM in-line. Since the accuracy of this method was not very reliable for the STI, as explained in Chapter II, we developed a scatterometry model able to measure the CD using a profile view. All the details about the model were previously explained in Chapter II (3.2.3.).

However, the development of this model took place in parallel with the analyses here presented. For this reason, most of these results were obtained with CDSEM.

3. CHARACTERIZATION

The characterization of the process here, is related to the study of all the parameters that can be the source of CD variations in order to understand its influence on the final CD of the STI. The goal is to propose a solution to keep the final CD under control, close to the target, after the plasma etching process.

3.1. Process Variability

The STI etch process is used to create shallow trenches in the silicon substrate, which are used to form isolation barriers between device elements. This process involves the etching of eight layers (see Figure V-4) and a complicate recipe including different steps such as stabilizations, transitions, EPD steps, overetch and fixed time steps. To complete this complicated process, together with the complexity of the plasma etching operation, undesired variations on the final CD can be induced. Furthermore, the previous steps, including the depositing stack and the photolithography can also cause unwanted variations that then change the input CD as soon as the etching operation starts. While STI CD variation gets worse, the wafer yields are reduced. To handle this issue, we took a "global picture" of the

situation at the beginning of this thesis at STMicroelectronics Rousset, where the STI etching process was not under control. This initial situation is shown in Figure V-6.

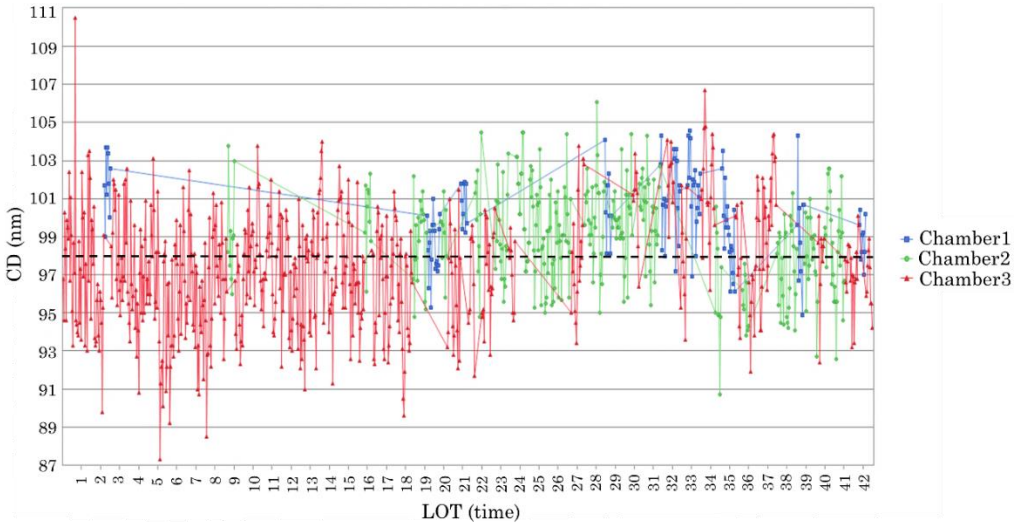

Figure V-6. SPC chart of the STI CD after etching. The black dashed line represents the target. The three process chambers show obvious different behaviors over time.

The variations on the CD can be easily perceived in Figure V-6 where the CD is often on or off the target with a big deviation. To keep the STI CD close to the target and reduce the range, effective models and strategies are required. As more and more data can be collected nowadays, it is very important to filter out the most significant sources of variations that interact with the etching process before constructing the model. The following sections start with the introduction to the impact of previous steps and the variation induced by the etching process itself. Based on these results, we decided the best strategy for keeping the CD on target.

3.2. Impact of Previous Steps

In addition to the complexity of the etching process itself, there are two main external factors impacting the STI CD. The **thickness variation** of each layer in the stack and the **CD post photolithography**, which is the starting point of the CD after etching.

- **<u>The Influence of Thickness Variation</u>**

The standard STI etch process involves etching the bottom antireflective coating (BARC), the nitride, the underlying pad oxide, and a shallow trench into the silicon substrate. At the 90-nm technology node, STI etch requires a hard-mask process to reduce defectivity and improve chamber performance. In our research, we added the NFARL and the AHM layers, which

enable to reduce the STI CD. However, there was no possibility of measuring these two layers separately, as they had the same refractive index. Therefore, we were not able to see the different influences that each one provides. In order to increase our knowledge about the impact of the two additional layers on the final CD, we did an experiment to induce the variations on their thickness during the deposition step while maintaining each time one of these materials in its standard conditions. We could then differentiate how the variation of each material influences the final STI CD. To perform these experiments, the EPD steps were avoided in order not to correct the intentional difference in thickness. These results are presented in Figure V-7.

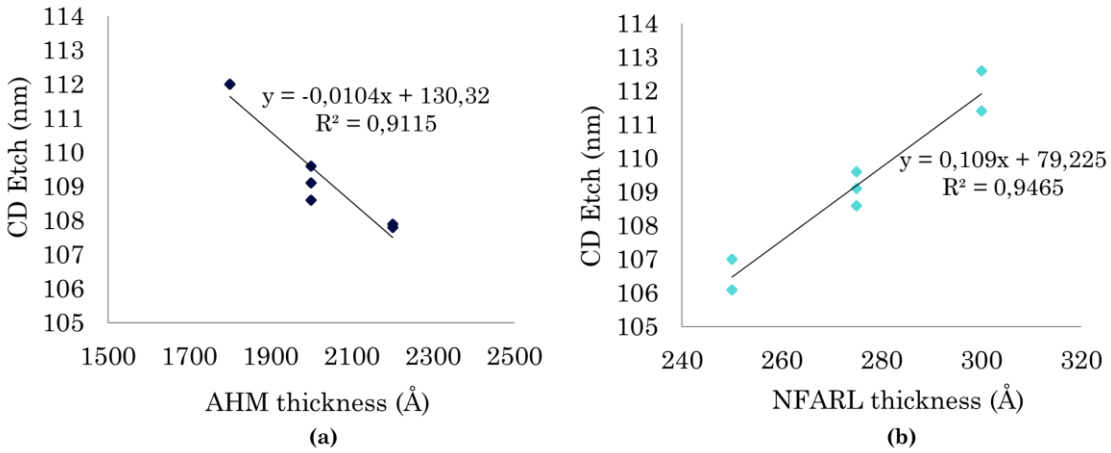

Figure V-7. AHM (a) and NFARL (b) individual influence on the STI CD without EPD system.

From analytical results shown in Figure V-7, we concluded that the NFARL has stronger influence on the STI CD than the AHM does. With the variation of 79Å in NFARL thickness, the influence on the CD is the same as when varying 130Å of the AHM thickness. In both cases, the influence would be 1nm of the final CD.

Since we are using EPD system when etching these layers, as well as for the other materials, we supposed that the thickness variation coming from the previous steps, such as the deposition thickness variations, are corrected by the EPD. As explained in Chapter II, the EPD does not perform etching in a fixed process duration, instead, the etching process stops when the end of the target material is detected. In order to verify that EPD system are actually correcting these possible thickness variations, we did a regression analysis to identify the impacts of the layers on the CD. We then tested the EPD performance on this layer. The study was performed with the software provided by *KLA-Tencor*, and the results of the analysis are shown in Figure V-8.

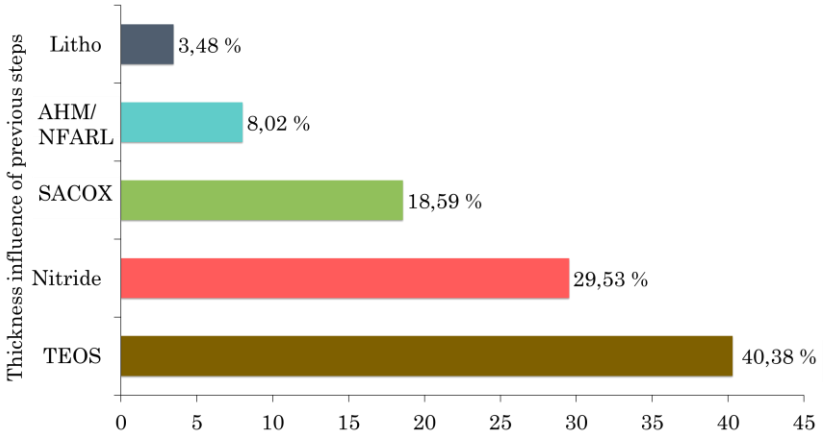

Figure V-8. Influence of the thickness variation of each layer on the final CD.

From Figure V-8, we decided to test the EPD performance with respect to the TEOS thickness variation, as it appeared to be the most influential one. Thus, we induced several variations on the thickness deposition of this layer by making the experiments in one lot, i.e., 25 wafers. Knowing the standard thickness of the TEOS layer is 490Å, we divided a complete lot into five groups of thickness 440Å, 465Å, 490Å, 515Å and 540Å. If the EPD worked well, no matter what the thickness of the TEOS layer is, the final CD would be always the same. The differences in this case, shall be only related to the process time. The results of this study are shown in Figure V-9.

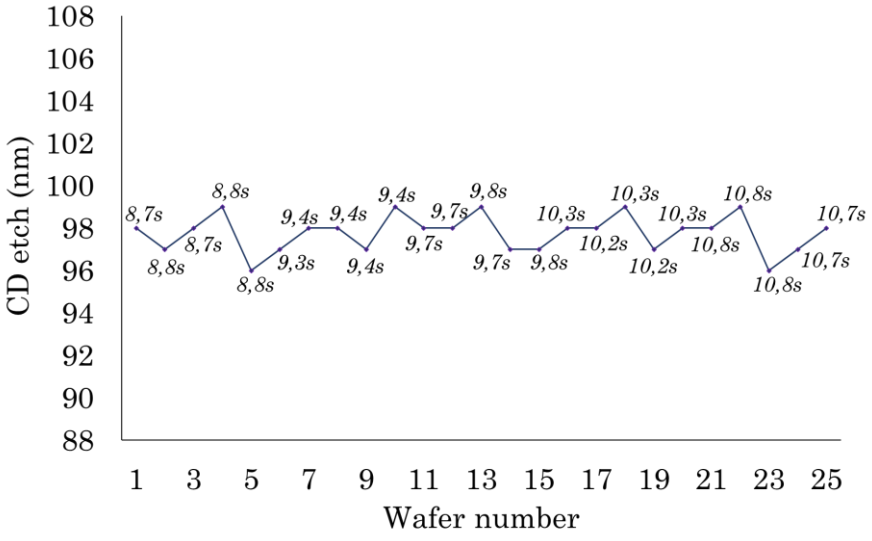

Figure V-9. Study of the EPD performance during the etching of the TEOS layer.

The results, as shown in Figure V-9, demonstrated that the EPD can correct the thickness variation induced by the previous steps.

Even if the performance of the EPD systems is good enough to control the variation of thickness induced for the previous steps, there is still another important factor to be responsible for the CD drifts, as mentioned before, this is the photolithography CD.

- **<u>The Influence of Photolithography</u>**

It is expected that the bigger post-photolithography CD leads to larger post-etching CD (see Figure V-10).

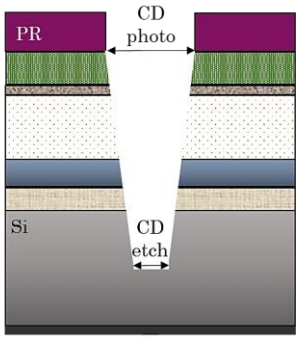

Figure V-10. The process physics of the post-photolithography and the post-etching CD's.

To further understand the influence of photolithography process on the CD after etching, the CD correlation between the two workshop is illustrated in Figure V-11.

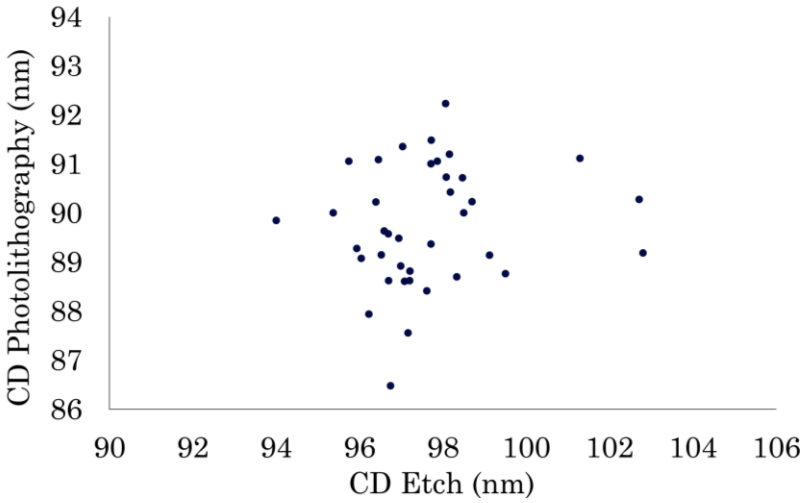

Figure V-11. The lot-level CD's after the photolithography and etching are plotted together to observe any possible correlations.

Surprisingly, we did not find a significant correlation of the CD's after the photolithography and etching process. This may be due to the rework strategy of the photolithography step at

STMicroelectronics Rousset. If the post-photolithography CD of one wafer deviates more than ±3nm from the target, the wafer is sent to rework. To further verify this conjecture, we performed a study including CD at its biggest and smallest limits of the photolithography, i.e., 80nm and 100nm, in contrast to the CD target at 90nm, while the rework policy is disabled temporarily. The results of this study are presented in Figure V-12.

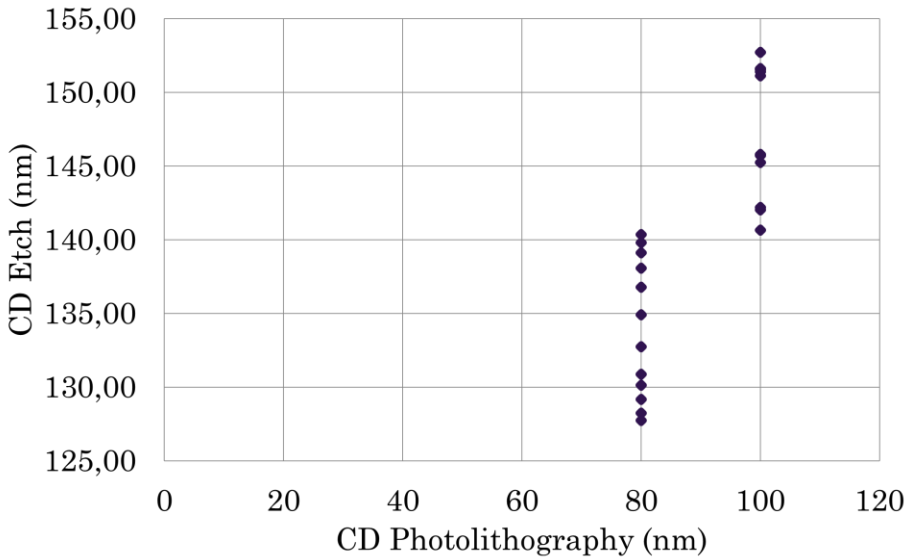

Figure V-12. The impacts of different post-photolithography CD's on the post-etching CD.

As can be confirmed from Figure V-12, bigger CD variation after the photolithography leads to the different CD's after etching. Given the reworking of photolithography at STMicroelectronics Rousset, the influence of the post-photolithography CD, can be neglected because the variation will be very small (within ±3nm).

In summary, the influences of the previous steps can be ignored since the thickness variations are corrected by using the EPD systems and the impact of the photolitigraphy CD is negligible when the rework strategy is applied. One can conclude that the variation on the post-etching CD (see Figure V-6) should lie within the etching process itself. Consequently, the effect of the etching step on the STI CD was of the next study focus

3.3. The Influence of Etching

In order to study the source of variation within the etching process, we identified these factors as effects coming from process chamber, lot-to-lot, wafer-to-wafer, intra-wafer product type, silicon supplier, and the unexplainable source. The analysis of variance was performed by using the *KLA-Tencor* software which allows to select the factors of our interest. This result is shown in Figure V-13.

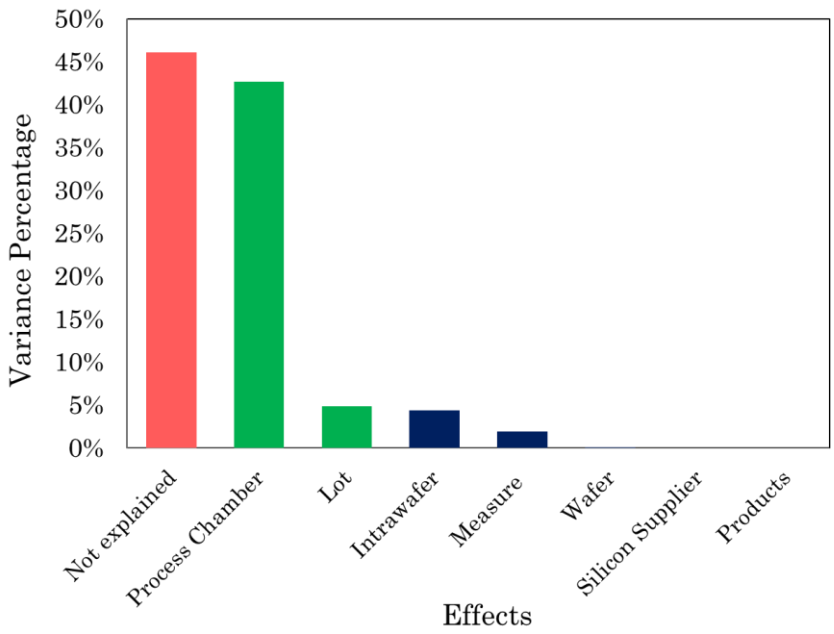

Figure V-13. Analysis of variance of the etching CD.

From Figure V-13, we can see that the two green bars, which account for 48% of the CD variation, can be improved using R2R controllers. The most important effect which influences the variation of the STI CD is the process chamber effect (43%). Furthermore, the three process chambers are clarified to be rather mismatched. This chamber effect (43%) together with the lot-to-lot effect (5%) can be corrected by developing a FB R2R. There is also an unexplained effect, which appears to be the most critical one. We could only optimize the variability due to the chamber and lot-to-lot effects (48%). However, at that stage, we started to develop the scatterometry model with the metrology equipment, as explained previously in Chapter II (3.2.). Even if we didn't know the source of this unexplained effect, we thought that maybe by improving the measurement system, we could reduce this effect.

During the development of this scatterometry model, we started to develop the strategy for controlling the CD; the FB R2R, which is the main goal of this research in order to reduce the part of the variability that was related to the chamber and lot-to-lot effect.

4. OPTIMIZATION

The strategy employed for optimizing the process control of the STI etching by improving the CD drifts, was based on a Feedback Run-to-Run (FB R2R) controller. Details about this model are presented in this section.

4.1. The EWMA R2R Strategy

Although there exist numerous ways to design a R2R controller, as explained in the first section of this chapter, the most widely implemented design is based on an Exponentially Weighted Moving Average (EWMA) scheme [300]. In 1959, Roberts [305] firstly suggested that the EWMA control scheme can be used for process monitoring. By choosing a proper weighting factor λ, the EWMA control procedure can become sensitive and detect the small or gradual drift in the process. The basic equation of exponentially smoothing established by Roberts can be expressed as:

$$EWMA_t = \lambda Y_t + (1-\lambda)EWMA_{t-1} \text{ , for } t=1,2,\ldots,n, \tag{V.4.}$$

where,

$EWMA_0$ is the mean of historical data,
Y_t is the observation at time t,
n, is the number of observations to be monitored including $EWMA_0$, and
$0 < \lambda \leq 1$ is a constant that determines the depth of memory.

Equation (V.4) is from Roberts [305], but there are some alternative approaches. For instance, according to Hunters [306], Y_{t-1} is used instead of Y_t. The parameter λ determines the rate at which "older" data enter into the calculation of the EWMA statistics. A value of $\lambda=1$ implies that only the most recent measurement influences the EWMA. Thus, a large value of $\lambda=1$ gives more weight to the recent data and less weight to the older data while a small value of λ gives more weight to older data [307]. The value of λ is usually set between 0.2 and 0.3 [306], although this choice is somewhat arbitrary and based on engineering knowledge.

Another approach (V.6.) is found in Campbell et all [300]. They explained that usually the typical EWMA R2R Controllers are based on a linear regression model for describing the process model of the form:

$$\hat{Y}_{k+1} = bu_k + c_k \tag{V.5.}$$

where $\hat{Y}_{k+1}$ is the predicted output at batch $k+1$, b is the process gain, u_k is the process input calculated based on previous observations through batch k, and c_k is the estimate for the disturbance entering system. The basic equation of exponential smoothing (V.4.) is explained in a different way [300], under the form:

$$c_{k+1} = \lambda(Y_{k+1} - bu_k) + (1-\lambda)c_k \tag{V.6.}$$

Equation (V.6.), compared to (V.4.), requires the calculation of the desired output (T) with the EWMA-based R2R controller, expressed as:

$$u_k = \frac{T - c_k}{b} \tag{V.7.}$$

The strategy that we followed for developing the FB R2R model is related to these EWMA designs.

4.2. The STI-Etch R2R Controller

The final element of the R2R controller is the control law which specifies how the recipe of the process should be updated. The FB R2R controller that we developed is illustrated in Figure V-14.

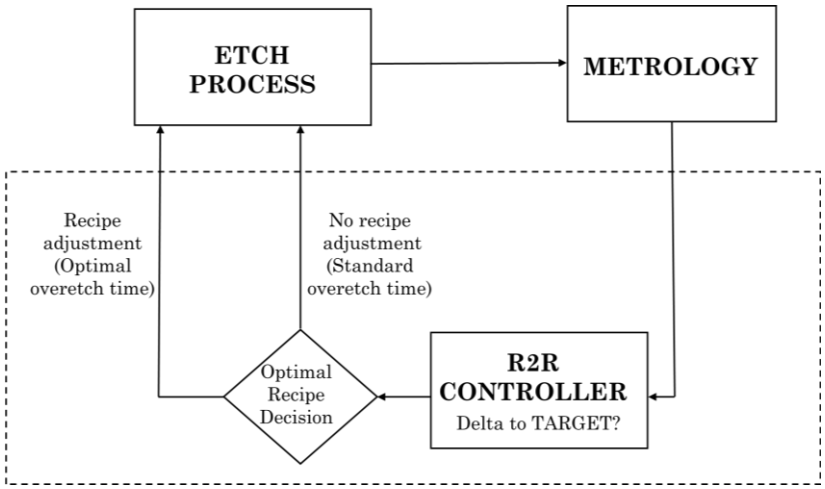

Figure V-14. Schematic diagram of the R2R controller developed for the STI CD.

It firstly required to select the parameter in charge of adjusting the CD. The photoresist trim is often used as the main factor. However, the photoresist disappeared during the AHM step in this research. The AHM then becomes the most influential on the STI CD. This is the novel finding for the process engineers such that this step is employed to control the CD. Furthermore, the overetch of the material AHM_OE is indeed due to the shrinking CD, since the O_2 is a selective chemistry which is able to etch the AHM laterally without etching the following materials. For the AHM_OE, we performed a study in order to see if overetching the material at this layer within a fixed duration has a constant etch rate in all chambers. The result is shown in Figure V-15.

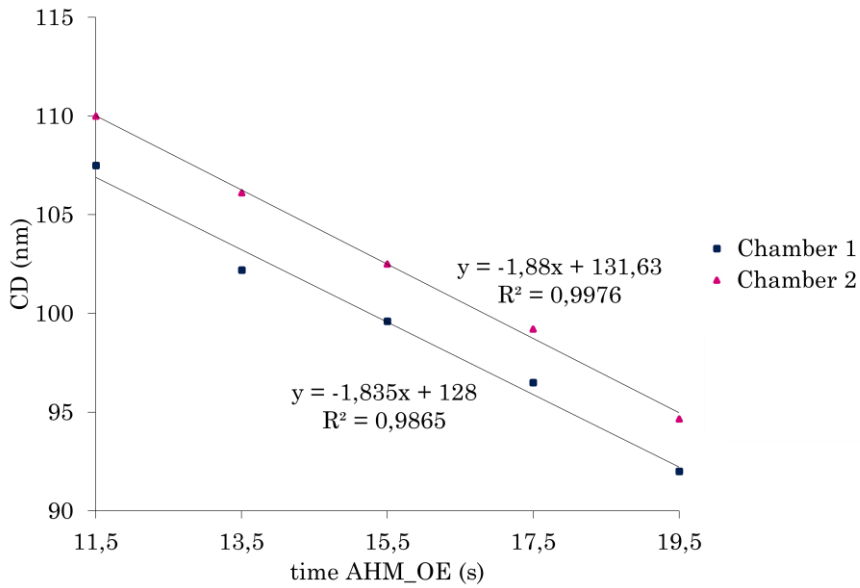

Figure V-15. AHM_OE etch rate in two different chambers.

As can be seen in Figure V-15, the etch rates, i.e., the slopes, of the two chambers are constant and present a constant offset in-between. As a result, this step (AHM_OE) is kept to control the STI CD.

4.2.1. R2R Operation

The model automatically takes into account the changes in the CD target specification. The final CD is fed back into the control model and used to update the model parameters, which in this research is the overetch of the AHM (AHM_OE). The standard etching time during the overetch (a) is 15.5s. All the model parameters are defined in Table V-1.

Table V-1. The definitions of model parameters.

Notation	Definition
τ	CD target
Y_t	Observed CD at time t
$\widehat{Y}_t$	Predicted CD based on R2R controller at time t, for $t \geq 2$
a	AHM etching time during the overetch (constant=15.5s)
$\widehat{a}_t$	Predicted time AHM OE at time t, where $\boldsymbol{\widehat{a}_t = a + \widehat{S}_{t-1}}$ (V.8.)
b	Etch rate (constant per chamber)
λ	Smoothing factor EWMA ($0 < \lambda \leq 1$)
S_t	Offset time, where $\boldsymbol{S_t = \frac{Y_t - \tau}{b}}$ (V.9.)
$\widehat{S}_t$	EWMA predicted Offset time, where $\boldsymbol{\widehat{S}_t = \lambda \cdot S_t + (1 - \lambda) \cdot \widehat{S}_{t-1}}$ (V.10.) for $t \geq 2$

The smoothing scheme starts by setting $\widehat{S_1} = \lambda \cdot S_1 = \lambda \frac{Y_1 - \tau}{b}$ (there is no S_o), where $\hat{S}_t$ stands for smoothed observation or EWMA, and S_t stands for the offset time (V.9.). The subscripts refer to the time period 1, 2, 3…n. For example, the second period, based on (V.10.) is:

$$\hat{S}_2 = \lambda \cdot S_2 + (1 - \lambda) \cdot \hat{S}_1$$

The first prediction can be calculated for $\widehat{Y_t}$ since we start with $t \geq 2$. The predicted CD basic equation, based on the EWMA controller, is under the form:

$$\widehat{Y_t} = Y_t - b \cdot \hat{S}_{t-1} \tag{V.11.}$$

By substituting $\hat{S}_{t-1}$ in the predicted CD basic equation (V.7.), the predicted CD equation would be expanded as:

$$\widehat{Y_t} = Y_t - b \cdot \lambda \cdot \sum_{j=0}^{t-2} (1 - \lambda)^j \cdot S_{t-1-j} \tag{V.11.a}$$

By substituting $S_t = \frac{Y_t - \tau}{b}$, V.11.a:

$$\widehat{Y_t} = Y_t - b \cdot \lambda \cdot \sum_{j=0}^{t-2} (1 - \lambda)^j \cdot \left(\frac{Y_{t-1-j} - \tau}{b}\right) \tag{V.11.b}$$

The final equation to predict the CD, can be written as:

$$\widehat{Y_t} = Y_t - \lambda \cdot \sum_{j=0}^{t-2} (1 - \lambda)^j \cdot \left(Y_{t-1-j} - \tau\right) \tag{V.11.c}$$

The R2R operation over the timeline is shown in Figure V-16.

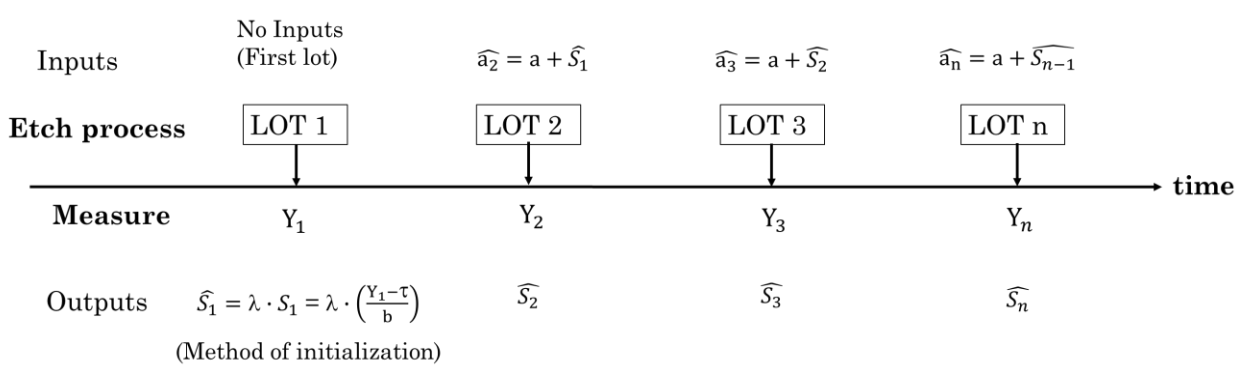

Figure V-16. FB R2R operation is illustrated from lot to lot over time.

By varying the weighting factor, i.e., λ, the EWMA control procedure can be sensitive to a small or gradual drift in the process. In this research, λ was set to 0.4, in order to avoid the

variations that could be induced by the metrology variability. This value was experimentally calculated.

4.2.2. Model Validation

For validating the model before putting into practice in the production line, some "simulations" were performed based in (V.11.) and evaluated. The results related to the process chamber effect and the lot-to-lot effect are shown in Figure V-17 and Figure V-18, respectively.

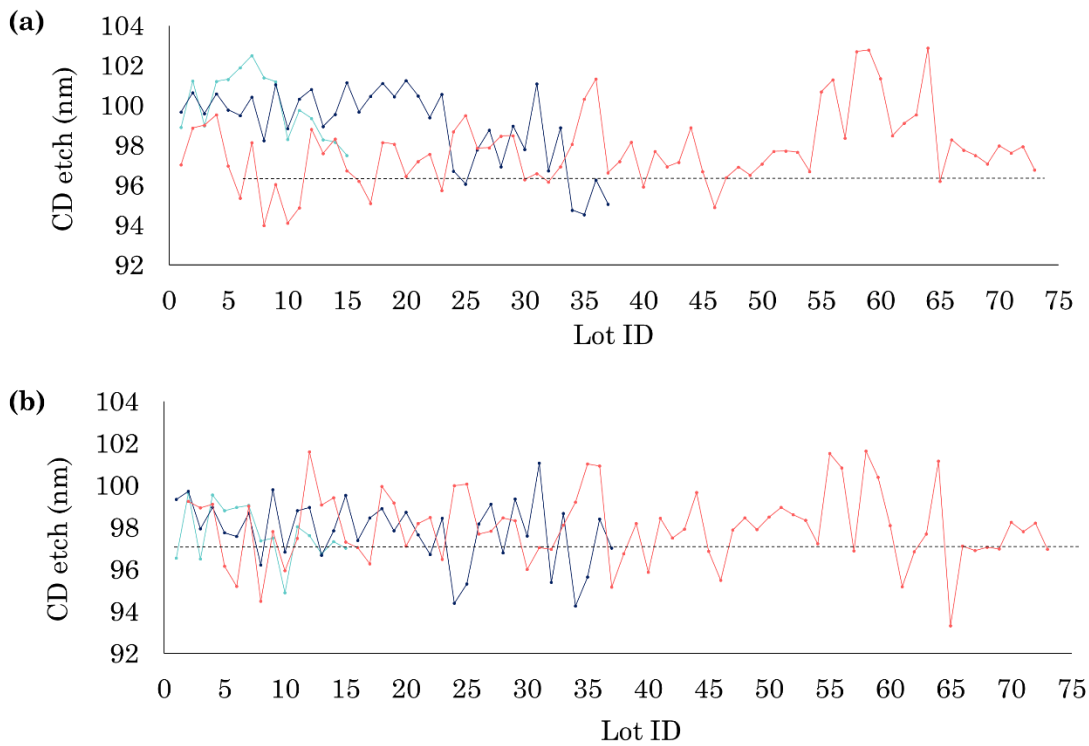

Figure V-17. Comparison between (a) the observed data and (b) the predicted CD by using the proposed R2R controller. Three chambers are denoted in different colors while the dashed lines indicate the targets.

Respect to these results, the model was validated since the process chamber effect which was the one that we were interested in correcting, improved 88% of the 43% that this effect induced to the total variability. Thus, 38% of the total variability. In this Figure V-17, the standard deviation between chambers goes from 0.79 (a) to 0.09 (b).

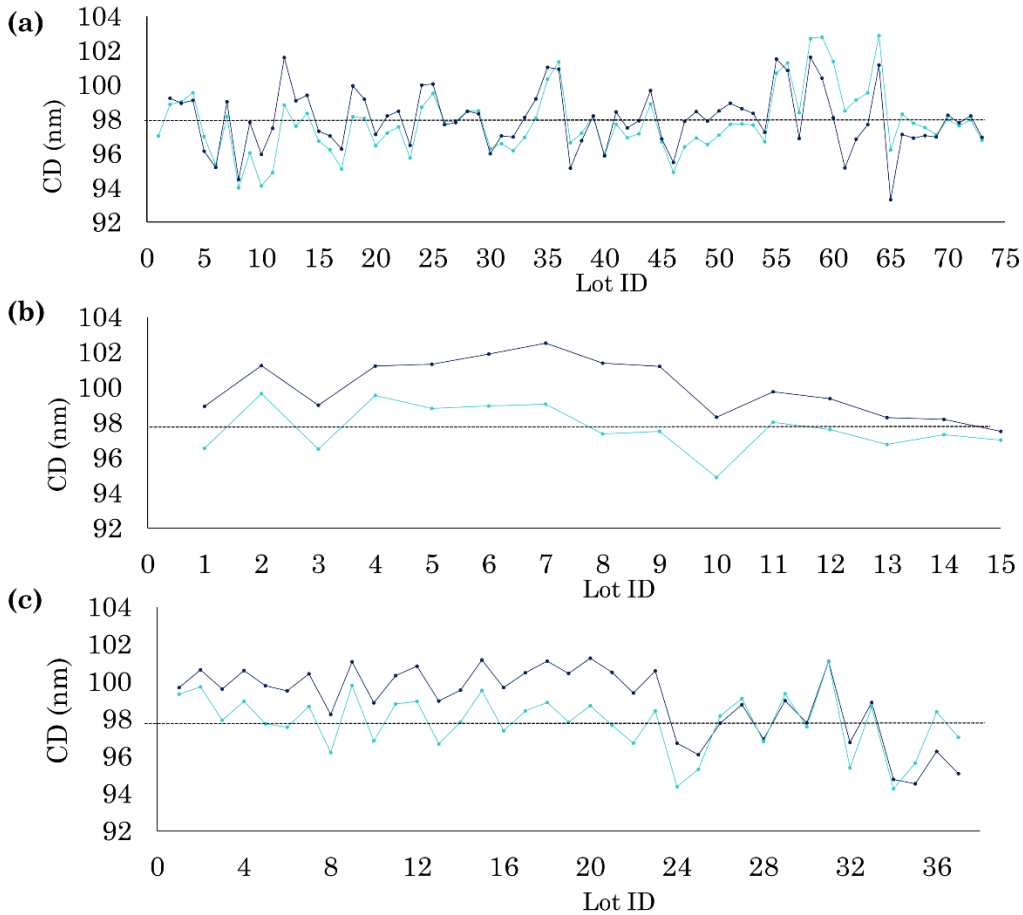

Figure V-18. Lot-to-Lot variations in the three chambers are observed in (a), (b) and (c), where the dark blue line indicates the observed data and light blue line represents the predicted value.

However, even if with the R2R we were able to correct a significant percentage of the variability, we wanted also to improve the metrology system since it could allow to keep reducing the variability due to the better accuracy of the measures.

4.2.3. New Metrology

Once the scatterometry model was completely developed, we did some variations on the plasma parameters in order to have different CD values for testing the accuracy of this model. The model was able to be representative in all cases and therefore nowadays the scatterometry model is used in the cleanroom as a representative measure of the CD and the height of the STI trench, not only after the etching but also after the photolitography step.

5. CONCLUSIONS

This chapter shows the characterization and optimization of the STI process. First, the characterization of the sources of variation have been studied. The results showed that the variation induced by the previous steps, especially the thickness variations, could be improved during the etching process by using the EPD systems. The post-photolithography CD is already corrected due to the implementation of the rework strategy, which reworks the wafers with large CD deviations from the desired targets. Therefore, the variations coming from the deposition thickness of the previous steps or the photolithography was negligible.

The etching variability was analyzed. A R2R controller was developed for keeping the STI CD in control by reducing the most important effects; the process chamber and the lot-to-lot variation. To develop the R2R model based on the EWMA control scheme, the time of exposition of the AHM to O_2 during the AHM overetch step was selected as the control parameter. The AHM overetch step was usually performed in fixed process duration. By varying the duration, we get bigger and smaller CD with respect to the predicted one. The experimental study showed that the etch rate remains constant for all chambers under different settings of durations and thus the control model can be built based on the chosen parameter with less confounding effects. The smoothing factor λ in the R2R model is set to 0.4, experimentally. The R2R model was further validated with historical data. The variation due to the chamber effect has dropped from 43% to 5% of the total variation. The objective is to keep improving/reducing the variation with the new scatterometry metrology system. The unexplained effect could be actually improved by this more accurate metrology system to measure the CD's. All the study was performed and the R2R control was deployed for the technology already existing in production, where the historical data coming from the technology have been validated. Then, the next goal is to put the R2R model into practice for the STI process of the eSTM technology in production mode.

"I applied streaks and blobs of colors onto the canvas with a palette knife, and I made them sing with all the intensity I could..." (W. Kandinsky)

Conclusions and Future Work

This thesis was conducted within the framework of a joint collaboration between industrial and academics. Thus, the work presented in this manuscript is intimately linked to the industrial development of the newest STMicroelectronics Rousset technology; the eSTM. This thesis aimed to study and optimize a very specific stage: the plasma etching processing of the embedded trench for advanced microelectronics applications. Throughout these years, a link has been established between academia and industry trying to explain the phenomena and problems appearing in the process via the process characterization and modelling.

The objectives of this work can be divided into three parts. Firstly, the study of the eSTM trench including the characterization of the process and the design optimization to achieve a model able to predict the CD (Critical Dimension) of the eSTM trench for the optimal electric results. Secondly, the development of the floating sample method at STMicroelectronics Rousset which allowed us to study the reactor walls deposition and the implementation of the cleaning strategy. And, finally, the characterization of the STI process for controlling the CD by developing a controller model. In addition, within the timeframe of this thesis, a new scatterometry model was also developed. This model can be used to measure the STI CD after the photolithography and etching steps, which could stand up as a potential alternative candidate to CDSEM measures. Each of these parts was divided into two main sections; the characterization and the optimization. In the following, the major contributions of each of these parts are summarized.

- Contributions to the characterization and optimization of the eSTM

The characterization of the eSTM trench during the etching process contributed to improve our knowledge of the process. It allowed us to identify the role of the species of the etching gases and to understand the composition of the sidewalls passivation through surface analysis. From these characterizations, we could interpret the role of the gases during the etching. Furthermore, the protocol employed for the characterization of the passivation layer is nowadays ready at ST Microelectronics Rousset and it can be used for characterizing other samples. Even if, for the moment, the analyses can only be performed ex-situ.

A model was developed by using DOE in order to optimize the eSTM trench etching process in terms of CD. The related-study also improved our knowledge of the physical behavior in

relation to the final trench CD process. Respect to the industrial contributions, the eSTM CD of the trench was reduced based on the electrical results. The optimal CD proposed during this study is nowadays the target CD of this trench, which is obtained with the recipe proposed by the DOE model. Furthermore, the designated model can be used to predict the CD such that it enables reaching the desired CD for better product performances (ex: electrics, morphology, etc.).

- Contributions to the characterization and optimization of the Reactor Walls

Thanks to the *Floating Sample* Method, we could analyze the composition of the reactor walls deposits during the process and the cleaning by using XPS. During the eSTM process more CF_x polymers were deposited on the chamber than SiO_xBr_y or SiO_xF_y as expected, knowing this, we could improve the WAC used for cleaning the reactor walls after each process. The two cleaning steps were reduced, so that the total WAC time was reduced from 65s to 38s. That made also an impact to the production process time, which is also reduced. For the industrialization, the pressure was increased. With the optimal WAC proposed, the percentage of fluorine on the coatings was reduced from 30.8% to 26.9%.

- Contributions to the characterization and optimization of the STI

A process control solution was required to reduce the etch process variability related to the STI CD. A R2R controller was developed for keeping the STI CD under control by improving the variability due to the process chamber and lot-to-lot effects. This R2R is nowadays up to be set in place for the technology in production, the one which historical data have been used for these analyses. The idea is to set the same model in place for the STI CD of the eSTM technology, once it will be in production mode. Moreover, the scatterometry model developed at the same time, is already working in the production line.

- Future work

The studies performed in this thesis are far from reaching its full potential yet. Indeed, many improvements are still possible:

- A better characterization of the wafer surface and the deposits created on the reactor walls could be performed with analyses in-situ. Since the experiments were performed in the industrial reactor of STMicroelectronics, we did not have this option. However, if an improvement of the equipment would be possible, or trying to find the same equipment in a laboratory which could do it, the mechanism taking place for the plasma-surface and plasma-reactor walls could be explained avoiding the contamination influence of air exposition.

- Even if the cleaning strategy (WAC) was improved for the process and the deposits created on the reactor walls, it could be better optimized by avoiding the cleaning gases or using a conditioning strategy, as explained in Chapter IV. For that, the line gases must be changed. A study related to the influence of the F-contamination once the eSTM technology would be in production mode, should be performed in order to understand the influence of this contamination on the variability of the process. Even a study could be performed for analyzing the possibilities of performing the process without using F-based chemistries.

- The R2R model was validated during the time that was set of-line. However, a new analysis of variance should be performed now that the scatterometry measures are in place. Furthermore, FDC analyses would help to improve the variability due to the equipment.

- The R2R controller was developed for controlling the CD of the STI that can be used both for the technology studied which is already in production and for the STI of the eSTM technology. Furthermore, based on this model, a similar controller could be developed for controlling the CD variabilities of the eSTM trench, once it will be in production mode.

Although the technology studied in this manuscript (eSTM) is still not a technology in production at STMicroelectronics Rousset, the results obtained in our study were transferred and used for an overall improvement of the manufacturing process in order to maximizing the performance of the device still in development. Furthermore, the R2R model is already scheduled to be put in place for the technology which shares the STI process with the eSTM technology in the coming months.

Résumé (French)

Contenu

1. Introduction
2. Expérimental : Matériaux et Équipement
3. eSTM: Caractérisation et Optimisation des Processus
4. Interactions Plasma-Parois du Réacteur
5. STI: Contrôle de Procédé de Gravure Plasma par rapport aux Dimensions Critiques
6. Conclusions

1. Introduction

Ces dernières années, de grands progrès ont été observés dans la technologie des semiconducteurs et dans les techniques de conception de circuits. Pourtant, la fabrication de puces électroniques est une tâche très difficile, principalement en raison de la complexité et la sensibilité de son processus de production [1]. De plus, comme le marché des mémoires entre dans un marché où les consommateurs exigeant des performances toujours plus élevées et des applications plus diversifiées, de nouveaux types de dispositifs sont en cours de développement afin de suivre les exigences d'échelle en vue de la réduction des coûts. Dans ce scénario, les mémoires [43, 44] jouent un rôle important.

Les mémoires volatiles sont rapides et sont utilisées pour le stockage temporaire de données car elles perdent l'information lorsque l'alimentation est coupée. Cela signifie qu'elles doivent être en permanence sous tension pour conserver leurs informations. Les Mémoires Non Volatiles (NVM) [39,49] conservent les informations même lorsque l'alimentation est coupée. Elles ont été conçues pour stocker l'information sans aucune consommation d'énergie pendant une longue période.

Pour la compréhension de cette thèse, la différence entre l'EEPROM et les mémoires Flash, toutes deux à base flottante, doit être introduite. La structure de base de chaque mémoire est présentée à la Figure 1. Les principales différences entre ces deux NVM sont:

• **EEPROM** (de l'anglais, Electrically Erasable Programmable Read Only Memory). Une ROM électriquement effaçable/programmable, qui peut être effacée électriquement, mais également sélectivement par adresse d'octet. Pour effacer sélectivement, un transistor de sélection est nécessaire pour chaque cellule, conduisant à une cellule à deux transistors (2T); la grille flottante et le transistor de sélection. Le transistor de sélection augmente la taille des mémoires et la complexité de l'organisation de la matrice, mais la matrice mémoire peut être effacée par bit.

• **Mémoire FLASH.** Le nom "flash" provient de son mécanisme d'effacement rapide. Elle ressemble à la mémoire EEPROM mais sans le transistor de sélection. Contrairement à une EEPROM, elle peut être effacée électriquement, mais seulement par un grand bloc de cellules simultanément. Elle perd la sélectivité des octets mais permet d'avoir une cellule à un transistor (juste la grille flottante). Aujourd'hui c'est la mémoire la plus produite.

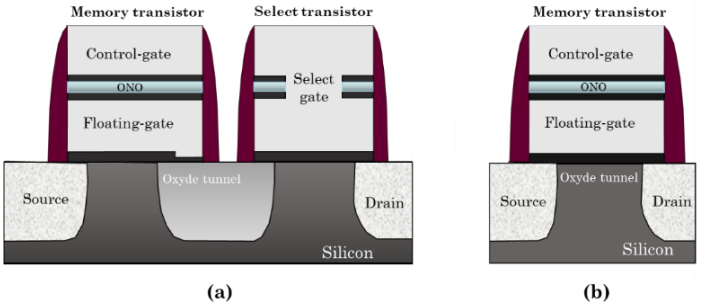

Figure 1. Schéma des mémoires EEPROM (a) et Flash (b).

La mémoire idéale doit entre autres avoir une faible consommation d'énergie, permettre une lecture/écriture/effacement rapides et une solution haute densité ... Mais l'appareil "idéal" n'existe pas encore. Cependant, différents types de mémoires ont été inventés afin d'atteindre ces propriétés spécifiques [43,44]. Exemple de cette tentative est l'eSTM (de l'anglais, Embedded Select Trench Memory) qui est représenté dans la Figure 2. Cette mémoire a été présentée par STMicroelectronics en 2012 [53,54].

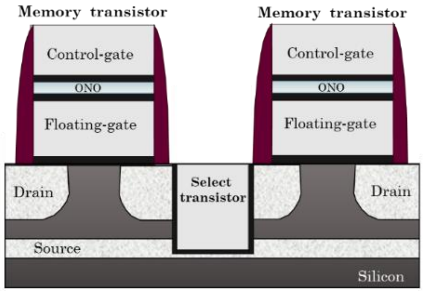

Figure 2. Schéma de la structure eSTM.

L'eSTM à pour objectif combiner les avantages de faible consommation énergétique et d'isolement de l'EEPROM, en raison de son transistor de sélection, avec la taille réduite de la mémoire Flash en réduisant sa taille. Sur cette base, deux transistors de sélection ont été fusionnés en un seul transistor vertical de sélection. Grâce à cela, il est possible de convertir une grande cellule (2T), en une nouvelle cellule, plus petite en taille et encore à faible consommation, malgré un processus de fabrication légèrement plus complexe mais toujours compatible avec une technologie CMOS. Les propriétés des mémoires EEPROM, Flash et eSTM sont comparées dans le Tableau 1.

Tableau 1. Propriétés des EEPROM, Flash et eSTM.

	EEPROM	**FLASH**	**eSTM**
Low Consumption	x		x
Fully-Bit alterable	x		x
High Density		x	x
Fast Write/Erase		x	x

TECHNOLOGIE CMOS

La technologie CMOS à base de silicium a été la force motrice de progression de l'industrie de la microélectronique depuis plus de quatre décennies. La diminution remarquable de la règle de conception et de l'augmentation du nombre de composants sur un circuit intégré individuel ont nécessité un changement majeur dans la technologie utilisée pour fabriquer ces circuits. La gravure et le dépôt subséquents de motifs, ont permis de produire des composants microélectroniques comme les transistors et les lignes d'interconnexion sur un

substrat semi-conducteur. Les principales étapes telles que le dépôt, la lithographie et la gravure plasma sont représentées dans la Figure 3.

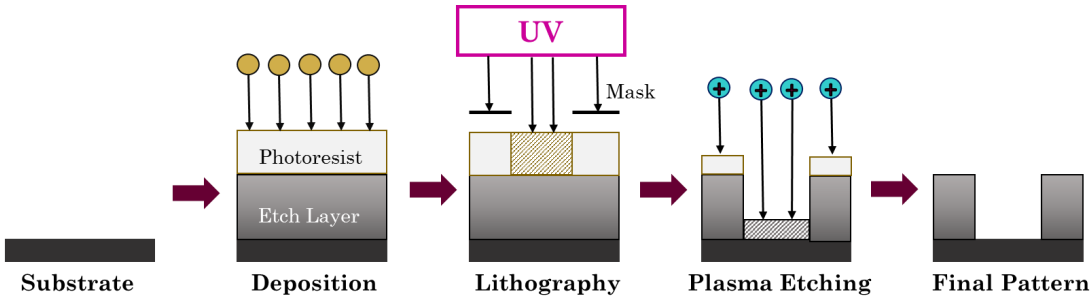

Figure 3.

Représentation des principales étapes de fabrication CMOS [Adapté de 59].

De nos jours, l'un des principaux défis auxquels est confrontée l'industrie des semi-conducteurs est la fabrication de ces composants [19] et le contrôle des variations à l'échelle nanométrique [62-64]. Pour relever ce défi, les études se portent sur la gravure par plasma [59,65,66,67]. Le plasma ou la gravure sèche de silicium joue un rôle majeur dans la fabrication des semi-conducteurs. Elle permet le transfert de motifs de circuits complexes par photolithographie sur le silicium, le dioxyde de silicium et les métaux qui construisent les circuits intégrés.

Une grande partie de la compréhension des plasmas provient des procédées de gravure plasma développées pour la technologie CMOS, où la génération de plasma [70] nécessite l'application d'une forte radiofréquence (RF), sous vide. Le principal avantage de la gravure sèche ou plasma repose sur son anisotropie, ce qui est hautement préférable pour des dimensions plus petites. De plus, la gravure anisotrope a la capacité de graver avec une meilleure résolution des motifs plus fine et un rapport d'aspect plus élevé que la gravure isotrope. Ainsi, à la fin des années 1970, l'industrie de la microélectronique entraîne la transition de la gravure humide vers la gravure plasma, et aujourd'hui presque tous les processus de transfert de modèle sont effectués par gravure plasma. La gravure anisotrope est rendue possible par la combinaison d'approches physiques et chimiques. La partie physique peut être réalisée par bombardement neutre, ionique, électronique ou photonique qui assiste les réactions de gravure d'une surface exposée à un agent de gravure chimique. Ce bombardement est anisotrope et non sélectif. La partie chimique implique une réaction chimique entre les gaz d'attaque et la surface du silicium. Cette réaction est spontanée, isotrope et expose de façon sélective. Coburn et Winters, dans leur expérience classique en 1979 [71], ont montré que la gravure plasma est le résultat synergique de la combinaison entre ces deux mécanismes; le bombardement ionique et la réaction chimique neutre.

L'ETAT DE L'ART EN GRAVURE PLASMA

Depuis l'introduction des procédés de gravure sèche ou gravure plasma dans la fabrication des circuits à base semi-conducteurs à la fin des années 60 et au début des années 70, il était

établi que la gravure plasma est une technique incroyablement complexe. Bien qu'il y ait eu une discussion sur le contrôle du profil dès le début, ce n'est que vers le milieu des années 1970 que sous-cotation dans le processus de gravure plasma a pu être éliminé [93].
Au début, la majeure partie du travail de gravure sèche impliquait l'utilisation des molécules halocarbonées, le CF_4 étant le plus courant. Puis, un article important, décrivant un procédé pour graver SiO_2 sélectivement par rapport à Si en utilisant une chimie sans fluor (polymérisation), a révolutionné les procédés. Pour la première fois, le terme de *passivation des flancs* a été introduit. En effet, les produits chimiques fluorés étaient connus pour avoir tendance à graver de façon isotopique, de sorte que la passivation des parois latérales était nécessaire pour maintenir un profil acceptable. L'utilisation d'un dépôt de polymères comme couche de passivation, a permis de contrôler le profil et la sélectivité. Il existe deux mécanismes possibles pour la formation de cette *passivation*; par des réactions chimiques ou par pulvérisation physique [94]. Des analyses chimiques utilisant des techniques de spectroscopie sont aujourd'hui couramment utilisées pour révéler la composition de cette couche de passivation.
À la fin des années 1970, d'importantes études sur la gravure ont été menées, confirmant l'importance de la synergie entre le bombardement ionique et les réactions chimiques lors de la gravure plasma [71]. Un développement important des équipements de gravure plasma a commencé à cette époque. La première méthode utilisée pour augmenter la densité du plasma dans l'équipement de gravure sèche à une seule plaquette était le magnétron RIE (de l'anglais, Reactive Ion Etching). Cette méthode avait peu de marges en termes de chargement de plaquettes résultant d'un plasma non uniforme. Vers la fin des années 80, un système utilisant des sources alimentées par induction pour générer des plasmas de densité plus élevée a été introduit avec succès. C'est en 1985 que Hitachi a commercialisé la gravure plasma ECR (de l'anglais, Electron Cyclotron Resonance). Le réacteur ECR a besoin d'une grande bobine magnétique pour former un champ magnétique fort, ce qui rendait difficile d'avoir une chambre de gravure compacte. La nécessité d'aborder cette question a conduit au développement du ICP (de l'anglais, Inductively Coupled Plasma). Avec une bobine simple placée au-dessus de la chambre de gravure, il était possible de générer un plasma de haute densité par induction électromagnétique [61,95,96].

2. Expérimental : Matériaux et Équipement

MATERIAUX

L'empilement (stack) de semi-conducteurs classiques en industrie microélectronique comprend un substrat, une couche semi-conductrice et un masque. Pour le travail présenté dans cette thèse, le stack est composé de photorésine (PR), BARC, a-C:H, TEOS, NFARL,

Nitrure, SiO_2, d'une couche semi-conductrice et d'un substrat dont la nature et fonction sont décrites ci-dessous.

• **Photorésine (PR).** La photorésine est un matériau photosensible utilisé dans le procédé de photolithographie pour former un revêtement à motifs sur la surface à graver. La PR utilisée dans cette étude est une photorésine de 193nm. Ces résines ont une sélectivité inférieure et une résistance mécanique médiocre par rapport à celles de 248nm [109]. Pour cette raison, un masque épais est nécessaire.

• **BARC.** De l'anglais, Bottom Anti-Reflective Coating, cette couche anti-réflect organique appliqué avant le PR afin d'absorber la lumière. Il empêche l'interaction chimique entre le PR et le substrat et augmente le contrôle du CD.

• **a-C:H ou AHM.** De l'anglais, Hydrogenated Amorphous Carbon Mask. Il s'agit d'une couche de carbone de type diamant [111,112], dur, amorphe et avec une fraction importante d'atomes de carbone hybrides sp^3, contenant une quantité significative d'hydrogène [111]. Ce matériau servira de masque pour la gravure une fois la résine consommée.

• **TEOS.** De l'anglais, Tetraethylorthosilicate. Préparé par l'alcoolyse du tétrachlorure de silicium, il s'agit d'une molécule tétraédrique utilisée comme précurseur du dioxyde de silicium [113]. Il s'agit d'un matériau à base d'oxyde également utilisé comme masque dur.

• **NFARL.** De l'anglais, Nitrogen-Free Anti-Reflective Layer. Il s'agit d'un oxyde riche en silicium avec une sélectivité élevée vers l'a-C:H. Les propriétés optiques et les caractéristiques de gravure des films AHM et NFARL les rendent bien adaptés à l'intégration dans un espaceur à double motif [115]. Il s'agit d'une autre couche anti-réfléchissante, mais contrairement au BARC, le NFARL aura tendance à maintenir une épaisseur constante indépendamment du relief de la couche inférieure. C'est pourquoi il est dit « planarisant » et aura tendance à réduire les inégalités du relief.

• **Nitrure.** Le nitrure de silicium (Si_3N_4) est un matériau amorphe, similaire aux films de SiO_2. Il est largement utilisé comme barrière d'oxyde. Il est généralement utilisé comme masque dur de gravure dans les applications STI [116]. En raison de la différence de coefficient de dilatation thermique entre le silicium et le Si_3N_4, le nitrure de silicium est déposé sur Si avec une mince couche tampon d'oxyde, appelée oxyde de chemin, afin d'éviter les dommages induits par le stress à l'interface à température élevée [58].

ÉQUIPEMENT DE GRAVURE

L'équipement utilisé pour le développement dans cette thèse est le réacteur TCP®, de l'anglais Transformer Coupled Plasma, lancé par Lam Research en 1992 [93,95]. Cet équipement est un exemple de réacteur ICP. Dans cet équipement, un DC-BIAS est créé en appliquant une puissance RF à l'électrode inférieure, puis, le DC-BIAS contrôlable dirige les ions normaux à la surface de la tranche et donc il y a très peu d'interaction entre les champs électriques supérieur et inférieur. Le rendement énergétique élevé crée un plasma à haute

densité où l'énergie ionique et la directionnalité sont contrôlées par la puissance appliquée à l'électrode inférieure [97]. La Figure 4 présente cet équipement : un cluster comprenant 4 chambres de gravure.

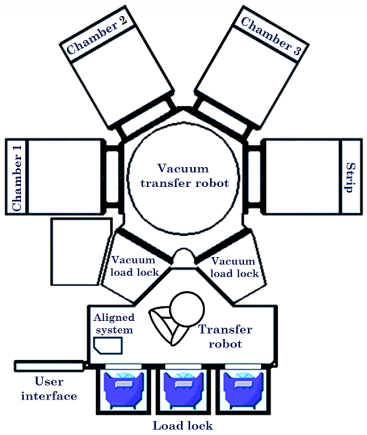

Figure 4. Représentation schématique de la plateforme de gravure LAM Versys.

Lam Research a lancé cet équipement de type ICP [93,95] où le plasma est généré par une bobine en forme d'anneau planaire avec enroulements multiples comme dans un transformateur [65]. Cette conception est capable de fournir une densité de plasma beaucoup plus élevée par rapport à une conception de chambre standard. Un schéma de la chambre de gravure est donné dans la Figure 5.

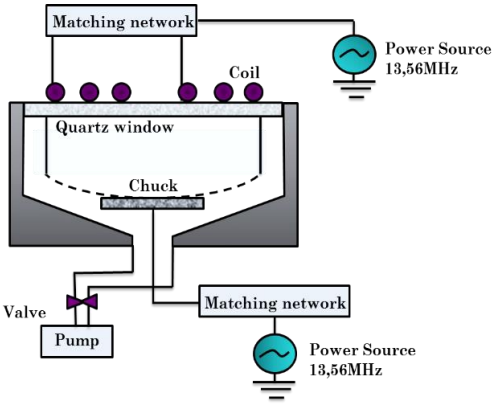

Figure 5. Représentation schématique de la plateforme de gravure LAM Versys 2300 [Adapté de 65].

Dans cette configuration TCP, capacitive comme inductive, la puissance est complétée par une source RF couplée capacitive pour contrôler l'énergie ionique. Le plus grand avantage est que la séparation du couplage RF offre la possibilité de contrôler le courant ionique (TCP inductif) indépendamment du contrôle de l'énergie ionique (bias capacitif). Dans ces outils capacitifs, la puissance est souvent fournie avec des fréquences multiples, permettant un certain contrôle indépendant de la densité ionique et de l'énergie.

Afin de maintenir la chambre aux conditions initiales, un nettoyage WAC (De l'anglais, Waferless Auto Clean) est appliqué entre chaque procédé. Il se compose de recettes similaires

à la recette du procédé, en sachant qu'il n'y a pas de plaquettes dans la chambre. Il existe deux types de WAC:

• **Le Conditionnement:** démarre automatiquement avant le passage de la première plaquette de chaque lot. Il peut être utilisé à la fois pour amener la chambre à la bonne température et pour nettoyer l'intérieur de la salle blanche.

• **Le Post-WAC:** est lancé pour nettoyer la chambre après gravure de chaque plaquette.

La recette de WAC doit être sélectionnée en fonction du sous-produit de dépôt sur la chambre après le procédé.

3. eSTM: Caractérisation et Optimisation des Procédés

Le fonctionnement de la cellule eSTM est identique à un flash NOR avec un transistor de sélection. Cependant, des développements sont nécessaires pour mettre en place le procédé de réalisation du transistor vertical, car il est complètement nouveau. La fabrication de la cellule consiste en une succession d'étapes, semblables à la Flash mais avec des étapes supplémentaires où réside toute la complexité du procédé.

SPECIFICATIONS DU PROCEDE

L'eSTM partage les étapes standard du procédé flash jusqu'à la définition des zones actives/STI. Une fois ces zones définies, la STI est remplie de SiO_2. Ensuite, une tranchée perpendiculaire aux lignes actives est créée. Pour ce faire, une masque dure est nécessaire. Ensuite, la tranchée sera remplie de Si. Puisque cette étude est basée sur la caractérisation et l'optimisation du procédé de gravure plasma impliqué dans la création de cette tranchée, ces étapes sont représentées dans la Figure 6.

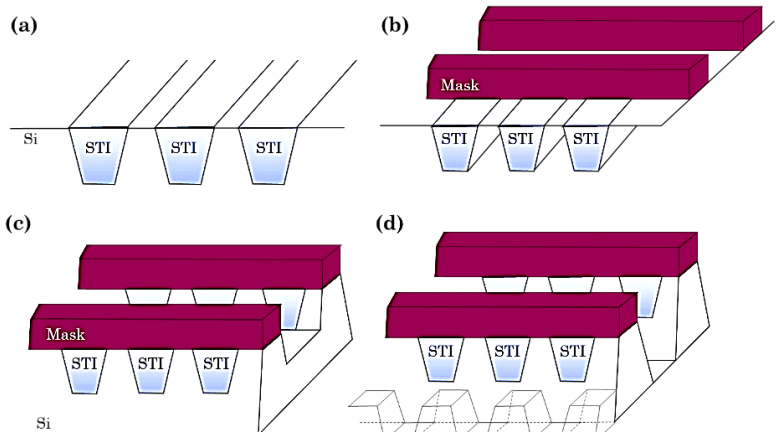

Figure 6. Représentation schématique des principales étapes de réalisation de la tranchée eSTM. A) à partir du flash active/STI standard, b) masquage et photolithographie, c) gravure de la première partie de la tranchée et d) étape de gravure finale pour atteindre la tranchée eSTM.

Considérations de gravure

La Figure 7 illustre le procédé utilisé pour graver la tranchée eSTM. Il est composé de 5 étapes de gravure. Ces 5 étapes sont la gravure du NFARL, la gravure de l'AHM, la sur-gravure de l'AHM, la première étape de gravure de tranchée (Si/SiO_2) et la deuxième étape (Si) qui est la dernière. La vitesse de gravure du SiO_2 pendant la quatrième étape de cette recette est beaucoup plus élevée que pour la gravure de Si. Cependant, au cours de l'étape finale, la vitesse de gravure de Si augmente fortement en utilisant un plasma à base de brome.

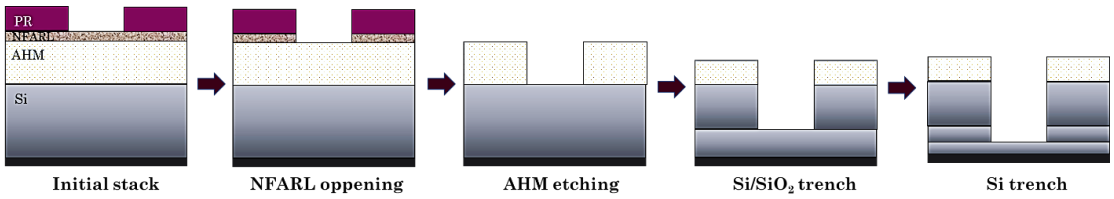

Figure 7. Représentation schématique des cinq étapes de gravure de la tranchée eSTM.

Ici, l'étape de sur-gravure de l'AHM n'est pas représentée, puisqu'elle est en quelque sorte incluse dans l'étape de gravure de l'AHM. Au cours de cette sur-gravure, la chimie utilisée est la même. L'objectif, est de "nettoyer" les résidus d'AHM qui pourraient rester après la gravure principale de ce matériau. Désormais, nous pouvons nous référer à la quatrième étape (Si/SiO_2) comme tranchée STI et à la dernière (Si) comme tranchée eSTM. La chimie utilisée lors de l'étape NFARL, $CF_4/CH_2F_2/He$, n'est responsable que de l'ouverture NFARL. Une chimie à base de fluor est nécessaire puisque le NFARL est un matériau de type oxyde. Ensuite, l'AHM qui est un matériau à base de carbone est gravé avec $Cl_2/HBr/O_2$. Cette chimie est sélective et grave uniquement l'AHM. La couche suivante est le STI, mais tout d'abord, juste après la gravure de l'AHM qui prend 50sec nous effectuons une sur-gravure de 29% du temps afin d'éliminer les résidus possibles de AHM qui peuvent rester sur les parois latérales. Pendant cette étape, la gravure est latérale. Il n'y a aucun risque de gravure de la couche suivante (Si/SiO_2). Après avoir gravé le masque dur, la première étape principale démarre, la tranchée STI. Comme expliqué précédemment, au cours de cette étape, la vitesse de gravure du SiO_2 est plus rapide que pour le Si (3780Å/min contre 840Å/min, respectivement), mais comme elle est à base de fluor ($CF_4/CH_2F_2/He$) et donc non sélective, elle est capable de graver les deux. Enfin, la gravure de la tranchée eSTM, à base de Br (HBr/O_2), grave le silicium profondément et verticalement tout en étant fortement sélective par rapport au SiO_2. La vitesse de gravure de Si au cours de cette étape est de 3015Å/min. La température est constante pendant toute la recette (Intérieur/Extérieur: 60/60°C).

CARACTERISATION

Le but de cet étude est de caractériser le processus de gravure de la tranchée eSTM car il s'agit d'un procédé complètement nouveau chez STMicroelectronics. Les méthodes utilisées

pour cette étude sont OES (de l'anglais, Optical Emission Spectroscopy) et l'XPS (de l'anglais, X-Ray Photoelectron Spectroscopy). OES est utilisée afin de connaître les espèces dans le plasma et XPS pour analyser la composition chimique des parois latérales; la couche de passivation. L'objectif est d'accroître notre connaissance sur les interactions plasma-surface.

Caractérisation du plasma par OES

La première partie de la caractérisation est liée à l'identification des espèces activées par/présentes dans le plasma lors de la gravure de la tranchée. La plupart des espèces atomiques et diatomiques peuvent être surveillées par OES, mais en raison de la complexité du mécanisme d'excitation, l'OES est généralement une technique qualitative. Seules les espèces excitées dans les plasmas sont détectées et le spectre observé donne des informations sur la densité de l'état excité et ne reflète pas directement le profil de la population au sol [213].

Le spectromètre, « OES Plus sur Flex45 », est monté sur l'équipement du plasma afin de collecter ses émissions. La lumière émise par le plasma, qui est étudiée à l'aide d'OES, a été analysée dans la gamme 220-840nm. Les différents systèmes d'émission optique étudiés comprenaient les contributions de la chimie (plasmas à base F et Br) et des matériaux liés au masque et à la tranchée (AHM et silicium). Les principales espèces détectées étaient CF_x*, CH*, H* et F* pour la première chimie et Br*, O* et F* pour la seconde. Le film a-C:H (masque) produit des radicaux CH et C_2 pendant la gravure au plasma à base de F. Les lignées d'émission de Balmer d'hydrogène étaient très intenses dans les plasmas à base de F (pour AHM et Si) comme pour la gravure de tranchée eSTM. Lors de la première gravure ($CF_4/CH_2F_2/He$), la présence de H_α a été clairement détectée. Pour les spectres de plasma à base de Br, la deuxième chimie, une ligne observée à 656,6nm, pourrait être plutôt associée au Br, en raison de l'absence de H_β et de H_δ dans les autres spectres. Néanmoins, pour la gravure eSTM, nous avons associé cette ligne à H_α puisque d'autres lignes de cette série ont été détectées. Il est intéressant de noter que le fluor est présent sur tous les spectres, même pendant la deuxième chimie (plasma bromé). Cette détection de F est probablement liée à la présence de fluor résiduel de la première chimie dans la chambre, ou dans les lignes de gaz.

En plus de ces analyses, une autre étude a été réalisée pour améliorer la compréhension de la gravure de la tranchée de l'eSTM liée à la composition de surface de plaquette.

Caractérisation de surface par XPS

Le procédé de gravure de la tranchée eSTM est sensible à plusieurs paramètres qui permettent la gravure anisotrope. La caractérisation superficielle par XPS des différents substrats nous a permis de comprendre la composition de la couche de passivation de la tranchée eSTM. Les principaux éléments détectés étaient C 1s, F 1s, O 1s et Si 2p pour les deux chimies, avec quelques traces de Br 3d détectées après la deuxième chimie (HBr/O_2). Etant données les très faibles dimensions par rapport aux caractéristiques étudiées dans la

littérature, plusieurs analyses ont été réalisées afin de développer le protocole et de mieux comprendre le mécanisme de passivation de la tranchée eSTM.

Premièrement, lors de la première chimie, les principaux contributeurs à la passivation étaient C, F, O et Si. Le silicium était principalement oxydé sous sa forme SiO_2 et avait une contribution plus grande d'oxygène que de fluor. La contribution fluorée, même si plus faible que la contribution oxygénée, était plus présente sur le bord que sur le centre. Nous avons associé cet effet à l'influence des parois du réacteur, car une certaine passivation F est également attendue sur les parois du réacteur pendant le processus en utilisant une chimie à base de F. Pour nous, il était très difficile d'identifier les pièces provenant du masque et celles provenant des flancs de silicium, puisque dans toutes nos analyses, l'effet de charge différentielle n'était pas très prononcé.

Lors de l'analyse de la passivation après la deuxième chimie, la couche de passivation était principalement composée d'oxygène et de silicium. Il y avait encore avec une certaine contribution fluorée restante de la première étape. Selon la littérature, la couche de passivation formée lors de l'attaque avec HBr doit être SiO_xBr_y [249,250]. Dans notre cas, la passivation était du type SiO_xF_y, car même si certaines contributions de Br ont été détectées, elles étaient trop faibles pour être quantifiées. En effet, puisque nos analyses ont été effectuées ex-situ, le brome pu désorber avec l'exposition à l'air. La désorption du brome et l'oxydation des couches de passivation des flancs de silicium en présence d'oxygène (par ajout d'oxygène aux chimies à base de HBr ou par exposition à l'air) est un effet qui a été étudié de manière approfondie dans la littérature [249,250]. Avertin [67], a également observé ce phénomène au cours de ses études pour un plasma $SF_6/HBr/O_2$. Il a expliqué que le brome, n'étant pas détecté, peut aisément être remplacé par F ou O et qu'il est donc difficile de détecter Br sur les surfaces. Puisque nos analyses ont été réalisées ex-situ, en raison des limitations industrielles, la passivation étudiée a été soumise à ces facteurs. De plus, nous avons non seulement exposé les échantillons à l'air, mais aussi ajouté de l'oxygène à la chimie HBr. Cependant, ces analyses nous ont permis d'avoir une idée du mécanisme de la surface du plasma qui a lieu au cours du processus eSTM. Avec une passivation SiO_xF_y sur les parois latérales, nous avons voulu différencier la partie STI (SiO_2) de la tranchée par rapport à la tranchée eSTM elle-même (Si). À cette fin, nous avons utilisé la technique de l'échantillon flottant développé par Joubert et al [155] en 2004. Cette méthode est principalement utilisée pour simuler les parois du réacteur, cependant, certaines études l'ont utilisée pour analyser la passivation des flancs [67,125,260]. Ces études ont montré que l'échantillon flottant n'est pas aussi précis pour l'analyse de la passivation que pour la caractérisation du dépôt des parois du réacteur. En effet, les parois du réacteur en tant qu'échantillon flottant sont bombardées par des ions à incidence normale avec une énergie égale au potentiel plasma tandis que les parois latérales des structures sont bombardées par des ions d'incidence de pâturage avec une énergie fixée par la puissance de polarisation du substrat. La technique de l'échantillon flottant permet donc d'accéder à des informations sur la présence d'un

nouveau dépôt de la phase gazeuse qui peut éventuellement être formé sur les parois latérales des structures gravées. Cette méthode a été utilisée en corrélation avec les autres méthodes de caractérisation. Elle a permis de confirmer la conclusion effectuée auparavant, qu'une passivation SiO_xF_y principalement oxydée est détectée à la fois sur la partie STI (SiO_2) et la partie Si de la tranchée eSTM après la gravure finale.
Dans tous les cas, la formation de la couche de passivation des flancs est une combinaison de mécanismes complexes et son absence a des conséquences désastreuses pour le profil de gravure et les dimensions critiques. Dans notre cas, certains problèmes ont été confrontés. Des problèmes comme la difficulté de faire l'analyse ex-situ avec le faible effet induit par l'effet de charge différentielle. Le but de ces analyses était de caractériser la passivation, qui est liée à la CD (de l'anglais, Critical Dimension). Mais pour garder la CD sous contrôle, plusieurs paramètres doivent être pris en compte. La partie suivante est liée à l'étude de l'influence de ces paramètres sur le CD.

OPTIMISATION

La dimension critique (CD) est fortement influencée par la gravure RIE du silicium dans la technologie CMOS. Cette CD doit être bien contrôlée, car il s'agit d'un des paramètres les plus importants pour les résultats électriques. Cependant, le procédé RIE dépend de nombreux paramètres, ce qui complique sa compréhension.
L'objectif de cette étude était de décrire et d'évaluer les paramètres qui entrent en jeu au cours du procédé afin de sélectionner les plus importants en termes de variations de CD pour la tranchée eSTM. Ainsi, nous pourrions optimiser les performances de la cellule en améliorant le CD de la tranche eSTM en termes de résultats électriques. Pour cela, quelques expériences ont été réalisées afin de proposer un modèle analytique développé à l'aide de plans d'expériences ou « DOE » pour ses sigles en anglais Design of Experiments. L'objectif final était d'avoir un modèle adapté au procédé de telle sorte qu'il puisse prédire le CD chaque fois que nous aurions eu besoin d'un changement industriel.

Partie Expérimentale

Il y avait 11 principaux paramètres impliqués dans la recette utilisée pour cette étude, comme la pression, la température, TCP, BIAS et les flux de gaz. Plusieurs gaz sont nécessaires pour graver chaque couche. Par exemple, comme il a été expliqué précédemment, lors de la gravure du Si/SiO_2, la chimie choisie est à base F alors que celle pour la gravure au silicium est à base de Br. Pour commencer à concevoir un ensemble d'expériences nécessaires, il était essentiel de connaître les facteurs les plus importants (entrées) liées aux sorties, c'est-à-dire le CD dans cette étude. Étant donné que le procédé à l'étude comporte 10 paramètres dans chacune des 4 étapes, la réduction du nombre d'entrées est obligatoire même si l'on soupçonne qu'ils sont des facteurs clés. Il y avait deux objectifs dans cette recherche: le premier était de découvrir les facteurs et les étapes avec les plus grandes influences en termes

de CD final afin de construire un modèle mathématique et donc la « fenêtre de procédé » significative; le second objectif était de pouvoir prédire le CD avec le modèle de sorte qu'il permet d'ajuster le CD au besoin (ex: pour les performances électriques, la morphologie, etc.). Ces objectifs seront satisfaits en choisissant les facteurs appropriés pour effectuer la modélisation du DOE et en évaluant le modèle. Pour l'ensemble de l'étude, le CD final a été mesuré sur le haut de la tranchée en utilisant le CDSEM en ligne.

- ***Identification des paramètres et étapes les plus influentes***

Dans notre étude, « l'analyse de sensibilité » utilisée est un test qui consiste à faire varier un paramètre de la recette à la fois afin d'explorer ce que le modèle fait avec la nouvelle valeur. Dans ces analyses, la valeur de référence a été maintenue constante. Les facteurs ont été écartés de la ligne de base une seule fois (ou deux fois) et la ligne de base n'a pas été modifiée tout au long de l'analyse. L'existence d'interactions est initialement ignorée. Nous supposons qu'il n'y a pas d'interactions entre les étapes puisque la chimie utilisée était sélective. Ainsi, cette étude a été utilisée comme étape de dépistage avant l'analyse du DOE.

- ***Analyse de sensibilité des processus***

Le nombre total d'expériences requises pour effectuer l'analyse de sensibilité était de 20, étant donné que le nombre de paramètres était de 10. Les résultats de cette analyse de sensibilité du procédé concernant la variation attendue du CD sont présentés en Figure 8.

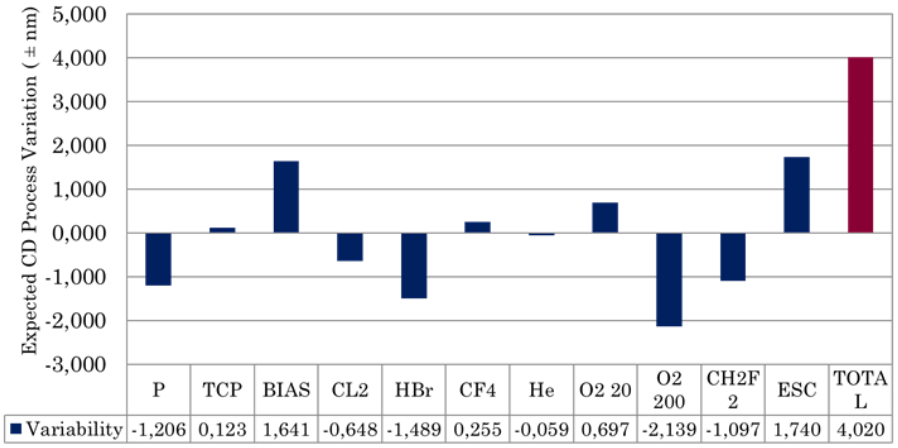

Figure 8. Variation de CD attendue à partir de l'analyse de sensibilité du procédé.

La Figure 8 montre que, la sensibilité la plus élevée était liée au débit d'O_2 (200sccm), à la température ESC, à la tension BIAS, au débit d'HBr, à la pression et au débit du CH_2F_2. Il y avait encore trop de paramètres à utiliser pour la prochaine analyse de sensibilité. Un découpage procédé ou « partitioning » était donc nécessaire pour identifier les étapes les plus importantes.

- ***Partitioning***

Faire un découpage procédé ou « partitioning » consiste à graver une plaquette par étape. En arrêtant le processus après chaque étape, chaque plaquette est représentative de l'une des étapes.

Après avoir identifié les principaux paramètres du processus avec l'analyse de sensibilité, l'étape suivante était de faire un partitioning pour découvrir les étapes les plus importantes en analysant l'influence de chaque couche par rapport au CD final. Les résultats de ce partitioning sont présentés dans le Tableau 2.

Tableau 2. Partitioning par étapes de gravure par rapport au CD.

Step	CD variation	Δ CD*
PHOTOLITOGRAPHY	Starting CD: 100nm	-
NFARL	100nm → 90nm	10nm
AHM	90nm → 152nm	62nm
STI trench	152nm → 184nm	32nm
Si trench	184nm → 172nm	12nm

*Values absolutes

Dans le Tableau 2, on peut noter que le CD à changé d'une étape à l'autre. Les différences entre deux étapes consécutives ont été calculées pour étudier la source de variation en termes d'étapes. Selon ce tableau, les étapes qui induisent la plus grande variation CD sont l'AHM et la tranchée STI. En particulier, l'étape AHM qui induit 62nm de variation de CD. Après cette étape, le CD a augmenté de 90 nm après l'ouverture NFARL à 152nm après la gravure AHM.

- ***Sélection des facteurs clés pour l'analyse du DOE***

Avec l'identification des paramètres et des étapes critiques, les paramètres critiques (débit de O_2, température ESC, tension BIAS, débit HBr, pression et CH_2F_2) ont ensuite été corrélés aux étapes les plus importantes (AHM et STI). Pour sélectionner les facteurs de conception pour le DOE, deux nouvelles analyses de sensibilité ont été réalisées.

Les effets des paramètres lors de la gravure AHM sur le CD final de la tranchée eSTM ont été classés comme suit: O_2> P> HBr> BIAS> ESC. Les contributions des paramètres à la variabilité dans cette étape étaient de 41%, 28%, 17%, 13% et 1%, respectivement. Les effets des paramètres pendant la gravure de la tranchée STI sur le CD final de la tranchée eSTM ont été classés comme suit: P> BIAS> CH_2F_2> ESC. Les contributions des paramètres classés à la variabilité survenue dans cette étape étaient de 40%, 28%, 28% et 4%, respectivement. En conséquence, les facteurs d'entrée pour le DOE étaient **O_2 (AHM), P (AHM), P (tranchée STI), BIAS (tranchée STI) et CH_2F_2 (tranchée STI)**. Considérant que ces cinq facteurs de contrôle étaient les paramètres/étapes les plus critiques liés au CD final de la tranchée eSTM, un modèle de surface de réponse doit être construit pour tenir compte des principaux

effets et des interactions entre les paramètres clés. Le modèle doit pouvoir prévoir/optimiser le CD en ajustant les paramètres.

- ***Design of Experiments (Plan d'experience)***

Le logiciel Design Expert a proposé plusieurs modèles DOE. Celui utilisé pour cette étude était un modèle de réponse de surface D-Optimale. Il a utilisé des facteurs discrets avec n'importe quel nombre de niveaux.

- Conception expérimentale

Pour étudier les effets principaux et toutes les interactions des facteurs choisis, la matrice de conception idéale est sûrement basée sur la conception factorielle complète. Compte tenu des 5 facteurs à 3 niveaux, la conception factorielle complète avait nécessite 243 wafers. Avec la contrainte d'utiliser un seul lot, c'est-à-dire 25 wafers, le nombre d'expériences a été réduit à 21 pour évaluer les effets principaux et toutes les interactions de second ordre. Trois expériences supplémentaires au centre de l'espace de conception, appelées répétitions, ont été ajoutées afin d'étudier la répétabilité et la robustesse de la conception [269]. Pour éviter le premier effet de plaque et avoir la condition de chambre stable, on traite 24 wafers expérimentals et on mesure leurs CD de la tranchée de silicium, c'est-à-dire la réponse du modèle de DOE après le procédé.

Le Tableau 3 résume les niveaux de conception des 5 paramètres sélectionnés. Les 24 expériences (21 tests avec 3 répétitions) ont été générées sur la base des critères D-Optimal, où le niveau 0, c'est-à-dire S_A, S_B, S_C, S_D et S_E, indique le réglage standard pour les cinq facteurs.

Table 3. Niveaux de conception pour les paramètres sélectionnés .

Step	Parameters	-1	0	+1	Variations
AHM	O_2	S_A-10	S_A	S_A+10	20sccm
	P	S_B-0,5	S_B	S_B+0,5	1mTorr
STI trench	P	S_C-0,75	S_C	S_C+0,75	1,5mTorr
	BIAS	S_D-27,5	S_D	S_D+27,5	55V
	CH_2F_2	S_E-7,5	S_E	S_E+7,5	15sccm

Ce DOE a été réalisé à travers les étapes de la tranchée AHM et STI, puisque les deux étapes ont été évaluées comme les plus importantes. Cependant, le CD a toujours été mesuré en haut de la tranchée finale de l'eSTM, qui était donc le CD final. Aucune interaction entre les étapes n'a lieu puisque la chimie change pour chaque étape et elle est sélective pour graver le matériau cible. Par conséquent, on s'attendait à voir seulement les interactions entre paramètres dans la même étape.

- Résultats

En menant les 24 essais expérimentaux et en recueillant les réponses au processus, c'est-à-dire le CD de tranchée finale, les modèles de surface de réponse ont été construits et évalués

à l'aide du logiciel « Design Expert ». Le meilleur modèle, étant le modèle linéaire, a été sélectionné et analysé. Ce modèle peut être exprimé comme (**1**) en fonction des 5 facteurs et du terme d'interception.

$$CD= +172.67-7.88\cdot A-3.95\cdot B-1.01\cdot C+1.36\cdot D-2.32\cdot E \quad (1)$$

Le modèle CD dans (**1**) a été construit en termes de niveaux codés, c'est-à-dire, -1 et +1, par rapport aux paramètres de ligne de base. L'équation (**1**) est utile pour identifier l'impact relatif des facteurs en comparant les coefficients.

- Prédictions et Validation

Une comparaison des résultats expérimentaux et des résultats prédits pour les différentes réponses du DOE est représentée dans la Figure 9.

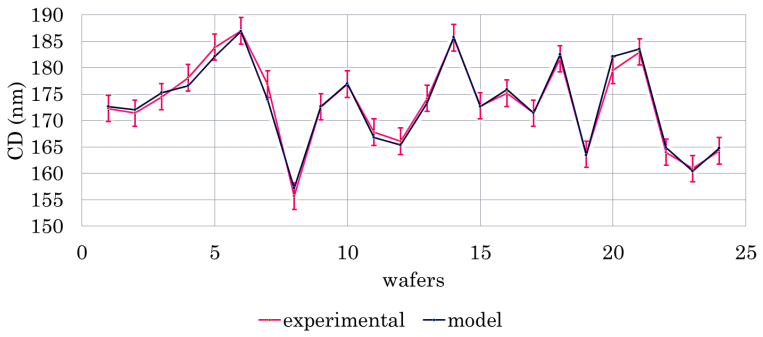

Figure 9. Comparaison entre les valeurs CD expérimentales et calculées.

Pour vérifier que le modèle a fonctionné pour faire des prédictions, une plaquette complémentaire a été traitée et les réponses correspondantes ont été recueillies. Comme on peut le voir sur la Figure 9, les mesures prédites et les vraies mesures de CD pour ces essais ont été fortement corrélées. En conclusion, le modèle est significatif et donc il peut être utilisée pour prédire les CD.

CONCLUSIONS

Ce chapitre présente la caractérisation et l'optimisation du processus eSTM. Tout d'abord, on a discuté de la caractérisation des différentes parties qui interagissent pendant la gravure de processus. Par conséquent, les diagnostics du plasma lui-même en utilisant OES et la composition de la couche superficielle en cours d'attaque par XPS ont été étudiés. Dans un second temps, pour réduire le CD dans le but d'optimiser les résultats électriques, un modèle a été proposé en utilisant le DOE. Ce modèle est capable de prédire et de contrôler le CD en établissant les unités pour les paramètres les plus importants.

4. Interactions Plasma-Parois du Réacteur

Pendant les processus de gravure plasma, il y a les interactions plasma-surface, comme expliqué précédemment, mais aussi les interactions plasma-parois du réacteur. En raison des

différences sur l'énergie du bombardement ionique et de la composition chimique des parois du réacteur par rapport à la surface de la plaquette, les effets sont complètement différents.

INFLUENCE DES CONDITIONS DE LA PAROI DU REACTEUR SUR LES PROCESSUS D'ATTAQUE

Le contrôle de la stabilité des processus de plasma devient un problème majeur à mesure que les dimensions des grilles diminuent à chaque nouvelle génération. Parmi les différentes raisons qui conduisent à contrôler les dimensions des caractéristiques, la composition chimique du revêtement formé sur les parois du réacteur est l'une des plus importantes [155]. Lors de la gravure de tranches successives, les surfaces de paroi exposées au plasma vont changer progressivement. En conséquence, les caractéristiques de gravure du plasma changent. Les couches de revêtement formées sur les parois du réacteur ont été étudiées pour plusieurs auteurs pour différentes chimies de plasmas. De plus, il existe plusieurs études relatives au mécanisme fluoré des parois des réacteurs irradiées par des plasmas à haute densité à base de fluor. Lorsque la surface du réacteur est bombardée par des ions positifs à haut flux d'un plasma fluor, les parois sont significativement fluorées. En outre, les parois des réacteurs des usines de production de masse sont composées de parois intérieures d'Al_2O_3 et Y_2O_3 qui présentent des problèmes d'érosion et de génération de particules significatives lorsqu'elles sont immergées dans des plasmas à base de fluor [283]. Ce problème est accentué du fait que la plupart des stratégies de nettoyage utilisent également des plasmas contenant du fluor. Ces problèmes de fluor ont été largement étudiés en raison de l'importance de maintenir des conditions stables de traitement au plasma.

Chez STMicroelectronics, le nettoyage effectué après chaque plaquette liée au procédé eSTM est le WAC (Wafer-less Auto Clean) [289]. Comme introduit précédemment, il s'agit d'un nettoyage périodique du réacteur dans lequel des plaquettes ne sont pas nécessaires. Le WAC de nos expériences utilise une chimie à base de SF_6/O_2. Il se compose de deux étapes principales de nettoyage. Le *Clean-1* (à base de F) est utilisé pour nettoyer le dépôt «vitreux» ; les oxi-halogénures de silicium. Le *Clean-2* (à base de O_2), est utilisé pour nettoyer le dépôt de polymères de type C_xF_y. Cependant, comme le *Clean-1* utilise également O_2, certains dépôts contenant du carbone sont également gravés pendant cette étape. Puisque l'eSTM est une nouvelle technologie encore en développement, au début le WAC a été prise d'autre technologie. Ce WAC impliquait 30s pour le *Clean-1* et 35s pour le *Clean-2* (30_35). La Figure 10 présente une représentation schématique du processus opérationnel de WAC utilisé dans notre étude.

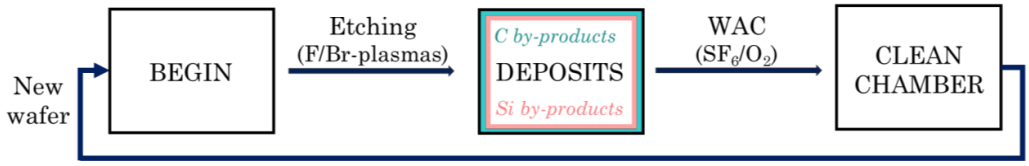

Figure 10. Principe du WAC utilisé pour le nettoyage des produits C- et Si-.

Concernant le problème du fluor, qui n'est pas seulement lié au procédé, mais aussi au WAC, nous voulions caractériser le revêtement déposé lors du procédé et pendant le WAC sur les parois du réacteur. L'objectif est d'étudier la présence du fluor dans la chambre de gravure pendant le procédé et pendant le WAC a fin de réduire cette concentration et maintenir le réacteur toujours dans les mêmes conditions.

CARACTERISATION DES REVETEMENTS

L'étude des interactions plasma-parois est difficile en raison de l'absence de méthodes de diagnostic pour contrôler la nature chimique des films formés sur les parois du réacteur pendant la gravure. En 2004, Joubert et al [155] ont proposé la méthode de l'échantillon flottant. Cette méthode est la méthode la plus largement utilisée pour caractériser la composition des parois du réacteur car elle permet l'analyse quantitative de la composition chimique des revêtements sans nécessiter d'équipement spécifique, en utilisant un échantillon flottant électriquement au-dessus d'une plaquette standard où le même dépôt que sur le réacteur va se déposer. En transférant la tranche portant l'échantillon électriquement flottant dans la chambre d'analyse XPS, on peut déterminer la composition chimique. En exploitant cette méthode [155], nous avons pu analyser les parois du réacteur de l'équipement de gravure plasma de STMicroelectronics Rousset sans contaminer la chambre. Le protocole expérimental consistait à fixer les échantillons sur les plaquettes, mais à les séparer par un *gap* calculé pour chaque procédé. Des rouleaux adhésifs *Kapton* ont été utilisés pour créer ce *gap* entre la plaquette et l'échantillon. Comme mentionné précédemment, lorsque la tension de polarisation RF est appliquée à la plaquette, si le *gap* est suffisamment épais, il empêche la polarisation DC de l'échantillon. La plaquette contenant l'échantillon est gravée dans des conditions régulières alors que l'échantillon est électriquement flottant, et ainsi les mêmes dépôts se développent sur l'échantillon et les parois du réacteur [155]. Cependant, notre analyse XPS a été effectuée ex-situ, puisqu'il n'y avait pas d'autre possibilité. Par conséquent, une certaine contamination doit être prise en compte.
Le protocole expérimental utilisé dans cette recherche a consisté à analyser les dépôts créés au cours de la gravure de la STI (chimie à base de fluor), celle créée lors de la gravure de tranchée eSTM et celle créée lors de la WAC.

Substrats

Les parois de la chambre du LAM Versys 2300 sont en Al_2O_3 mais enrobées de Y_2O_3 puisque LAM a découvert que ce composé est plus stable que l'Al_2O_3. Pour analyser les parois de la chambre en utilisant la méthode de l'échantillon flottant, des échantillons de type Y_2O_3 étaient essentiels. Nos échantillons ont été déposés sur silicium par pulvérisation ionique au xénon à l'Université de Poitiers (CNRS). L'épaisseur était d'environ 200 nm.

Résultats

La première chose que nous voulions étudier était l'influence du processus sur les parois du réacteur, celle liée à la tranchée eSTM. Ainsi, des analyses sur l'influence de l'étape STI (chimie à base de F) et de l'étape eSTM (chimie à basée de Br) sur les parois du réacteur ont été effectuées. A partir de ces résultats, nous avons conclu que la présence du fluor était la contribution la plus importante pour les deux processus, après la chimie F- (étape STI) et après la Br- (étape eSTM). Les deux compositions étaient assez semblables à l'exception de la présence du brome par rapport à l'échantillon lié au eSTM qui provient clairement de la chimie. Le C a été lié au F (CF_x) avec une contribution de la contamination de l'air (CC:CH). Cependant, aucun silicium n'a été détecté dans aucun échantillon, seules quelques traces au cours de l'étape eSTM qui ne sont même pas quantifiables. Cela a été vraiment surprenant puisque de l'étape de l'eSTM (HBr/O_2), certains dépôts « vitreux » étaient attendus sur les parois du réacteur. Dans tous les cas, nous avons toujours été en mesure de détecter la composition de l'échantillon (Y_2O_3) ce qui signifie que l'épaisseur du revêtement était inférieure à 10nm qui est la capacité de détection du XPS. La réduction des atomes d'oxygène a été expliquée par l'incorporation de fluor. Les atomes Y étaient moins liés aux atomes O (Y-O) et plus liés à F (Y-F) puisque sa présence était plus importante après le processus. Ainsi, après le procédé, l'yttrium est principalement lié au fluor sous la forme YF_x.

Toujours concernées par le problème du fluor, nous avons également caractérisé les revêtements déposés sur les parois du réacteur pendant le WAC, qui est destiné à nettoyer les revêtements d'un procédé à l'autre. Puisque le WAC était également à base F (SF_6/O_2), et sachant par la littérature que ce type de plasma laisse également une contamination F sur les parois du réacteur, nous voulions savoir si les revêtements étaient plus ou moins fluorés que pendant les procédés (STI et eSTM). Puisque la pression utilisée pendant le WAC est plus élevée que celle utilisée pendant les processus, elle est supposée réduire ces formations contenant du fluor. Après les analyses, nous avons pu voir une réduction du fluor en ce qui concerne les analyses précédentes (55% pour la gravure de la STI et 52,3% pour cela de l'eSTM), mais encore la présence de fluor après le WAC était encore très inquiétante (30,8%). Après avoir analysé le processus et les influences du WAC sur les parois du réacteur, toutes concernées par le problème du fluor, nous devions trouver une solution pour améliorer la situation.

OPTIMISATION DE LA STRATEGIE DE NETTOYAGE

L'optimisation de la recette WAC a été nécessaire afin d'obtenir celle qui correspond le mieux à notre recette. L'objectif était également de réduire l'exposition au fluor pour réduire les formations YF_x. La stratégie suivie alors, était d'optimiser le WAC. En optimisant le WAC, des conditions plus reproductibles peuvent être obtenues, ce qui est essentiel car la taille du CD continue de diminuer.

Stratégie

La stratégie suivie consistait à enregistrer l'émission optique de 5 wafers de production. Deux WAC ont été effectués après chacun d'eux. Le premier, c'était celui que nous voulions tester. Le second, était un WAC de référence, dont les temps de *Clean-1* et de *Clean-2* étaient plus longs (60_60) que le WAC standard (30_35) pour être utilisés comme référence de chambre propre.

- ***Etape 1: Définition du temps pour Clean-1 (SF_6/O_2) en utilisant la méthode d'itération***

Afin de définir le temps du *Clean-1*, les traces enregistrées pour 703nm (F) ont été comparées avec la référence de nettoyage de la chambre (60_60). La trace qui se chevauchent avec la référence était la bonne. Plusieurs références sont nécessaires pour confirmer que les résultats ne sont pas dus à la variabilité du processus. Cinq temps de WAC ont été essayés pour le *Clean-1*. Ces temps étaient entre 10s et 25s, plus le standard qui est de 30s. Même en sachant que les restrictions LAM ne permettent pas un *Clean-1* inférieur à 12s, nous avons voulu le tester afin de voir si 10s seraient déjà assez. Aussi, pour vérifier les analyses précédentes, où nous n'avions pas trouvé beaucoup de dépôts « vitreux » à nettoyer.

- ***Etape 2: Définition du temps pour Clean-2 (O_2) en utilisant la méthode de détection de point final***

Une fois que le temps pour le *Clean-1* a été défini, nous avons recherché un WAC avec le temps optimal sélectionné pour *Clean-1* et 60s pour *Clean-2*. Ensuite, les *EndPoint* du *Clean-2* ont été évalués en utilisant la ligne 516nm (C). Le temps optimisé pour *Clean-2* doit être égal au point final plus 30% de ce point final.

- ***Étape 3: Nouvelle méthodologie de vérification de la propreté de WAC***

Un WAC long et une référence propre (WAC 60_60) étaient nécessaires pour être sûr que la chambre avait été nettoyée. Nous avons traité une plaquette standard avec le nouveau WAC optimisé, sélectionné avec les temps optimaux pour les étapes 1 et 2. Ensuite, on a utilisé une nouvelle référence WAC de chambre pour comparer ses traces relatives au 703nm (F) et vérifier si les traces chevauchaient. Cela confirmerait que la WAC a réussi.

- ***Étape 4: Utilisation de la méthode d'échantillon flottant pour vérifier l'optimisation***

Après avoir vérifié que le WAC était le bon avec des analyses OES, nous avons utilisé la méthode de l'échantillon flottant pour comparer si le dépôt de fluor a été réduit avec ce nouveau WAC.

Résultats

La Figure 11 et la Figure 12 montrent les résultats relatifs à l'étape 1, la définition de temps pour *Clean-1* (SF_6/O_2) en utilisant la méthode d'itération.

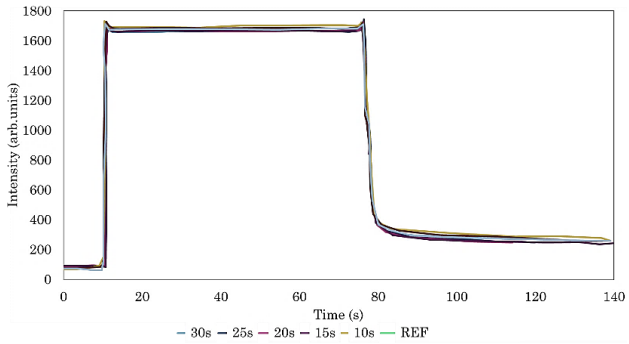

Figure 11. Définition de temps pour *Clean-1* (SF_6/O_2) en utilisant la méthode d'itération.

Dans la Figure 11, toutes les lignes se chevauchent. Pour clarifier ceci, un zoom entre 10s et 26s est montré dans la Figure 12, où on peut facilement apprécier le fait que même en utilisant un nettoyage de 1 de 10s, la chambre était déjà bien nettoyée.

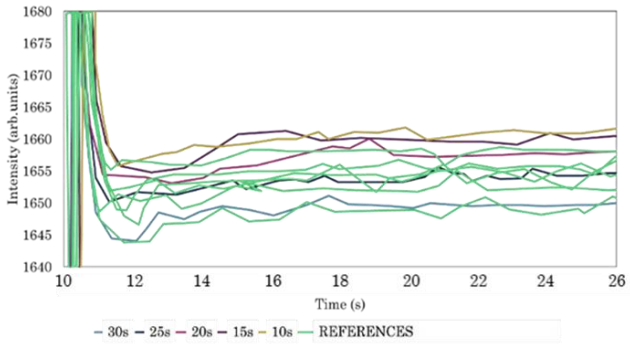

Figure 12. Zoom de la Figure 11 entre 10s et 26s avec plus de références.

Dans la Figure 12, des références supplémentaires ont été introduites afin de confirmer que la variation était due à l'équipement et non au temps du WAC. En introduisant ces références, il était facile de voir que les expériences étaient mélangées entre elles et que la seule différence était la variabilité liée à l'équipement lui-même. Par conséquent, la chambre était toujours propre. En outre, pour envisager une variation réelle, il devrait être autour de 250a.u., ici, l'échelle a été fixée entre 1640a.u. et 1680a.u et d'ailleurs, les différents temps employés ne respectaient aucune logique. La variation entre elles est totalement arbitraire, ce qui confirme qu'elle était associée à la variabilité et non au temps de processus. Ainsi, même à 10s, le *Clean-1* était suffisant. Ceci correspondait aux analyses effectuées en utilisant l'échantillon flottant, lorsque nous avons vu l'influence du procédé sur les parois du réacteur. L'absence de silicium lors de l'utilisation de l'échantillon Y_2O_3 a donc été confirmée avec ces expériences du fait que déjà à 10s la chambre est totalement nettoyée de dépôts "vitreux". Cependant, nous avons fixé le temps de *Clean-1* à 12s, ce qui était le minimum recommandé par LAM.

Une fois le temps de *Clean-1* sélectionné (12s), nous avons analysé la ligne de 516nm liée au carbone en exécutant un WAC 12_35. Le résultat de cette deuxième étape du protocole, lié à

la définition de temps pour *Clean-2* (O_2) en utilisant la méthode de détection de point final, est montré dans la Figure 13.

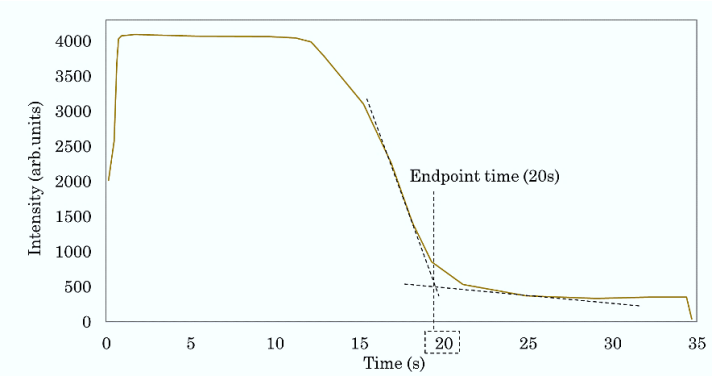

Figure 13. Définition du temps pour *Clean-2* (O_2) en utilisant la méthode de détection de point final pour la ligne 516nm (C).

Comme on peut l'apprécier à partir de la Figure 13, le temps du *Clean-2* a été fixé à 20s. Cependant, 30% de ce temps doit être ajouté afin d'être sûr que nous avons totalement nettoyé tous les polymères C. Ainsi, le temps optimisé pour le *Clean-2* était de 26s, en comptant le 30% supplémentaires. Par conséquent, notre WAC optimisé était 12_26s, où 12s étaient nécessaires pour *Clean-1* et 26s pour le *Clean-2*. En effet, pendant le *Clean-1* (SF_6/O_2) en même temps que les dépôts « vitreux » sont nettoyés par SF_6, le O_2 nettoie aussi les polymères carbonés. Puisque nous avons réduit le temps pour le *Clean-1*, le *Clean-2* ne pouvait pas être autant réduit car de polymères C (CF_x) ont été trouvés dans les analyses.
L'étape 3 était liée à la vérification du WAC, qu'a été validée avec succès. Cependant, même si le WAC était déjà optimisé pour le procédé eSTM, où peu de dépôts « vitreux » étaient impliqués dans la gravure de procédé, nous voulions voir comment la présence du fluor a été affectée par cette réduction de temps pour le *Clean-1* (de 30s à 12s). Pour cela, nous avons utilisé la technique de l'échantillon flottant. Avec ce technique on a pu caractériser les dépôts sur la chambre lors du nouveau WAC (12_26s) et le comparer au précédent (30_35s), comme expliqué dans le protocole (étape 4). De plus, puisque nous voulions réduire autant que possible le fluor, nous avons également caractérisé le nouveau WAC en augmentant sa pression (de 60mTorr à 85mTorr). En sachant que le nombre de molécules est proportionnel à la pression du système, et le libre parcours moyen (λ) dépend du nombre de molécules; sous une pression trop élevée, le λ est trop court et donc les électrons et les ions ne peuvent pas atteindre la vitesse nécessaire pour les collisions ionisantes, donc il y en a moins d'attaque Y_2O_3 et donc moins de formations YF_x.
A partir de ces résultats, nous avons vérifié que la réduction du fluor était liée à la réduction du temps (nouveau WAC) et à l'augmentation de la pression (nouvelle WAC haute pression). Pour le standard et le nouveau WAC, la pression utilisée était de 60mTorr alors que pour le nouveau WAC (à haute pression), nous avons utilisé 85mTorr, ce qui est le maximum permis

par LAM Research. En raison des résultats obtenus avec les analyses d'échantillons flottants, le WAC optimal qui est aujourd'hui en production est le nouveau WAC à haute pression (85mTorr). Ainsi, le temps pour le *Clean-1* est 12s à 85mTorr et le *Clean-2* est 26s.

CONCLUSIONS

L'objectif de cette étude était d'analyser les interactions entre les parois du réacteur et le plasma. En utilisant la méthode de l'échantillon flottant, nous avons compris que pendant la gravure de la tranché eSTM, plus de polymères CF_x sont déposés sur la chambre que SiO_xBr_y ou SiO_xF_y comme prévu. En optimisant le WAC, nous avons réduit les formations YF_x, mais il faut néanmoins envisager de nouvelles stratégies pour éviter complètement ces formations, car tant que nous continuerons à utiliser une chimie à base de fluor, ces formations seront toujours présentes sur les parois du réacteur. Pour le moment, d'autres analyses doivent être réalisées chez ST Microelectronics Rousset afin de voir l'importance de la présence des revêtements à base de fluor sur les parois du réacteur pour la reproductibilité du procédé afin de voir si d'autres stratégies plus appropriées pourraient être utilisées. Un exemple pourrait être la stratégie de « conditionnement », résumée à la Figure 14.

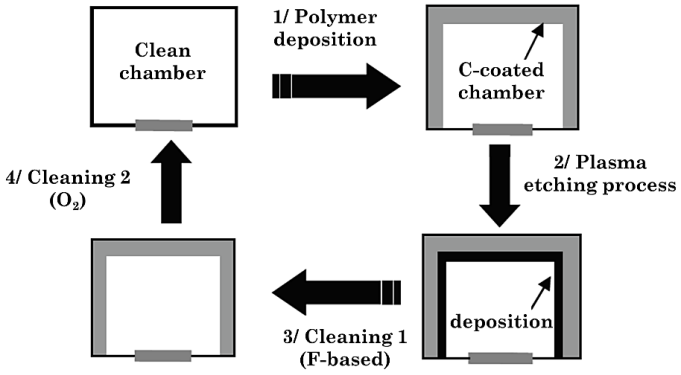

Figure 14. Principe de la stratégie de revêtement en utilisant un film riche en carbone [66].

Cette stratégie, employée par Cunge et al [156] propose un nouveau conditionnement des parois de la chambre pour améliorer la stabilité des processus plasmatiques en se débarrassant des particules d'AlF_x. Avec cette stratégie, obtenue en revêtant les parois du réacteur entre les plaquettes avec un polymère riche en carbone, le procédé de gravure commencerait toujours dans les mêmes conditions.

5. STI: Contrôle de Procédé de Gravure Plasma par rapport aux Dimensions Critiques

Comme les dimensions critiques continuent à diminuer, le contrôle du processus est devenu essentiel pour contrôler le profil et l'uniformité du CD [294]. Afin de réduire la variabilité du

procédé lié au CD des STI après gravure, des solutions de contrôle de processus doivent être réalisées.

LE PROCÉDÉ STI

Le procédé STI est considéré comme une étape de fabrication très critique parce qu'elle limite toutes les couches de motifs ultérieures en définissant les régions actives pour les structures électriques [295]. Il s'agit de la technique d'isolation utilisé sur les nœuds de processus CMOS sous-0,5µm parce qu'il évite complètement la forme du *bec d'oiseau* caractéristique du LOCOS, qui était traditionnellement la technique d'isolement [296]. Le STI est créé au début du procédé de fabrication du dispositif semi-conducteur, avant la formation des transistors. De plus, lorsqu'elle est utilisée comme base de processus complexes tel que l'eSTM, les CD doivent être vraiment bien définies pour éviter des problèmes électriques.
La STI est effectué au début du flux de procédés. Afin de comprendre l'étude réalisée pour contrôler le CD de la STI, quelques concepts expérimentaux doivent être introduits avant. Ainsi, le « stack » nécessaire et les spécifications de gravure liées à ce procédé sont présentées dans cette partie.

Caractéristiques

Le masque requis pour atteindre la tranchée STI est composé de NFARL, AHM, TEOS et nitrure. Les étapes les plus importantes nécessaires à la définition du processus de la tranchée STI sont montrées dans la Figure 15.

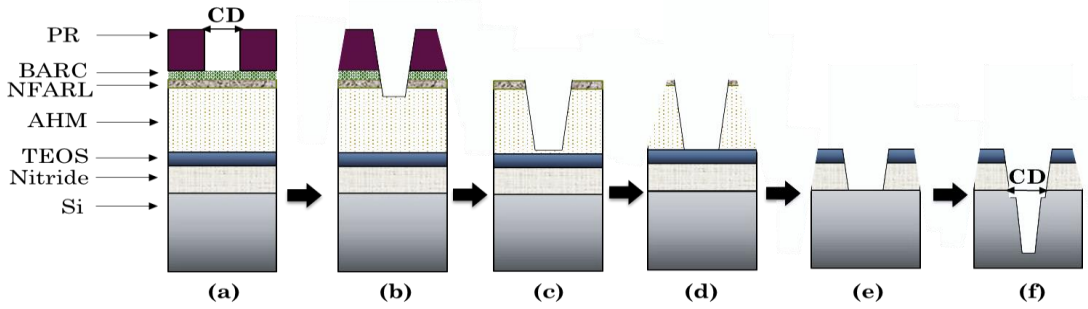

Figure 15. Représentation schématique des principales étapes de gravure requises pour atteindre la tranchée STI: Empilement initial (a), gravure BARC et NFARL (b), gravure AHM (c), recouvrement AHM (d), TEOS/Nitrure/Découpe et décapage AHM), la tranchée TCR et STI (f).

Dans la Figure 15, le premier CD (a) est représentatif du CD après l'étape de la photolithographie, qui est notre CD d'entrée. Le dernier CD (f), est le CD qui sera le cas d'étude au cours de cette thèse, qui est le CD de la tranchée STI après le procédé de gravure. Cet énorme empilement ainsi que la complexité du procédé de gravure plasma sont directement responsables des dérives de CD. La recette compte avec 32 étapes, y compris les étapes de stabilisation et de transitions. Cependant, elle pourrait être résumée en 8 étapes

principales, où 5 de ces étapes nécessitent des systèmes EPD (EndPoint) ou detection de fin d'attaque, et donc aussi un « overetch ».

CARACTERISATION

La caractérisation de procédé ici, est liée à l'étude de tous les paramètres qui peuvent être la source de variations du CD, afin de comprendre leurs influences sur le CD final du STI. L'objectif est de proposer une solution pour maintenir le CD final sous contrôle, proche de la valeur cible (target), après le procédé de gravure plasma.

Variabilité du procédé

En plus de la complexité du procédé de gravure plasma, il existe deux principaux facteurs externes qui ont une incidence sur le CD du STI. La variation d'épaisseur de chaque couche dans les étapes de dépôt et le CD post-photolithographie, qui est le point de départ du CD après gravure. Cependant, après avoir analysé l'influence de ces étapes, nous avons vu que la variation induite par les étapes précédentes, en particulier les variations d'épaisseur, pouvaient être améliorées au cours du procédé de gravure en utilisant les systèmes EPD. Respect du CD post-photolithographie, il est déjà corrigé en raison de la mise en œuvre de la stratégie de « re-working » de l'atelier de photolithographie, qui retravaillent les plaquettes avec des écarts importants de CD par rapport aux cibles souhaitées. Par conséquent, les variations provenant de l'épaisseur de dépôt des étapes précédentes ou de la photolithographie étaient négligeables.

Afin d'étudier la source de variation dans le procédé de gravure, nous avons identifié ces facteurs comme des effets provenant de la chambre de gravure, lot à lot, wafer-wafer, intra-wafer, type de produit, fournisseur de silicium, et la source inexplicable. L'analyse de variance a été réalisée en utilisant le logiciel *KLA-Tencor* qui permet de sélectionner les facteurs qui nous intéressent. Les 48% de la variation du CD peuvent être améliorés en utilisant des contrôleurs R2R. L'effet le plus important qui influence la variation du CD de la STI est l'effet de la chambre de gravure (43%). Cet effet de chambre (43%) ainsi que l'effet lot-à-lot (5%) peuvent être corrigés en développant un FeedBack R2R. Il y a aussi un effet inexpliqué, qui semble être le plus critique. Nous avons seulement pu optimiser la variabilité due à la chambre et les effets de lot à lot (48%). Cependant, nous avons pensé que peut-être en améliorant le système de mesure, nous pourrions réduire cet effet. Pour cela, nous avons développé un modèle de scatterométrie. Dans le même temps, nous avons commencé à développer la stratégie de contrôle du CD; le FB R2R qui est le principal objectif de cette recherche afin de réduire la part de la variabilité liée à la chambre et l'effet lot-à-lot.

OPTIMISATION

Une fois que la variabilité de gravure a été analysée, la stratégie employée pour optimiser le contrôle de procédé de la gravure du STI en améliorant les dérives de CD a été basée sur une boucle de control (FB R2R).

Le contrôleur R2R a été développé pour maintenir le CD du STI sous contrôle en réduisant les effets les plus importants; les variations dues a la chambre de gravure et l'effet du lot. Pour développer le modèle R2R basé sur le schéma de contrôle EWMA, le temps d'exposition d'AHM (chimie O_2) pendant l'étape de surgravure (overetch) d'AHM a été sélectionnée comme paramètre de contrôle. Cette étape était habituellement effectuée en temps fixe. En faisant varier la durée du temps, on obtient un CD plus grand ou plus petit par rapport à ce qui à été prédit.

L'élément final du contrôleur R2R est la loi de contrôle qui spécifie comment la recette du procédé doit être mise à jour. Le régulateur FB R2R que nous avons développé est illustré à la Figure 16.

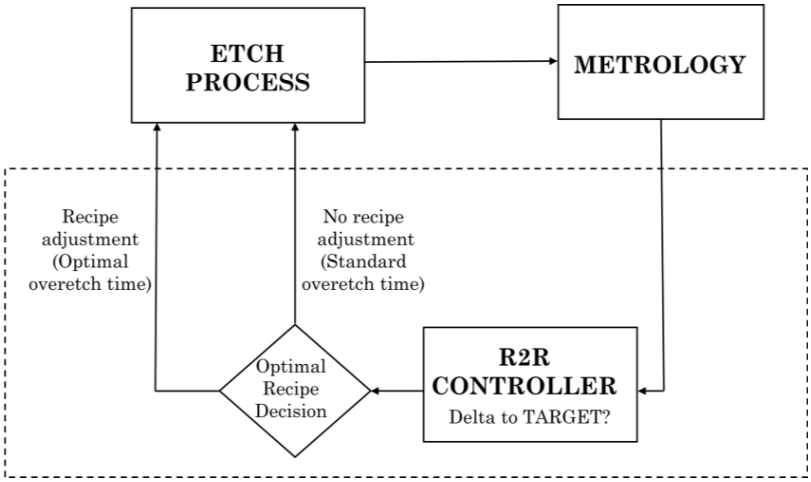

Figure 16. Diagramme schématique du contrôleur R2R développé pour le CD de la STI.

Fonctionnement R2R

Le modèle prend automatiquement en compte les changements dans la spécification de target du CD. Le CD final est réintroduit dans le modèle de contrôle et utilisé pour mettre à jour les paramètres du modèle, qui dans cette recherche est le *overetch* d'AHM (AHM_OE). Le temps de gravure standard pendant le *overetch* (a) est de 15,5 s. Tous les paramètres du modèle sont définis dans le Tableau 4.

Tableau 4. Les définitions des paramètres du modèle.

Notation	Definition
τ	CD target
Y_t	Observed CD at time t
$\widehat{Y_t}$	Predicted CD based on R2R controller at time t, for $t \geq 2$
a	AHM etching time during the overetch (constant=15.5s)
$\widehat{a_t}$	Predicted time AHM OE at time t, where $\boldsymbol{\widehat{a}_t = a + \widehat{S}_{t-1}}$ (2)
b	Etch rate (constant per chamber)
λ	Smoothing factor EWMA ($0 < \lambda \leq 1$)
S_t	Offset time, where $\boldsymbol{S_t = \frac{Y_t - \tau}{b}}$ (3)
$\widehat{S_t}$	EWMA predicted Offset time, where $\boldsymbol{\widehat{S}_t = \lambda \cdot S_t + (1-\lambda) \cdot \widehat{S}_{t-1}}$ (4) for $t \geq 2$

Le schéma de lissage commence par le réglage $\widehat{S_1} = \lambda \cdot S_1 = \lambda \frac{Y_1 - \tau}{b}$ (il n'y a pas S_0). Par rapport à notre équation d'EWMA (4) $\hat{S}_t$ représente l'observation lissée, et S_t représente le temps de décalage (3). Les indices se réfèrent à la période 1, 2, 3 ... n.

La première prédiction peut être calculée pour $\hat{Y}_t$ puisque nous commençons par $t \geq 2$. L'équation de base pour prédire le CD, basée sur le contrôleur EWMA, peut s'écrire sous la forme:

$$\widehat{Y_t} = Y_t - b \cdot \hat{S}_{t-1} \qquad (5)$$

En substituant $\hat{S}_{t-1}$ dans l'équation de base du CD prédit, L'équation de CD prédite serait comme suit:

$$\widehat{Y_t} = Y_t - b \cdot \lambda \cdot \sum_{j=0}^{t-2} (1-\lambda)^j \cdot S_{t-1-j} \qquad (5.a)$$

En remplaçant $S_t = \frac{Y_t - \tau}{b}$, (5.a), l'équation finale pour prédire le CD, peut s'écrire:

$$\widehat{Y_t} = Y_t - \lambda \cdot \sum_{j=0}^{t-2} (1-\lambda)^j \cdot \left(Y_{t-1-j} - \tau\right) \qquad (5.b)$$

En faisant varier le facteur de pondération, c'est-à-dire, λ, la procédure EWMA peut être sensible à une dérive faible ou progressive dans le procédé. Dans cette étude, λ a été fixé à 0.4, afin d'éviter les variations qui pourraient être induites par la variabilité de la métrologie. Cette valeur a été calculée expérimentalement.

Validation du modèle

Pour valider le modèle avant mise en production, certaines *simulations* ont été réalisées et évaluées. Les résultats relatifs à l'effet de chambre et à l'effet de lot sont indiqués respectivement dans la Figure 17 et la Figure 18.

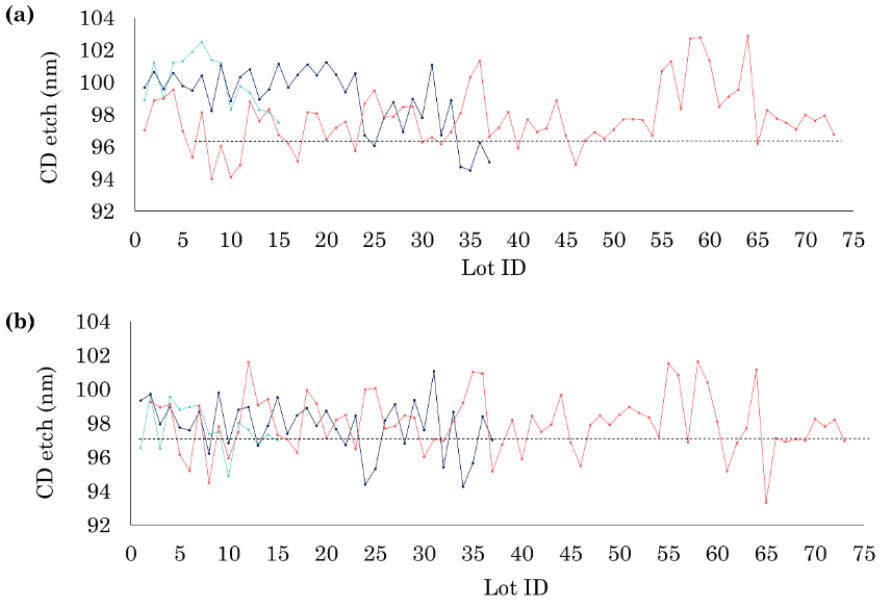

Figure 17. Comparaison entre (a) les données observées et (b) le CD prédit en utilisant le contrôleur R2R proposé. Trois chambres sont indiquées en différentes couleurs tandis que les lignes en pointillé indiquent les cibles.

En ce qui concerne ces résultats, le modèle a été validé puisque l'effet de chambre qui était celui que nous nous intéressions à corriger, s'est amélioré de 88% dur les 43% que cet effet induit à la variabilité totale. Ainsi, 38% de la variabilité totale a été corrigé. Dans cette Figure 17, l'écart type entre les chambres passe de 0,79 (a) à 0,09 (b).

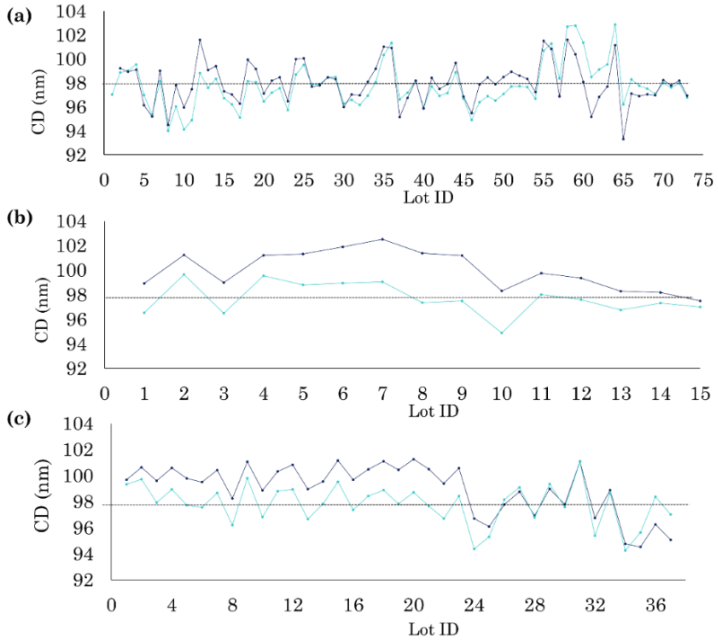

Figure 18. Les variations de Lot à Lot dans les trois chambres sont observées en (a), (b) et (c), où la ligne bleu foncé indique les données observées et la ligne bleu clair représente la valeur prédite.

Cependant, même si avec le R2R nous avons pu corriger un pourcentage significatif de la variabilité, nous voulions aussi améliorer le système de métrologie car il pourrait permettre de continuer à réduire la variabilité due à une meilleure précision des mesures. Une fois que le modèle de scatterométrie a été complètement développé, nous avons fait quelques variations sur les paramètres plasma afin d'avoir différentes valeurs de CD pour tester la précision du modèle. Le modèle a pu être représentatif dans tous les cas et aujourd'hui, le modèle de scatterométrie est utilisé dans la salle blanche comme mesure représentative du CD et de la hauteur de la tranchée STI, non seulement après la gravure mais aussi après l'étape de la photolithographie.

CONCLUSIONS

Cette étude montre la caractérisation et l'optimisation du CD par rapport à la gravure de la tanche d'isolation (STI). Premièrement, la caractérisation des sources des variations a été étudiées. La variabilité de la gravure a également été analysée. Un contrôleur R2R a été développé pour maintenir le CD du STI contrôlé en réduisant les effets les plus importants; l'effet de chambre et l'effet du lot. Le modèle R2R a été validé avec des données historiques et le facteur de lissage λ dans le modèle R2R est fixé à 0.4, expérimentalement. La variation due à l'effet de chambre est passée de 43% à 5% de la variation totale. L'objectif est de continuer à améliorer/réduire la variation avec le nouveau système de métrologie (scatterométrie). L'effet inexpliqué pourrait être réellement amélioré par ce système de métrologie plus précis pour mesurer les CD.

6. Conclusions

Cette thèse a été menée dans le cadre d'une collaboration entre industriels et universitaires. Ainsi, le travail présenté dans ce manuscrit est intimement lié au développement industriel d'une nouvelle technologie de STMicroelectronics Rousset; l'eSTM. Cette thèse visait à étudier et à optimiser une étape très spécifique: le traitement par gravure plasma de la tranchée pour des applications microélectroniques avancées.

Les objectifs de ce travail peuvent être divisés en trois parties. Tout d'abord, l'étude de la tranchée eSTM en incluant la caractérisation et l'optimisation du procédé pour obtenir un modèle capable de prédire le CD de la tranchée eSTM par rapport aux résultats électriques. Deuxièmement, le développement de la méthode de l'échantillon flottant à STMicroelectronics Rousset qui nous a permis d'étudier le dépôt sur les parois du réacteur et la mise en œuvre de la nouvelle stratégie de nettoyage (WAC). Enfin, la caractérisation du procédé STI pour contrôler le CD en développant un modèle de control R2R. De plus, parallèlement aux travaux de cette thèse, un nouveau modèle de scatterométrie a également été développé. Ce modèle est utilisé pour mesurer le CD de la STI après les étapes de photolithographie et de gravure et permet d'avoir mesures plus représentatives.

TRAVAIL FUTUR

Les études effectuées dans cette thèse sont loin d'être exhaustives encore. En effet, de nombreuses améliorations sont encore possibles:

- Une meilleure caractérisation de la surface de la plaquette et des dépôts créés sur les parois du réacteur pourrait être réalisée avec des analyses in-situ. Puisque les expériences ont été réalisées dans le réacteur industriel de STMicroelectronics Rousset, nous n'avions pas cette option. Cependant, si une amélioration de l'équipement est possible en utilisant des équipements des caractérisation in-situ, on pourrait éviter l'influence de la contamination induite par l'exposition de l'échantillon à l'air.
- Même si la stratégie de nettoyage (WAC) a été améliorée, elle pourrait être optimisée en évitant les gaz de nettoyage fluorés ou en utilisant une stratégie de *conditionnement*, comme expliqué dans la conclusion de cette étude. Pour cela, les gaz de ligne doivent être changés. Une étude portant sur l'influence de la contamination fluor sur le CD de l'eSTM devrait être réalisée afin de comprendre l'influence de cette contamination sur la variabilité du procédé.
- Le modèle R2R a été validé pour réduire la variabilité de CD du STI par rapport à la cible (target). Cependant, une nouvelle analyse de la variance devrait être effectuée maintenant que les mesures de scatterométrie sont en place. En outre, des analyses FDC contribueraient à améliorer la variabilité due à l'équipement.
- Le contrôleur R2R a été développé pour contrôler le CD du STI.Un contrôleur similaire pourrait être développé pour contrôler les variations de CD de la tranchée eSTM, une fois qu'elle sera en mode production.

Bien que la technologie étudiée dans ce manuscrit (eSTM) ne soit pas encore une technologie en production chez STMicroelectronics Rousset, les résultats obtenus dans notre étude ont été transférés et utilisés pour une amélioration globale du procédé de fabrication afin de maximiser les performances du dispositif encore en développement.

Bibliography

[1] H.C.M. Andrade, B. Gedik, D.S. Turaga. Fundamentals of Stream Processing: Application Design, Systems, and Analytics. Pages 467-468.
[2] Riordann, Hoddeson and Herring. "The Invention of the transistor", Rev. Mod. Phys., Vol.71, No.2, Centenary 1999.
[3] J.S. Kilby, "Invention of the Integrated Circuit", IEEE Transaction on Electron Devices ED-23.7 (1976): 648-654.
[4] F.Fagin, T.Klein, and L.Vadasz, "Insulated gate field effect transistor integrated circuits with silicon gates", IEEE Transactions on Electron Devices 16, 236 (1969).
[5] G.E.Moore. Cramming more components onto integrated circuits. Electronics, 38:8, 1965.
[6] Haissam El-Aawar. "Increasing the transistor count by constructing a two-layer crystal square on a single chip". International Journal of Computer Science & Information Technology (IJCSIT) Vol 7, No 3, June 2015.
[7] ITRS roadmap for semiconductors http://www.itrs.net/reports.html
[8] D.R.S. Cumming, S.B. Furber and D.J. Paul "Beyond Moore's law". Phil. Trans. R. Soc. A 372: 20130376, 2014. Doi: 10.1098/rsta.2013.0376
[9] R.M. Warner, B.L. Grung. "MOSFET Theory and Design 1st Edition". Oxford University Press, January 1999.
[10] S.M.Sze. Physics of Semiconductor Devices, 3rd Edition.
[11] J.R. Brews and E.H. Nicollian. MOS (metal oxide semiconductor) physics and technology. Vol. 1987. New York et al. Wiley, 1982.
[12] http://www.cs.mun.ca/~paul/transistors/node1.html Paul Gillard courses. Department of Computer Science, Memorial University of Newfoundland.
[13] M.H. Rasid, V. González, and P.A. Suárez Fernández. Power electronics handbook: device, circuits and applications, 3rd Edition. Elsevier, 2004.
[14] M.K. Achuthan and K.N. Bhat, Fundamentals of semiconductor devices. Tata McGraw-Hill Education Pvt. Ltd., 2007.
[15] Semiconductors. Chapter 4: Bipolar Junction Transistors. http://www.allaboutcircuits.com/textbook/semiconductors/
[16] W.C. O'Mara, R.B. Herring, L.P. Hunt. Handbook of Semiconductor Silicon Technology, 1st Edition. Materials science and process technology series. Noyes Publications, 1990.
[17] http://www.rsc.org/periodic-table/element/14/silicon
[18] High Purity Silicon VIII: Proceedings of the International Symposium. Vol 2004-2005. Electronics Division, The Electrochemical Society, 2004.
[19] S.M.Sze . Semiconductor Devices, Physics and Technology, 2nd Edition.
[20] P. Yu and M. Cardona. Fundamentals of Semiconductors: Physics and Materials Properties, 4th Edition. Springer Berlin Heidelberg, 2010.
[21] E. D. Jones. "Control of Semiconductor Conductivity by Doping" pp 155-171. Electronic Materials: From Silicon to Organics. Springer US, 1991.
[22] Donald Neamen. Semiconductor Physics And Devices. Irwin, 1992.

[23] http://www.rsc.org/periodic-table
[24] http://www.rsc.org/periodic-table
[25] Luca Varani. "Physics of Semiconductor Devices. Part III: Semiconductor at Equilibrium". University Montpellier, 2011.
[26] M.M. Atalla. "Semiconductor Devices Having Dielectric Coatings," U.S. Patent 3,206,670. Filed 1960. Granted 1965.
[27] D. Kahng and M.M. Atalla. "Silicon-Silicon Dioxide Field Induced Surface Devices". Carnegie Inst. of Tech., Pittsburgh, PA. IRE-AIEE Solid-state Device Res. ConJ, 1960.
[28] Jim Fraser. "Wafer FAB Process technology". Microelectronics technology & manufacturing maagement, 2010.
[29] Wai-Kai Chen. The VLSI Handbook, 2nd Edition. University of Illinois , Chicago, USA. CRC Press, 2010.
[30] Kevin McGowan. Semiconductors: From Book to Breadboard. Cengage Learning, 2012.
[31] J.R. Barnes. Robust Electronic Design Reference Book. Vol-1. Springer Science & Business Media, 2004.
[32] J.P. Uyemura. Circuits design for CMOS VLSI. Georgia Institute of technology, 1952. Doi : 10.1007/978-1-4615-3620-8
[33] http://ecee.colorado.edu/~bart/book/book/chapter7/ch7_6.htm
[34] D.V. Hall and SSSP Rao. Microprocessors and its Interfacing, 3rd Edition. McGraw Hill Education, 2012.
[35] B.RM. Dhanpat. Fundamentals of Microprocessors and Microcontrollers. Rai Publications, 2010.
[36] A.Pal. Microcontrollers: Principles and Applications. Phi learning private limited, 2011.
[37] A. Gupta, S.K. Kataria & Sons. Microcontroller and Embedded Systems, 2013.
[38] G. Campardo, R. Micheloni and D. Novosel. VLSI-Design of Non-Volatile Memories. Spinger, 2005.
[39] P.C. Lacaze and J.C. Lacroix. Non-volatile Memories: Electronics engineering series. Wiley-ISTE, 2014.
[40] W.D. Brown and J. Brewer. Nonvolatile Semiconductor Memory Technology: A Comprehensive Guide to Understanding and Using NVSM Devices, 1st Edition. Wiley-IEEE Press, 1997.
[41] B. de Salvo. Silicon non-volatile memories; Paths of Innovation. Wiley-ISTE, 2009.
[42] C. Kim, "Future Memory Technology Trends and Challenges in Quality Electronic Design". 7th International Symposium on, vol., no., pp.513-513. ISQED '2006. Doi: 10.1109/ISQED.2006.69
[43] Jonathan Bartoli PhD thesis. "Developpement de nouvelles architectures de cellules memoires non volatiles pour des applications a ultra basse consummation", 2015.
[44] Vincenzo Della Marca PhD thesis. "Characterization and modelling of advanced charge trapping nonvolatile memories", 2013.
[45] Ashok K. Sharma. Advanced Semiconductor Memories: Architectures, Designs, and Applications, 1st Edition. Wiley-IEEE, 2002.
[46] D.A. Hodges. J.Wiley & Sons. Semiconductor Memories. Inc, 1972.

[47] S.K. Kurinec and K. Iniewski. Nanoscale Semiconductor Memories: Technology and Applications. CRC Press, 2013.
[48] B. Prince. Semiconductor Memories: A Handbook of Design, Manufacture and Application. Wiley-Blackwell, 2nd Edition, 1995.
[49] J.S. Meena, S.M. Sze, U. Chand, and T-Y Tseng. Overview of emerging nonvolatile memory technologies. Nanoscale Res Lett., 2014. Doi: 10.1186/1556-276X-9-526
[50] D. Kahng and S. M. Sze, "A Floating Gate and Its Application to Memory Devices" Bell Syst. Tech. J., 46, 1283 (1967).
[51] P. Pavan, L. Larcher and A. Marmiroli. Floating Gate Devices: Operation and Compact Modeling. Springer US 2004. Doi: 10.1007/b105299.
[52] P. Dimitrakis. Charge-Trapping Non-Volatile Memories: Vol.1 - Basic and Advanced Devices. Springer, 1st Edition, 2015.
[53] Y. Goasduff, F.de la Rosa, S. Niel, A. Regnier. "Method of forming the source line of a vertical select transistor in NVM memory array". Patent Europa 12-RO-0410, 2012.
[54] Y. Goasduff, F.de la Rosa, S. Niel, A. Regnier. "Floating gate fowler nordheim non-volatile memory cell with vertical finger select transistors and method of forming". Patent Europa 12-RO-0656, 2012.
[55] I. Suchy. Handbook of Die Design. McGraw-Hill Education, 2 Edition, 2005.
[56] G.R. Rodriguez-Verjan PhD thesis "Smart Sampling for Risk Reduction in Semiconductor Manufacturing", 2014.
[57] M. Quirk and J. Serda. Semiconductor Manufacturing technology. Vol 1. Prentice Hall, 1st Edition, 2001.
[58] Y. Nishi and R. Doering. Handbook of Semiconductor Manufacturing Technology. CRC Press, Second Edition, 2007.
[59] Moritz Haass PhD thesis. "Pulsed plasmas for etch applications : Développement de procédés de gravure à base de plasmas réactifs pulsés", 2012.
[60] J. Reece Roth. Industrial Plasma engineering, vol.2. Applications to nonthermal processing. Department of electrical and computer engineering, university of tenneessee, knoxville. IOP.Bristol and Philadelphia. 2001.
[61] K. Nojiri. Dry Etching Technology for Semiconductors. Springer Cham Heidelberg New York Dordrecht London. Doi: 10.1007/978-3-319-10295-5
[62] Hyung Joo Lee B.S. Advanced Process Control and Optimal Sampling in Semiconductor Manufacturing. The University of Texas at Austin. Chemical Engineering. ProQuest, 2008.
[63] T. Sonderman and C. Spanos. Advanced Process Control in Semiconductor Manufacturing, 2005.
[64] Control of Manufacturing Processes. Spring Lecture #2: Semiconductor Process Variation, 2008. http://ocw.mit.edu
[65] D. Dries PhD thesis. "Study of photon induced volatilization of copper and process control of metal etch plasmas", 2011.
[66] R. Ramos PhD thesis. "Interactions entre les plasmas de gravure à couplage inductif et les parois du réacteur", 2008.

[67] S. Avertin PhD thesis “Développement et caractérisation de procédés de gravure plasma de T.S.V (Through Silicon Via) pour l’Intégration Tridimensionnelle de Circuits Intégrés”, 2012
[68] Langmuir, Proc. Natl. Acad. Sci. U.S.A. 14, 627 (1928).
[69] Richard Fitzpatrick. Plasma Physics: An Introduction. CRC Press, 2014.
[70] S.M.Rossnagel, J.J.Cuomo and W.D.Westwood. Handbook of plasma processing Technology: Fundamental, etching, Deposition, and Surface Interactions, 1990.
[71] J.W.Coburn and H.F. Winters. “Ion-and electron-assisted gas-surface chemistry: An important effect in plasma etching”. J. Appl. Phys. 50,3189 (1979).
[72] F.F. Chen, Introduction to Plasma Physics and Controlled Fusion, vol.1. New York: Plenum Press, 1984.
[73] M. Lieberman and A. Lichtenberg, Principles of Plasma Discharges and Materials Processing, New York: John Wiley and Sons, 1994.
[74] R. J. Goldston and P. H. Rutherford. Introduction to Plasma Physics. London: Institute of Physics Publishing, 1995.
[75] A. T. Forrester. Large Ion Beams. New York: John Wiley and Sons, 1988.
[76] R.L. Merlino. Understanding Langmuir probe current-voltage characteristics. Am. Phys. 75 12, December 2007. Doi: 10.1119/1.2772282
[77] I. Langmuir and L. Tonks, "General Theory of the Plasma of an Arc", Phys. Rev. 34, 876 - 922 (1929).
[78] Maxwell and J. Clerk. "Maxwell–Boltzmann distribution."
http://www.self.gutenberg.org/articles/maxwell%E2%80%93boltzmann_distribution
[79] M.I. Boulos, P. Fauchais and E. Pfender. Thermal Plasmas: Fundamentals and Applications. Springer Science, 1994.
[80] J. Meichsner, M. Schmidt, R. Schneider and H-E. Wagner. Nonthermal Plasma Chemistry and Physics. CRC Press, 2012.
[81] E.G. Harris. Physics of Hot Plasmas. Chapter 4: Plasma Instabilities, pp 145-201. Springer US, 1968. Doi: 10.1007/978-1-4615-8639-5_4
[82] A. Grill. Cold Plasma Materials Fabrication: From Fundamentals to Applications. Wiley IEEE Press, 1994.
[83] M.A. Lieberman. “A mini-course on the principles of plasma discharges”, 2003.
[84] D. Flamm, V. Donnelly, and J. Mucha. “The reaction of fluorine atoms with silicon”. Journal of Applied Physics 52, 3633 (1981).
[85] D. Flamm. “Mechanisms of silicon etching in fluorine- and chlorine-containing plasmas”. Pure and Applied Chemistry 62, 1709 (1990).
[86] J. McVittie. Fundamentals of plasma etching: Plasma-surface interactions. Standford Nanofabrication acility university. NNIN Etch Workshop, 2008.
[87] F.F. Cheng and J.P. Chang. Lecture notes on Principles of plasma processing. Springer, 2003. Doi: 10.1007/978-1-4615-0181-7
[88] H. Jansen, H. Gardeniers, M.de Boer, M. Elwenspoek and J. Fluitman. “A survey on the reactive ion etching of silicon in microtechnology”. Journal of micromechanics and microengineering 6.1, 14–28. Printed in the UK, 1996.

[89] P. Verdonck. Plasma etching, lecture notes. http://www.che.ufl.edu/unit-ops-lab/experiments/semiconductors/etching/Etching-theory.pdf
[90] Wet and Dry Etching, Class notes. Chemical Engineering University, Forida
[91] Romain de Paris thesis "Eco-conception de la gravure poly m10+", 2013.
[92] G.S. Mathad. Plasma Processing: Proceedings of the International Symposium, Science and Technology Division, Vol.13. The Electrochemical Society, 2000.
[93] J.W.Coburn ."The evolution of plasma etching in integrated circuit manufacturing", Dpto of Chemical Engineering, University of California.
[94] Shih-Po Lin et all. "Investigation of the time-delay effect on the critical dimension of tungsten silicide/polysilicon gate after reactive ion etching". Electrochemical Society Proceedings Volume 99-30. Pages 186-192
[95] V.M. Donnelly and A. Kornblit. Plasma etching: Yesterday, today, and tomorrow. Review Article. J. Vac. Sci. Technol. A 31(5), 2013.
[96] R.J. Shul and S.J. Pearton. Handbook of Advanced Plasma Processing Techniques. Springer Science & Business Media, 2011.
[97] Etch process introduction pdf.
[98] G. Cunge, N. Sadeghi and R. Ramos. "Influence of the reactor wall composition on radicals' densities and total pressure in Cl2 inductively coupled plasmas: II. During silicon etching". J. Appl. Phys. 102, 093305 (2007). http://dx.doi.org/10.1063/1.2803881
[99] G Cunge, B Pelissier, O Joubert, R Ramos and C Maurice. "New chamber walls conditioning and cleaning strategies to improve the stability of plasma processes". Plasma Sources Science and Technology, Volume 14, Number 3, 2005.
[100] K. Miwa, K. Usami, N. Takada and K. Sasaki. "Modification of Fluorinated Al_2O_3 Surface by Irradiating H2 and O2 Plasmas". Japanese Journal of Applied Physics, 2009.
[101] K. Miwa, K. Usami, N. Takada and K. Sasaki. "Fluorination mechanisms of Al2O3 and Y2O3 surfaces irradiated by high-density CF4/O2 and SF6/O2 plasmas". Journal of Vacuum Science & Technology A Vacuum Surfaces and Films, 2009.
[102] K. Miwa, T. Sawai, M. Aoyama, F. Inoue, A. Oikawa, K. Imaoka. "Particle reduction using Y2O3 material in an etching tool". Conference paper IEEE, 2007.
[103] M. Meyyappan and D.J. Economou. Proceedings of the Second International Symposium on Process Control, Diagnostics, and Modeling in Semiconductor Manufacturing. The Electrochemical Society, 1997.
[104] TF Edgar et al., "Automatic Control in Microelectronics Manufacturing: Practices, Challenges and Possibilities". *Automatica* 36, no. 11: 1567–1603 (2000).
[105] M-S. Chen, T.F. Yen, B. Coonan, Straatum and T. Cheyney. "Controlling etch tools using real-time fault detection and classification". Micromagazine, 2007.
[106] E. Bluem and J.P. Vassilakis. "Advanced Process Control Increases Yield of Low Open Area Via Etches". - Application Scientists - Thin Film Division Horiba.
[107] John V. Ringwood et all. "Estimation and Control in Semiconductor Etch: Practice and Possibilities". IEEE transactions on semiconductor manufacturing, vol. 23, no.1, 2010.
[108] H. Enami, M. Sakaguchi, N. Itabashi and M. Izawa. "Plasma Etching System and its Applications to 45–32-nm Leading-edge Devices". Hitachi Review, 2007.

[109] P. Subramonium, P. Fang, J. Henri, G.A. Antonelli, S. Varadarajan, I. Kalinovski and S.H. Hong. "Low temperature Ashable Hardmask (AHMTM) Films for sub-45nm patterning", Nouvellus System, Inc.
[110] "Understanding Brewer Science's. Bottom Anti-Reflective Coatings". Brewer science Inc, Rolla MO, USA.
[111] A.D. McNaught, A. Wilkinson. "Diamon-like carbon films" IUPAC Compendium of Chemical Terminology: the "Gold Book", 2Edition, Oxford Blackwell Scientific, 1997.
[112] R.E.Clausing, L.L.Horton, J.C.Angus, P.Koidl. Diamond and Diamond-like films and coatings. Springer Science & Business Media, 2012.
[113] D.A.P. Bulla, N.I. Morimoto. "Deposition of think TEOS PECVD silicon oxide layers for integrated optical waveguide application" Thin Solid Films 334:60. Doi: 10.1016/S0040-6090(98)011117-1.
[114] S. Rojas, P. Serra, W. S. Wu, F. Santarelli, G. C. Sarti, and F. Minni. "Process characterization for LPCVD deposition of SIO_2 films from TEOS liquid source" Le J. Phys. Colloq., vol. 50, no. C5, pp. C5–83–C5–90, May 1989.
[115]http://www.sematech.org/meetings/archives/litho/8940/pres/Process%20Control%20Requirements%20for%20Double%20Patterning_Litho_Ext_Symp_2010_21OCT10_Final.pdf
[116] A.M. Chatterjee, M. Manson, K. Joyner, D. Rogers, D. Mercer, J. Kuehne and A. Esquivel. Microelectronic Device and Multilevel Interconnection Technology II, 39 .SPIE 2875 (1996). Doi: 10.1117/12.250874.
[117] https://www.crystec.com/triende.htm
[118] B.E. Goodlin PhD thesis "Multivariate Endpoint Detection of Plasma Etching Processes". University of Texas at Austin, 2002.
[119] D.M. Manos and D.L. Flamm. Plasma Etching: An Introduction. Elsevier, 1989
[120] P.J. Marcoux and P.D. Foo. Optical Methods of End-Point Detection for Plasma Etching. Solid State Technology, Vol.0276, p.115-122. 1981. Doi: 10.1117/12.931703
[121] P. Hariharan. "Basics of Interferometry". Academic Press, 2012.
[122] W.H. Steel. "Interferometry". Vol 1 Cambridge University Press, ISSN 0959-6208. 1985.
[123] A.Holland. "General training manual for jobin yvon horiba thin film group end point detection equipment", Horiba group, 1999.
[124] F.F.Chen and J.P.Chang. Lecture notes on principles of plasma processing. Kluwer Academic/Plenum Publishers, New York, 233 Spring. ISBN:0-306-47497-2
[125] Laurene Babaud PhD "Développement et optimisation d'un procédé de gravure grille polysilicium pour les noeuds technologiques 45 et 32nm", 2010.
[126] Erwine Pargon PhD « Analyse des mécanismes mis en jeu lors de l'élaboration par gravure plasma de structures de dimensions deca-nanométriques : Application au transistor CMOS ultime", 2012.
[127] R. Westerman et all. "Endpoint detection methods for time division etch processes"
[128] D.M. Devia et al. "Methods Employed in Optical Emission Spectroscopy Analysis: a Review". Ingeniería y Ciencia Vol. 11, no. 21, pp. 239–267 Doi:10.17230/ingciencia.11.21.12
[129] A. Zaidel et al. "Tables of spectral lines", IFI/Plenum. NY, 1970.

[130] Peak Sensor System. Spectral Lines Technical Reference for Endpoint and Fault Recipe Formulation on ProPak, OmniPak & DataPak Systems
[131] J.E. Sansonetti et al. "Handbook of Basic Atomic Spectroscopic Data". National Institute of Standards and Technology, Gaithersburg, Maryland. American Institute of Physics, 2005. DOI: 10.1063/1.1800011
[132] R. Pearse et al. "The identification of Molecular Spectra" 4th Edition, Jhon Wiley & Sons, NY, 1976.
[133] Z.Karpas. "Analytical Chemistry of Uranium: Environmental, Forensic, Nuclear, and Toxicological Applications". CRC Press, 2014
[134] N. Bohr. On the constitution of atoms and molecules part i. Philosophical Maga-zine, 26(151):1{26, Jul. 1913.
[135] S.Lynn thesis "Virtual Metrology for Plasma Etch Processes" 2011.
[136] 2300 Exelan Process Module Maintenance, Revision B
[137] O.Ros PhD "Development and characterization of plasma etching processes for the dimensional control and LWR issues during High-k Metal gate stack patterning for 14FDSOI technologies", 2016.
[138] H.S. Nalwa. "Handbook of Surfaces and Interfaces of Materials, Five-Volume Set". Academic Press, 2001.
[139] Society of Photo-optical Instrumentation Engineers, Semiconductor Equipment and Materials International, SEMATECH (Organization). "Metrology, Inspection, and Process Control for Microlithography, Volumen 3677, Part 1". SPIE, 1999.
[140] K.D. Sattler. "Handbook of Nanophysics: Nanoelectronics and Nanophotonics". CRC Press, 2010.
[141] A.C. Diebold. "Handbook of Silicon Semiconductor Metrology". CRC Press, 2001.
[142] A. Vauselle PhD "Métrologie des dimensions critiques: scatterométrie et développements avancés". Aix-Marseille university, 2013.
[143] P. van der Heide. "X-ray Photoelectron Spectroscopy: An introduction to Principles and Practices". John Wiley & Sons, 2011.
[144] Einstein A. Ann. Physik 1905, 17, 132 (http://casanchi.com/fis/einstein1905/uno/uno_a.pdf). English version of Einstein's original article: http://casanchi.com/fis/einstein1905/uno/uno_i.pdf
[145] MAE 649 Microscopy and Spectroscopy, Chapter 3: X-ray photoelectron spectroscopy. http://www2.cemr.wvu.edu/~wu/mae649/xps.pdf
[146] S. Diplas. "X-ray photoelectron spectroscopy – An Introduction". SINTEF-UIO, 2013.https://www.uio.no/studier/emner/matnat/fys/MENA3100/v13/undervisningsmateriale/xps_spyros.pdf
[147] G.W.F. Drake. "Springer Handbook of Atomic, Molecular, and Optical Physics". Springer Science & Business Media, 2006.

[148] R. Paynter. "XPS theory", INRS- Énergie, Matériaux et Télécommunications, Quebec. http://saturno.fmc.uam.es/web/solidoII/propiedades_de_transporte/XPS_Paynter_t.pdf
[149] http://www.lasurface.com/xps/
[150] D.A. Shirley. "High-Resolution X-Ray Photoemission Spectrum of the Valence Bands of Gold". Phys. Rev. B 5, 4709-4714 (1972).
[151] http://www.casaxps.com/help_manual/manual_updates/peak_fitting_in_xps.pdf
[152] JF. Watts and J.Wolstenholme. "An introduction to surface analysis by xps and aes". Wiley Editions. Available at: http://202.38.64.11/~mams/escalab/An.Introduction.To.Surface.Analysis.By.XPS.And.AES.pdf
[153] D.Briggs and M.P.Seah. "Practical Surface Analysis (Second edition) Vol1: Auger and X-ray Photoelectron Spectroscopy". John wiley & sons.
available at: http://www.gbv.de/dms/ilmenau/toc/030968801.PDF
[154] K.Shen. "Experimental approaches to the study of insulating materials by electron spectroscopy". Literature report for CEM924.
[155] O. Joubert et al. "Monitoring chamber walls coating deposited during plasma processes : Application to silicon gate etch processes". J. Vac. Sci. Technol. A 22, 553 (2004)
[156] G. Cunge et al. "New chamber walls conditioning and cleaning strategies to improve the stability of plasma processes". Plasma Sources Sci. Technol. 14 (2005) 599–609. Doi: 10.1088/0963-0252/14/3/025
[157] http://www.nobelprize.org/educational/physics/microscopes
[158] P. Echlin. "Handbook of Sample Preparation for Scanning Electron Microscopy and X-Ray Microanalysis". Springer Science & Business Media, 2011.
[159] J. Goldstein et al. "Scanning Electron Microscopy and X-ray Microanalysis: Third Edition". Springer Science & Business Media, 2012.
[160] R. Egerton. "Physical Principles of Electron Microscopy: An Introduction to TEM, SEM, and AEM". Springer Science & Business Media, 2011.
[161] D.B. Williams and C.B. Carter. "Transmission Electron Microscopy: A Textbook for Materials Science. Diffraction. II". Springer Science & Business Media, 1996.
[162] L. Reimer. "Transmission Electron Microscopy: Physics of Image Formation and Microanalysis". Springer, 2013.
[163] J.C. Vickerman, D. Briggs. "TOF-SIMS: Materials Analysis by Mass Spectrometry". IM Publications, 2013.
[164] S. Fearn. "An Introduction to Time-of-Flight Secondary Ion Mass Spectrometry (ToF-SIMS) and its Application to Materials Science". Morgan & Claypool Publishers, 2015.
[165] G. Robert et al. "Secondary ion mass spectrometry: a practical handbook for depth profiling and bulk impurity analysis". Wiley, 1989.
[166] V.T. Cherepin. "Secondary Ion Mass Spectroscopy of Solid Surfaces". VSP, 1987.

[167] J.E. deVries. “Surface characterization methods-XPS, TOF-SIMS, and SAM-A complementary ensemble of tools”. J. of material engineering and performance, Vol.7. 1998
[168] https://www.phi.com/surface-analysis-techniques/tof-sims.html
[169] G. Tao et al. “Characterization and modelling of program/erase induced device degradation in 2T-FNFN-NOR Flash memories”, Physical and Failure Analysis of Integrated Circuits, 2008. IPFA 2008. 15th International Symposium on the. IEEE, 2008. DOI: 10.1109/IPFA.2008.4588191
[170] Y. K. Lee et al. “2T-FN eNVM with 90nm Logic Process for Smart Card”, 2008 Joint Non-Volatile Semiconductor Memory Workshop and International Conference on Memory Technology and Design. 2008. DOI: 10.1109/NVSMW.2008.13
[171] A. Watsona and S. H. Voldman. "The effect of deep trench and sub-collector on the latchup robustness in BiCMOS silicon germanium technology." Bipolar/BiCMOS Circuits and Technology Meetings. 2004. DOI: 10.1109/BIPOL.2004.1365772
[172] A. T. Tilke et al. "Highly scalable embedded flash memory with deep trench isolation and novel buried bitline integration for the 90-nm node and beyond." Electron Devices, IEEE Transactions on 54.7 (2007): 1681-1688. DOI: 10.1109/TED.2007.898040
[173] A. T. Tilke, et al. "Novel Buried Bitline Integration for compact Cell Design in High-Performance embedded Flash Memory with Deep Trench Isolation." Non-Volatile Semiconductor Memory Workshop, 2006. IEEE NVSMW 2006. 21st. IEEE, 2006. DOI: 10.1109/TED.2007.898040
[174] H. L. Tu et al. “High performance spiral inductor on deep-trench mesh silicon substrate", IEEE Microwave and Wireless Components Letters 16.12,p.654-656, 2006. DOI : 10.1109/LMWC. 2006.885608.
[175] H. Sunami. “Development of three-dimensional MOS structures from trench-capacitor DRAM cell to pillar-type transistor", International Conference on Solid-State and Integrated Circuits Technology Proceedings, ICSICT, p. 853-856, 2008. DOI 10.1109/ICSICT.2008.4734677.
[176] D. Lee et al. “Vertical floating-gate 4.5F2 split-gate NOR ash memory at 110nm node”, Digest of Technical Papers. 2004 Symposium on VLSI Technology, p. 72-73, 2004. DOI : 10.1109/VLSIT.2004.1345400.
[177] H. V. Tran et al. “An experimental 1Mb 0.11 um 4.5F2 1.8Volt multilevel vertical split gate source side injection test vehicle for giga-bit density NOR ash memory”, 2005 IEEE Asian Solid-State Circuits Conference, ASSCC 2005, p. 125-128, 2005. DOI: 10.1109/ASSCC.2005.251681.
[178] B. Chen. “Highly reliable SuperFlash embedded memory scaling for low power SoC”, International Symposium on VLSI Technology, Systems and Applications, Proceedings, p. 8-9. 2007. DOI :10.1109/VTSA.2007.378941.
[179] Plasma technology for advances devices: http://www.clarycon.com/

[180] M.L.Wagner and R.Nine. “The use of HBr in polysilicon etching”. Gases and instrumentation. www.gasesmag.com
[181] Dr. Bo Cui, waterloo nanofabrication group courses- etching-. https://ece.uwaterloo.ca/~bcui/
[182] V.M.Donelly and A.Kornblit. “Plasma etching: Yesterday, today and tomorrow” Journal of Vacuum Science & Technology A 31.5. 2013. DOI: 10.1116/1.4819316
[183] M.J.Madou. “Fundamentals of microfabrication: the science of miniaturization” 2nd Edition. CRS Press, 2002.
[184] N.G.Einsprunch and D.M.Brown. “Plasma processing for VLSI, Vol.8”. Electronics microstructure science.
[185] S.Franssila. “Introdcution to microfabrication”. J.Wiley and sons, 2004.
[186] R.A. Haring et al. "Mass and energy distribution of particles sputter etched from Si in a XeF2 environment." Applied Physics Letters 41.2 (174-176), 1982.
[187] G.C. Tyrrell et all. "Ion beam assisted etching of silicon with bromine: The role of the adsorbed state." Applied Surface Science 43.1-4 (439-446), 1989.
[188] T.D.Bestwick and G.S.Oehrlein. “Reactive ion etching of silicon using bromine containing plasmas”. J.Vac.Sci.Technol.A.8(3) May/Jun, 1990. DOI: 10.1116/1.576832
[189] Anthony Ricci. “Dry Etch Process Application Note”. PALL Microelectronics, ABG-106-0405. https://www.pall.com/pdfs/Microelectronics/ABG-106-0405.pdf
[190] G.S. Oehrlein et al. "Fluorocarbon high- density plasmas. II. Silicon dioxide and silicon etching using CF4 and CHF3." Journal of Vacuum Science & Technology A 12.2 (333-344), 1994. DOI:10.1116/1.578877
[191] T. E. F. M. Standaert et al. "Role of fluorocarbon film formation in the etching of silicon, silicon dioxide, silicon nitride, and amorphous hydrogenated silicon carbide." Journal of Vacuum Science & Technology A 22.1 (53-60), 2004. DOI: 10.1116/1.1626642
[192] Oehrlein, Gottlieb et al. "Surface science issues in plasma etching." IBM Journal of Research and Development 43.1.2 (181-197), 1999. DOI: 10.1147/rd.431.0181
[193] Schaepkens, Gottlieb and Oehrlein. "A review of SiO2 etching studies in inductively coupled fluorocarbon plasmas." Journal of The Electrochemical Society 148.3 (C211-C221), 2001.
[194] J.W. Coburn. “Insitu Auger electron spectroscopy of Si and SiO2 surfaces plasma etched in CF4-H2 glow discharges”. Journal of Applied Physics, 50(8), (5210-5213), 1979. DOI: 10.1063/1.326660
[195] T.E.F.M. Standaert et al. "High density fluorocarbon etching of silicon in an inductively coupled plasma: mechanism of etching through a thick steady state fluorocarbon layer." Journal of Vacuum Science & Technology A 16.1 (239-249), 1998.
[196] L. Rolland et al. "SiO 2/Si selectivity in high density CHF 3/CH 4 plasmas: Role of the fluorocarbon layer." Microelectronic engineering 53.1 (375-379), 2000. DOI: 10.1016/S0167-9317(00)00337-3

[197] R. Hyun-Kyu, et al. "Effects of CH2F2 Addition on a High Aspect Ratio Contact Hole Etching in a C4F6/O2/Ar Plasma." Electrochemical and solid-state letters 6.9 (C126-C129),2003.
[198] R D'Agostino et al. "Spectroscopic diagnostics of CF4- O2 plasmas during Si and SiO2 etching processes." Journal of applied physics 52.3 (1259-1265), 1981. DOI: 10.1063/1.329748
[199] C. J. Mogab, A. C. Adams and D. L. Flamm. " Plasma etching of Si and SiO2-The effect of oxygen additions to CF4 plasmas". J. Appl. Phys. 49, 3796. 1978. DOI:10.1063/1.325382
[200] X. Li, et al. "Effects of Ar and O2 additives on SiO2 etching in C4F8-based plasmas." Journal of Vacuum Science and Technology-Section A-Vacuum Surfaces and Films 21.1 (284-293), 2003. DOI: 10.1116/1.1531140
[201] X. Li, et al. "Characteristics of C4F8 plasmas with Ar, Ne, and He additives for SiO2 etching in an inductively coupled plasma (ICP) reactor." Journal of Vacuum Science & Technology A 21.6 (1955-1963), 2003. DOI: 10.1116/1.1619420
[202] D. Zhang and M.J. Kushner. "Investigations of surface reactions during C2F6 plasma etching of SiO2 with equipment and feature scale models." Journal of Vacuum Science and Technology-Section A-Vacuum Surfaces and Films 19.2 (524-538), 2001. DOI: 10.1116/1.1349728
[203] S. Gomez et al. "Etching of high aspect ratio structures in Si using SF6/O2 plasma." Journal of Vacuum Science & Technology A 22.3 (606-615), 2004. DOI: 10.1116/1.1710493
[204] S. Gomez et al. "Etching of high aspect ratio features in Si using SF6/O2/HBr and SF6/O2/Cl2 plasma." Journal of vacuum science and technology a vacuums surfaces and films 23.6 (1592), 2005. DOI: 10.1116/1.2049303
[205] Hwang et al. "Etching of Silicon in HBr Plasmas for High Aspect Ratio Features." (2002).
[206] K-W. Chang et al. "Highly selective etching for polysilicon and etch-induced damage to gate oxide with halogen-bearing electron-cyclotron-resonance plasma." Journal of applied physics 80.5 (3048-3055). 1996. DOI: 10.1063/1.363164
[207] G.C. Schwartz and P. M. Schaible. "Reactive ion etching of silicon." Journal of Vacuum Science & Technology 16.2, (410-413), 1979. DOI: 10.1116/1.569962
[208] T. Hattori. "Cleaning and Surface Conditioning Technology in Semiconductor Device Manufacturing 10, Número 2". The Electrochemical Society, 2007
[209] M. Fukasawa et al. "Structural and electrical characterization of HBr/O2 plasma damage to Si substratea)." Journal of Vacuum Science & Technology A 29.4 (041301), 2011. DOI: 10.1116/1.3596606
[210] J.McVittie. "HBr and NF3 based silicon etching". 2008 NINN Etch Workshop. http://www.prism.gatech.edu/~gtg928x/NNIN_reading_material/HBr-NF3.pdf
[211] M.A. Vyvoda et al. "Effects of plasma conditions on the shapes of features etched in Cl2 and HBr plasmas. I. Bulk crystalline silicon etching." Journal of Vacuum Science & Technology A 16.6 (3247-3258); 1998. DOI: 10.1116/1.581530

[212] V.M.Donnelly, “Optical Diagnostic techniques for low pressure plasmas and plasma processing”, AT & T Bell Laboratories. Vol. I, Chapter 1, p. 1. Academic Press, Boston, 1989. (O. Auciello and D. L. Flamm, eds. “Plasma Diagnostics: Discharge parameters and chemistry.).
[213] I.P.Herman. “Optical Diagnostics for Thin Film Processing”. Academic Press, 23 oct. 1996
[214] R.W. Dreyfus, J.M. Jasinski, R.E. Walkup, and G.S. Selwyn. “Optical diagnostics of low pressure plasmas”. Pure and Appl. Chem., Vol 57, No.9 pp. 1265-1276. 1985
[215] W.R. Harshbarger et al. "A study of the optical emission from an RF plasma during semiconductor etching." Applied Spectroscopy 31.3 (201-207), 1977.
[216] T.Y. Jung, D. H. Kim, and H. B. Lim. "Molecular Emission of CF 4 Gas in Low-pressure Inductively Coupled Plasma." Bulletin of the Korean Chemical Society 27.3 (373-375), 2006.
[217] T.A.R. Hansen and R.Engeln “Detection of hydrocarbon radicals during plasma etching”. Dpt of Appl. Phys. Eindhoven University of Technology.
[218] R. D’Agostino, Cramarossa, and S.De Benedictis. "Diagnostics and decomposition mechanism in radio-frequency discharges of fluorocarbons utilized for plasma etching or polymerization." Plasma Chemistry and Plasma Processing 2.3 (213-231), 1982.
[219] D. Field, A. J. Hydes, and D. F. Klemperer. "Spectroscopic studies of fluorescent emission in plasma etching of Si and SiO2 and the mechanism of gas-surface interactions." Vacuum 34.5 (563-578), 1984.
[220] P.E. Clarke, D. Field, and D. F. Klemperer. "Optical spectroscopic study of mechanisms in CCl4 plasma etching of Si." Journal of applied physics 67.3 (1525-1534), 1990.
[221] J.G. Shabushnig and P.R. Demko. "Application of optical-emission spectroscopy to semiconductor-device fabrication." American Laboratory 16.8. 1984.
[222] G.G. Gifford. “Applications of optical emission spectroscopy in plasma manufacturing systems”. Santa Cl-DL tentative. International Society for Optics and Photonics, 1991.
[223] N. Hershkowitz and R.A. Breun. "Diagnostics for plasma processing (etching plasmas)." Review of scientific instruments 68.1 (880-885), 1997.
[224] K. Ino, et al. "Plasma enhanced in situ chamber cleaning evaluated by extracted-plasma-parameter analysis." IEEE transactions on semiconductor manufacturing 9.2 (230-240), 1996.
[225] K. Miwa and Y. Kawabata. "In-situ quantification of deposition amount in a Poly-Si etch chamber using optical emission spectroscopy of etching plasmas." IEEE International Symposium, Sept.
[226] G..Selwyn, Optical Diagnostic Techniques for Plasma Processing. AVS Press, New York, 1993.
[227] M.J.Cohen. “Optical emission spectroscopy for plasma processing”. Bussines element manager for semiconductor instruments, EG1G Princenton Applied Research, New Jersey. http://infohouse.p2ric.org/ref/31/30708.pdf

[228] LAM Research. “Representative emission lines used in endpoint detection of plasma etching. Hardware specifications” [132,213,226,228a,228b]
[228a]. “CRC Handbook of Chemistry and Physics”, CRC Press, Inc, 1978
[228b]. “Optics diagnostics for thin film processing” Academic Press, Singer, 1988.
[229] G. Scott Douglas PhD thesis. “A Study of Plasma Ignition Enhancement for Aeroramp Injectors in Supersonic Combustion Applications”, 2001.
[230] R. Barni, S. Zanini and C. Riccardi. “Experimental study of bromoform plasmas”. 30th ICPIG, Belfast, Northern Ireland, UK, 2011.
[231] C. Vallée et all. “correlation between an optical plasma diagnostic (OES) and in-situ thin film diagnostic (SE)". Laboratoire des plasmas et couches minces, IMN-CNRS-Université de Nantes. Simulation 150: 200.
[232] R. Martinez et al. "Electron-impact-induced light emission from CF_2Cl_2." Journal of Physics B: Atomic, Molecular and Optical Physics 25.22 (4951), 1992.
[233] J.M. Keane and R.C. Fry. "Red and near-infrared inductively coupled plasma emission spectra of fluorine, chlorine, bromine, iodine, and sulfur with a photodiode array detector." Analytical Chemistry 58.4 (790-797), 1986.
[234] S.J. Strickler. "The identification of molecular spectra (Pearse, RWB; Gaydon, AG)." Journal of Chemical Education 41 (398), 1964. DOI: 10.1021/ed041pA398
[235] S. Koda. "Emission and energy transfer of triplet difluoromethylene produced in the reaction of oxygen atoms with tetrafluoroethylene." Chem. Phys. Letters 55.2 (353-357), 1978.
[236] S. Koda. "Mechanism of oxygen (3P) atom reaction with tetrafluoroethylene and quenching processes of the emission of difluoromethylene (3B1)." Journal of Physical Chemistry 83.16 (2065-2073), 1979.
[237] M. Suto, and N. Washida. "Emission spectra of CF3 radicals. II. Analysis of the UV emission spectrum of CF3 radicals." The Journal of Chemical Physics 78.3 (1012-1018), 1983.
[238] T. Cao et al. "Optical emission spectroscopy diagnostic and thermodynamic analysis of thermal plasma enhanced nanocrystalline silicon CVD process." RSC Advances 4.29 (15131-15137), 2014. DOI: 10.1039/C4RA01306A
[239] E.D. Lancaster et al. "Spectroscopic analysis of fire suppressants and refrigerants by laser-induced breakdown spectroscopy." Applied optics 38.9 (1476-1480), 1999.
[240] I. Radivojevic et al. "Detection of bromine in thermoplasts from consumer electronics by laser-induced plasma spectroscopy." Spectrochimica Acta Part B: Atomic Spectroscopy 59.3 (335-343), 2004.
[241] Endpoint-manual-wavelengths. Functional description, Chapter 3. https://snf.stanford.edu/SNF/equipment/dry-etching/applied-materials-precision-5000-etcher-p500etch-semi-clean/endpoint-wavelengths/at_download/file
[242] N. Hershkowitz and R.A. Breun. “Diagnostics for plasma processing (etching plasmas)”. Review of scientific instruments 68.1 (880-885), 1997.

[243] M. Matsui et al. "Surface analysis of polysilicon gate etching by pulsed-microwave plasma." Japanese Journal of Applied Physics 53.3S2 (03DD04), 2014.
[244] J. Pereira et al. "In situ x-ray photoelectron spectroscopy analysis of SiOxFy passivation layer obtained in a SF6/O2 cryoetching process." Appl. Phys. Lett 94.7 (71501), 2009.
[245] C.C. Cheng et al. "Competitive halogenation of silicon surfaces in HBr/Cl2 plasmas studied with x-ray photoelectron spectroscopy and in situ, real-time, pulsed laser-induced thermal desorption." Journal of Vacuum Science & Technology A 13.4 (1970-1976), 1995.
[246] M. Haass, M. Darnon, and O. Joubert. "Sidewall passivation layer thickness and composition profiles of etched silicon patterns from angle resolved x-ray photoelectron spectroscopy analysis." Journal of Applied Physics 111.12, 2012.
[247] S. Bouchoule et al. "Sidewall passivation assisted by a silicon coverplate during Cl2-H2 and HBr inductively coupled plasma etching of InP for photonic devices." Journal of vacuum science and technology b microelectronics and nanometer structures 26.2 (666), 2008.
[248] S. Bouchoule et al. "Effect of Cl2-and HBr-based inductively coupled plasma etching on InP surface composition analyzed using in situ x-ray photoelectron spectroscopy." Journal of Vacuum Science & Technology A 30.3 (031301), 2012.
[249] L. Desvoivres, L. Vallier, and O. Joubert. "X-ray photoelectron spectroscopy investigation of sidewall passivation films formed during gate etch processes." Journal of Vacuum Science & Technology B 19.2 (20-426), 2001.
[250] L. Vallier et al. "Chemical topography analysis using XPS during plasma etching in Si processing." FLTPD, Frontiers in low temperature plasma diagnostics IV. 2001.
[251] F.H. Bell, O. Joubert, and L. Vallier. "Polysilicon gate etching in high density plasmas. II. X-ray photoelectron spectroscopy investigation of silicon trenches etched using a chlorine-based chemistry." Journal of Vacuum Science & Technology B 14.3 (1796-1806), 1996.
[252] F.H. Bell and O. Joubert. "Polysilicon gate etching in high density plasmas. III. X-ray photoelectron spectroscopy investigation of sidewall passivation of silicon trenches using an oxide hard mask." Journal of Vacuum Science & Technology B 14.4 (2493-2499), 1996.
[253] F.H. Bell and O. Joubert. "Polysilicon gate etching in high density plasmas. IV. Comparison of photoresist and oxide masked polysilicon etching-thickness determination of gate oxide layers using x-ray photoelectron spectroscopy." Journal of Vacuum Science & Technology B 14.6 (3473-3482), 1996.
[254] F.H. Bell and O. Joubert. "Polysilicon gate etching in high density plasmas. V. Comparison between quantitative chemical analysis of photoresist and oxide masked polysilicon gates etched in HBr/Cl2/O2 plasmas." Journal of Vacuum Science & Technology B 15.1 (88-97), 1997.
[255] G.S. Oehrlein et al. "Surface analysis of realistic semiconductor microstructures." Journal of Vacuum Science & Technology A 7.3 (1030-1034), 1989.
[256] G.S. Oehrlein and Y. Kurogi. "Sidewall surface chemistry in directional etching processes." Materials Science and Engineering: R: Reports 24.4 (153-183), 1998.

[257] K. Siegbahn et al. ESCA Atomic, Molecular and Solid State Structure Studied by Means of Electron Spectroscopy (Almqvist&Wiksells, Uppsala, 1967), p. 251.

[258] Olivier Luere PhD "Analyse des differentes strategies de procedes de gravure de grille metal -high k pour les nœuds technologiques 45nm et 32nm", 2011.
[259] Xavier Mellhaouil PhD " Mécanismes physico-chimiques dans le procédé de gravure plasma du Silicium", 2006.
[260] Thomas Morel PhD " Developpement de procedes de gravure de grille metallique W, WN pour les noeuds technologiques sub-45 nm", 2006.
[261] R.Fisher, The design of experiment, Oliver-Boyd, Edinburgh (1935)
[262] Ronald A. Fisher. Philosophical Transactions of the Royal Society of Edinburgh. 1918. (volume 52, pages 399–433)
[263] Ronald A. Fisher. "Probable Error" of a Coefficient of Correlation Deduced from a Small Sample. Metron, 1: 3-32 (1921)
[264] C. Chung Wang et al. "Optimizing the rapid prototyping process by integrating the Taguchi method with the Gray relational analysis." Rapid Prototyping Journal 13.5 (304-315), 2007.
[265] A. Saltelli et al. "Global Sensitivity Analysis: The Primer". John Wiley and Sons, 2008.
[266] H. Rabitz. "Systems analysis at the molecular scale." Science 246.4927 (221-226), 1989.
[267] T. Turányi. "Sensitivity analysis of complex kinetic systems. Tools and applications." Journal of Mathematical Chemistry 5.3 (203-248), 1990.
[268] A. Saltelli. "Sensitivity analysis: Could better methods be used." Journal of Geophysical Research 104.D3 (3789-3793), 1999.
[269] R. Buxton. "Design Expert 7: Introduction". Mathematics learning, 2007. http://www.lboro.ac.uk/media/wwwlboroacuk/content/mlsc/downloads/Design%20Expert%207.pdf
[270] F. Pasqualini. "Design of experiments. Application to microelectronics". Master in microelectronics technology and manufacturing management, STUniversity.
[271] R. Legtenberg et al. "Anisotropic reactive ion etching of silicon using SF 6/O 2/CHF 3 gas mixtures." Journal of The Electrochemical Society 142.6, (2020-2028), 1995
[272] K. Prasad et al. "Application of design of experiments to plasma arc welding process: a review." Journal of the Brazilian Society of Mechanical Sciences and Engineering 34.1: (75-81), 2012
[273] KS. Chen et al. "Effect of process parameters on the surface morphology and mechanical performance of silicon structures after deep reactive ion etching (DRIE)." Journal of Microelectromechanical Systems 11.3: (264-275), 2002
[274] Sivarao et al. "Comparison between Taguchi Method and Response Surface Methodology (RSM) in modelling CO2 laser machining." Journal of Mechanical and Industrial Engineering 8.1.35-42, (2014)
[275] R.I.Haque PhD thesis. "Design et développement d'un capteur acoustique imprimé", 2015.

[276] L.F. Alvarez PhD thesis. “Design optimization based on genetic programming”, University of Bradford, UK, 2000.
[277] R.H. Myers and D.C.Montgomery. “Response surface methodology: Process and product optimization using designed experiments” 2nd edition. Wiley series in probability and statistics. John Wiley and sons, INC.
[278] A.B. Eldin. “General Introduction to Design of Experiments (DOE)”, Sigma Pharmaceutical Corp., Egypt.
[279] M. Schaepkens et al. “Influence of reactor wall conditions on etch processes in inductively coupled fluorocarbon plasmas”. J. Vac. Sci. Technol. A 16, (2099),1998.
[280] S. Xu et al. "Fluorocarbon polymer formation, characterization, and reduction in polycrystalline–silicon etching with CF4-added plasma." Journal of Vacuum Science & Technology A 19.3 (871-877), 2001.
[281] G. Cunge, O. Joubert and N. Sadeghi. “Enhancement of the recombination rate of Br atoms by CF4 addition and resist etching in HBr/Cl2/O2 plasmas”. Journal of applied physics 94 (6285-6290), 2003.
[282] G. Cunge et al. “Plasma-wall interactions during silicon etching processes in high-density HBr/Cl2/O2 plasmas”. Plasma Sources Science and Technology 14.2 (S42), 2005.
[283] K. Miwa, N. Takada, and K. Sasaki. "Fluorination mechanisms of Al2O3 and Y2O3 surfaces irradiated by high-density CF4/O2 and SF6/O2 plasmas." Journal of Vacuum Science and Technology A 27.4 (831-835), 2009.
[284] R. Ramos et al. "Plasma/reactor walls interactions in advanced gate etching processes." Thin Solid Films 515.12 (4846-4852), 2007.
[285] R. Ramos et al. “Cleaning aluminum fluoride coatings from plasma reactor walls in SiCl4/Cl2 plasmas”. Plasma Sources Science and Technology 16.4 (711), 2007.
[286] K. Miwa et al. “Modification of Fluorinated Al2O3 Surface by Irradiating H2 and O2 Plasmas”. Japanese Journal of Applied Physics 48.12R (126002), 2009.
[287] Pattent n° 20040221869 by B.C.Smith and D.J.James, 2004. Serial: 10786996
[288] M. Abdolahad, N. Nilchi, and S. Mohajerzadeh. “Fluorine-free high-resolution selective plasma etching of silicon-oxide layers on silicon substrates”. Journal of Physics D: Applied Physics 43.39 (395402), 2010.
[289] H. Singh et all. LAM Research corporation, US patent n°WO02/091453 A1. 2002.
[290] G.C.H. Zau and H.H. Sawin. "Effects of O 2 Feed Gas Impurity on Cl2 Based Plasma Etching of Polysilicon." Journal of the Electrochemical Society 139.1 (250-256), 1992.
[291] A.R. Godfrey et al. "New diagnostic method for monitoring plasma reactor walls: Multiple total internal reflection Fourier transform infrared surface probe." Review of Scientific Instruments 72.8 (3260-3269), 2001.
[292] S.J. Ullal et al. "Maintaining reproducible plasma reactor wall conditions: SF6 plasma cleaning of films deposited on chamber walls during Cl2/O2 plasma etching of Si." Journal of Vacuum Science & Technology A 20.4 (1195-1201), 2002.

[293] G. Cunge et al. "Time-resolved measurements of Cl2 density in high-density plasmas and application." Applied physics letters 88.5, 2006.
[294] B. Parkinson et al. "Increased uniformity control in a 45nm polysilicon gate etch process." SPIE Advanced Lithography. International Society for Optics and Photonics, 2009.
[295] R. Chong et al. "Optimizing STI etch process control using optical digital profilometry." Micro. vol. 22. no. 5. Canon communications inc, 2004.
[296] Ch. Hollauer, "Modeling of Thermal Oxidation and Stress Effects" http://www.iue.tuwien.ac.at/phd/hollauer/node7.html
[297] NIST/SEMATECH e-Handbook of Statistical Methods, http://www.itl.nist.gov/div898/handbook
[298] J. Isotalo. "Basics of statistics." University of Tampere, Findland, 2001. http://www.mv.helsinki.fi/home/jmisotal/BoS.pdf
[299] Introduction to STATISTICAL PROCESS CONTROL TECHNIQUES. Statit Software, Inc., Corvallis, Oregon, 2007. http://www.statit.com/services/SPCOverview_mfg.pdf
[300] W.J. Campbell et al. "A comparison of run-to-run control algorithms." Proceedings of the 2002 American Control Conference (IEEE Cat. No. CH37301). Vol. 3. IEEE, 2002.
[301] J.Moyne, "APC: A factory-wide strategy for ultimate yield improvement" , SolidState Technology, Insights for Electronics Manufacturing. http://electroiq.com/blog/2003/10/apc-a-factory-wide-strategy-for-ultimate-yield-improvement/
[302] J.R. Moyne and N.S. Patel. "Special section on advanced process control." IEEE Transactions on Semiconductor Manufacturing 20.4 (343-344), 2007.
[303] J. Moyne, E. Del Castillo, and A.M. Hurwitz, eds. "Run-to-run control in semiconductor manufacturing". Vol. 200. Chichester: CRC press, 2001.
[304] Z. Ning et al. "A comparative analysis of run-to-run control algorithms in the semiconductor manufacturing industry." ASMC 96 Proceedings. IEEE/SEMI 1996. IEEE, 1996.
[305] S.W. Roberts. "Control chart tests based on geometric moving averages." Technometrics 42.1 (97-101), 2000.
[306] J.S. Hunter. "The exponentially weighted moving average." J. Quality Technol. 18.4 (203-210), 1986.
[307] P. Čisar and S.M. Čisar. "Optimization methods of EWMA statistics." Acta Polytechnica Hungarica 8.5 (73-87),2011.

[I] K.Hazell. "Cold Plasma stops the cold virus from spreading in minutes". The Huffington Post, 2011.
[II] X-Ray photoelectron spectroscopy. http://en.wikipedia.org/wiki/X-ray_photoelectron_spectroscopy
[III] J.Holden. "Science looks beyond silicon in search for computer speed". The Irish Times, 2

List of Publications/ Communications

Journals (under submission):

1. "Key Effects and Process Parameters Extraction on the CD of Reactive Ion Etching (RIE) based on DOE Modelling" M.Rizquez, A.Roussy, J.Blue, L.Bucelle, J.Pinaton and J.Pasquet. IEEE Transactions on Semiconductor Manufacturing. (Submitted in 2016).

Oral presentations:

1. "Comparison study between optical emission spectroscopy and x-ray photoelectron spectroscopy techniques during process etch plasma" M.Rizquez, A. Roussy, A. James, J.Pinaton and Y.Goasduff. ASMC Conference, New York (USA), May 2014.
25th Annual SEMI IEEE (pp. 417-422). Available at: http://dx.doi.org/10.1109/ASMC.2014.6846967
2. "Plasma-Reactor Wall Interactions: Bromine-Fluorine Chemistry Duality in an Industrial Dry Etch Process" M.Rizquez, A.Roussy, B.Bortoloti, J.Pinaton and Y.Goasduff.MRS conference, San Francisco (USA), April 2015.
MRS Proceedings, Vol. 1803, Cambridge University Press. Available at: http://dx.doi.org/10.1557/opl.2015.600
3. "Developing R2R controller by means of studying the sources of variability in plasma etch process" M.Rizquez, D.Pompier, A.Roussy, Y.Goasduff, J.Pinaton and J.Pasquet. APCM Conference, Munich (Germany), April 2015.

Poster presentations:

1. "An approach to the passivation breakthrough during silicon plasma etching with a hydrogenated amorphous carbon (a-C:H) mask" M.Rizquez, A.James, A.Roussy, J.Pinaton and Y.Goasduff. JNRDM, Lille (France), May 2014.
2. "Passivation study using XPS: investigating F/Br species during plasma etching processes" M. Rizquez, A.Roussy, A.James, B.Bortolotti, J.Pinaton, J.Pasquet and Y.Goasduff. PESM conference, Leuven (Belgium), May 2015.

École Nationale Supérieure des Mines
de Saint-Étienne

NNT : *2016LYSEM024*

María RíZQUEZ

CHARACTERIZATION AND OPTIMIZATION OF HIGH DENSITY PLASMA ETCHING PROCESSES FOR ADVANCED MEMORIES APPLICATION

Speciality : Microelectronics

Keywords : Semiconductors, Plasma etching, Process control, Characterization

Abstract :

Among other characteristics, the ideal memory should have low power consumption, fast read/write/erase and high density solution. Different types of memories have been developed to pursuit these specific properties. Example of this attempt is the eSTM (Embedded Select Trench Memory). The eSTM aims to have the advantages of consumption and isolation from the EEPROM, due to its select transistor, together with the advantage of the Flash by reducing its size at the expense of a slightly more complex manufacturing process but still compatible with a CMOS technology. This PhD work studies the characterization and optimization of the plasma etching processes for this new technology developed by STMicroelectronics, the eSTM. This work has been highly related to the characterization of the reactor walls, the plasma itself and the wafer surface. The main objectives of this thesis are to understand the fundamental mechanisms of the etching processes and to propose innovative solutions to reduce the variations of CD by reaching the good control of the process desired. This thesis would help for the enhancement and increase of our knowledge on the physical phenomena which happens during this process, especially the passivation. This would offer the possibility of optimize the etch process and get the best CD (Critical Dimension) in terms of electrical results. The emphasis, was put on the characterization to get the maximum knowledge about the interactions taking place during the process inside of the reactor walls, such as plasma-surface interactions and plasma-reactor wall interactions. In order to characterize those films (both passivation as coatings on the reactor walls) and their composition, different techniques are used. Since the interactions between the plasma and the walls of reactors are responsible for a lack of reproducibility of the etching processes, this study also aims at the understanding of the cleaning of the reactor walls. Notably, the problem of the Fluorine has been shown in the reactor that is used for this study. As a new technology still in development, the study of the plasma-reactor wall interactions was required in order to develop the optimal cleaning after the etching in an industrial reactor at STMicroelectronics. Furthermore, this thesis was also focused on the optimization of the process drifts at STI (Shallow Trench Isolation) level, since the reproducibility of production processes generates serious concerns in making the component of the chips. Therefore, corrective actions were developed to control the source of variations by creating a regulation loop able to correct the CD dispersion between lots (25wafers). Such kind of R2R would play a key role for controlling the CD of the STI (Shallow Trench Isolation). Additionally, this model could be applied for controlling the CD of the new eSTM product.

École Nationale Supérieure des Mines
de Saint-Étienne

NNT : *2016LYSEM024*

María RíZQUEZ

CARACTÉRISATION ET OPTIMISATION DES PROCÉDÉS DE GRAVURE PLASMA HAUTE DENSITÉ POUR APPLICATION SUR DES DISPOSITIFS DE TYPE MÉMOIRES ÉLECTRONIQUES AVANCÉES

Spécialité: Microélectronique

Mots clefs : Semi-conducteurs, Gravure par plasma, Control de procédé, Caractérisation

Résumé :

Parmi d'autres caractéristiques, la mémoire électronique idéale doit présenter une faible consommation d'énergie, haute densité et de la rapidité en lecture/écriture/effacement. Différents types de mémoires ont été ainsi développées. Un exemple en l'eSTM, de l'anglais Embedded Select Trench Memory. Ce travail de thèse étudie la caractérisation et l'optimisation des procédés de gravure plasma utilisés dans la fabrication de cette nouvelle technologie développée par STMicroelectronics Rousset, l'eSTM. Ce travail a été fortement lié à la caractérisation des parois du réacteur, le plasma lui-même et la surface de la plaquette de silicium. Lors de cette thèse, la caractérisation chimique des surfaces exposées aux plasmas a permis de caractériser et d'optimiser ce nouveau procédé de gravure. De plus, les interactions entre le plasma et les parois des réacteurs sont responsables de l'absence de reproductibilité des procédés de gravure. Cette étude vise également à comprendre les dépôts sur les parois du réacteur qui se produisent pendant la gravure de la tranchée de l'eSTM. L'étude de ces dépôts a été nécessaire afin de développer un protocole de nettoyage optimal au sein d'un réacteur industriel, à STMicroelectronics. L'un des paramètres les plus critiques dans le développement des nouveaux dispositifs et dans l'amélioration des performances sont les Dimensions Critiques (CD) des transistors qui jouent un rôle fondamental au niveau des résultats électriques. La gravure plasma est contrôlée par la formation d'une couche de passivation se formant en surface des flancs du silicium. La maitrise de cette couche par les conditions du plasma (pression, puissance source débit de gaz...) a permis de développer un model innovant afin d'optimiser le CD de la tranchée. De plus, cette thèse a également porté sur l'étude des dérives des CD au niveau des STI (Shallow Trench Isolation). Des mesures correctives ont été développées afin de contrôler les sources de variations en créant une nouvelle stratégie de gravure pour corriger la dispersion des CD entre lots (25 plaquettes de silicium). Cette correction est possible par la mise en place base de boucles de régulations (R2R) permettant le contrôle de procédé de fabrication de la STI. Cette correction peut être aussi appliqué sur des tranchées type eSTM.